nagra
National Cooperative for
the Disposal of Radioactive Waste

TECHNICAL REPORT 91-09

GRIMSEL TEST SITE

INTERPRETATION OF CROSSHOLE HYDRAULIC TESTS AND A PILOT FLUID LOGGING TEST FOR SELECTED BOREHOLES WITHIN THE BK-SITE

JULY 1992

S. Vomvoris[1] and B. Frieg[1] (eds)

D. Guyonnet[3], V. Kelley[2], J.-M. Lavanchy[3]
S. Löw[3] and S. Mishra[2]

[1] NAGRA, CH-5430 Wettingen
[2] INTERA Inc., Austin, Texas
[3] Colenco Power Consulting Ltd., Baden

GRIMSEL TEST SITE/SWITZERLAND
A JOINT RESEARCH PROGRAM BY

- NAGRA – National Cooperative for the Disposal of Radioactive Waste, Wettingen, Switzerland
- BGR – Federal Institute for Geoscience and Natural Reseources, Hannover, Federal Republic of Germany
- GSF – Research Centre for Environmental Sciences, Munich, Federal Republic of Germany

Hardstrasse 73, CH-5430 Wettingen/Switzerland, Telephone + 41-56-37 11 11

nagra
National Cooperative for
the Disposal of Radioactive Waste

TECHNICAL REPORT 91-09

GRIMSEL TEST SITE

INTERPRETATION OF CROSSHOLE HYDRAULIC TESTS AND A PILOT FLUID LOGGING TEST FOR SELECTED BOREHOLES WITHIN THE BK-SITE

JULY 1992

S. Vomvoris[1] and B. Frieg[1] (eds)

D. Guyonnet[3], V. Kelley[2], J.-M. Lavanchy[3]
S. Löw[3] and S. Mishra[2]

[1] NAGRA, CH-5430 Wettingen
[2] INTERA Inc., Austin, Texas
[3] Colenco Power Consulting Ltd., Baden

GRIMSEL TEST SITE/SWITZERLAND
A JOINT RESEARCH PROGRAM BY

- NAGRA – National Cooperative for the Disposal of Radioactive Waste, Wettingen, Switzerland
- BGR – Federal Institute for Geoscience and Natural Reseources, Hannover, Federal Republic of Germany
- GSF – Research Centre for Environmental Sciences, Munich, Federal Republic of Germany

Hardstrasse 73, CH-5430 Wettingen/Switzerland, Telephone + 41-56-37 11 11

National Cooperative for the
Disposal of Nuclear Waste
NAGRA

NAGRA TECHNICAL REPORT NTB 91-09

INTERPRETATION OF CROSSHOLE HYDRAULIC TESTS AND A PILOT FLUID LOGGING TEST FOR SELECTED BOREHOLES WITHIN THE BK-SITE, GRIMSEL TEST SITE

PART I
INTRODUCTION AND REPORT OVERVIEW
S. Vomvoris & B. Frieg

PART II
METHODS FOR ANALYZING SINGLE- AND MULTI-WELL HYDRAULIC TEST DATA
S. Mishra

PART III
ANALYSIS OF SINGLE AND CROSSHOLE TESTS AT THE BK-SITE, GRIMSEL TEST SITE
D. Guyonnet & J.-M. Lavanchy

PART IV
ANALYSIS OF A PILOT CROSSHOLE FLUID LOGGING TEST AT THE BK-SITE, GRIMSEL TEST SITE
V. Kelley & S. Löw

PART V
INTERPRETATION OF SELECTED 1990 HYDRAULIC AND FLUID LOGGING TESTS: SYNTHESIS AND CONCLUSIONS
D. Guyonnet & V. Kelley

FOREWORD

Concepts for the disposal of radioactive waste in geological formations lay great weight on acquiring extensive knowledge of the proposed host rock and the surrounding rock strata. For this reason, Nagra has, since May 1984, been operating the **Grimsel Test Site (GTS)** which is located at a depth of 450 m in the crystalline rock of the Aare Massif of the Central Swiss Alps. The general objectives of the research being carried out in this underground laboratory include

- the build-up of know-how in planning, performing and interpreting field experiments in various scientific and technical disciplines.

- the acquisition of practical experience in the development of investigation methodologies, measuring techniques and test equipment which will be of use during actual repository site explorations.

The GTS is operated by Nagra and, on the basis of a German-Swiss co-operative agreement, various experiments are carried out by Nagra, the Federal Institute for Geoscience and Natural Resources (Bundesanstalt für Geowissenschaften und Rohstoffe, BGR) and the Research Center for Environmental Sciences (Forschungszentrum für Umwelt und Gesundheit GSF). The Grimsel projects of both GSF and BGR are supported by the German Federal Ministry for Research and Technology (BMFT). NTB 85-46 (English version) and NTB 85-47 (German version) provide an overview of the German-Swiss investigation programme. In a special issue of the Nagra Bulletin 1988 (English version) and in Nagra Informiert 1+2/1988 (German version) the status of the programme up to 1988 is described.

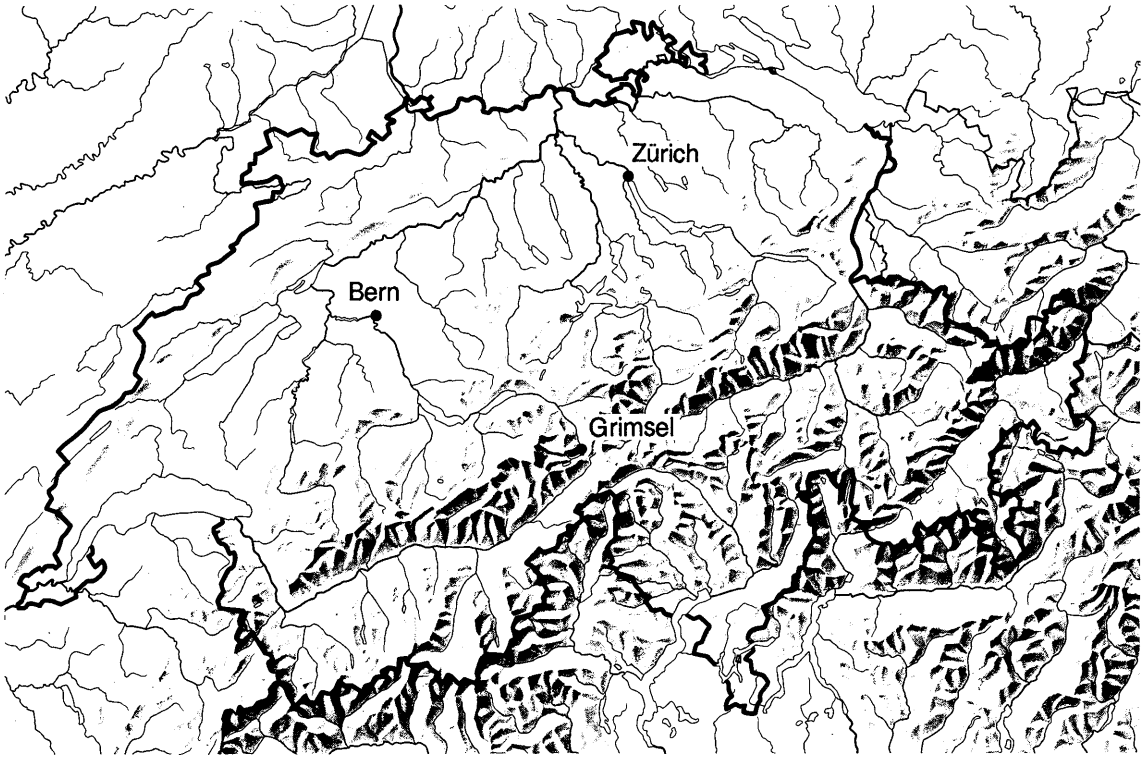

Location of Nagra's underground test facility at the Grimsel Pass in the Central Alps (Bernese Alps) of Switzerland (approximate scale 1 cm = 25 km).

Geographische Lage des Nagra Felslabors am Grimselpass (Berner Oberland) in den schweizerischen Zentralalpen (Massstab: 1 cm = ca. 25 km)

GRIMSEL-GEBIET

Blick nach Westen

1 Felslabor
2 Juchlistock
3 Räterichsbodensee
4 Grimselsee
5 Rhonetal

GRIMSEL AREA

View looking West

1 Test Site
2 Juchlistock
3 Lake Raeterichsboden
4 Lake Grimsel
5 Rhone Valley

FLG FELSLABOR GRIMSEL
GTS *GRIMSEL TEST SITE*

Situation

0 100 m

- Zugangsstollen/*Access tunnel*
- Fräsvortrieb/*by tunnel boring machine*
- Sprengvortrieb/*excavated by blasting*
- Zentraler Aaregranit ZAGR / *Central Aaregranite CAGR*
- Biotitreicher ZAGR / *CAGR with high content of biotite*
- Grimsel-Granodiorit / *Grimsel-Granodiorite*
- Scherzone/*Shear zone*
- Lamprophyr/*Lamprophyre*
- Wasserzutritt/*Water inflow*
- SB Sondierbohrung/*Exploratory borehole*
- US US Bohrung/*US borehole*

ZB	Zentraler Bereich/*Central facilities*
AU	Auflockerung/*Excavation effects*
BK	Bohrlochkranz/*Fracture system flow*
EM	El.magn. HF-Messungen/*-measurements*
FRI	Kluftzone/*Fracture zone investigation*
GS	Gebirgsspannungen/*Rock stresses*
HPA	Hydr. Parameter/*Hydr. parameters*
MI	Migration/*Migration*
MOD	Hydrodyn. Modellierung/*H. modeling*
NM	Neigungsmesser/*Tiltmeters*
UR	Untertageradar/*Underground radar*
US	Seismik/*Underground seismic testing*
VE	Ventilationstest/*Ventilation test*
WT	Wärmeversuch/*Heat test*

A — A Schnitt/*Section*

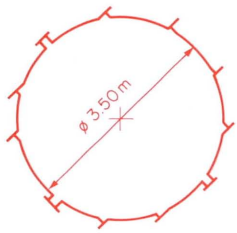

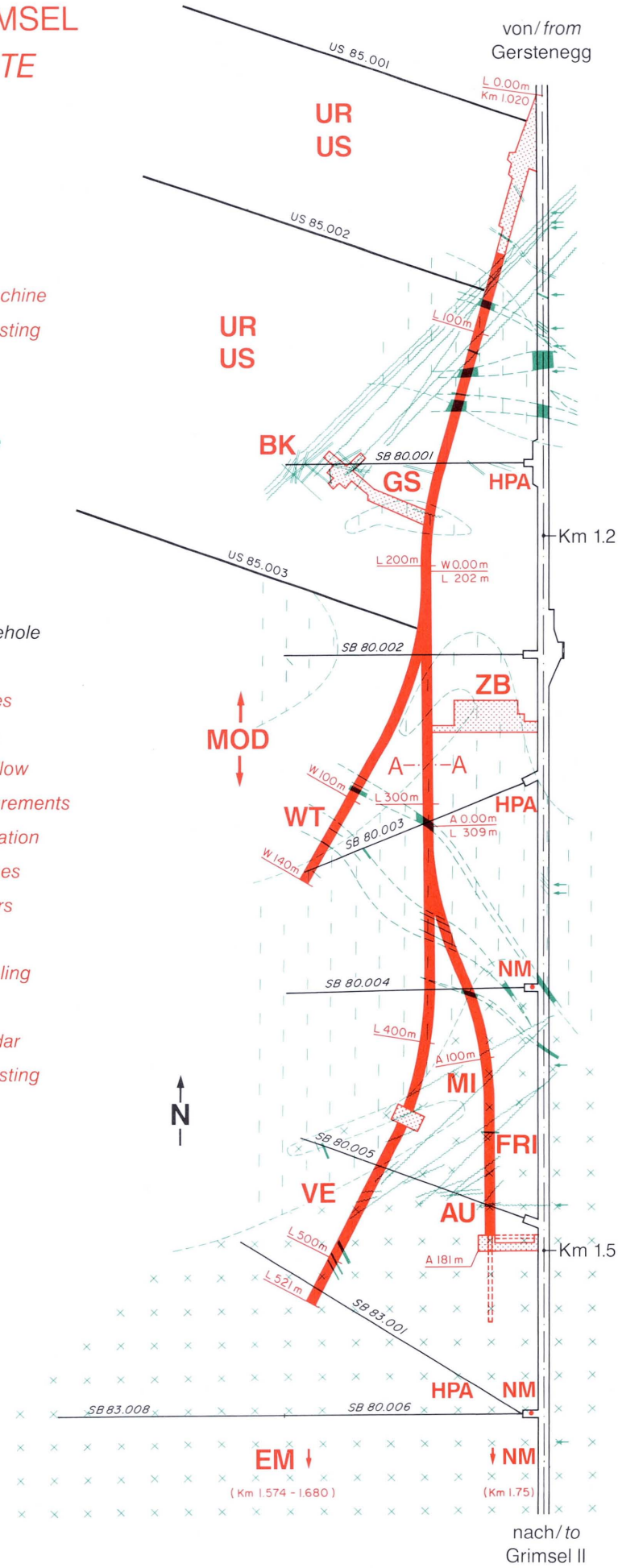

6/88

ZUSAMMENFASSUNG

Der vorliegende Bericht beinhaltet die theoretischen Grundlagen und die Auswertung von hydrogeologischen Versuchen, welche durch COLENCO (im Auftrag der NAGRA) und die Bundesanstalt für Geowissenschaften und Rohstoffe (BGR) am Standort "Bohrlochkranzversuch" (BK) des Felslabors Grimsel (FLG) im Januar bis März 1990 durchgeführt worden sind. Die Feldversuche im stark zerklüfteten kristallinen Gebirge beinhalten sowohl hydraulische Mehrbohrloch-Packerversuche wie ein Fluid-Logging Mehrbohrloch-Versuch über eine Distanz von wenigen Dekametern. Die Zielsetzung der Versuche bestand darin, mit relativ begrenztem Aufwand einen Ueberblick über die grundlegenden Fliessverhältnisse im Bereich einer komplizierten Störungszone im zentralen BK-Bereich zu erhalten.

Die hydraulischen Tests bestanden aus mehrstündigen Ein- und Mehrbohrloch-Injektionsversuchen mit der Bohrung BK 85.004 als aktiver Bohrung, und längeren Druckerholungsphasen vor und nach der aktiven Testserie. Die neu zur Anwendung gekommene (und in Teil II hergeleitete) Auswertungs-Philosophie beruht auf diagnostischen Plots der Messdaten, welche Hinweise auf das wirksame Fliessregime und das für die Parameterbestimmung zu verwendende Fliessmodell ergeben. Die Auswertung der Druck/-Fliessdaten der aktiven Bohrung BK 85.004 deuten auf ein heterogenes Fliessfeld mit radialen 2-dimensionalen Fliessverhältnissen zu frühen Zeiten (Bohrloch-Nahbereich) und linearen 1-dimensionalen, beziehungsweise berandeten Fliessverhältnissen zu späteren Zeiten. Die Druckreaktionen in den Beobachtungsbohrungen deuten auf die Existenz von diskreten, sehr hochdurchlässigen Fliesswegen (Kurzschlüssen) und bestätigen die Schlussfolgerungen, welche auf den Daten der aktiven Bohrungen beruhen.

Der Fluid-Logging-Mehrbohrlochversuch stellt in seiner Art einen Pilotversuch dar, da die Fluid-Logging-Methode bisher ausschliesslich als Einbohrloch-Methode eingesetzt wurde. Zu diesem Zweck wurden in der Bohrung BK 85.004 kontinuierlich Salzlauge injiziert und in verschiedenen Beobachtungsbohrungen eine Serie von kombinierten Salinitäts/Temperatur-Logs der Bohrlochflüssigkeit gefahren. Jede frei ausfliessende Beobachtungsbohrung wurde zu Beginn einer Log-Serie mit Frischwasser klargespült uns anschliessend während etwa 10 Stunden gelogt, während alle anderen Bohrungen mit Packern verschlossen waren. Der Versuch ergab sehr erfolgreiche Resultate, indem innerhalb von 9 Tagen 7 Bohrung detailliert hydraulisch charakterisiert werden konnten. Aus der Art der Zuflüsse (mit/ohne Salztracer) konnten Fliesswege mit schnellen und langsamen Verbindungen zur Injektionsbohrung bestimmt werden und mittels analytischen (Momenten-Methode) und numerischen Verfahren (BORE Simulator) bezüglich der Fliessraten und Durchbruchskonzentrationen quantifiziert werden. Die Zuflussstellen (Klüfte) mit hoch-mineralisierten Zuflüssen (wahrscheinlich direkte Fliessverbindungen) entsprechen genau denjenigen Packerintervallen der hydraulischen Versuche, welche sehr hohe hydraulische Verbindungen (Kurzschlüsse) aufweisen.

RESUME

Ce rapport présente l'analyse de tests hydrauliques effectués par le Bundesanstalt für Geowissenschaft und Rohstoffe (BGR) et d'un test pilote de diagraphie de fluides entres forages effectué par NAGRA/COLENCO, dans la roche cristalline fracturée de la zone du BK (Laboratoire Souterrain du Grimsel).

Les tests hydrauliques sont des tests simples et d'interférence d'injection à charge constante dans le forage 85.004. La philosophie d'interprétation est basée sur l'utilisation de graphes dits diagnostiques. Ces graphes fournissent des indications concernant le modèle d'écoulement et la présence éventuelle de limites. Les résultats de l'analyse des tests simples indiquent une réponse mixte avec une première fenètre de données présentant des caractéristiques d'écoulement radial suivie d'une deuxième fenètre présentant des caractéristiques d'écoulement linéaire ou limité. L'analyse des tests d'interférence indiquent la présence d'une zone hautement perméable et confirme la présence de limites.

Pour le test pilote de diagraphie de fluides, une saumure a été injectée dans le forage 85.004 tandis que des diagraphies de conductivité et de température étaient mesurées dans divers forages de la zone du BK. Le test identifia avec succès des fractures productrices dans les forages d'observation qui étaient (1) connectées au forage d'injection ou (2) apparemment non-connectées au forage d'injection. Une quantité importante d'information concernant la localisation de fractures productrices (53 fractures) a été obtenue en un temps relativement court (9 jours de tests). L'application de la méthode des Moments Partiels fournit malgré des conditions non-optimales pour cette méthode, des valeurs d'écoulement aux fractures dont les sommes pour chaque forage sont très proches des valeurs mesurées. Le modèle de différences finies BORE est utilisé pour simuler les diagraphies de conductivité électrique ce qui permet d'estimer les écoulements aux fractures ainsi que les concentrations dans les fluides produits par ces fractures. La position des fractures présentant les plus hautes concentrations (donc a-priori les mieux connectées a l'intervalle d'injection), correspondent aux positions des intervalles dont les tests hydrauliques ont montré qu'ils intersectaient une zone hautement transmissive.

SUMMARY

This report presents the analysis of hydraulic tests performed by the Bundesanstalt für Geowissenschaft und Rohstoffe (BGR) and of a pilot crosshole fluid logging test performed by NAGRA/COLENCO, in the fractured crystalline rock of the BK area in the Grimsel Test Site (GTS).

The hydraulic tests were single- and crosshole constant-head injection tests into borehole 85.004. The test analysis philosophy is based on the use of diagnostic plots. These plots provide indications relative to the flow model and to the presence of boundaries. Results of the single-hole analysis indicate a mixed response with an early-time portion dominated by radial flow followed by a later-time portion showing linear or bounded-flow characteristics. Analysis of the observation interval response shows evidence of a highly transmissive feature and confirms the presence of low permeability boundaries indicated by the single-hole analysis.

For the pilot crosshole fluid logging test, a salt brine was injected into borehole 85.004 and electrical conductivity and temperature logs were measured in various boreholes of the BK area. The test successfully identified flowing fractures in observation boreholes which were (1) connected to the injection borehole or (2) apparently not connected to the injection borehole. A large amount of information relative to flowing fracture locations (53 individual fractures) was obtained in a relatively short period of time (9 days of testing). The method of Partial Moments was used to calculate interval flow rates and, despite non-optimal conditions for application of this methodology, provided interval flow rates for each borehole which added up to values in good agreement with measured total borehole flow rates. The BORE finite-difference model was used to simulate the measured conductivity logs and provided estimates of fracture flow rates as well as fracture inflowing fluid concentrations. The locations of the fractures with the highest inflowing fluid concentrations (and therefore supposedly those best connected to the injection interval), correspond to the locations of the intervals which intersect a highly transmissive feature as shown by the hydraulic tests.

TABLE OF CONTENTS

		page
ZUSAMMENFASSUNG		I
RESUME		II
SUMMARY		III
TABLE OF CONTENTS		IV
LIST OF FIGURES		VII
LIST OF TABLES		XII
PART I		
I.1	Background and Scope	3
I.2	Report Organisation	4
PART II		
ABSTRACT		9
II.1	INTRODUCTION	9
II.1.1	Basic Background	9
II.1.2	Interpretation Philosophy	10
II.1.3	Pressure Derivative Analysis	10
II.1.4	Scope and Objectives	10
II.2	SINGLE-WELL TEST ANALYSIS	11
II.2.1	Introduction	11
II.2.2	Early-time (Borehole Dominated) Response	11
II.2.3	Middle-time (System Dominated) Response	12
II.2.4	Late-time (Boundary Dominated) Response	16
II.2.5	Analysis of Variable Rate/Pressure Test Data	16
II.2.6	Pressure Buildup Analysis	18
II.2.7	Constant Head (Pressure) Testing	20
II.3	MULTI-WELL TEST ANALYSIS	22
II.3.1	Introduction	22
II.3.2	Borehole Storage Effects	22
II.3.3	Constant Rate Interference Testing	22
II.3.4	Constant Pressure Interference Testing	25
II.4	CONCLUDING REMARKS	26
PART III		
ABSTRACT		31
III.1	SINGLE-HOLE TEST ANALYSIS	31
III.1.1	INTRODUCTION	31
III.1.1.1	Site description	31

III.1.1.2	Scope and objectives of the analysis	34
III.1.2	BOREHOLE HISTORY PRIOR TO TESTING	36
III.1.3	ANALYSIS OF THE PRESSURE RECOVERIES	37
III.1.3.1	Method of analysis	37
III.1.3.2	Results of the Horner analysis	37
III.1.3.3	Conclusions of the pressure recovery analysis	40
III.1.4	CONSTANT HEAD INJECTION TEST ANALYSIS	43
III.1.4.1	Hydraulic gradients within the BK zone prior to testing	43
III.1.4.2	Diagnostic plots for flow dimension analysis	45
III.1.4.2.1	Methodology	45
III.1.4.2.2	Results of the diagnostic plot analysis	46
III.1.4.3	Numerical analysis of the constant head tests	49
III.1.4.3.1	Methodology	49
III.1.4.3.2	Results of the numerical analysis	50
III.1.4.3.3	Implications for the conceptual model of the BK zone	52
III.1.5	SUMMARY AND CONCLUSIONS	55
III.2	CROSSHOLE TEST ANALYSIS AT THE BK SITE	56
III.2.1	Introduction	56
III.2.1.1	Objectives	56
III.2.1.2	Approach	56
III.2.2	Diagnostic Plots	56
III.2.2.1	Diagnostic Plots for Heterogeneity Diagnosis	56
III.2.2.1.1	Methodology	56
III.2.2.1.2	Results	57
III.2.2.2	Diagnostic Plots for Flow Dimension Diagnosis	59
III.2.2.2.1	Methodology	59
III.2.2.2.2	Results of the Flow Dimension Analysis	60
III.2.3	Determination of Hydraulic Parameters	62
III.2.3.1	Methodology	62
III.2.3.2	Sensitivity Analysis	63
III.2.3.3	Results of Hydraulic Parameter Calculations	64
III.2.4	Summary and Conclusions	69
III.2.4.1	Implications for the Conceptual Model of the BK Zone	69
III.2.4.2	Significance of the Calculated T and S Values	69

PART IV

ABSTRACT		75
IV.1	INTRODUCTION	76
IV.2	TEST HISTORY	77
IV.2.1	Test Objectives and Test Design	77
IV.2.2	Test Description	79
IV.3	ANALYSIS OF FLUID LOGGING TESTS	81
IV.3.1	Conceptual Model for Analysis	81
IV.3.2	Data Measured and Analysis Tools	84
IV.3.3	Test VE458, Borehole 85.007	86
IV.3.3.1	Qualitative Description and Analysis	86
IV.3.3.2	Quantitative Analysis	92
IV.3.4	Test VE459, Borehole 85.006	95
IV.3.4.1	Qualitative Description and Analysis	95

IV.3.4.2	Quantitative Analysis	99
IV.3.5	Test VE460, Borehole 88.017	104
IV.3.5.1	Qualitative Description and Analysis	104
IV.3.5.2	Quantitative Analysis	106
IV.3.6	Test VE461, Borehole 85.008	112
IV.3.6.1	Qualitative Description and Analysis	112
IV.3.6.2	Quantitative Analysis	117
IV.3.7	Test VE462, Borehole 85.005	120
IV.3.7.1	Qualitative Description and Analysis	120
IV.3.7.2	Quantitative Analysis	124
IV.3.8	Test VE463, Borehole 88.015	125
IV.3.8.1	Qualitative Description and Analysis	125
IV.3.8.2	Quantitative Analysis	129
IV.3.9	Test VE464, Borehole 85.009	135
IV.3.9.1	Qualitative Description and Analysis	135
IV.3.9.2	Quantitative Analysis	139
IV.4	ASSESSMENT OF THE COMPLEX DEVELOPMENT OF THE MEASURED CONDUCTIVITY LOGS	144
IV.4.1	Transient Flow Rate	144
IV.4.2	Transient Inflowing Concentration	144
IV.4.3	Measurement of Non-Radially Averaged Concentrations	147
IV.5	SUMMARY OF RESULTS, CONCLUSIONS, AND RECOMMENDATIONS	150

PART V

V.1	INTRODUCTION	157
V.2	BRIEF SUMMARY OF INFORMATION FROM PREVIOUS GEOLOGICAL, STRUCTURAL AND GEOPHYSICAL INVESTIGATIONS AT THE BK-SITE	158
V.3	SUMMARY OF HYDRAULIC AND FLUID LOGGING RESULTS WITH RESPECT TO BK FRACTURE-SYSTEM CHARACTERIZATION	160
V.3.1	Results from hydraulic testing	160
V.3.2	Results from the pilot crosshole fluid logging test	162
V.4	OPEN QUESTIONS AND RECOMMENDATIONS FOR FUTURE INVESTIGATIONS	165
REFERENCES		167
APPENDIX		171

LIST OF FIGURES

Figure II.1: Pressure response at flowing well following a rate change 13

Figure II.2: Diagnostic plots for the wellbore storage dominated (early-time) period 13

Figure II.3: Incomplete Gamma Function, with $\upsilon=\{1-n/2\}$, and $u=\{S_s r^2/4Kt\}$ (after BARKER, 1988) 13

Figure II.4: Conceptual flow models 14

Figure II.5: Diagnostic plots for integral flow dimensions, constant rate case 17

Figure II.6: Semi-log derivative diagnostics 17

Figure II.7: Diagnostics for boundary dominated period 19

Figure II.8: Schematic representation of variable flow rate history (after EARLOUGHER, 1977) 19

Figure II.9: Schematic of Horner method of analysis for pressure buildup data 21

Figure II.10: Transient rate response at the flowing well following a pressure change 21

Figure II.11: Diagnostic plots for integral flow dimensions, constant pressure case. 23

Figure II.12: Areal schematic of observation well pressure response after an active well rate change 24

Figure III.1: Plan view of the BK Test Site with the test boreholes shown (modified after Bräuer et al. 1989) 32

Figure III.2: Total depths and inclinations of boreholes in planes A, B, C, and D 33

Figure III.3: Log-Log plot diagnostic. 2^{nd} recovery, interval 85.004 i2 39

Figure III.4: HORNER plot for flow dimension = 2. 1^{st} and 2^{nd} recoveries, interval 85.004 i2 39

Figure III.5: Diagnostic semi-log derivative plot for flow dimension = 2. 1^{st} and 2^{nd} recoveries, interval 85.004 i2 41

Figure III.6: HORNER plot for flow dimension = 1. 1^{st} and 2^{nd} recoveries, interval 85.004 i2 41

Figure III.7: Diagnostic derivative plot for flow dimension = 1. Interval 85.004 i2 42

Figure III.8: Gradients between test interval (85.004 i2) and other intervals 44

Figure III.9: Test VE457. Radial flow diagnostic 47

Figure III.10: Test VE457. Diagnostic for bounded system 47

Figure III.11: Test VE457. Linear flow diagnostic 48

Figure III.12: GTFM simulation for test VE455 51

Figure III.13: GTFM simulation for test VE457 51

Figure III.14: Lamprophyre dykes in the BK area (from Bräuer et al. 1989) 53

Figure III.15: Best-fit transmissivities from the GTFM simulations. Tests VE451-457, borehole 85.004 54

Figure III.16: Responses in observation intervals during test VE455 58

Figure III.17: Responses in observation intervals during test VE455 58

Figure III.18: Responses in selected intervals during test VE457 61

Figure III.19: Selected semi-log derivative plots for dimensional analysis 61

Figure III.20: Head variations used in the sensitivity analysis 66

Figure III.21: Evaluation of the flux-normalized Theis approach 66

Figure III.22: Best-fit matches to the Theis curve. Test VE453 67

Figure III.23: Parameters obtained from the best fits to the Theis solution for all observation intervals 67

Figure III.24: Parameters obtained from best fits to the Theis solution. r is taken as straight line distance 68

Figure III.25: Parameters obtained from best fits to the Theis solution. r is a unit value 68

Figure III.26: Conceptual model of flow at the BK site 71

Figure IV.1: Time line showing when BK boreholes were open during the pilot fluid logging cross-hole test 80

Figure IV.2: Borehole conceptual model (after TSANG et al. 1990) 82

Figure IV.3: Conductivity and Temperature Logs 5,6,7,8,9, 10,11,12 and 13 Borehole 85.007, logging times 15,53,122,158,198,262,326,380 and 425 minutes after first borehole flushing 87

Figure IV.4: Conductivity logs 13 and 14, borehole 85.007 Logging times 425 and 1372 min after flushing 89

Figure IV.5: Conductivity and Temperature Logs 15,16,17,18 and 19, borehole 85.007, logging times 5,36,54,95 and 153 minutes after second borehole flushing 90

Figure IV.6: Inflow locations, borehole 85.007 91

Figure IV.7: Zero moments for fluid logging test VE458 borehole 85.007, logs 15,16,17,18 and 19 96

Figure IV.8: Interval flowrate as calculated by MOMENT, Test VE458, borehole 85.007, logs 15,16,17,18 and 19 96

Figure IV.9: Conductivity and Temperature logs 21,22,23,24 and 25 borehole 85.006, logging times - 1036,6, 27,63 and 123 minutes after borehole flushing 98

Figure IV.10: Inflow locations, borehole 85.006 100

Figure IV.11: Zero moments for fluid logging test VE459 logs 22,23,24 and 25, borehole 85.006 103

Figure IV.12: Interval flowrate as calculated by MOMENT test VE459, logs 22,23,24 and 25, borehole 85.006 103

Figure IV.13: Conductivity and temperature logs 26,27,28,29 and 30, borehole 88.017, logging times -84,7, 28, 47 and 108 minutes after first borehole flushing 105

Figure IV.14: Conductivity and temperature logs 31,32,33 and 34, Borehole 88.017, logging times 6,26,43 and 100 minutes after second borehole flushing 107

Figure IV.15: Conductivity logs 34 and 35, borehole 88.017 logging times 100 and 3490 minutes after second borehole flushing 108

Figure IV.16: Inflow locations, borehole 88.017 109

Figure IV.17: Zero moments for fluid logging test VE 460 borehole 88.017, logs 27,28,29 and 30 113

Figure IV.18: Interval flowrate as calculated by MOMENT test VE460, logs 27,28,29 and 30, borehole 88.017 113

Figure IV.19: Conductivity and temperature logs 36,37,38,39,40 and 41, borehole 85.008, logging times -73,9,30, 50,83 and 166 minutes after borehole flushing 114

Figure IV.20: Inflow locations, borehole 85.008 116

Figure IV.21: Zero moments for fluid logging test VE461 logs 37,38,39,20 and 41, borehole 85.008 119

Figure IV.22: Interval Flowrate as calculated by MOMENT test VE461, logs 37,38,39,40 ans 41, borehole 85.008 119

Figure IV.23: Conductivity and temperature logs 42,43,44,45, 46,47 and 48, borehole 85.005, logging times -64,8,22,38,68,149 and 226 minutes after borehole flushing 121

Figure IV.24: Inflow locations, borehole 85.005 123

Figure IV.25: Conductivity and temperature logs 51,52,53,54, 55,56 and 57, borehole 88.015, logging times -67,6,22,42,78,160 and 263 minutes after borehole flushing 126

Figure IV.26: Inflow locations, borehole 88.015 128

Figure IV.27: Zero moments for fluid logging test VE463 logs 52,53,54,55,56 and 57, borehole 88.015 131

Figure IV.28: Partial zero moments calculated by MOMENT, test VE463, logs 52,53,54,55,56 and 57, borehole 88.015 131

Figure IV.29: Borehole flowrates calculated by MOMENT logs 52,53,54,55,56 and 57, borehole 88.015 132

Figure IV.30: Interval flowrate as calculated by MOMENT test VE463, logs 52,53,54,55,56 and 57, borehole 88.015 132

Figure IV.31: Trial Bore simulation, test VE463, borehole 88.015, calibration to logs 52,53,54,55,56 and 57 measured 0.1, 0.37, 0.7, 1.3, 2.67 and 4.38 hours after borehole flushing 134

Figure IV.32: Conductivity and temperature logs 60,61,62,63, 64,65,66 and 67 borehole 85.009, logging times -70,6,25,44,77,118,181 and 278 minutes after borehole flushing 136

Figure IV.33: Inflow locations, borehole 85.009 138

Figure IV.34: Zero moments for fluid logging test VE464 borehole 85.009, logs 61,62,63,64,65,66 & 67 141

Figure IV.35: Interval flowrate as calculated by MOMENT, test VE464, borehole 85.009, logs 61,62,63, 64,65,66 & 67 141

Figure IV.36: Trial Bore simulation, test VE464, borehole 85.009 calibration to logs 61,62 and 63 measured 0.1, 0.42 and 0.73 hours after borehole flushing 143

Figure IV.37: Potential effect of transient inflowing concentration 146

Figure IV.38: Possible scenario for late time peaks 148

Figure V.1: Preliminary geologic model of the BK site. 159

Figure V.2: Three-dimensional views of the BK Site. 164

LIST OF TABLES

Table I.1:	Test overview in the BK-area (period 14.12.1989 -22.03.1990)	5
Table III.1:	Hydraulic test sequence and chronology	35
Table III.2:	Apparent depths of intervals and distances between	36
Table III.3:	Couple identifiers used in Figure III.8.	43
Table III.4:	Summary of diagnostic plot variables.	45
Table III.5:	Summary of diagnostic plot results.	49
Table III.6:	Summary of parameters which yielded the best fits during the numerical analysis	50
Table III.7:	Schematic representation of borehole 85.004	55
Table III.8:	Results of Sensitivity Analysis	63
Table III.9:	Transmissivities and storativities obtained from the best-fit matching procedure	65
Table IV.1:	Measurements of Conductivity and Flow Rate Measured at the Borehole 85.007 Wellhead During Logging	88
Table IV.2:	Comparison of Significant Permeability Zones as Determined by Fluid Logging and Bräuer, Borehole 85.007	92
Table IV.3:	Borehole Average Mass Flux and Inflowing Concentration, Borehole 85.007	94
Table IV.4:	Measurements of Conductivity and Flow Rate Measured at the Borehole 85.006 Wellhead During Logging	97
Table IV.5:	Comparison of Significant Permeability Zones as Determined by Fluid Logging, Lugeon Tests, and Bräuer, Borehole 85.006	101
Table IV.6:	Borehole Average Mass Flux and Inflowing Concentration, Borehole 85.006	102
Table IV.7:	Comparison of Significant Permeability Zones as Determined by Fluid Logging and Bräuer, Borehole 88.017	110
Table IV.8:	Borehole Average Mass Flux and Inflowing Concentration, Borehole 88.017	111

Table IV.9: Comparison of Significant Permeability Zones as Determined by Fluid Logging, Lugeon Tests, and Bräuer 117

Table IV.10: Borehole Average Mass Flux and Inflowing Concentration, Borehole 85.008 118

Table IV.11: Measurements of Conductivity and Flow Rate Measured at the Borehole 85.005 Wellhead During Logging 120

Table IV.12: Comparison of Significant Permeability Zones as Determined by Fluid Logging, Lugeon Tests, and Bräuer, Borehole 85.005 124

Table IV.13: Measurements of Conductivity and Flow Rate Measured at the Borehole 88.015 Wellhead During Logging 125

Table IV.14: Comparison of Significant Permeability Zones as Determined by Fluid Logging and Bräuer, Borehole 88.015 127

Table IV.15: Borehole Average Mass Flux and Inflowing Concentration, Borehole 88.015 129

Table IV.16: Calibrated Parameters Input to BORE for Test VE463 Calibration 135

Table IV.17: Measurements of Conductivity and Flow Rate Measured at the Borehole 85.009 Wellhead During Logging 137

Table IV.18: Comparison of Significant Permeability Zones as Determined by Fluid Logging, Lugeon Tests, and Bräuer, Borehole 85.009 139

Table IV.19: Borehole Average Mass Flux and Inflowing Concentration, Borehole 85.009 140

Table IV.20: Calibrated Parameters Input to BORE for Test VE464 Calibration 142

Table IV.21: Inflow Within Each Borehole having the Highest Inflowing Concentration 152

Table IV.22: Average Borehole Inflow Parameters 152

PART I

INTRODUCTION AND REPORT OVERVIEW

Stratis Vomvoris and Bernhard Frieg

I.1 Background and Scope

The determination of hydraulic properties in fractured rock as a basis for modeling possible nuclide migration from a deep underground repository is one of the key hydrogeological questions for site characterisation programs in such host formations. The Grimsel Test Site (GTS) offers a unique opportunity to investigate some of the relevant methodological and technical questions.

The Fracture System Flow Test (Bohrlochkranzversuch-BK) has focused on questions related to the hydrogeology of fractured rock at the scale of about 100 m. The underlying questions can be summarized as follows:

- What type of tests need to be performed to adequately characterize flow and mass transport in a segment of the fractured rock mass?

- What "tools", hardware or software, are required for the execution and interpretation of a test?

- How should information, such as structural geology, geological core analysis, geophysical imaging, be integrated with hydrogeology to form a consistent conceptual model?

- What should be an efficient exploration strategy to characterize fractured rock from an underground access drift?

The Federal Institute of Geoscience and Natural Resources (BGR) in Hannover, Federal Republic of Germany has been the principal investigator since 1985 at the BK-site focusing on most of the above mentioned questions. An overview of BGR's activities for Phase 1 and Phase 2 of GTS (1985-1990) and a list of the numerous publications can be found in NTB 91-01 (PAHL et al., 1992).

An overview of the GTS experiments up to Phase 2 (1990) can be found in LIEB (1988). Currently GTS has entered its Phase 3 program of an overall duration of 3 years (1991-1993). During the 3rd Phase Nagra has been able to allocate more effort and therefore, increase its participation in the joint programs at the GTS, among which the BK3.

The present report focuses on part of Nagra's activities as a preparation for the participation in the BK3 phase. A series of tests was proposed by Nagra and jointly carried out in the field with BGR. Additional field support was provided by the group for in-situ testing (UGIV) from COLENCO/INTERA; the geophysical aspects of the fluid logging tests were carried out by GEOTEST. BGR's cooperation and support in performing these tests is appreciated.

The proposed test design was built up on the experience previously accumulated by BGR and NAGRA, as documented in the various reports (e.g. KEUSEN et al., 1989; BRÄUER et al., 1989; PAHL et al., 1992) or discussed in various meetings. A conscious effort was made to introduce and test Nagra's approach for: a) type of test; b) test execution and documentation; and c) test interpretation.

The geometry of the BK-site is depicted in Figures III.1 and III.2. A total of 17 boreholes have been drilled from the BK cavern intersecting

a fracture zone with a NNE-SSW strike (Figure V.1). The majority of the boreholes lies in 4 parallel vertical planes as shown in the mentioned Figures. In the period between December 1989 and March 1990 a series of tests was performed as shown in Table I.1. Thematically the tests can be grouped in four categories: i) static pressure build-up; 2) single- and cross-hole hydraulic tests; 3) cross-hole fluid logging; and 4) long duration withdrawal test. The flexibility for program adjustment as new information was collected was part of the testing philosophy. With the pressure build-up observations and the series of seven cross-hole hydraulic tests data with respect to the connectivity of the system were successively collected. They formed the basis for the final design of the fluid logging tests.

In turn the fluid logging results in the seven inclined boreholes provided the basis for adjusting the packed-off intervals for the monitoring of the long-duration pumping test. During the fluid logging the following test design was adopted: constant saline tracer injection in a central borehole (85.004/Interval 2; Figures III.1 and III.2) and logging of fluid electrical conductivity and temperature in observation boreholes at successively larger distances.

I.2 Report Organisation

The form of this report as an edited volume was chosen to give credit to all persons involved at the particular subtasks; four relatively stand-alone parts are included as described below. The results cover the period up to the end of the fluid logging test (Table I.1). The references can be found in a separate section at the end of the report.

Part II (S. Mishra) presents the theoretical aspects for analyzing single- and multi-well hydraulic test data. The emphasis is on deriving simple diagnostic plots corresponding to variable pumping rates and different flow-dimensionalities.

Part III (D. Guyonnet and J.-M- Lavanchy) documents the hydraulic tests performed. It shows the heterogeneity and relative complexity of the site. In particular, the almost identical slow transient behavior of all intervals at late times and the rapid almost instantaneous reaction (independent of distance) of the connected intervals are characteristics of the system that deserve special attention and will be the focus of future tests.

Part IV (V. Kelley and S. Löw) describes a novel test performed for the first time within an Underground Laboratory. The pilot cross-hole fluid logging is a direct technique to investigate the connectivity of various domains of the system. There were technical challenges to overcome, as for example the inclined boreholes or the limited access space, as well as theoretical ones, as for example test design, actual "tracers" utilized (electrical conductivity and temperature). The results were very promising and the gained experience forms the basis for the design of a series of similar tests within the BK-Phase 3 program.

Part V (D. Guyonnet and V. Kelley) serves as a summary of the results and an outlook/set of recommendations for future tests. The emphasis has been placed on outlining components of the conceptual model that could

Table I.1: Test overview in the BK-area (period 14.12.1989 - 22.03.1990)

Test-Name	Date/Duration	Remarks	Reporting/Analysis
Static pressure build-up:			
VE 450	14.12.1989- 18.01.1990/35 days	Installation of packers and beginning of Recovery	KELLEY & FRIEG 1990
Single- and crosshole hydraulic tests:			
VE 451	18.01.1990 / 1.3 hrs	Constant head injection in interval 16.6 - 44.6 m (BK 85.004/i2)	Part III GUYONNET & LAVANCHY
VE 452	19.01.1990 / 6 hrs	Repetition of VE 451 with longer duration	Part III GUYONNET & LAVANCHY
VE 453	22.01.1990 / 2 hrs	Constant head injection in interval 1.9 - 14.9 m (BK 85.004/i1)	Part III GUYONNET & LAVANCHY
VE 454	23.01.1990 / 3 hrs	Constant head injection in interval 7.7 - 15.7 m (BK 85.004/i2)	Part III GUYONNET & LAVANCHY
VE 455	23.01.1990 / 1 hrs	Constant rate injection in interval 2 - 6 m (BK 85.004/i1)	Part III GUYONNET & LAVANCHY
VE 456	24.01.1990 / 1.5 hrs	Constant head injection in interval 16.7 - 28.7 m (BK 85.004/i2)	Part III GUYONNET & LAVANCHY
VE 457	25. - 26.01.1990 / 24 hrs	Constant head injection in interval 6.7 - 10.7 m (BK 85.004/i2)	KELLEY & FRIEG 1990
VE 457	26. - 29.01.1990 / 69 hrs	Recovery after hydraulic testing	
Crosshole fluid-logging:			
VE 457/458	29. - 31.01.1990	Temp./Cond.-logging in borehole BK 85.007 (15 runs)	Part IV KELLEY & LOEW
VE 458/459	31.01. - 01.02.1990	Temp./Cond.-logging in borehole BK 85.006 (6 runs)	Part IV KELLEY & LOEW
VE 459/460	02.02. - 05.02.1990	Temp./Cond.-logging in borehole BK 88.017 (10 runs)	Part IV KELLEY & LOEW
VE 461	05.02.1990	Temp./Cond.-logging in borehole BK 85.008 (6 runs)	Part IV KELLEY & LOEW
VE 462	06.02.1990	Temp./Cond.-logging in borehole BK 85.005 (7 runs)	Part IV KELLEY & LOEW
VE 462	06. - 07.02.1990	Temp./Cond.-logging in borehole BK 88.015 (9 runs)	Part IV KELLEY & LOEW
VE 463	07. - 08.02.1990	Temp./Cond.-logging in borehole BK 85.009 (10 runs)	Part IV KELLEY & LOEW
VE 464/465	08.02. - 07.03.1990 27 days	Recovery after fluid-logging and pressure build-up	KELLEY & FRIEG 1990
Long duration withdrawal test:			
VE 465/466	07.03. - 22.03.1990 15 days	Constant rate withdrawal test in borehole BK 85.004 (i2/6.7 - 10.7 m)	KELLEY & FRIEG 1990

be investigated with additional tests rather than perform a complete in-depth synthesis of all available information.

If the data and methods presented in this report are further used for the development of in-situ characterisation programs the editors believe that the objectives of performing these tests in Grimsel will have been successfully accomplished.

PART II

METHODS FOR ANALYZING SINGLE- AND MULTI-WELL HYDRAULIC TEST DATA

Srikanta Mishra

ABSTRACT

Methods for analyzing single and multi-well hydraulic test data are outlined. Diagnostic plots for selecting the appropriate equivalent continuum flow model (and identifying wellbore and boundary conditions) are described. Interpretive equations for estimating hydraulic parameters are presented.

II.1 INTRODUCTION

II.1.1 Basic Background

Transient pressure and/or rate testing is a commonly used technique for estimating the hydraulic characteristics of permeable rock bodies. Typically, the system is stressed at a borehole by perturbing the pressure or the flow rate, and the response of the system (i.e., pressure or rate change) is measured at the same well and/or adjacent well(s). Analysis of such an input-output experiment then yields the hydraulic properties of the formation.

The classical assumption invoked in hydraulic test analysis is that of 2-dimensional converging (diverging) radial flow to (from) a well from (to) an aquifer. This is a reasonable assumption whenever the aquifer can be represented as an equivalent continuum - as is the case with most sedimentary formations. However, the situation is much more complicated when hydraulic testing of fractured rock masses is considered. Such systems typically consist of a network of discrete and permeable fractures embedded in a relatively impermeable matrix. Even though an equivalent continuum representation might be applicable for describing the hydraulic test response, the corresponding flow dimension need not be restricted to the familiar 2-D case. In fact, the system response may appear to mimic that of equivalent 1-, 2-, 3- or even non-integral dimensional flow geometries, depending on: (a) connectivity of the fracture network, (b) location of the well(s) in the network, (c) volume of rock influenced by the applied hydraulic stress, etc. Thus, the observed 'dimensionality' of flow in a fracture network is a complex function of the tested volume, test duration, and the geometry of the fracture network (ALMEN et al., 1986; BARKER, 1988).

Further complications in test interpretation arise due to inner and outer boundary effects. At the inner boundary, i.e., at the active well, wellbore storage can cause significant attenuation of the early-time pressure response. The near-wellbore pressure profile might also be altered due to the presence of a 'skin' zone. The late-time pressure response is influenced by outer boundary effects such as 'leaky' faults, no-flow boundaries, and constant pressure boundaries. It is thus necessary to isolate the middle-time (system) pressure response from early-time (inner boundary) and late-time (outer boundary) effects in order to accurately estimate desired hydraulic characteristics.

II.1.2 Interpretation Philosophy

Interpretation of hydraulic test data involves two main aspects: (i) selection of an appropriate well-aquifer flow model, and (ii) estimation of the corresponding model parameters. A judicious methodology for selecting an equivalent continuum flow system model is an important first step in our work, in view of the complex hydraulic responses which characterize fractured rock masses.

The nature of the flow system is diagnosed by examining pressure (or rate) vs. time graphs, or variations thereof, for characteristic traces that signify a particular flow configuration. Once the flow model is selected, its parameters can then be obtained in a variety of ways. Common approaches for this purpose include: (i) log-log type-curve matching, (ii) specialized graphical analysis with simple interpretive equations, and (iii) automated parameter estimation via linear or nonlinear regression techniques.

II.1.3 Pressure Derivative Analysis

Historically, the primary diagnostic tool for flow model selection in hydraulic test interpretation has been the pressure vs. time graph, plotted either in log-log, semi-log or cartesian formats (EARLOUGHER, 1977; GRINGARTEN, 1982). Recent developments in petroleum reservoir testing suggest that a graph of the rate of pressure change (pressure derivative) vs. time provides more information than the simple pressure-time graph (BOURDET et al., 1983). In particular, the derivative graph has been shown to enhance trends and characteristics in the pressure response signal that are only weakly apparent from an examination of the pressure-time data.

Although several possibilities exist for forming the derivative group, the measure of choice in this work is the semi-log derivative, i.e., the rate of pressure change with respect to the natural logarithm of time. This is essentially the slope of a graph of pressure vs. log time. As will be shown subsequently, the semi-log derivative response for a homogeneous infinite-acting radial flow system is constant with respect to time. Thus, an examination of the semi-log derivative graph can indicate the degree to which the equivalent continuum response for a given hydraulic test is similar to that of 2-D radial flow.

II.1.4 Scope and Objectives

In the following sections, we provide the theoretical basis for the interpretation of single- and multi-well hydraulic test data. The primary emphasis is on describing how diagnostic plots (pressure/rate vs. time and semi-log derivative vs. time graphs) can be used for flow model selection. A secondary aspect is the use of simple interpretive equations for estimating hydraulic properties, e.g., hydraulic conductivity (transmissivity) and/or specific storage (storativity). We begin by documenting various methods for analyzing single-well tests. The constant rate flow test is used as the basic test sequence to demonstrate the various techniques. These methods are then extended for variable

rate/pressure testing, constant head testing and pressure recovery analysis. Subsequently, we discuss the interpretation of multi-well hydraulic test data for constant rate and constant head conditions at the active well. Finally, we present some general observations regarding the application of the interpretation methodology presented in this section to single- and multi-well test data obtained from the hydraulic test campaign conducted at the BK site during the period from December 1989 to March 1990, and described in greater detail by GUYONNET & LAVANCHY (this volume).

II.2 SINGLE-WELL TEST ANALYSIS

II.2.1 Introduction

In single-well tests, the pressure or the rate response of the system is measured at the borehole where the hydraulic stress is imposed (Fig. II.1). Thus, the tested volume of rock is localized to some region around the well itself. For a constant rate flow test, the pressure response will typically exhibit three regimes: (i) an early-time period, influenced by borehole storage and/or skin effects, (ii) a middle-time period, characterized by the response of the system itself, and (iii) a late-time period, affected by boundaries. Typical characteristics of each of these regimes is discussed next.

II.2.2 Early-time (Borehole Dominated) Response

During a constant rate flow test, the fluid withdrawn at the surface initially comes from the packed-off interval in the borehole, rather than from the formation. Pressure data from this early-time period therefore contain no information about the formation proper. The early-time pressure response can be described by (EARLOUGHER, 1977):

$$C\ dh_w/dt = q \quad \Rightarrow \quad \Delta h_w = \{q/C\}\ \Delta t \qquad (II.1)$$

where q is the surface withdrawal rate [L^3/T], h_w is the wellbore pressure head [L], and C is the wellbore storage coefficient [L^3/L]. Eq. (II.1) also applies for injection testing, when all of the fluid injected at the surface essentially goes to compress the wellbore fluid at early times. Now, taking the logarithm of both sides of (II.1), and rearranging, one obtains:

$$\log(\Delta h_w) = \log(q/C) + \log(\Delta t) \qquad (II.2)$$

Thus, a log-log graph of the change in head, Δh_w, vs. elapsed time, Δt, during the wellbore storage dominated period will yield a line of unit slope. A cartesian graph of Δh_w vs. Δt will also yield a straight line but with slope {q/C}, from which the wellbore storage coefficient, C, can be estimated if the surface rate, q, is known. These diagnostics are indicated in Fig. II.2.

The semi-log derivative of Eq. (II.1) is given by:

$$\Delta h_w' = d(\Delta h_w)/d(\ln \Delta t) = \{q/C\}\ \Delta t \qquad (II.3)$$

which has exactly the same form as (II.1). Thus, the diagnostic plots for Δh_w and $\Delta h_w'$ should overlie each other and also exhibit the same characteristics (i.e., unit-slope line in a log-log plot, and straight line in a cartesian plot).

Wellbore storage being the initial perturbation to affect the pressure response, the first diagnostic plot should be a log-log plot of Δh_w or $\Delta h_w'$ vs. Δt to check for a line of unit slope.

II.2.3 Middle-time (System Dominated) Response

The propagation of pressure pulses in a porous and permeable continuum is a diffusional process, and hence can be expressed as:

$$\{S_s/K\}\ \delta h/\delta t = 1/r^{n-1}\ \delta/\delta r\ \{r^{n-1}\ \delta h/\delta r\} \qquad (II.4)$$

where S_s is specific storage [1/L], K is hydraulic conductivity [L/T], h is pressure head [L], r is radius [L], t is time [T], and n is the flow dimension. Note that the above equation is valid for all positive and non-zero values of n, and is not restricted to the familiar integral values of n=1 (linear), n=2 (radial), and n=3 (spherical) flow geometries (BARKER, 1988) as shown schematically in Fig. II.4. Solution of (II.4) requires specifying the initial condition, an inner boundary condition, and an outer boundary condition. In the simplest case, the initial condition is taken to be one of stabilization:

$$h(r,0) = h_i \qquad (II.5)$$

where h_i is assumed to be the uniform initial pressure head in the system [L]. Similarly, the outer boundary condition is assumed to represent undisturbed conditions, viz.:

$$h(\infty,t) = h_i \qquad (II.6)$$

at an infinite distance from the borehole. At the inner boundary, the constant surface flow rate can be related to the local pressure gradient via a generalized version of Darcy's law:

$$q = Kb^{3-n}\alpha_n r_w^{n-1}\ \{\delta h/\delta r\}_{rw} \qquad (II.7)$$

where b denotes the extent of the flow region [L], α_n is the area of a unit sphere in n dimensions [L^2], r_w is the radius of the borehole [L], and q is the constant rate of flow from the well [L^3/T]. If the well is assumed to be a line source (i.e., with a vanishingly small wellbore radius), then Eq. (II.4)-(II.7) can be solved to yield the following closed-form expression for the drawdown at the well (BARKER, 1988):

$$\Delta h_w(t) = \{q r_w^{2\nu}/4\pi^{1-\nu}Kb^{3-n}\}\ \Gamma(-\nu,u) \qquad (II.8)$$

where $\Delta h_w=\{h_i-h(r_w)\}$, $\nu=\{1-n/2\}$, $u=\{S_s r^2/4Kt\}=\{1/4t_D\}$ with t_D being the classical definition of dimensionless time (EARLOUGHER, 1977), and $\Gamma(a,x)$ is the complementary incomplete Gamma function shown in Fig. II.3.

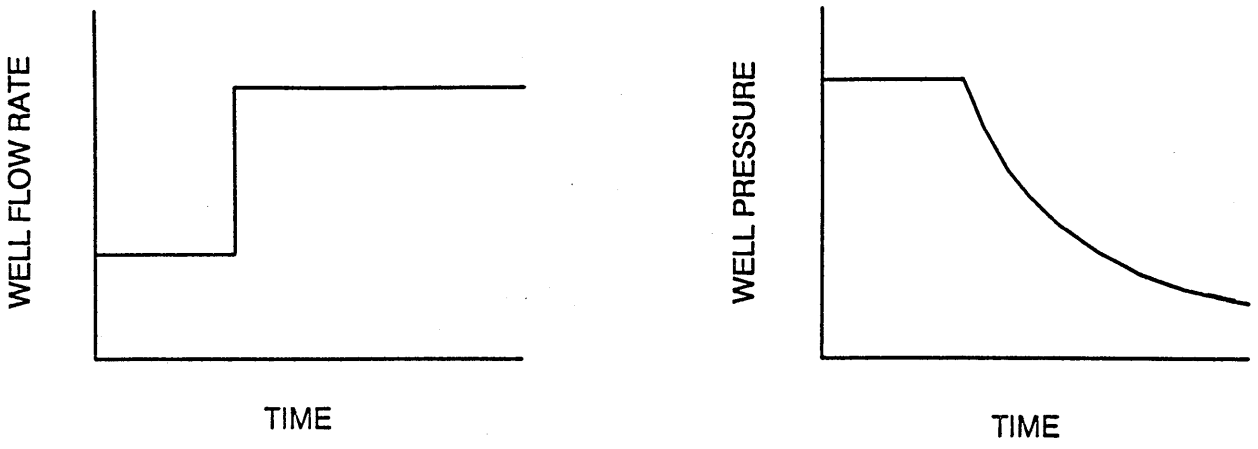

Fig. II.1: Pressure response at flowing well following a rate change

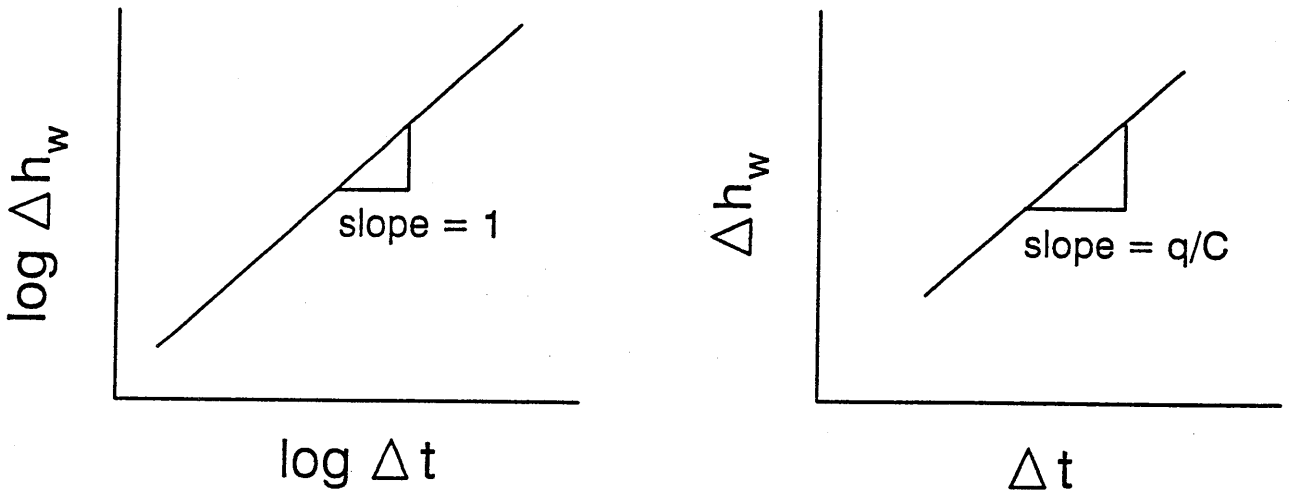

Fig. II.2: Diagnostic plots for the wellbore storage dominated (early-time) period

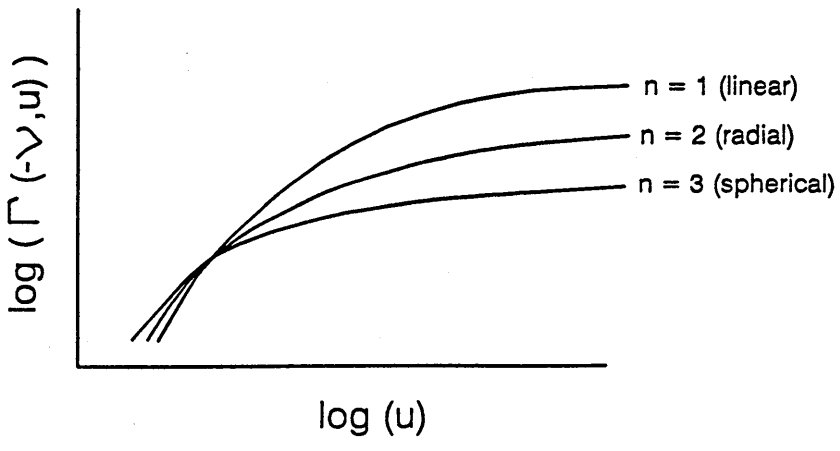

Fig. II.3: Incomplete Gamma Function, with $\upsilon=\{1-n/2\}$, and $u=\{s_s r^2/4Kt\}$ (after BARKER, 1988)

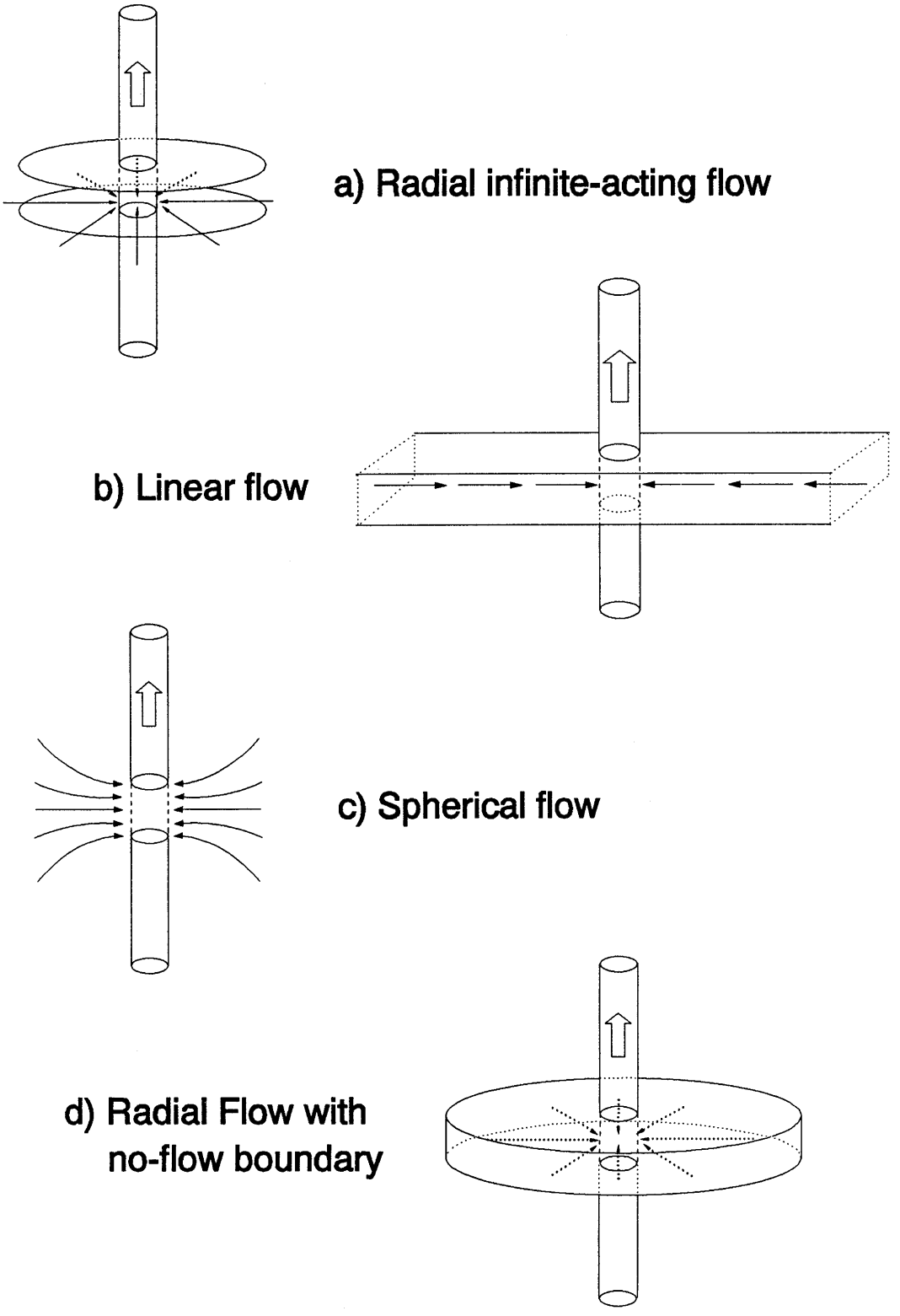

Fig. II.4: Conceptual flow models

Using special cases of the Gamma function corresponding to the integral dimensions (BARKER, 1988), we obtain the following:

$$\Delta h_w(t) = \{qr_w/2\sqrt{\pi Kb^2}\}\ \{1/\sqrt{u}\} \quad \underline{n=1} \tag{II.9a}$$

$$\Delta h_w(t) = \{q/4\pi Kb\}\ Ei(-u) \quad \underline{n=2} \tag{II.9b}$$

$$\Delta h_w(t) = \{q/4\pi Kr_w\}\ erfc(\sqrt{u}) \quad \underline{n=3} \tag{II.9c}$$

where $Ei(\cdot)$ denotes the exponential integral, and $erfc(\cdot)$ is the complementary error function. Note that as expected, Eq. (II.9b) yields the familiar THEIS (1935) solution for 2-D radial flow. Further simplifications of the above expressions are possible by taking the long-time approximations of (II.9), viz.:

$$\Delta h_w(t) = \{q/b^2\}\ \{t/\pi KS_s\}^{0.5} \quad \underline{n=1} \tag{II.10a}$$

$$\Delta h_w(t) = \{q/4\pi Kb\}\ \ln(2.25Kt/S_s r_w^2) \quad \underline{n=2} \tag{II.10b}$$

$$\Delta h_w(t) = \{q/4\pi Kr_w\}\ [1 - \{S_s r_w^2/\pi Kt\}^{0.5}] \quad \underline{n=3} \tag{II.10c}$$

Eq. (II.10b) may be recognized as the familiar COOPER-JACOB (1946) approximation of the Theis equation for the 2-D radial flow case. An examination of (II.10) also suggests the following rules for pressure response in different flow geometries:

(i) For the linear flow case (n=1), a <u>log-log</u> graph of Δh_w vs. t should form a straight line with slope 0.5. Further, a <u>cartesian</u> graph of Δh_w vs. $\sqrt{t}$ should also form a straight line with slope inversely proportional to the $\{KS_s\}$ product (Fig. II.5a).

(ii) For the radial flow case (n=2), a <u>semi-log</u> graph of Δh_w vs. ln(t) should form a straight line whose slope is inversely proportional to K (Fig. II.5b).

(iii) For the spherical flow case (n=3), a <u>cartesian</u> graph of Δh_w vs. $1/\sqrt{t}$ should form a straight line whose intercept is inversely proportional to K, and slope related to $\{S_s/K\}$ (Fig. II.5c).

Generalizations of such rules to non-integral flow dimensions is best achieved by examining the semi-log derivative response. Note that the derivative of the Gamma function is given by:

$$\delta\Gamma(a,x)/\delta x = -\ x^{a-1}\ e^{-x} \tag{II.11}$$

Thus, for $a=-\nu=\{n/2-1\}$, and $x=u=\{S_s r_w^2/4Kt\}$, and n being the flow dimension, we obtain after some manipulations:

$$\delta(\Delta h_w)/\delta(\ln t) = \{q/4\pi^{n/2}K^{n/2}S_s^{1-n/2}b^{3-n}\} \cdot \exp(-S_s r_w^2/4Kt) \cdot t^{1-n/2} \tag{II.12}$$

Since the exponential term in (II.12) quickly attains the value of unity (for $x \leq 0.01$), one can then take the logarithm of both sides to obtain the following relationship:

$$\log\{\delta(\Delta h_w)/\delta(\ln t)\} = \log(C_1) + \{1-n/2\}\log(t) \tag{II.13}$$

where C_1 is equal to the first term in braces of the right-hand side of (II.12). Eq. (II.13) suggests that a log-log graph of the semi-log derivative vs. time should yield a straight line with slope equal to {1-n/2}, where n is the flow dimension (Fig. II.6). Thus:

n = 0	=>	slope = 1	(wellbore storage)
n = 1	=>	slope = 0.5	(linear flow)
n = 2	=>	slope = 0	(radial flow)
n = 3	=>	slope = -0.5	(spherical flow)

This forms the basis for identifying the flow dimension by examining the semi-log derivative response. Once this step is accomplished, the hydraulic properties, K and S_s, can be determined by using (II.10) for the integral dimensions, or by using an asymptotic form of (II.8) for the non-integral dimensions (BARKER, 1988):

$$\Delta h_w(t) = \{q/4\pi^{1-\nu}Kb^{3-n}\nu\} \; [\{4Kt/S_s\}^{\nu} - \Gamma(1-\nu)r_w^{2\nu}] \qquad (II.14)$$

with ν={1-n/2}. Note that this equation also suggests the power-law scaling of the pressure-time response, previously obtained by examining the derivative behaviour (Eq. II.12).

II.2.4 Late-time (Boundary Dominated) Response

We distinguish between two types of conditions at the outer boundary which affect the late-time pressure response: (i) a constant pressure boundary, and (ii) a no-flow boundary. In the constant pressure case, the system will attain steady-state at late times, with the pressure response given by $\Delta h_w = C_2$, where C_2 is a constant which includes the hydraulic conductivity, the cross-sectional area open to flow, and other terms which depend on the dimensionality of flow. Thus, all graphs of Δh_w vs. t will approach a stabilization level at late time, with the semi-log derivative, $\Delta h_w'$ approaching zero.

For the no-flow outer boundary case, the wellbore response is:

$$\Delta h_w = C_3 \, t \qquad (II.15)$$

where C_3 is a constant which includes the compressibility and the pore volume of the tested formation, and other terms which depend on the geometry of the tested volume. Thus, a log-log graph of Δh_w vs. t will form a unit-slope line, and a cartesian graph of the same data would form a straight line with slope C_2. As in the case of the borehole storage dominated (early-time) data, the semi-log derivative group will show the same characteristics as the pressure graph because of the linear dependence on time. These diagnostics are shown in Fig. II.7.

II.2.5 Analysis of Variable Rate/Pressure Test Data

Practical reasons often cause rate fluctuations during a constant rate test, or wellbore head variations during a constant head test. Such problems render the straightforward application of the theory presented above difficult. However, a simple application of the principle of superposition provides a methodology for interpreting well test data

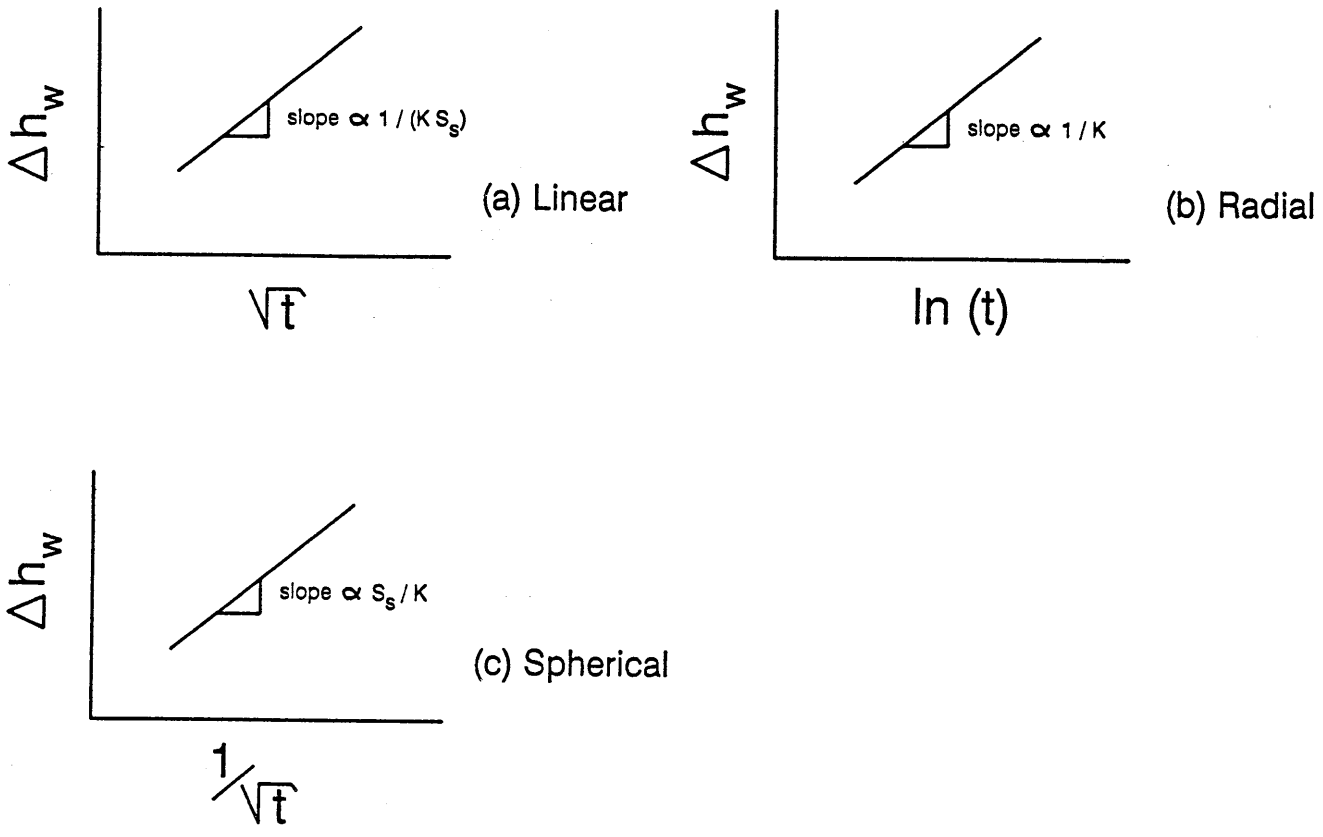

Fig. II.5: Diagnostic plots for integral flow dimensions, constant rate case

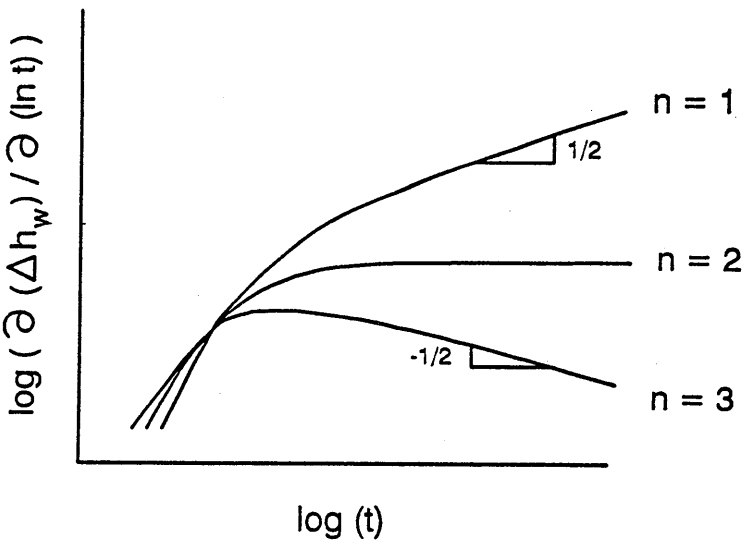

Fig. II.6: Semi-log derivative diagnostics

when both flow rate and wellbore pressure head change with time. Details of the methodology may be found in EARLOUGHER (1977) and STRELTSOVA (1988). Here, we present only some basic interpretive equations and techniques.

Consider a variable flow rate history, discretized into j=1,2,..,N-1,N periods of approximately constant rates as shown in Fig. II.8. Assuming that no inner and outer boundary effects are active, and that the long-time expressions given in (II.10) are valid, one can write:

$$\Delta h_w/q_N = [1/b^2\sqrt{\{\pi K S_s\}}] \Sigma \{q_j-q_{j-1}\}/q_N \sqrt{\{t-t_{j-1}\}} \quad \text{(II.16a)}$$

$$\Delta h_w/q_N = \{1/4\pi Kb\} \Sigma \{q_j-q_{j-1}\}/q_N \ln(t-t_{j-1}) + b_1 \quad \text{(II.16b)}$$

$$\Delta h_w/q_N = \{S_s^{0.5}/4(\pi K)^{1.5}\} \Sigma\{q_j-q_{j-1}\}/\sqrt{\{t-t_{j-1}\}} + b_2 \quad \text{(II.16c)}$$

for n=1 (linear), n=2 (radial), and n=3 (spherical) flow geometries, respectively. In the above, the constants b_1 and b_2 include formation and wellbore parameters. Eq. (II.16) suggests that analysis of variable rate/pressure test data should be based on <u>cartesian</u> graphs of $\Delta h_w/q_N$ vs. the appropriate summation term in the right-hand side (depending on the flow dimension). Such a graph should yield a straight line, the slope of which is related to K and/or S_s.

For non-integral dimensions, it is easily shown (from Eq. II.14) that the appropriate summation term, $G_n(t)$, is:

$$G_n(t) = \Sigma \{q_j-q_{j-1}\}/q_N \{t-t_{j-1}\}^{1-n/2} \quad \text{(II.17)}$$

where n is the flow dimension. Note, however, that because of the particular form of (II.17), the determination of the flow dimension for variable rate/pressure tests is a trial and error process. Cartesian graphs of $\Delta h_w/q_N$ vs. $G_n(t)$ should be prepared for various values of n and then tested for linearity. The value of n which corresponds to the highest degree of linearity between $\Delta h_w/q_N$ and $G_n(t)$ should then be chosen as the <u>first</u> guess for the flow dimension, and should thereafter be verified independently.

II.2.6 <u>Pressure Buildup Analysis</u>

Consider a well flowing at a constant rate for a period of t_p, subsequent to which it is shut-in, with the shut-in time being denoted by Δt. The pressure buildup response can then be generated by superimposing the effects of a well flowing at rate q for time $(t_p+\Delta t)$ and a well flowing at rate -q for Δt. In symbolic notation, we write:

$$\Delta h_{ws}(\Delta t) = \{h_i-h_{ws}(\Delta t)\} = \Delta h_w(t_p+\Delta t) - \Delta h_w(\Delta t) \quad \text{(II.18)}$$

where h_{ws} is the shut-in pressure head, and Δh_w is the flowing pressure head. For the familiar case of 2-D radial flow, the flowing pressure is given by Eq. (II.10b), the substitution of which in (II.18) gives:

$$\Delta h_{ws}(\Delta t) = \{q/4\pi Kb\} \{\ln(\{t_p+\Delta t\}/\Delta t)+\ln(2.25K/S_s r_w^2)\} \quad \text{(II.19)}$$

Thus, a semi-log graph of h_{ws} vs. $\ln(\{t_p+\Delta t\}/\Delta t)$ should produce a

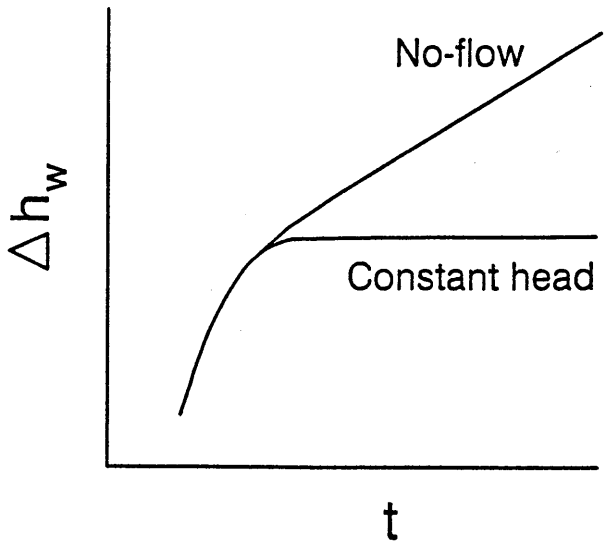

Fig. II.7: Diagnostics for boundary dominated period

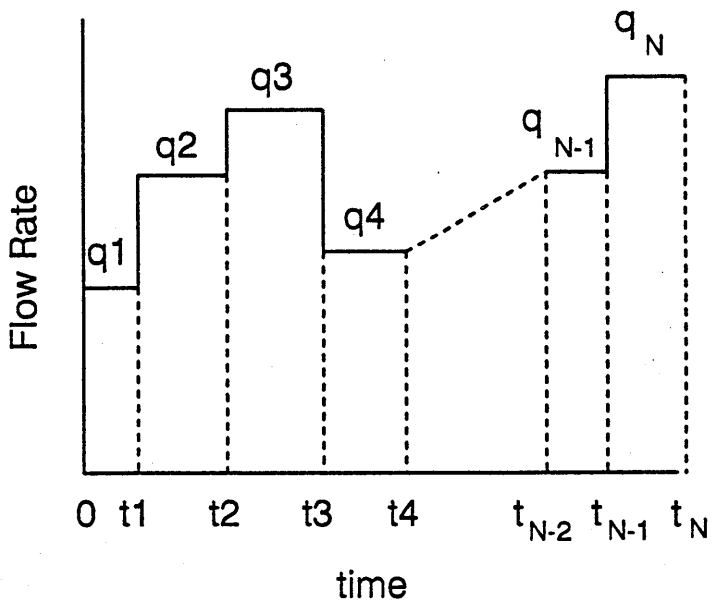

Fig. II.8: Schematic representation of variable flow rate history (after EARLOUGHER, 1977)

straight line with slope inversely proportional to K, and intercept equal to h_i. This method of buildup analysis, as depicted in Fig. II.9, was proposed independently by THEIS (1935) in the groundwater hydrology literature, and by HORNER (1951) in the petroleum engineering literature. It is generally referred to as the Horner method of analysis in view of the widespread use of pressure buildup testing for petroleum reservoir characterization.

In order to extend Horner's methodology to non-radial flow dimensions, we note that after an early time period, the pressure response scales as $t^{1-n/2}$ where n is the flow dimension (Eq. II.14). Hence we can write:

$$\Delta h_{ws} = C_4 \left[\{t_p+\Delta t\}^{\nu} - \{\Delta t\}^{\nu}\right] \qquad \text{(II.20)}$$

where $\nu=\{1-n/2\}$, and C_4 is a constant incorporating wellbore and formation parameters. Typically, C_4 involves a combination of K and S_s, thus precluding the independent determination of these two parameters in the absence of additional information. Note that as in the case of variable rate testing, the determination of the flow dimension from buildup data requires graphing h_{ws} vs. the time group shown in the right hand side of (II.20) for various values of n, and testing for linearity. The pressure derivative can also be effectively used in determining whether the pressure data exhibit linear trends or not (i.e., whether the derivative is constant or not).

The effects of wellbore storage on buildup data are essentially similar to that for the flowing period - provided the flow period lasts sufficiently beyond the end of wellbore storage. If the well was shut-in while wellbore storage effects were still active, the buildup data will yield no information about the formation proper (RAGHAVAN, 1980). Thus the importance of properly designing the durations of flow and shut-in periods prior to conducting a flow-recovery test sequence cannot be overemphasized.

II.2.7 Constant Head (Pressure) Testing

An alternative to the classical constant rate test is the case where a constant pressure (head) change is imposed at the well, and the subsequent change in the well flow rate is monitored as a function of time (Fig. II.10). One advantage of such testing is that wellbore storage effects can be effectively eliminated, thereby extending the data window containing the formation response. Note however that wellbore storage does affect any recovery period following a constant head flow period.

The theory presented in Section II.2.3 for the constant rate case can be easily extended to develop diagnostic methods and interpretive equations for analyzing constant head test data. Thus, we have:

$$\Delta H/q(t) = 1/[A/\{KS_s\}/\sqrt{\{\pi t\}}] \quad \underline{n=1} \qquad \text{(II.21a)}$$

$$\Delta H/q(t) = \{1/4\pi Kb\}\ [\ln(t)+\ln(2.25K/S_s r_w^2)] \quad \underline{n=2} \qquad \text{(II.21b)}$$

$$\Delta H/q(t) = 1/[1+\{S_s r_w^2/\pi Kt\}^{0.5}] \quad \underline{n=3} \qquad \text{(II.21c)}$$

for linear, radial and spherical flow, respectively, where ΔH is the

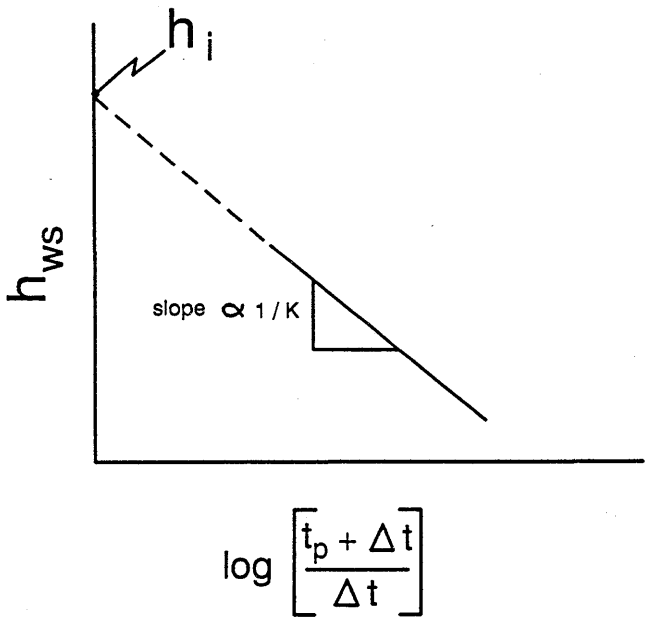

Fig. II.9: Schematic of Horner method of analysis for pressure buildup data

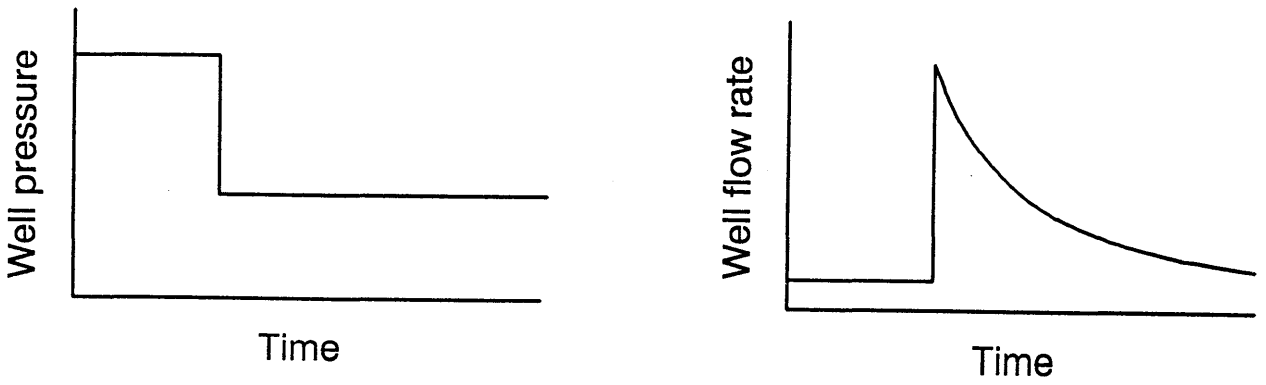

Fig. II.10: Transient rate response at the flowing well following a pressure change

constant head maintained at the well, and other terms are as described previously. Note that (II.21b) is the familiar JACOB-LOHMAN (1952) solution for the 2-D radial flow case.

Eq. (II.21) suggests that if the constant head is normalized with respect to the time-varying flow rate, then the time-dependent response $\{\Delta H/q(t)\}$ is similar to that for the constant rate case. Linear flow (n=1) shows a square-root of time dependence, radial flow (n=2) is indicated by a log-time dependence, while spherical flow (n=3) implies an inverse square-root of time dependence at early-time and constancy at late times, as shown schematically in Fig. II.11. Note that the corresponding quantity for the constant rate case is the time-varying head normalized by the constant rate, $\Delta h_w(t)/q$, as given in Eq. II.10. Thus, the diagnostic plots used for identifying the flow dimension in the constant rate case can be extrapolated to the constant head case, by appropriately modifying the time-dependent variable of interest from $\{\Delta h_w(t)/q\}$ to $\{\Delta H/q(t)\}$.

II.3 MULTI-WELL TEST ANALYSIS

II.3.1 Introduction

In multi-well testing (also referred to as cross-hole or interference testing), a constant rate or a constant pressure condition is imposed at the primary borehole or the active well and the pressure response is measured at one or more observation wells. Such a test, shown schematically in Fig. II.12, facilitates the determination of hydraulic properties at the inter-well scale. In this section, we briefly discuss the extension of single-well test analysis methods to multi-well tests.

II.3.2 Borehole Storage Effects

As in the case of single-well tests, the early-time pressure behaviour at the observation well is affected by borehole storage, which causes an attenuation of the pressure response. JARGON (1976) and OGBE & BRIGHAM (1989) have discussed the pressure response at the observation well during 2-D radial flow when wellbore storage effects are present at the active well and/or the observation well. Results from these studies suggest that the time beyond which wellbore storage effects can be neglected is proportional to $\{C/K\}$, where C is wellbore storage coefficient and K is hydraulic conductivity. This time is only weakly affected by specific storage (S_s), and the inter-well distance (r). Similar results have also been derived by MISHRA (unpublished memo, 1991) for constant pressure conditions at the active well.

II.3.3 Constant Rate Interference Testing

If a constant rate inner boundary condition is imposed at the active well, the observation well response for a system with any arbitrary flow dimension follows directly from the theory of BARKER (1988), presented previously in Section II.2.3.

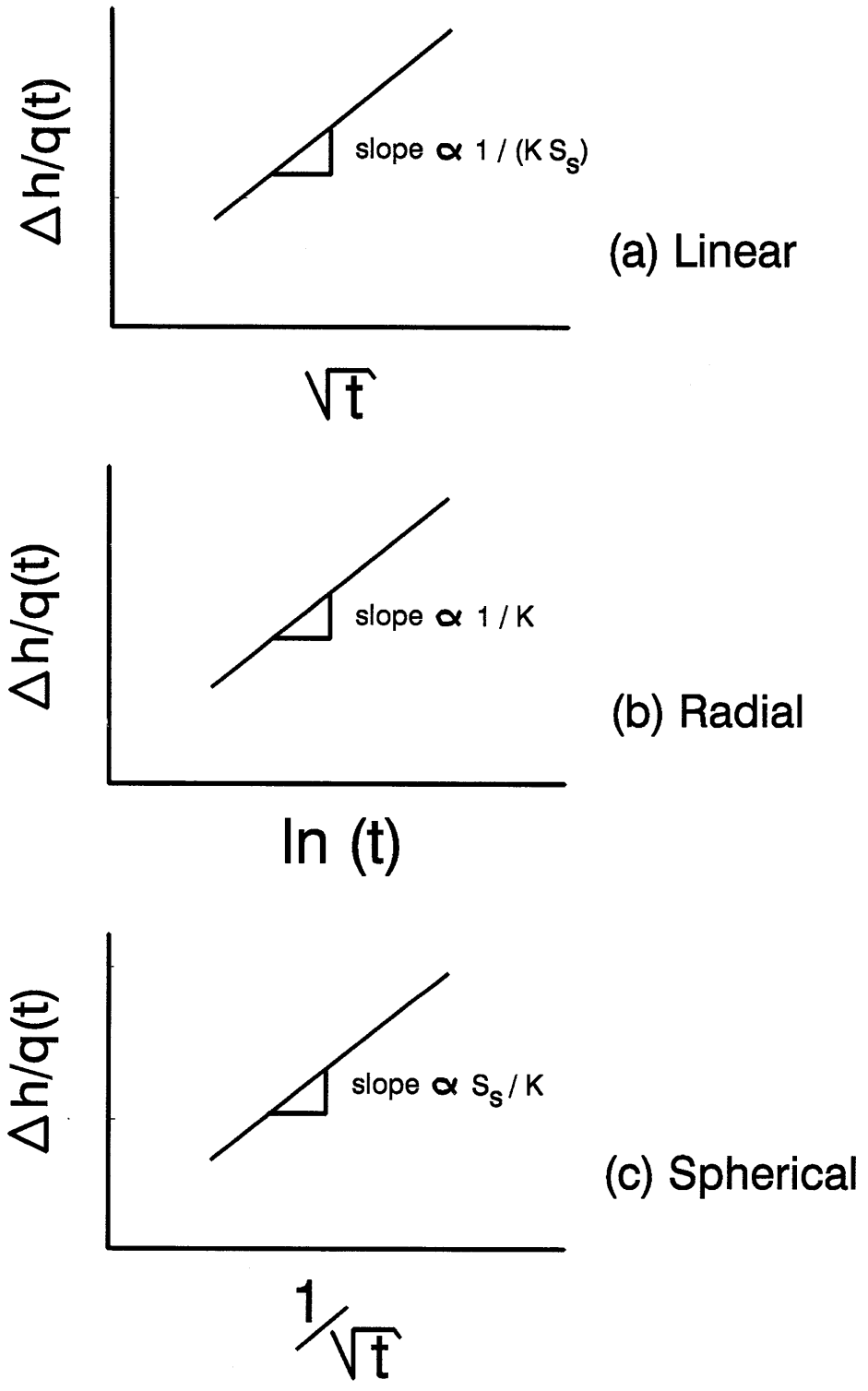

Fig. II.11: Diagnostic plots for integral flow dimensions, constant pressure case.

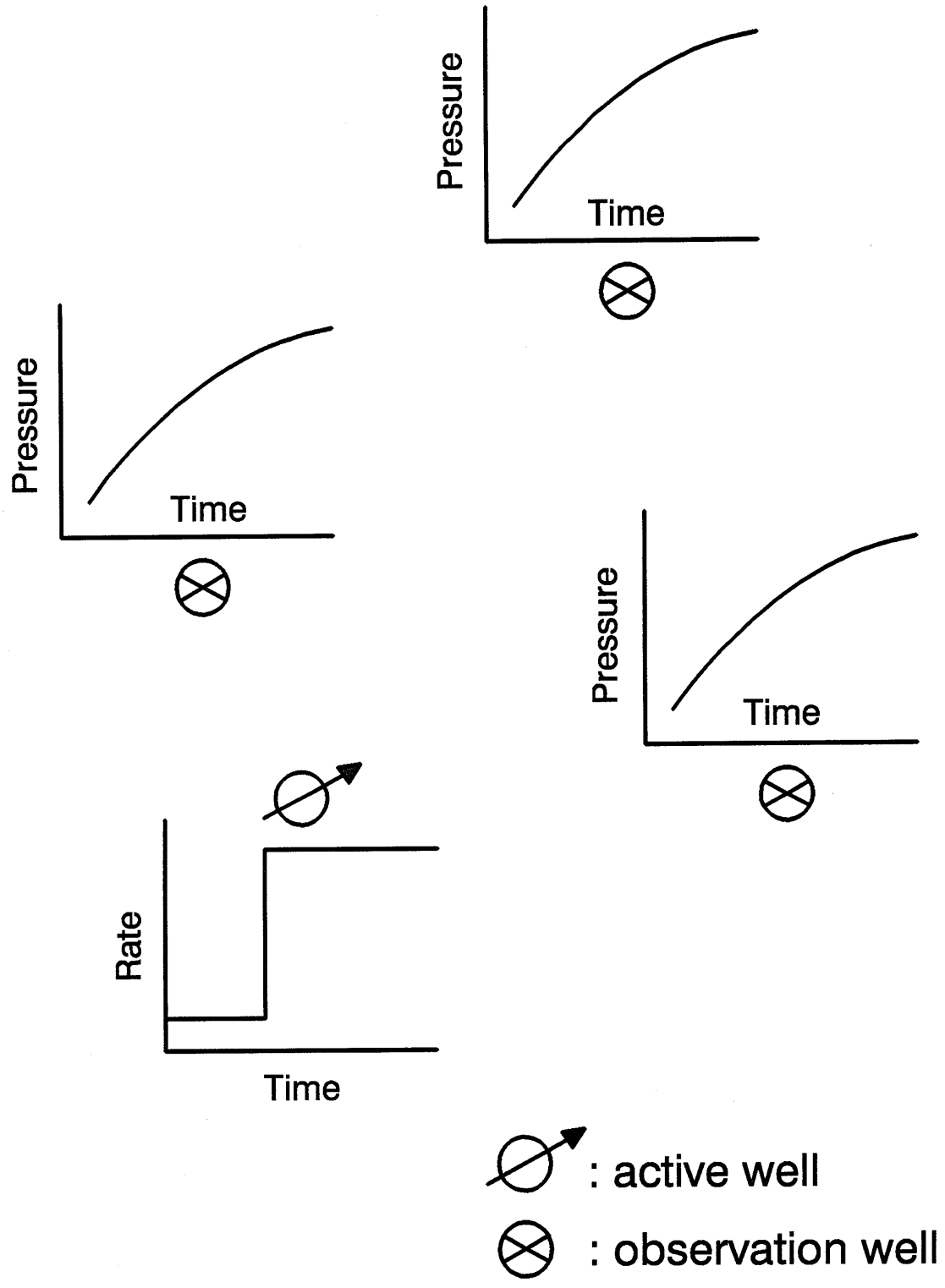

Fig. II.12: Areal schematic of observation well pressure response after an active well rate change.

Thus:

$$\Delta h(r,t) = \{qr^{2\nu}/4\pi^{1-\nu}Kb^{3-n}\}\ \Gamma(-\nu,u) \qquad (II.22)$$

where $\Delta h=\{h_i-h(r,t)\}$, $u=\{S_s r^2/4Kt\}$, $\nu=\{1-n/2\}$, r the inter-well distance, and other terms are as defined previously. Special forms of the above equation for the integral dimension cases can be easily obtained by substituting r for r_w in (II.9) and (II.10). These equations also provide the basic interpretive tools for parameter estimation.

Identification of the flow dimension involves log-log type-curve matching of the observation well data with Fig. II.3. An alternative approach, as discussed in Section II.2.3, requires the use of pressure derivatives. The semi-log derivative of Eq. (II.22) is given by:

$$\delta(\Delta h)/\delta(\ln t) = [q/\{4\pi K\}^{n/2}S_s^{1-n/2}b^{3-n}] \cdot \exp(-S_s r^2/4Kt) \cdot t^{1-n/2} \qquad (II.23)$$

The exponential term in (II.23) can be replaced by unity (to within 1%) whenever $\{S_s r^2/4Kt\}<0.01$, leading to the simple relationship:

$$\log[\delta(\Delta h)/\delta(\ln t)] \sim \{1-n/2\}\ \log(t) \qquad (II.24)$$

This suggests that a log-log graph of the semi-log derivative vs. time should form a straight line whose slope is related to the flow dimension. Note however that the condition under which the exponential term in (II.23) attains unity is easier to be satisfied for smaller values of r, other parameters being equal. Thus, only late-time data from the observation well pressure response will be amenable to the technique proposed via (II.24). This does not limit the practical utility of the derivative approach, since the early-time data are likely to be affected by borehole storage in any case.

An examination of the arguments of the Gamma function in Eq. (II.22), i.e., $\nu=\{1-n/2\}$ and $u=\{S_s r^2/4Kt\}$, suggests that for a given homogeneous system (i.e., uniform K and S_s) having a constant flow dimension, the pressure response will scale as $\{t/r^2\}$. Thus, the agreement (or deviation) between pressure data from different observation wells, when presented in a log-log graph of $\Delta h(r,t)$ (or $\Delta h/q$) vs. $\{t/r^2\}$, will indicate the homogeneity of the system with respect to S_s, K and/or n. Such a graph, with $\{t/r^2\}$ as the independent variable, is thus a more general diagnostic tool for comparing the pressure response from several observation intervals. Graphs which use either t or r^2 as the independent variable make implicit assumptions regarding the homogeneity of the system and/or the flow dimension, and are thus more restricted in their application.

II.3.4 Constant Pressure Interference Testing

When the active well is maintained at a constant pressure during cross-hole testing, it is useful to normalize the pressure change at the observation well, $\Delta h(r,t)$, with the time-varying flow rate at the active well, $q(r_w,t)$. Recall that the equivalent variable for the constant rate case is $\Delta h(r,t)/q(r_w)$. URAIET & RAGHAVAN (1980) and MISHRA & GUYONNET (1992) have shown that the constant pressure interference test

response for 2-D radial flow can be described via:

$$\Delta h(r,t)/q(r_w,t)|_{CH} \approx \Delta h(r,t)/q(r_w)|_{CR} = \{1/4\pi Kb\}\ Ei(-u) \qquad (II.25)$$

where $u=\{S_s r^2/4Kt\}$, CH denotes the constant head (pressure) case and CR denotes the constant rate case. This suggests that the active well flux normalized observation well pressure change can be matched to the familiar THEIS (1935) exponential integral solution in order to estimate hydraulic parameters.

Although not shown here, it can be demonstrated that similar equivalence between the constant head and the constant rate interference test solutions exist for other integral flow dimensions (e.g., linear and spherical). Eq. (II.21) may thus be generalized for integral and non-integral flow dimensions as follows:

$$\Delta h(r,t)/q(r_w,t) \approx \{r^{2\nu}/4\pi^{1-n}Kb^{3-n}\}\ \Gamma(-\nu,u) \qquad (II.26)$$

Asymptotic forms of (II.26), similar to those presented in (II.10) can then be used for estimating hydraulic properties. Furthermore, the flow dimension can be estimated by using a log-log graph of the semi-log pressure derivative vs. time, as suggested in Eq. (II.24):

$$\log[\delta(\Delta h(r,t)/q(r_w,t))/\delta(\ln t)] \sim \{1-n/2\}\ \log(t) \qquad (II.27)$$

As pointed out previously for the constant rate case, the arguments of the Gamma function suggest using $\{t/r^2\}$ as the independent variable in graphing observation well response from several wells. This would allow a more comprehensive evaluation of the degree of homogeneity existing in the tested flow system with respect to K, S_s and/or n.

II.4 CONCLUDING REMARKS

In this section, we have presented the basic theory for interpreting single- and multi-well hydraulic test data. The fundamental assumption underlying this presentation is that the tested formation behaves as a porous and permeable continuum. Fractured rock bodies may not always be amenable to an equivalent porous medium description with the classical 2-D radial flow geometry. Hence, there is a pragmatic need to make no a priori assumption regarding the equivalent dimensionality of flow when interpreting hydraulic test data from complex fractured systems.

The use of pressure derivatives for diagnostic purposes, widely used in petroleum reservoir testing, is described. We have shown how the derivative may be used for identifying the flow dimension, both for single-well and cross-hole test interpretation.
The equivalence between constant rate and constant pressure solutions is highlighted in an attempt to unify hydraulic test analysis procedures. The use of the flux normalized head change ($\Delta h/q$) as the dependent variable for test interpretation is recommended. It is shown that similar time-dependent responses result if the data are presented in terms of $\{\Delta h(t)/q(r_w)\}$ in the constant rate case, and as $\{\Delta H(r_w)/q(t)\}$ in the constant head case, for single-well tests - with $\Delta h(r,t)$ being used for multi-well tests. Furthermore, the use of $\{t/r^2\}$ as the independent variable in analyzing multi-well tests is recommended in order

to identify heterogeneous trends in a qualitative manner.

In summary, several classical techniques and their variations have been described for analyzing hydraulic tests in fractured media. A pragmatic approach, which combines the use of diagnostic plots for flow model selection, followed by the use of appropriate interpretive equations for parameter estimation, is recommended.

PART III

ANALYSIS OF SINGLE- AND CROSS-HOLE TESTS AT THE BK-SITE, GRIMSEL TEST SITE

Dominique Guyonnet and Jean-Marc Lavanchy

ABSTRACT

The analysis presented below attempts to apply the methodology described in MISHRA (1992, this volume) to a number of pressure-recovery and constant-head injection tests which were performed in the fractured crystalline rock of the BK-area at the Grimsel Test Site. Results clearly show that the flow system at this site is not homogeneous and 2-D radial. Diagnostic plots and numerical simulations for the single-hole analysis show evidence of hydraulic boundaries which affect the pressure responses observed during the recovery period and in the injection intervals. The geometry of the flow system is seen to change from radial or sub-radial at early times to linear or bounded at late times due most probably to the presence of lamprophyre dykes which act as low-permeability boundaries. Analysis of the observation intervals (cross-hole analysis) reveals the presence of a high transmissivity feature, the location of which is in good agreement with existing geological information. The single- and cross-hole analysis are successful in providing estimates of transmissivities for all monitored intervals (which range between 7.7E-07 and 3.6E-05 m^2/s) and of undisturbed hydraulic head for one interval (which lies between 1920 and 2078 m). However, little confidence can be assigned to estimates of storativity due to severe uncertainty relative to the true migration path of the pressure-pulse.

III.1 SINGLE-HOLE TEST ANALYSIS

III.1.1 INTRODUCTION

III.1.1.1 Site description

From the 14th of December 1989 to the 22nd of March 1990, NAGRA and the Bundesanstalt für Geowissenschaft und Rohstoffe (BGR) performed a number of hydraulic tests at the BK-site in the NAGRA Grimsel underground laboratory in central Switzerland. These tests are part of an investigation program which aims at localizing and characterizing the major hydraulic features in the BK-area. The design and fielding of the tests was performed by the COLENCO/INTERA group for in-situ testing (UGIV) and is described in LÖW & LAVANCHY (1990) and LAVANCHY (1990).

The Grimsel underground laboratory is situated in granitic to granodioritic fractured rock. Details concerning fracture and foliation orientation can be found in KEUSEN et al. (1989) and BRÄUER et al. (1989).

A schematic representation of the BK site is shown in Figure III.1. The majority of the boreholes are situated within four vertical planes which strike N-311° and are designated by the letters A, B, C and D (Figure III.2). Each plane includes three to four boreholes which radiate from the drift and deepen towards the N-W. The altitude of the drift is approximately 1730 m while the elevation of the rock surface above the site is approximately 2180 m.

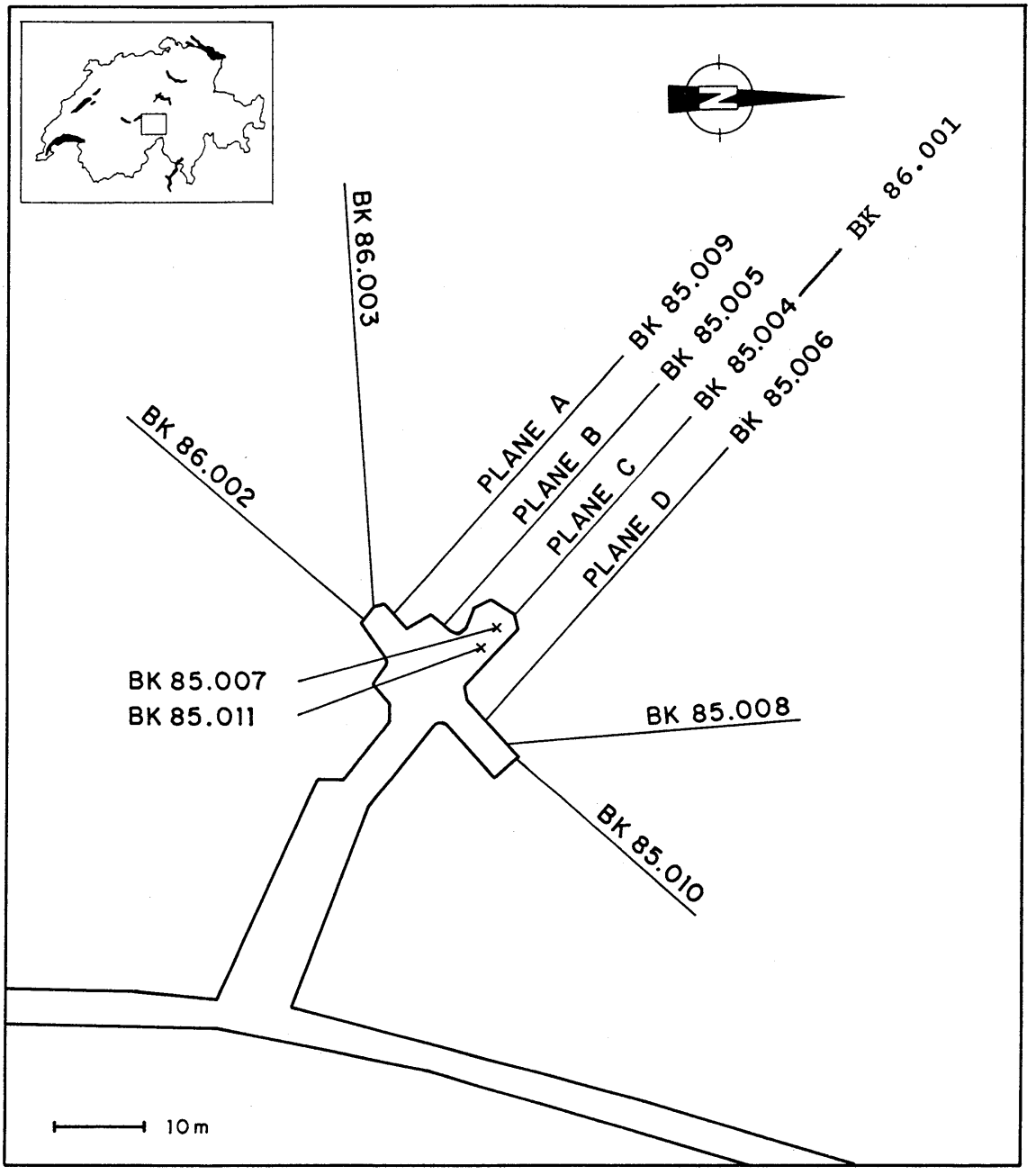

Figure III.1: Plan view of the BK Test Site with the test boreholes shown.
(modified after Bräuer et al. 1989)

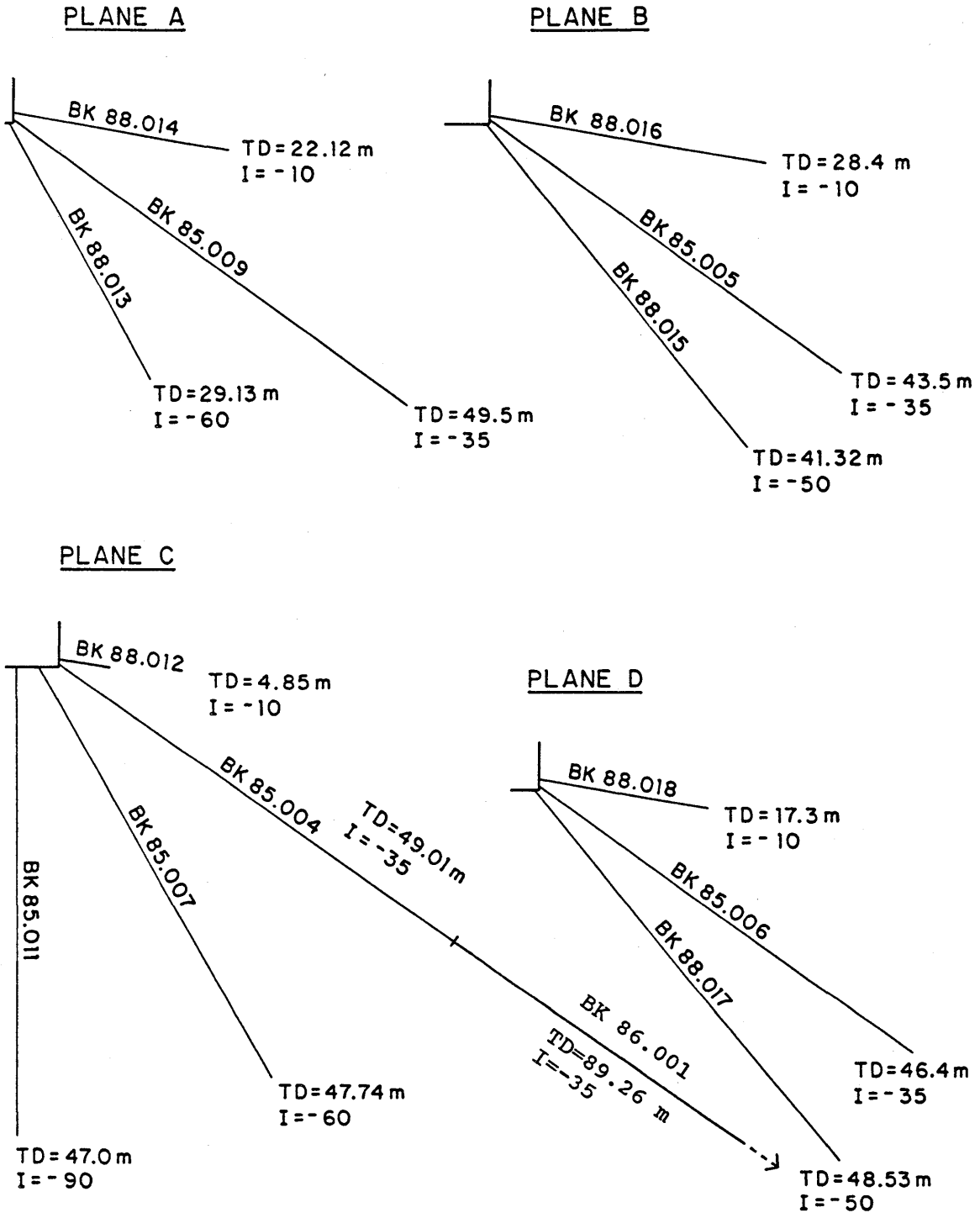

Figure III.2: Total depths and inclinations of boreholes in planes A, B, C, and D

The nature of the hydraulic tests and the sequence of events are summarized in Table III.1. As seen in this table, the tests started by a pressure-recovery which was followed by 7 constant-head injection tests (VE 451 through VE 457). At the outset of these injection tests, a fluid logging campaign was performed (KELLEY & LÖW 1992, this volume). This campaign was followed by a second pressure-recovery test and a constant-rate withdrawal test (VE 465) completed the hydraulic testing campaign.

All injection tests were performed at various depths in borehole 85.004. From one test to another, the apparent depth of the injection interval in 85.004 varied but the observation intervals remained the same. The apparent depths of the injection intervals and the distances between the injection interval and the observation intervals during each test are presented in Table III.2. The injection interval in borehole 85.004 during each test is indicated in Table III.2 by a distance to the injection interval equal to 0.

III.1.1.2 Scope and objectives of the analysis

The tests which are analyzed below are part of the NAGRA effort to understand flow within the fractured crystalline rock of the Grimsel underground laboratory. The specific objectives of the present analysis are:

- to improve the conceptual understanding of flow at the BK-site.
- to provide estimates of hydraulic parameters i.e. hydraulic head, transmissivity and storativity.
- to detect and analyze hydraulic boundaries.

This analysis attempts to apply the methodology of interpretation presented in MISHRA (1992, this volume). Rather than make an assumption concerning the flow model and carry out the interpretation based on this model, the hydraulic data are first analyzed to provide insight into which model is truly applicable to the problem at hand. Once the relevant model is identified, it is used to estimate the hydraulic parameters of interest. This approach differs conceptually with the one most commonly adopted, where the familiar radial flow system is assumed and the hydraulic data are analyzed accordingly.

The report is divided into two parts. Section III.1 presents the analysis of the pressure recoveries and the pressure responses in the injection intervals (single-hole analysis), while Section III.2 addresses the interpretation of the pressure responses in the observation intervals (cross-hole analysis).

Table III.1: Hydraulic test sequence and chronology

DATE	TIME	EVENT
14.12.89		Completion of Packer installation and beginning of 1st recovery
18.1.90	10:00	Start VE 451 injection (interval 85.004 i2)
18.1.90	11:15	End VE 451 injection
19.1.90	8:00	Start VE 452 injection (interval 85.004 i2)
19.1.90	14:00	End VE 452 injection
22.1.90	9:00	Start VE 453 injection (interval 85.004 i1)
22.1.90	11:00	End VE 453 injection
23.1.90	8:30	Start VE 454 injection (interval 85.004 i2)
23.1.90	11:30	End VE 454 injection
23.1.90	14:40	Start VE 455 injection (interval 85.004 i1)
23.1.90	15:40	End VE 455 injection
24.1.90	14:35	Start VE 456 injection (interval 85.004 i2)
24.1.90	16:05	End VE 456 injection
25.1.90	15:00	Start VE 457 injection (interval 85.004 i2)
26.1.90	15:00	End VE 457 injection
08.02.90	08:00	Start 2nd recovery
07.03.90	10:45	End of 2nd recovery
07.03.90	10:52	Start VE 465 pumping
22.03.90	11:00	End VE 465 pumping

Table III.2: Apparent depths of intervals and distances between injection interval and observation intervals (see also LAVANCHY 1990)

Interval Name	Interval apparent depth (m)		Distance between injection interval and observation intervals (m)					
	(valid for all tests except the 2nd recovery)							
			Test:	451	453	454	455	456	457
	from	to		+452					
85005 i1	1.80	14.80		27.91	7.88	10.31	6.09	20.27	8.08
85005 i2	15.80	28.80		14.56	10.82	8.29	14.67	8.08	10.57
85005 i3	29.80	36.80		6.46	20.86	17.73	25.10	8.29	20.57
85005 i4	36.80	45.00		8.09	28.22	25.00	32.53	14.58	27.92
85006 i1	2.00	11.00		33.80	13.30	16.06	10.12	26.19	13.54
85006 i2	12.00	19.00		25.15	8.13	9.37	8.42	17.83	8.19
85006 i3	21.00	27.00		17.29	10.50	8.71	13.78	10.90	10.30
85006 i4	28.00	45.00		8.45	20.92	17.91	25.04	9.42	20.64
85007	2.00	48.00		15.17	17.60	15.35	21.04	12.07	17.38
85008	1.00	49.00		31.54	24.96	24.82	25.82	27.38	24.93
85009	3.00	49.00		16.06	15.31	13.25	18.63	11.69	15.11
85010	1.00	43.00		46.26	34.37	35.52	33.30	41.06	34.47
85011	2.00	45.00		29.71	21.91	21.85	22.75	25.03	21.89
88013	3.50	29.00		28.16	15.95	16.50	16.28	22.10	15.98
88014	11.00	22.00		25.10	10.30	11.03	10.93	18.18	10.33
88015 i1	3.00	14.00		29.46	10.76	12.85	9.15	22.07	10.92
88015 i2	15.00	41.00		19.52	20.34	18.62	23.18	16.73	20.17
88016	7.00	28.00		21.05	7.06	6.78	9.43	13.79	6.97
88017 i1	2.00	11.00		34.78	14.95	17.55	12.05	27.31	15.18
88017 i2	12.00	21.30		27.91	14.18	14.98	14.26	21.45	14.22
88017 i3	22.00	49.00		22.91	26.56	24.83	29.30	21.82	26.39
88018	3.00	17.00		30.75	9.27	12.30	5.70	22.95	9.53
	(valid for 1st recovery, VE 451, VE 452, VE 453)								
85004 i1	1.90	14.90		22.20	0.00				
85004 i2	16.60	44.60		0.00	22.20				
			(valid for VE 454, VE 455)						
85004 i1	2.00	6.00				7.70	0.00		
85004 i2	7.70	15.70				0.00	7.70		
			(valid for VE 456)						
85004 i1	1.90	14.90						14.30	
85004 i2	16.70	28.70						0.00	
	(valid for VE 457 and 2nd recovery)								
85004 i1	2.00	5.00							5.20
85004 i2	6.70	10.70							0.00

III.1.2 BOREHOLE HISTORY PRIOR TO TESTING

The majority of the boreholes of interest were drilled in 1985 while the remainder was drilled in 1988 (see Table III.2). Since the time they were drilled until the time the packers were installed for testing on December 14th 1989, the boreholes were open most of the time and in communication with the drift. The pressure distribution in the vicinity of the boreholes can therefore be expected to be somewhat disturbed.

III.1.3 ANALYSIS OF THE PRESSURE RECOVERIES

III.1.3.1 Method of analysis

The pressure recovery in borehole 85.004 interval i2 is analyzed following the method presented in HORNER (1951) and outlined in MISHRA (1992, this volume). The method is used to estimate the undisturbed equilibrium pressure. The Horner method utilizes the principle of superposition to estimate the pressure in the borehole during the shut-in period. For a flow dimension n = 2 we have:

$$P_{ws}(\Delta t) = P_i - (Q / 4\Pi T) * \ln ((t_p + \Delta t)/\Delta t) \qquad (III.1)$$

where:
$P_{ws}(\Delta t)$ is the pressure in the borehole during the shut-in period
P_i is the undisturbed equilibrium pressure
Q is the flow rate during the open-hole period
T is transmissivity
t_p is the flow period duration (open hole)
Δt is the elapsed time since shut-in

It follows that a plot of P_{ws} versus $\ln((t_p +\Delta t)/\Delta t)$ has a slope of $Q / 4\Pi T$ and that the point where $\ln((t_p +\Delta t)/\Delta t)$ is equal to 0 is such that $P_{ws} = P_i$. Such a plot is commonly called a Horner plot.

If the available pressure data do not go to the point where $\ln ((t_p +\Delta t)/\Delta t) = 0$, the pressure curve must be extrapolated to that point. This assumes that the Horner plot displays a constant slope at late time. This assumption should be verified using the derivative of the pressure P_{ws} with respect to $\ln((t_p +\Delta t)/\Delta t)$: $\partial P_{ws} / \partial \ln((t_p +\Delta t)/\Delta t)$ should be constant at late times for extrapolation of P_i on the Horner plot.

As stated above, Equation III.1 is valid in the case of radial flow. If the flow dimension is not equal to 2 then a modified Horner plot must be used based on the following equation (see MISHRA 1992, this volume):

$$P_{ws}(\Delta t) = P_i - C * ((t_p + \Delta t)^{(1-n/2)} - \Delta t^{(1-n/2)}) \qquad (III.2)$$

where C is a constant which is a function of Q, T and the system geometry, n is the flow dimension and all other variables are as in Equation III.1.

The analysis procedure is identical to the radial flow case with the difference that the variable along the x-axis of the modified Horner plot is now $((t_p + \Delta t)^{(1-n/2)} - \Delta t^{(1-n/2)})$. As previously, extrapolation of the undisturbed pressure on the modified Horner plot should be done after the assumption of a constant slope at late times has been verified using a plot of the derivative. From Equation III.2 it follows that the relevant derivative is $\partial P_{ws} / \partial ((t_p + \Delta t)^{(1-n/2)} - \Delta t^{(1-n/2)})$.

III.1.3.2 Results of the Horner analysis

Borehole 85.004 was selected for the Horner analysis because it was the

injection borehole during the active hydraulic tests. The results of the analysis of the pressure data from both the 1st and the 2nd recovery periods in borehole 85.004 interval 2 are presented below. Note that interval 2 does not cover the same apparent depths during both recoveries (see Table III.2): during the 1st recovery interval 2 went from 16.6 to 44.6 m whereas during the 2nd recovery, it went from 6.7 to 10.7 m.

It should also be noted that the analysis of the 1st recovery period suffers from incompleteness of the data set: due to problems related to packer deflation during the 1st recovery, the data acquisition system was interrupted for periods of 10 to 22 days depending on the monitored interval (LAVANCHY, 1990). The data from the 2nd recovery was not affected by such interruptions and its analysis can be considered more reliable.

Prior to the Horner analysis, a plot of pressure versus time on a log-log scale was drawn to identify the duration of the wellbore storage dominated period (MISHRA, 1992 this volume). On a log-log plot this period is characterized by a slope of 1. Such information is of importance to any hydraulic analysis since data which fall within this period will be entirely controlled by the borehole conditions (storage, compressibility) and therefore will not yield any information concerning the actual formation parameters. Figure III.3 shows a log-log plot of the pressure response during the 2nd recovery. A linear best-fit to the data revealed a slope of 0.6 which suggests that this data is not dominated by wellbore storage. However, both the linearity and the slope of the pressure data suggest that the flow system has a dimension of 1 (linear flow). As was shown by MISHRA (1992 this volume), in the case of linear flow, a log-log plot of the pressure data should yield a slope of 0.5. The pressure response during the 1st recovery in 85.004 i2 showed a slope of 0.57 at late times on a log-log plot and provides further indication of non-radial flow in the vicinity of this borehole at late times.

Horner plots of the pressure response in borehole 85.004 interval 2 during both recovery periods are shown in Figure III.4 assuming a Horner time ratio valid for a flow dimension of 2. For the calculation of the Horner time ratio $(t_p+\Delta t)/\Delta t$, the flow period duration t_p was chosen as equal to 6 months. Plots were also constructed taking t_p = 6 years but the results were identical because in both cases t_p is very large compared with Δt. It should be noted that the very long duration of the open-hole period will affect the accuracy of the undisturbed hydraulic head determination since extrapolation must be performed over

a very long period. Also, extrapolation over such a long time interval assumes that conditions remain identical during this time and do not account for potential boundary effects.

From the Horner plots in Figure III.4 one could be tempted to extrapolate a value of the undisturbed head situated around 1840 m in the case of the 1st recovery and 1860 m in the case of the 2nd recovery. However the plot of the derivatives (Figure III.5) clearly shows that the derivative is constantly increasing even at late times. Therefore the

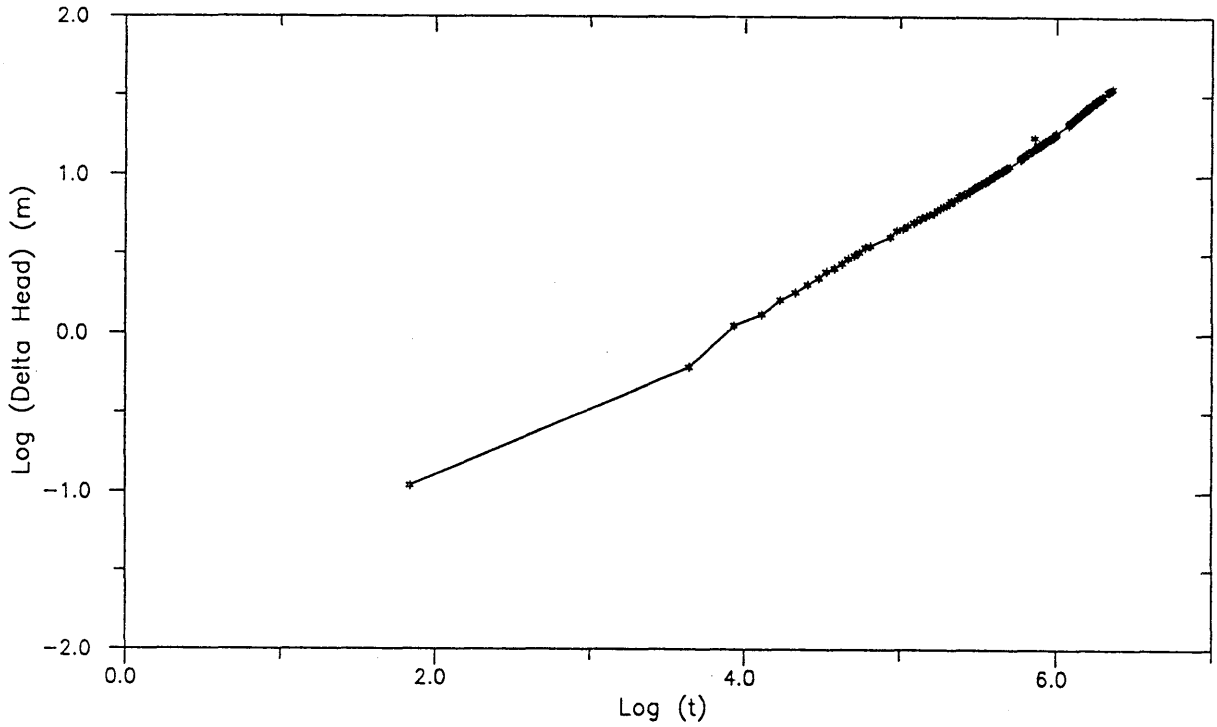

Figure III.3: Log-Log plot diagnostic. 2nd recovery, interval 85.004 i2

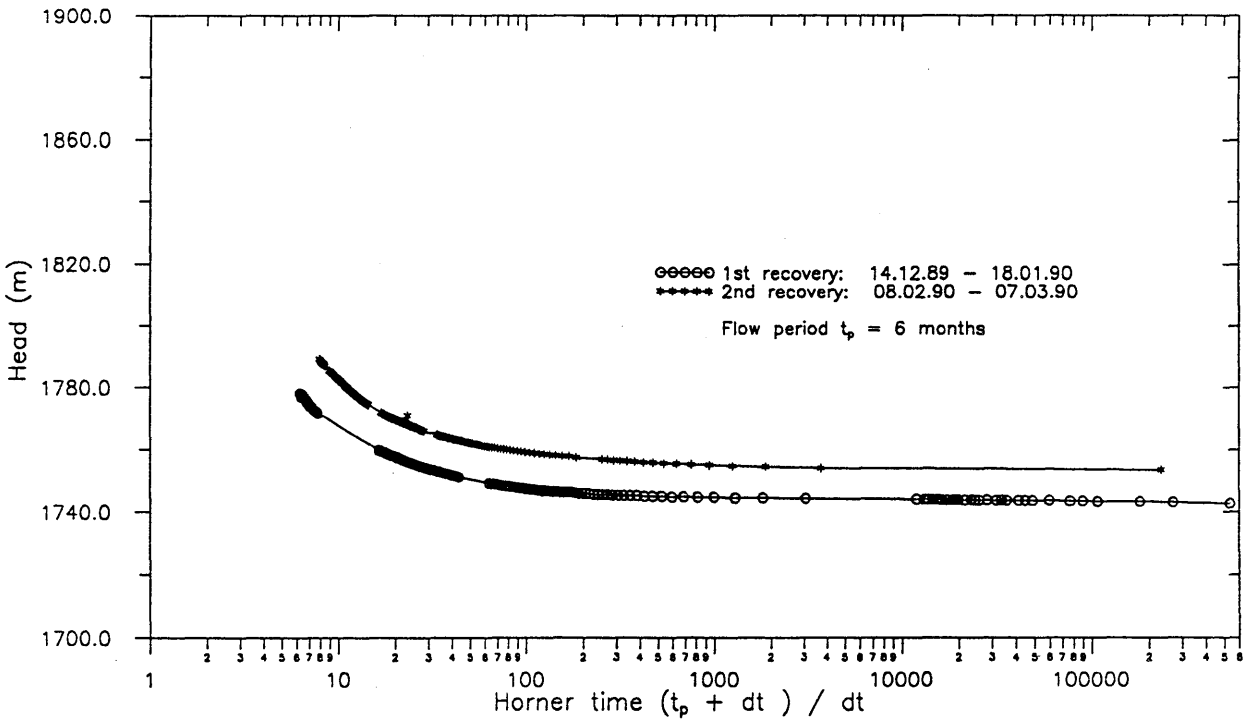

Figure III.4: HORNER plot for flow dimension = 2. 1st and 2nd recoveries, interval 85.004 i2.

slope of the Horner plot is also constantly increasing and an extrapolation assuming a constant slope cannot be made.

Based on the indication of linear flow provided by the log-log plot presented above, a Horner plot was constructed for a flow dimension n=1. The results are presented in Figure III.6 and the intercepts of the curves suggest an undisturbed hydraulic head situated around 1920 m in the case of the 1st recovery, and 1940 m in the case of the 2nd recovery. As previously, a plot of the derivative serves to establish whether the Horner plot has reached a true straight line. The derivatives are shown in Figure III.7. Although the graphs indicate that a constant slope of the Horner-plot has not yet been reached for either of the data sets, the range within which the derivatives vary is very small compared with the radial flow case (Figure III.5). The slope of the derivative was calculated and was taken into account in the head determination. This leads to a value of undisturbed hydraulic head of 2078 m which constitutes an upper limit for the head since we are assuming that the slope of the Horner plot increases in a constant fashion over the entire extrapolated time-interval.

III.1.3.3 Conclusions of the pressure recovery analysis

Horner plots were used for the estimation of the undisturbed hydraulic head in the vicinity of interval 85.004 i2. Due to the extremely long open-hole duration, the results of the analysis should be considered with caution. Extrapolation of the undisturbed head over such a long period does not account for any potential boundary effects which may have occurred had the test lasted long enough.

Diagnostic plots and pressure derivative analysis show that the classical Horner method assuming radial flow is not applicable to the pressure data measured in interval 2 of borehole 85.004 during recoveries 1 and 2. Indications of linear flow in the vicinity of this borehole during the two recovery periods led to a modified Horner analysis valid for a flow dimension of 1. Extrapolation shows that the undisturbed hydraulic heads lies between 1920 and 2078 m.

It should be noted that this undisturbed head is only applicable to borehole 85.004 interval 2 and cannot be assumed to be valid for the entire BK zone. In order to obtain a more complete picture of the head distribution in the BK zone, it is necessary to perform a similar analysis to the one described above, for all of the monitored intervals.

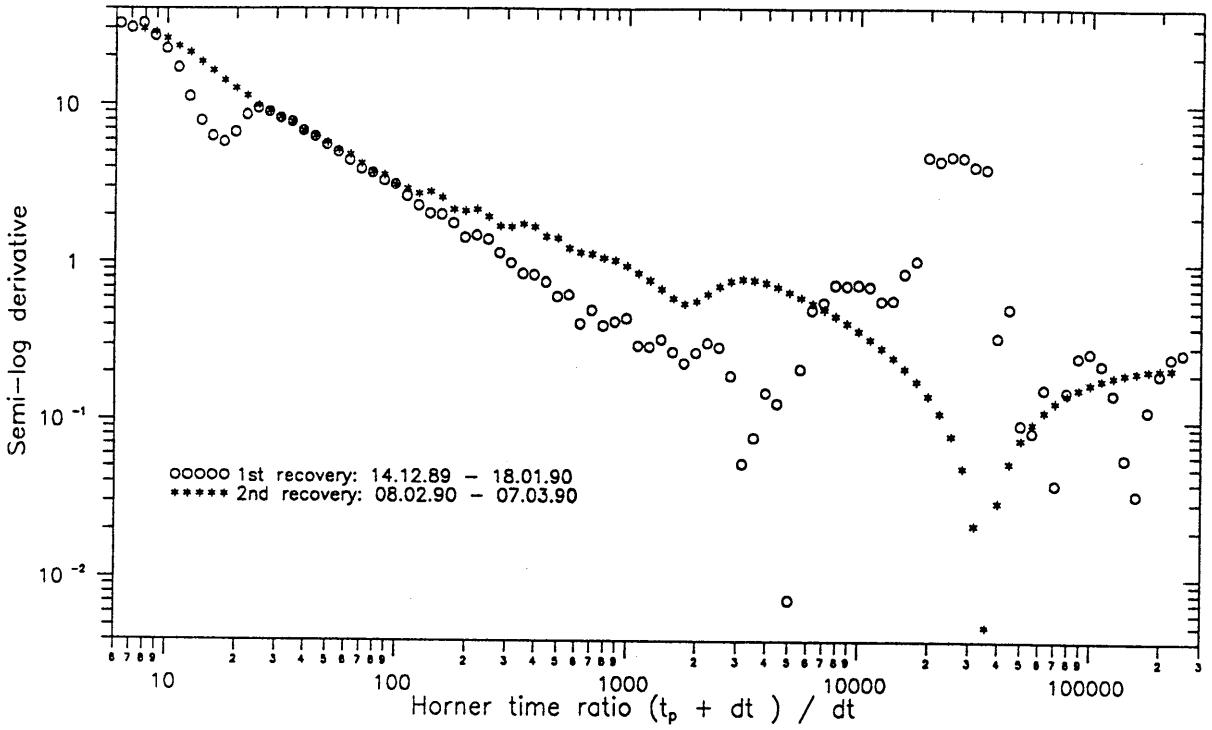

Figure III.5: Diagnostic semi-log derivative plot for flow dimension = 2. 1st and 2nd recoveries, interval 85.004 i2.

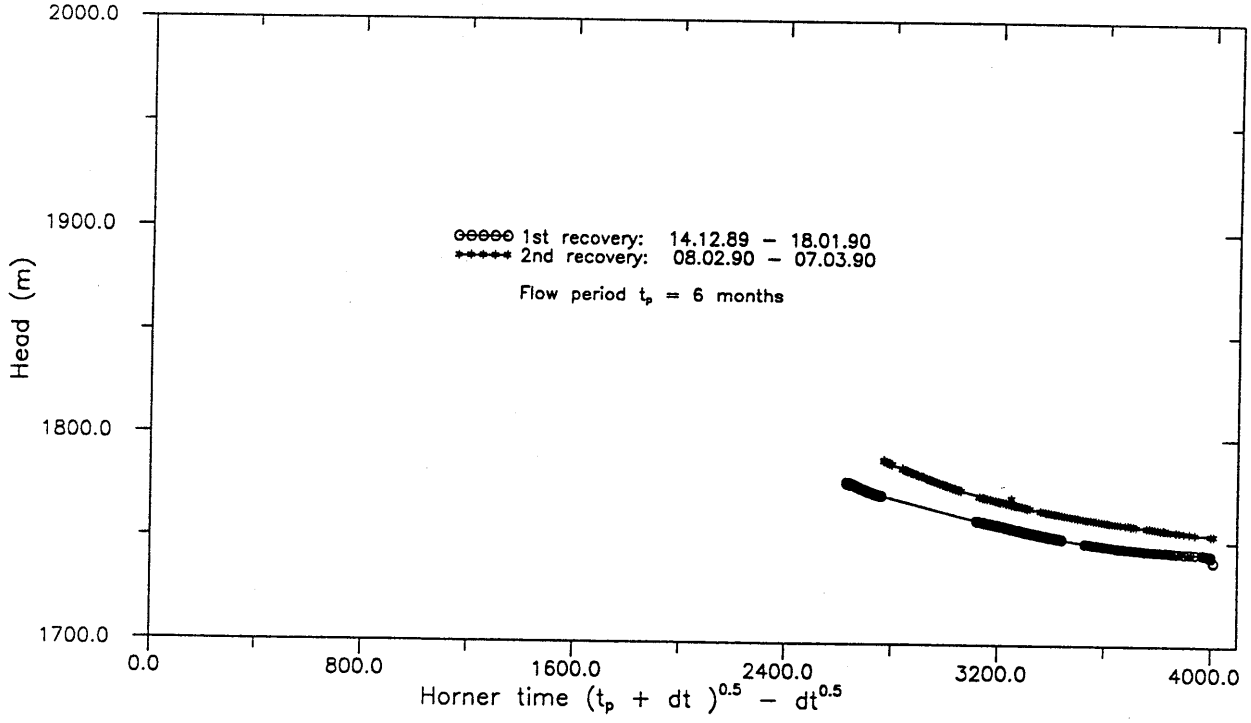

Figure III.6: HORNER plot for flow dimension = 1. 1st and 2nd recoveries, interval 85.004 i2.

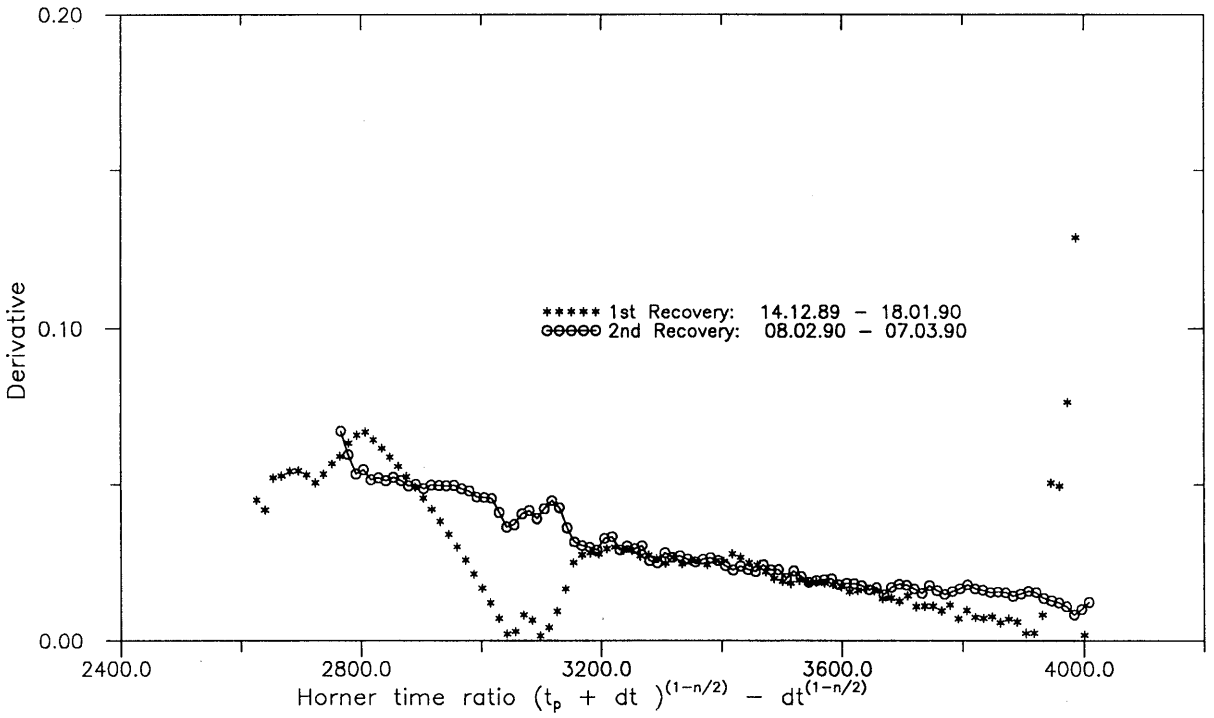

Figure III.7: Diagnostic derivative plot for flow dimension = 1. Interval 85.004 i2

III.1.4 CONSTANT HEAD INJECTION TEST ANALYSIS

III.1.4.1 Hydraulic gradients within the BK zone prior to testing

The purpose of a constant-head injection test is to induce an artificial stress in a system, monitor the system's response and interpret this response to estimate the hydraulic parameters. For the test to be meaningful, the magnitude of the artificial stress should be well above any natural stresses already existing within the test zone.

To test this hypothesis, hydraulic gradients between the injection interval and the observation intervals were calculated within the BK zone prior to the injection tests as well as during these tests. The results are presented in Figure III.8. Each injection interval-observation interval couple is identified by a number which can be found in Table III.3. Gradients are calculated at the end of the recovery period, at the end of test VE 452 and at the end of test VE 454. These two tests are chosen because they bracket the range of gradients which were observed during the tests.

Figure III.8 shows that the gradients induced by the tests are much greater than the natural gradients calculated at the end of the recovery period. This suggests that the tests were appropriately designed for the estimation of hydraulic parameters in the BK zone.

Table III.3: Couple identifiers used in Figure III.8.

Couple Identifier	Interval	Couple Identifier	Interval
1	85.009	9	85.006 i2
2	88.013	10	85.006 i3
3	88.014	11	88.017 i1
4	88.016	12	88.017 i2
5	88.015 i1	13	88.017 i3
6	85.007	14	88.018
7	85.011	15	85.008
8	85.006 i1	16	85.010

Note: Hydraulic gradients were calculated between interval 85.004 i2 and the intervals designated by their couple identifier.

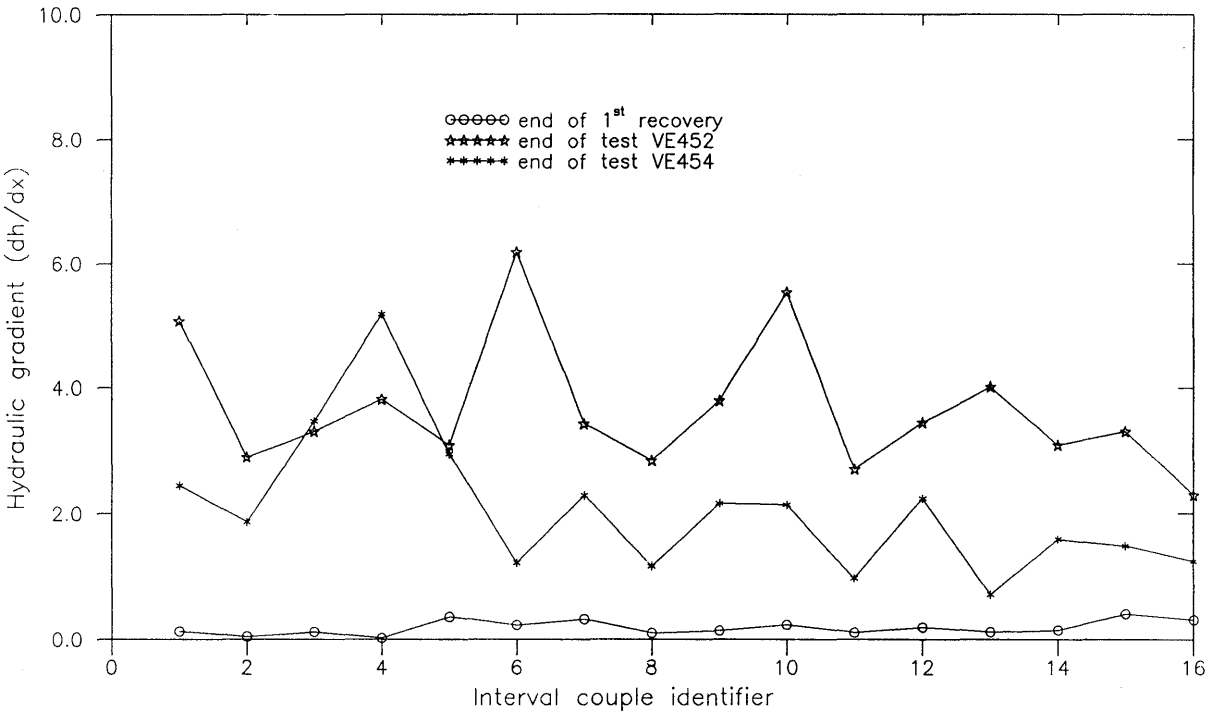

Figure III.8: Gradients between test interval (85.004 i2) and other intervals

III.1.4.2 Diagnostic plots for flow dimension analysis

III.1.4.2.1 Methodology

The purpose of diagnostic plots is to provide an easy way of identifying which flow model is applicable to a given pressure data-set. In MISHRA (1992 this volume), different ways of plotting the data for flow dimension determination are presented. Tests VE 451 through VE 457 were designed to be constant-head tests but in fact during certain tests, both the head and the flow at the injection interval varied. For this reason, it was not possible to use the diagnostic plots designed for constant-head tests where the inverse of the time-varying flow rate is plotted against a function of time. However, head variation could be accounted for by using the principal of superposition whereby the test is divided into a series of N constant flow periods and drawdowns at consecutive time intervals are added (STRELTSOVA, 1988). This leads to diagnostic plots which are very similar to the ones for constant head/ rate tests. Table III.4 summarizes the variables which are plotted for the different flow geometry diagnostics.

Table III.4: Summary of diagnostic plot variables.

X-axis variable	Y-axis variable	Geometry diagnosis
h_n/q_n	$B(t) = \Sigma_{i=1}^{n} (q_i-q_{i-1})/q_n * (t_n-t_{i-1})$	radial flow in a bounded system
h_n/q_n	$R(t) = \Sigma_{i=1}^{n} (q_i-q_{i-1})/q_n * \log(t_n-t_{i-1})$	radial infinite-acting flow (n=2)
h_n/q_n	$L(t) = \Sigma_{i=1}^{n} (q_i-q_{i-1})/q_n * (t_n-t_{i-1})^{0.5}$	linear infinite-acting flow (n=1)
h_n/q_n	$S(t) = \Sigma_{i=1}^{n} (q_i-q_{i-1})/q_n * 1/(t_n-t_{i-1})^{0.5}$	spherical infinite-acting flow (n=3)

Notes:

n = time interval number
h_n = hydraulic head at the injection interval over time interval n
q_n = flow at the test interval over time interval n
t_n = start time of time interval n

Note that the variables in Table III.4 should be plotted in cartesian coordinates since the relevant functions of t are already contained in the summation terms. In the case of the diagnostic plot for radial flow in a bounded system, the boundary is a circular no-flow boundary.

A flow geometry is diagnosed when a straight line is identified on the diagnostic plot for that specific flow geometry. Identification of a straight line can be made by visual inspection or through the use of a linear regression best-fit and the calculation of the coefficient of correlation r^2 according to:

$$r^2 = \Sigma(Y_{est} - Y_{avg})^2 / \Sigma(Y - Y_{avg})^2 * 100 \quad \text{(III.3)}$$

where:
r^2 = coefficient of correlation expressed as a percent
Y_{est} = estimated Y from linear regression
Y_{avg} = average Y

The plot which yields the largest value of r^2 can be selected as indicative of the most likely flow dimension.

III.1.4.2.2 Results of the diagnostic plot analysis

The pressure response measured during tests VE 451 through VE 457 was corrected for head variations and plotted for flow geometry diagnostic. First, log-log plots were drawn for identification of the borehole-storage dominated period. None of the plots exhibited a slope close or equal to 1 and therefore it can be concluded that none of the tests were significantly affected by borehole-storage.

Three diagnostic plots for the longest test (VE 457), are shown as examples in Figures III.9 to III.11. In Figure III.9, (a diagnostic plot for radial flow diagnosis), we see that the data exhibits a straight line until time 5160 s after which the data curves upwards. Such a sudden change in slope suggests the presence of a hydraulic boundary. In Figures III.10 and III.11, (diagnostic plots for a bounded system and for linear flow resp.), the data is curved until time 5160 s after which it shows a straight line. The diagnostic plot for spherical flow diagnosis is not shown because no portion of the data exhibited a straight line. The results presented in these figures suggest that the flow system in the vicinity of borehole 85.004 interval 2 during test VE 457 (interval 6.7 - 10.7 m), exhibits radial flow until the pressure pulse reaches a hydraulic boundary. The occurrence of a late-time straight line on both the bounded system and the linear flow diagnostic plots, suggests a system bounded on either side by boundaries causing channel-flow (STRELTSOVA, 1988). In such a system, flow is radial until the pressure-pulse hits the boundaries after which flow shows linear characteristics.

This mixed response in test VE 457 underlines a difficulty inherent to the diagnostic plot approach (and to any hydraulic analysis), since the "data window" within which the analysis is performed is of crucial importance to the result of the analysis. Linear regressions fitted to the entire data set on the diagnostic plots of test VE 457, without any prior visual inspection of the plots, would have led to erroneous flow geometry identification.

The results of the diagnostic plot analysis for all the tests are summarized in Table III.5. Inspection of this table reveals that none of the tests show spherical-flow characteristics. Tests VE 452, VE 455 and the early-time portion of test VE 457 show good evidence of radial flow. The late-time portion of test VE 457 presents linear flow or bounded-system flow characteristics. For tests VE 451, VE 453, VE 454

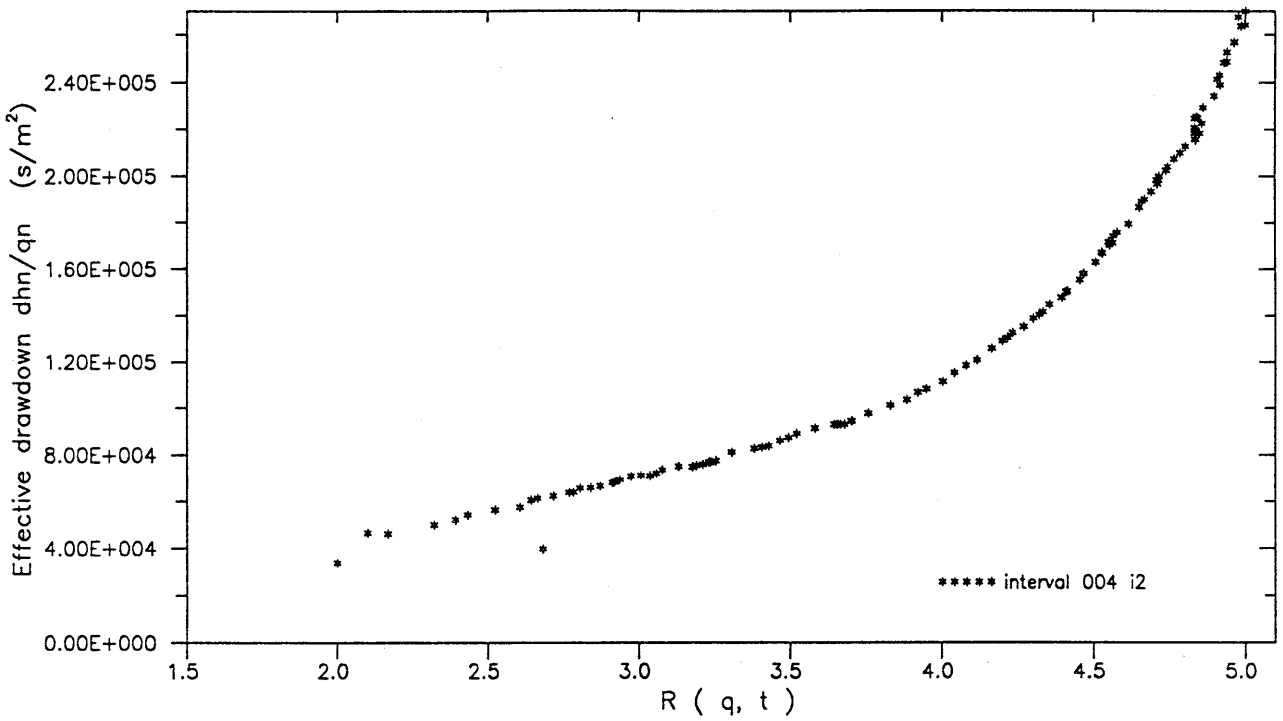

Figure III.9: Test VE457. Radial flow diagnostic.

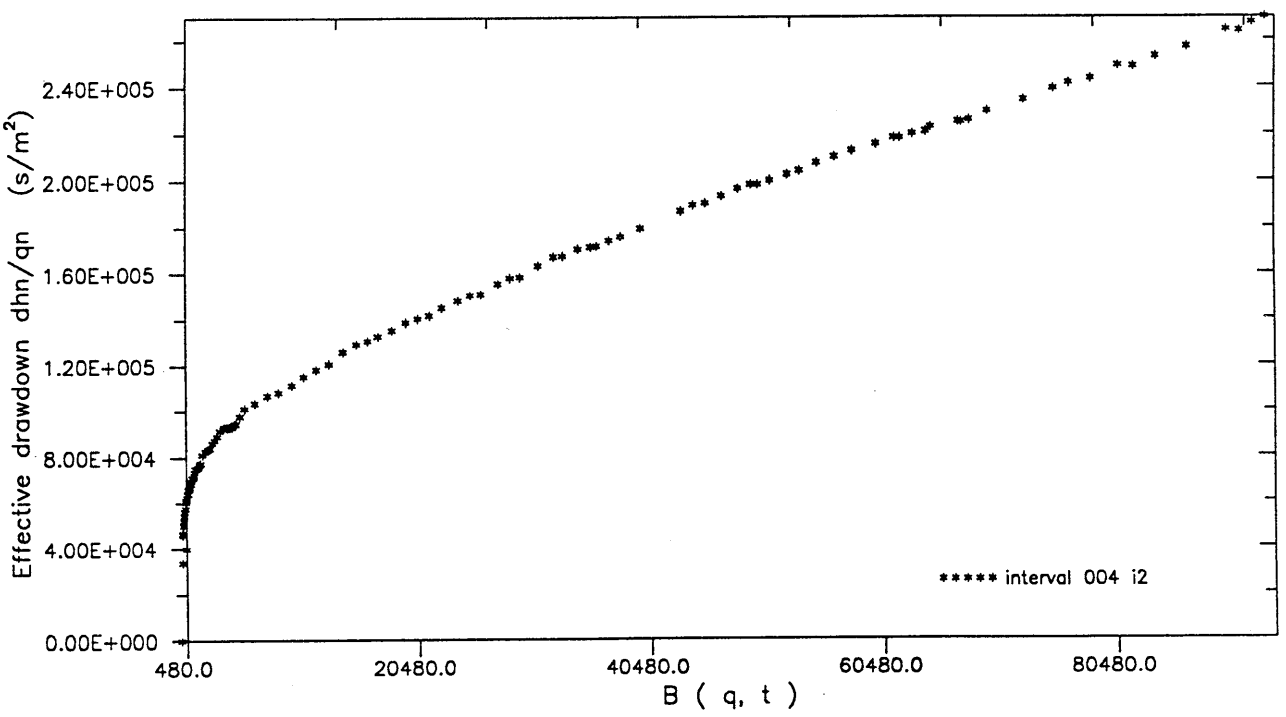

Figure III.10: Test VE457. Diagnostic for bounded system.

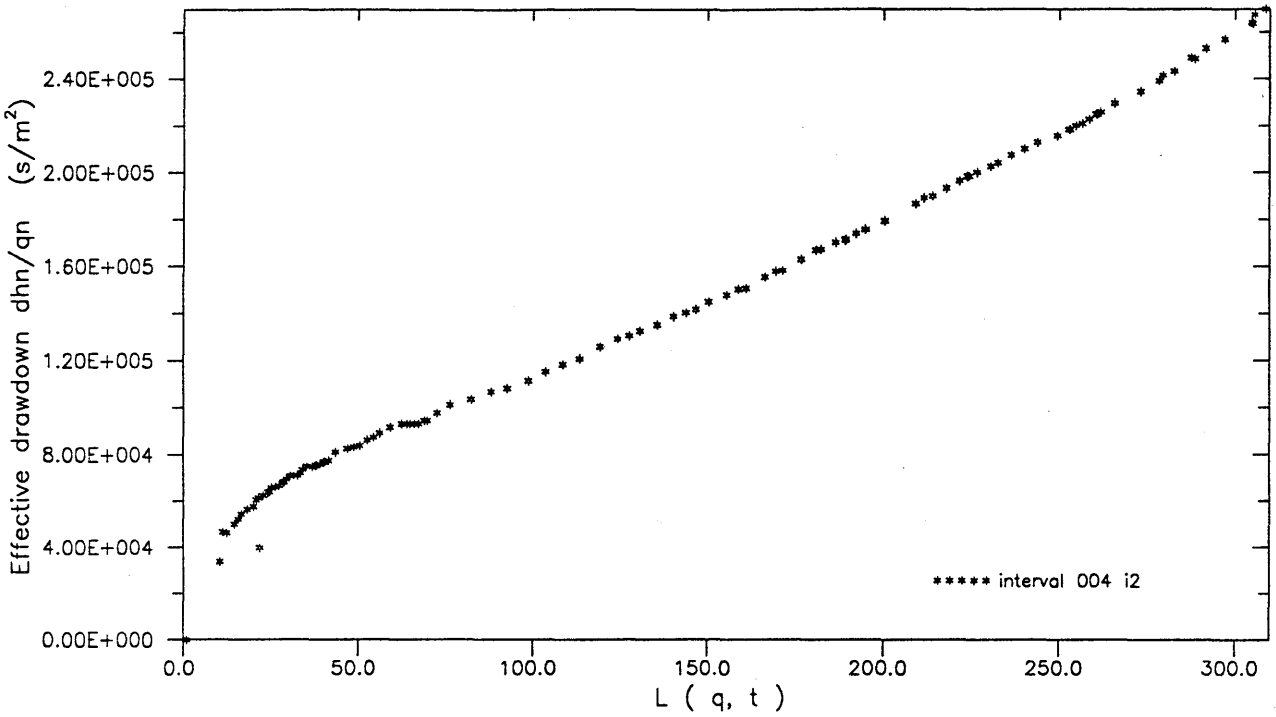

Figure III.11: Test VE457. Linear flow diagnostic.

and VE 456, it appears difficult to distinguish between radial and linear flow. It should be borne in mind that test VE 451 had a very short duration (4560 s), and therefore the flow characteristics may not have had sufficient time to develop.

From the results of the diagnostic plot analysis it was decided to analyze the pressure response measured during tests VE 451 through VE 457 using a numerical simulator of 2-D radial flow to a well.

Table III.5: Summary of diagnostic plot results.

Test	Time window (s)	Coefficient of Correlation (%)			
		Linear	Radial+ Boundary	Radial	Spherical
VE 451	901 - 4561	95	90	98	86
VE 452	121 - 21541	92	76	99	82
VE 453	780 - 7140	95	90	95	85
VE 454	3181 - 10981	91	90	91	89
VE 455	301 - 3841	94	87	98	94
VE 456	61 - 5581	97	94	95	86
VE 457	721 - 5161	92	70	96	85
VE 457	5161 - 85681	99.1	99.2	95	88

III.1.4.3 Numerical analysis of the constant head tests

III.1.4.3.1 Methodology

Numerical simulation of tests VE 451 through VE 457 was performed using GTFM, a numerical borehole simulator for 2-D radial flow. This model allows the simulation of radial flow to a borehole while including in particular borehole storage, double porosity, a finite skin and thermal effects. For details concerning the methodology used in this model for solving the partial differential equations, the reader is referred to GRISAK et al. (1985).

For each test, the simulation consisted of two sequences: a borehole history period and a flow period. For the borehole history, the pressure measured during the preceding test was entered as a file to be read by GTFM. The model computes the pressure perturbation within the formation caused by the pressures in the borehole. These perturbations are taken into account during the subsequent flow simulation. Since the tests were designed to be constant-head injection tests, the flow rate was variable. To account for this, the measured flow rate at the well

was also entered as a file to be read by the model. GTFM interpolates a flow rate versus time curve which fits the specified simulation time increment and calculates the head at the well.

Successive simulations were performed while adjusting the parameters by trial and error, until an acceptable match with the measured pressure response was obtained. The adjusted parameters are transmissivity and storativity, the static hydraulic head and the distance to a potential hydraulic boundary. A hydraulic boundary separating two zones of differing hydraulic parameters can be simulated using the finite skin option mentioned above. During the adjustment procedure, the parameters were submitted to certain constraints, for example the static head was not allowed to be lower than the elevation of the drift (1730 m).

III.1.4.3.2 Results of the numerical analysis

The parameters which yielded the best-fit matches to the pressure responses measured during each tests are summarized in Table III.6. Figures III.12 and III.13 show the best-fit matches in the case of tests VE 455 and VE 457. Very good fits to the measured data were obtained for all tests except VE 451. In this case no set of parameters was found which provided a match of the pressure response during both the flow and the recovery periods. However, this test was of very short duration and due to erratic variations in the head at the well, the quality of the data is questionable.

Table III.6: Summary of parameters which yielded the best fits during the numerical analysis

Test	interval depth (m)	Test Duration (s)	System Geometry	Inner Zone T (m2/s)	Inner Zone S	Outer Zone T (m2/s)	Outer Zone S	R (m)
VE451	16.6-44.6	4561	Inf.	5.04E-06	1.1E-05	none		
VE452	16.6-44.6	21541	Inf.	3.16E-06	1.1E-04	none		
VE453	1.9-14.	7140	Inf.	3.57E-05	1.9E-05	none		
VE454	7.7-15.	10981	Comp.	1.6E-05	3.2E-05	8.0E-09	1.6E-05	80
VE455	2-6	3841	Comp.	6.8E-06	4.0E-07	2.8E-07	8.0E-06	80
VE456	16.7-28	5581	Comp.	7.68E-07	8.0E-08	8.4E-08	8.4E-07	80
VE457	6.7-10.	85681	No-Fl.	1.2E-05	3.2E-05			70

Inf. : Infinite-acting radial flow
Comp. : Radial flow in a composite system (includes an inner and an outer zone)
No-Fl. : Radial flow in a bounded system (circular no-flow boundary)
R : Radial distance to outer zone or to no-flow boundary

As suggested by the diagnostic plot analysis (Section III.1.4.2.2), it was necessary to include a no-flow boundary at a certain distance from the well to reproduce the pressure data measured during test VE 457. Without a boundary, it was possible to reproduce the data until time

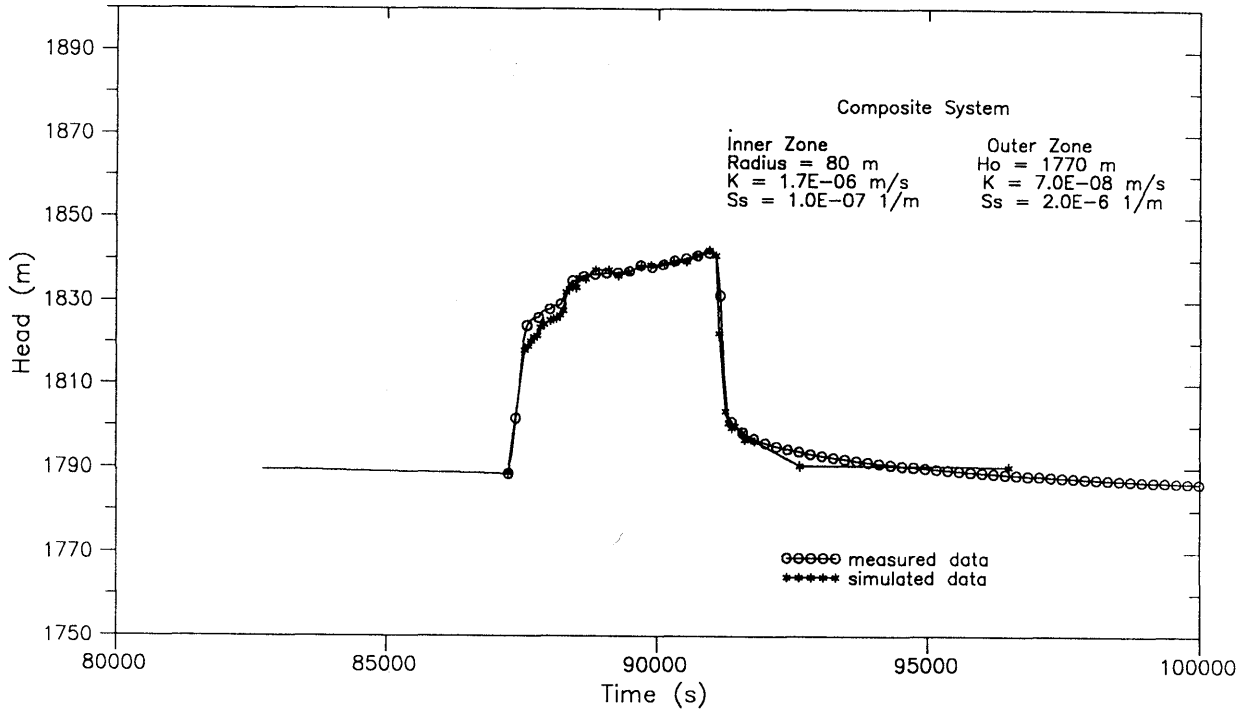

Figure III.12: GTFM simulation for test VE455.

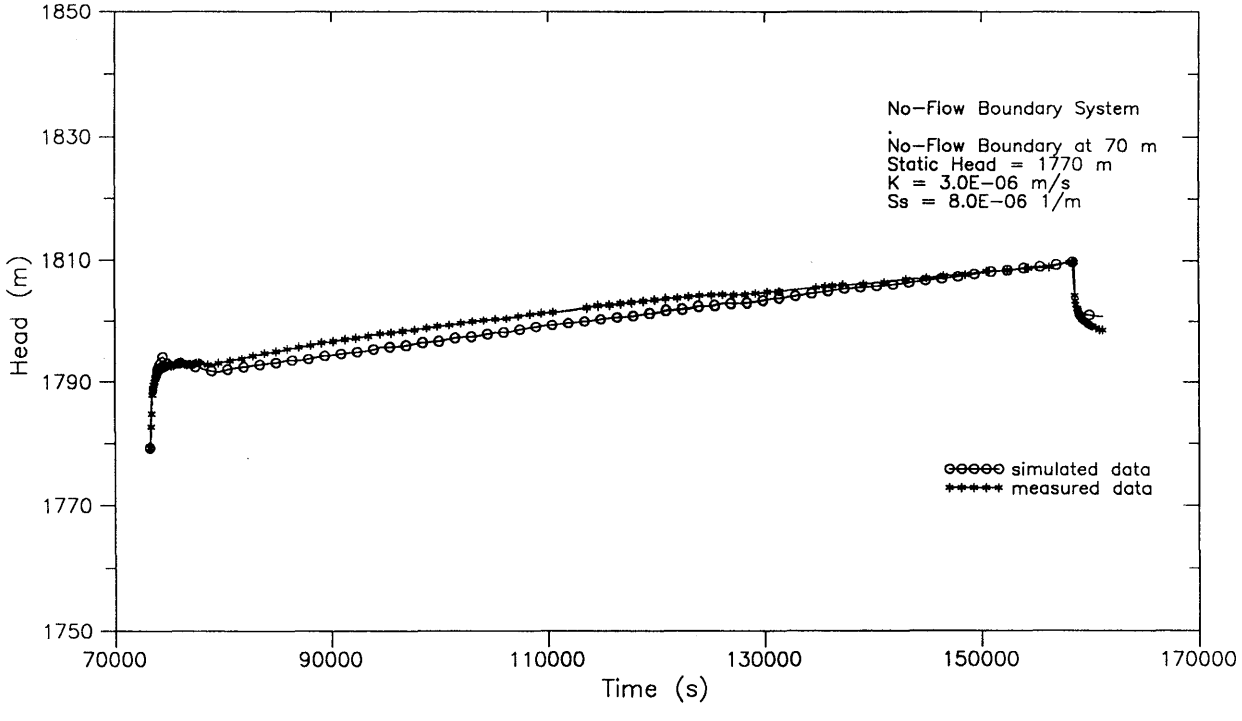

Figure III.13: GTFM simulation for test VE457.

5160 s when a deviation occurs, but no set of parameters provided a reasonable match with the entire data set. A no-flow boundary situated at 70 m from the well yielded the best fit to the observed data. It should be noted that the term "no-flow" can be viewed here as analogous to "low permeability" since a simulation using an outer zone with a transmissivity of 1E-10 m^2/s gave identical results.

Although this was not suggested by the diagnostic plot analysis, it was also necessary to include a hydraulic boundary in order to reproduce tests VE 454, VE 455 and VE 456. For these tests, composite systems with low permeability outer zones which appear at a radial distance of 80 m yielded good fits with the observed data.

As will be shown in the following section, the presence of a low permeability hydraulic boundary at a distance on the order of 80 m from borehole 85.004 is very consistent with existing geologic information concerning the BK site.

III.1.4.3.3 Implications for the conceptual model of the BK zone

The results of the diagnostic plots and the numerical analysis of tests VE 451 through VE 457 clearly show that the BK zone is not behaving as a homogeneous porous medium. Strong evidence of hydraulic boundaries separating zones of differing hydraulic parameters is provided by several tests. Test VE 457 showed an early-time radial flow response until 5160 s followed by either flow in a bounded system or by linear flow. The positive diagnostic for both flow geometries suggests flow in a system bounded on either side by boundaries which channel flow. Such a hypothesis is in good agreement with existing geologic information. It is well-known that two lamprophyre dykes delimit the test site to the north and to the south (Figure III.14). These lamprophyre dykes may well be acting as low permeability boundaries which channel flow at late times so that the pressure response exhibits linear flow characteristics. The distance to the boundaries (70 - 80 m) estimated in the numerical analysis is on the order of the distance between borehole 85.004 and the lamprophyre dykes as seen in Figure III.14. For the effect of the lamprophyre dykes to be observed in the pressure response, the test must last long enough as was the case for the pressure recoveries and for test VE 457.

The numerical analysis suggests that the dykes are not acting in the same way for all tests. Table III.7 summarizes the results of the numerical analysis and shows with the exception of the 2 to 6.5 m zone, the transmissivity of the outer zone appears to decrease as injection interval depth increases. This could explain why for certain tests, the diagnostic plots were unable to distinguish between radial and linear flow. In a composite system as opposed to a no-flow boundary system, the pressure response will show mixed characteristics and unequivocal determination of the flow geometry will not be possible.

The transmissivities of the inner zone are plotted versus depth in Figure III.15. This figure reveals a consistent pattern with two major intervals in borehole 85.004; an upper interval of relatively high transmissivity and a lower interval of lower transmissivity.

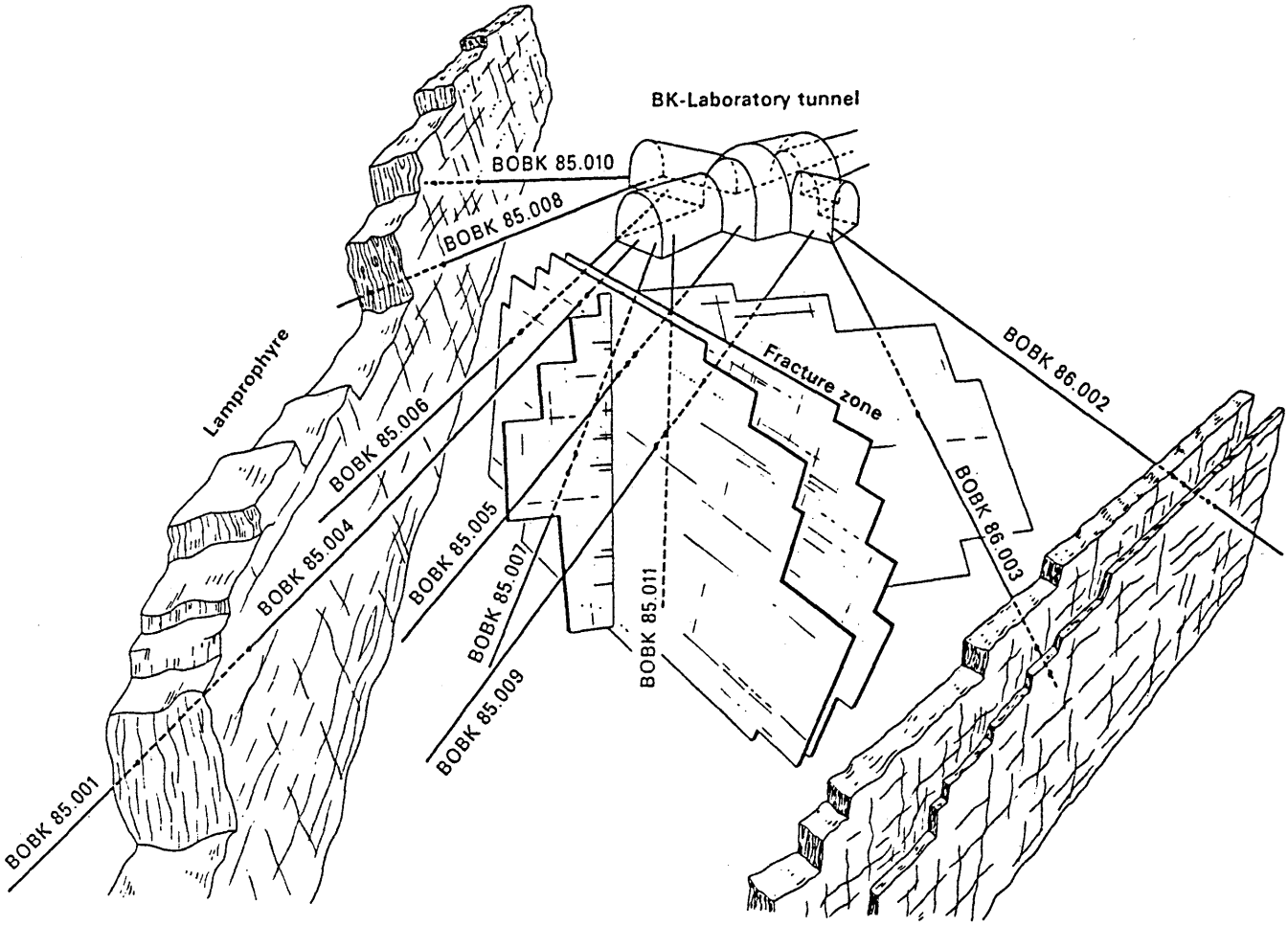

Figure III.14: Lamprophyre dykes in the BK area.
(from Bräuer et al. 1989)

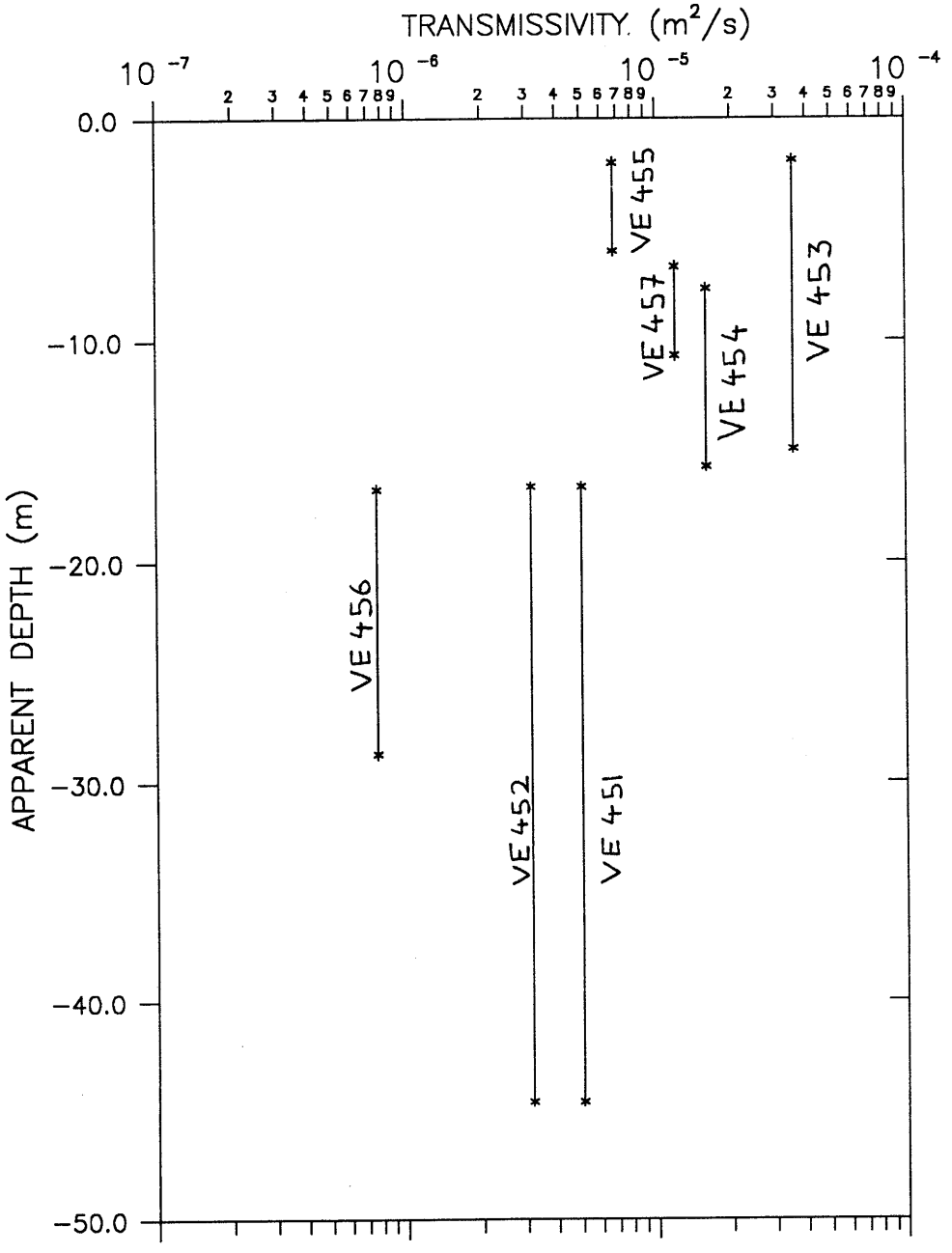

Figure III.15: Best-fit transmissivities from the GTFM simulations. Tests VE451-457, borehole 85.004.

Table III.7: Schematic representation of borehole 85.004

Depth (m)	85.004	Results of Simulations		
		T (inner zone) (m^2/s)	Boundary (m)	T (outer zone) (m^2/s)
2		7E-06	80	2E-07
6.5			70	1E-10
		2E-05		
			80	8E-09
15				
		8E-07	80	8E-08
29				
		2E-06	>40	?
45				

III.1.5 SUMMARY AND CONCLUSIONS

The hydraulic analysis presented in this chapter clearly suggests that the BK site is a highly complex flow system which cannot be assumed to be homogeneous 2-D radial. The analysis provided evidence for hydraulic boundaries, radial and linear flow in a composite system.

The analysis of the pressure recoveries measured in borehole 85.004 interval 2 during both recoveries showed indications of linear flow and provided estimates of the undisturbed hydraulic head which lie between 1920 and 1940 m. Derivatives indicate that these values may slightly be underestimating true values.

Diagnostic plots for tests VE 451 through VE 457 rule out the possibility of spherical flow for all tests. Clear evidence for radial flow is provided in the case of test VE 452, VE 455 and the early-time portion of test VE 457. The late-time portion of test VE 457 presents linear flow or bounded-system flow characteristics. The diagnostic plots are not successful in distinguishing between radial and linear flow geometries in the case of tests VE 451, VE 453, VE 454 and VE 456.

Numerical simulation of tests VE 451 through VE 457 confirm the presence of hydraulic boundaries and lead to the distinction between an inner zone and an outer zone. The transmissivities of the inner zone vary between 7.7E-07 and 3.6E-5 m^2/s. The transmissive characteristics of the outer zone vary from test to test. For example in the case of

test VE 457, the boundary is acting as a no-flow boundary, whereas in the case of test VE 456, the boundary separates two zones which have permeabilities differing by one order of magnitude.

The geometry suggested by the hydraulic analysis is in good agreement with existing geological information concerning the BK site which reveals the presence of two lamprophyre dykes at the north and the south of the test area. These two boundaries explain the occurrence of linear or bounded flow characteristics at late times suggested by the analysis of the pressure recovery tests and test VE 457.

III.2 CROSSHOLE TEST ANALYSIS AT THE BK SITE

III.2.1 Introduction

III.2.1.1 Objectives

Further to the analysis of the injection interval responses in the NAGRA BK boreholes during tests VE 451 through VE 457 (Section III.1), the responses in each of the observation intervals were analyzed and the results for selected intervals are presented below. For information concerning the geometry of the BK site and in particular the distances separating the injection interval and the observation intervals during each test, the reader is referred to Section III.1 (Table III.2).

The crosshole test analysis attempts to increase the conceptual understanding of the flow system at the BK site and to provide further evidence in support of results obtained during the analysis of the injection interval response. The emphasis of the analysis presented below is upon flow geometry, heterogeneity and estimating the hydraulic parameters transmissivity and storativity.

III.2.1.2 Approach

As for the analysis of the injection interval responses, the approach chosen here is to first perform diagnostic plots to provide indications concerning the dimension of the flow system as well as heterogeneity within the system. Once the flow system is understood conceptually, the appropriate flow model is applied to provide estimates of the hydraulic parameters transmissivity and storativity.

III.2.2 Diagnostic Plots

III.2.2.1 Diagnostic Plots for Heterogeneity Diagnosis

III.2.2.1.1 Methodology

In MISHRA (1992, this volume) it was shown that for the analysis of constant head tests, an extrapolation of the generalized flow equation

presented by BARKER (1988) can be made by normalizing the drawdown measured at the observation interval with respect to the flow rate at the injection interval.

Thus for any flow dimension we have:

$$\Delta h(r,t) \,/\, q(r_w,t) \approx f\,(\, t \,/\, r^2\,) \qquad \text{(III.4)}$$

where:
- Δh = drawdown
- r = the radial distance between injection interval and observation interval
- r_w = injection interval radius
- t = time
- $q(r_w,t)$ = flow rate at the injection interval
- and f denotes a functional relationship

It should be noted that Equation III.4 is not applicable to observation intervals which are very close to the injection interval at early times. According to MISHRA (1992, this volume), the error due to the approximation becomes negligible at all times when $r > 200\ r_w$:

It follows from Equation III.4 that when plotted as $\Delta h(r,t)/q(r_w,t)$ versus t/r^2 on a log-log graph, all the data from all of the observation intervals will fall onto a single curve if each of the following is true:

A: The flow system is homogeneous with respect to transmissivity and storativity.
B: The flow system is homogeneous with respect to the dimension of flow.
C: The pressure pulse moves along a straight-line between the injection interval and the observation interval.

Note that this approach is identical to that used during Theis curve matching, with the difference that in this case the flow rate at the well is variable and that we are not making any a-priori assumption on the flow dimension.

III.2.2.1.2 Results

Figure III.16 shows the flux-normalized pressure responses in various intervals during test VE 455. It is clearly seen that the data do not collapse onto one curve and therefore at least one of the assumptions **A**, **B** or **C** is not true.

An interesting result is obtained when r, the distance travelled by the pressure pulse, is taken as equal to unity rather than to the straight-line distance between the injection interval and the observation interval: the responses from several intervals presented in Figure III.16 now appear to collapse onto one plot (Figure III.17). This implies that there are certain intervals which are reacting in an identical manner as though they were one interval, independently of the radial distance which separates them from the injection interval. The intervals which

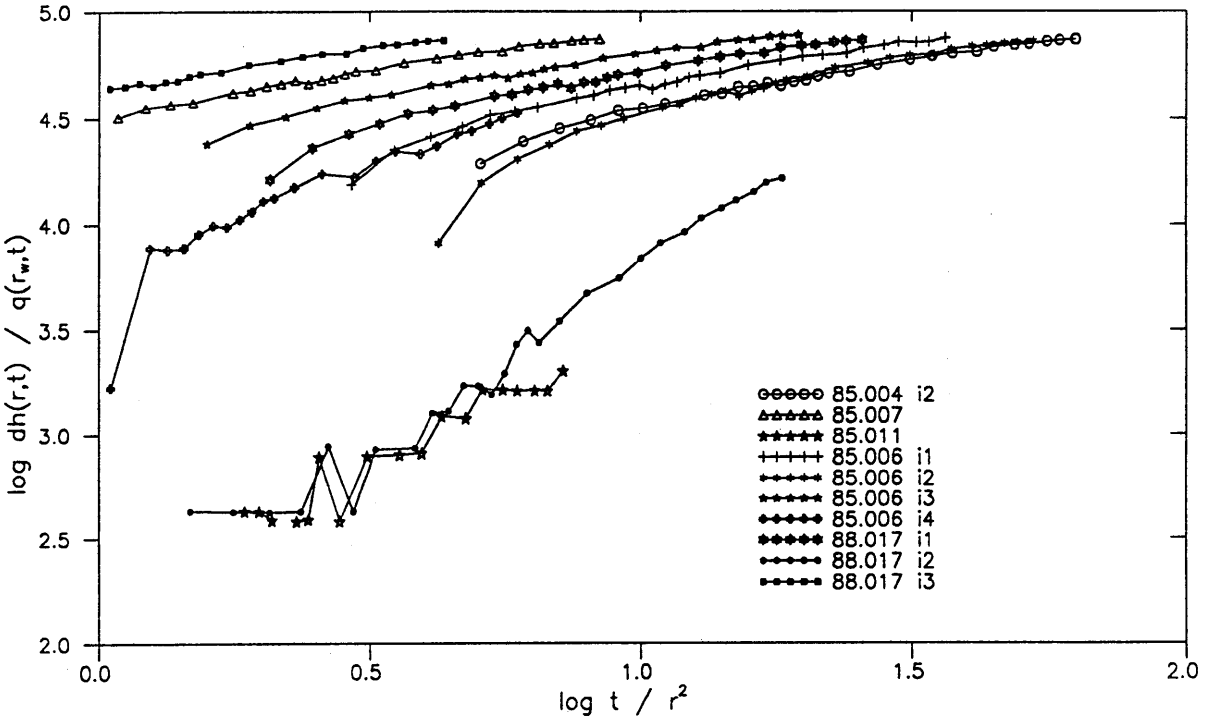

Figure III.16: Responses in observation intervals during test VE455.

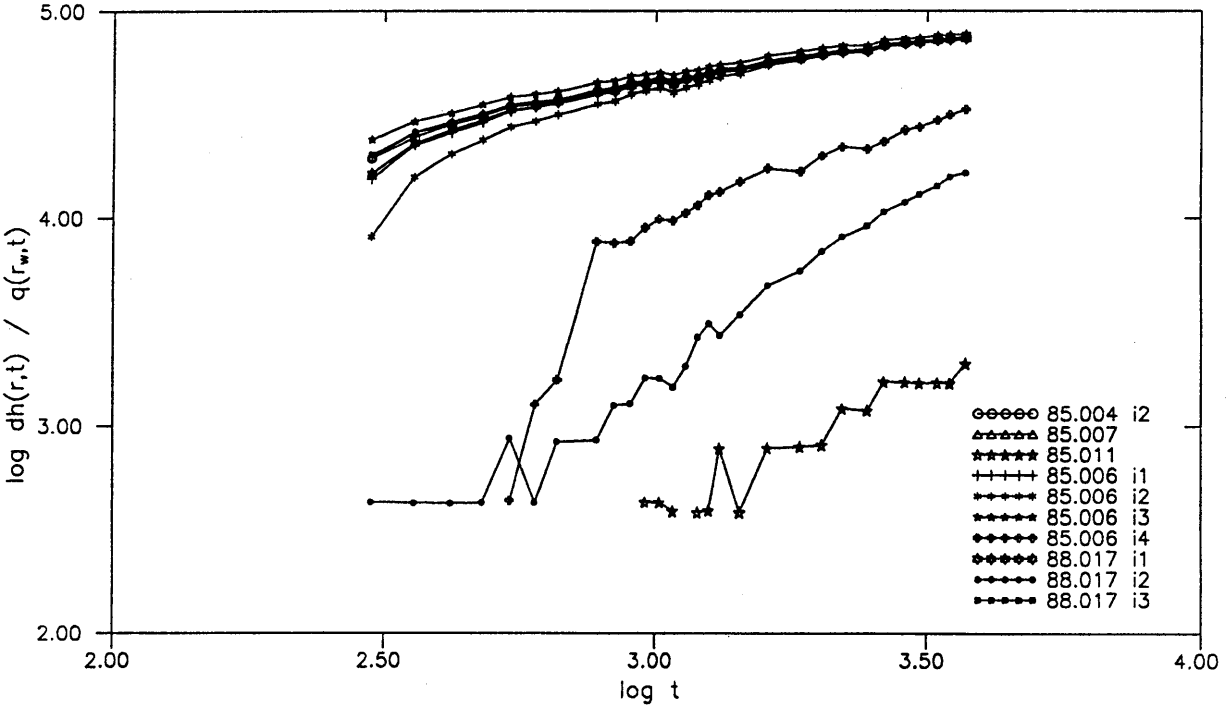

Figure III.17: Responses in observation intervals during test VE455.

consistently show a similar response during all the tests are:

borehole	85.005 i1
	85.006 i1, i2, i3
	85.007 i1
	88.015 i2
	88.017 i1, i2, i3
	88.018 i1

The responses measured within these selected intervals during test VE 457 are presented in Figure III.18 using a unit radial distance. The response measured in interval 85.004 i2 is also shown although it does not appear to collapse onto the other curves at least at early times. The intervals listed above must necessarily intersect a highly transmissive feature such that when the pressure pulse hits this feature, all the intervals which intersect it react in exactly the same way. The fact that the response in the injection interval is different than those measured in the intervals listed above, suggests that the injection interval does not intersect the highly transmissive feature. However, these responses were closest during test VE 457, indicating that the interval 6.7 - 10.7 m (injection interval during VE 457) is closer to the highly transmissive feature than the injected interval during any other test.

For the intervals listed above at least, the true migration path of the pressure pulse cannot be the straight line distance between the injection interval and the observation interval (hypothesis **C**). This high transmissivity feature is discussed in more detail in Section III.2.4.

Further doubt is shed on hypothesis **A** when the times of first interval-response are plotted as a function of the distance from the injection interval. If the flow system were perfectly homogeneous, one would expect the intervals situated furthest away from the injection intervals to start responding the latest. Such a plot showed that there is no clear correlation between first interval-response and distance from the injection interval during either of the tests.

The results presented above indicate that hypothesis **C** is not correct for certain intervals at least, and shed doubt on hypothesis **A** and **B**. This led to a flow dimension analysis with the objective of gaining some insight into the geometry of the flow system at the BK site.

III.2.2.2 Diagnostic Plots for Flow Dimension Diagnosis

III.2.2.2.1 Methodology

In MISHRA (1992, this volume), it was shown that for constant-head tests performed in a flow system of dimension n we have:

$$\log \left(\partial \left(\Delta h(r,t)/q(r_w,t)\right) / \partial(\ln t) \right) \sim (1-n/2) \log t \qquad \text{(III.5)}$$

where:
∂ denotes the partial derivative
$\Delta h(r,t)$ is the drawdown at radius r and time t

$q(r_w,t)$ is the flow at the injection interval at time t
n is the flow dimension
and ~ indicates a factor of proportionality

Therefore a plot of the semi-log flux-normalized pressure derivative versus time on a log-log graph should have a slope of 1-n/2 from which it follows that:

$$n = 2*(1-slope) \qquad (III.6)$$

From Equation III.6 we can distinguish between the following ideal cases:

- slope = -0.5: n = 3, spherical flow
- slope = 0 : n = 2, radial flow
- slope = 0.5 : n = 1, linear flow
- slope = 1 : n = 0, borehole storage dominated period

Since the quality of the raw head data from the observation intervals did not allow calculation of semi-log derivatives with sufficient accuracy (due to noise in the raw data), the data were first "treated" using a FORTRAN code named SMOOTH (Mishra pers. comm.). SMOOTH interpolates additional data points by splining and then smoothes the resulting curve using a Fourier transformation procedure. Semi-log derivatives were then calculated from the smoothed data. It should be noted that such a treatment for semi-log derivative calculation is a standard procedure in the petroleum industry.

III.2.2.2.2 Results of the Flow Dimension Analysis

Figure III.19 shows the semi-log flux-normalized pressure derivative for several intervals and different tests. It is seen that in the case of interval 85.005 i1 during test VE 454, the semi-log derivative exhibits a slope of 0 over the first portion of the test suggesting radial flow during this period. At approximately 2000 s however, the slope of the curve decreases and the curve forms a slight trough. This indicates the presence of a boundary the nature of which cannot be determined without further analysis.

Borehole 88.016, test VE 456 also exhibits radial flow behaviour at early times but the effect of the boundary is seen to be much more pronounced. The semi-log derivative for the response from interval 88.015 i2 is seen to have a slope greater than 0 which indicates that in this case the flow dimension is lower than 2. Fitting a straight line to the derivative on the log-log graph yields a slope of 0.42 and from Equation III.6 it follows that n = 1.2 indicating a tendency towards linear flow. The curve for interval 85.005 i3 test VE 452 is shown here as an example where n > 2, but it should be noted that very few intervals showed such behaviour. For this interval, the slope of the semi-log derivative curve yields a flow dimension of 2.3.

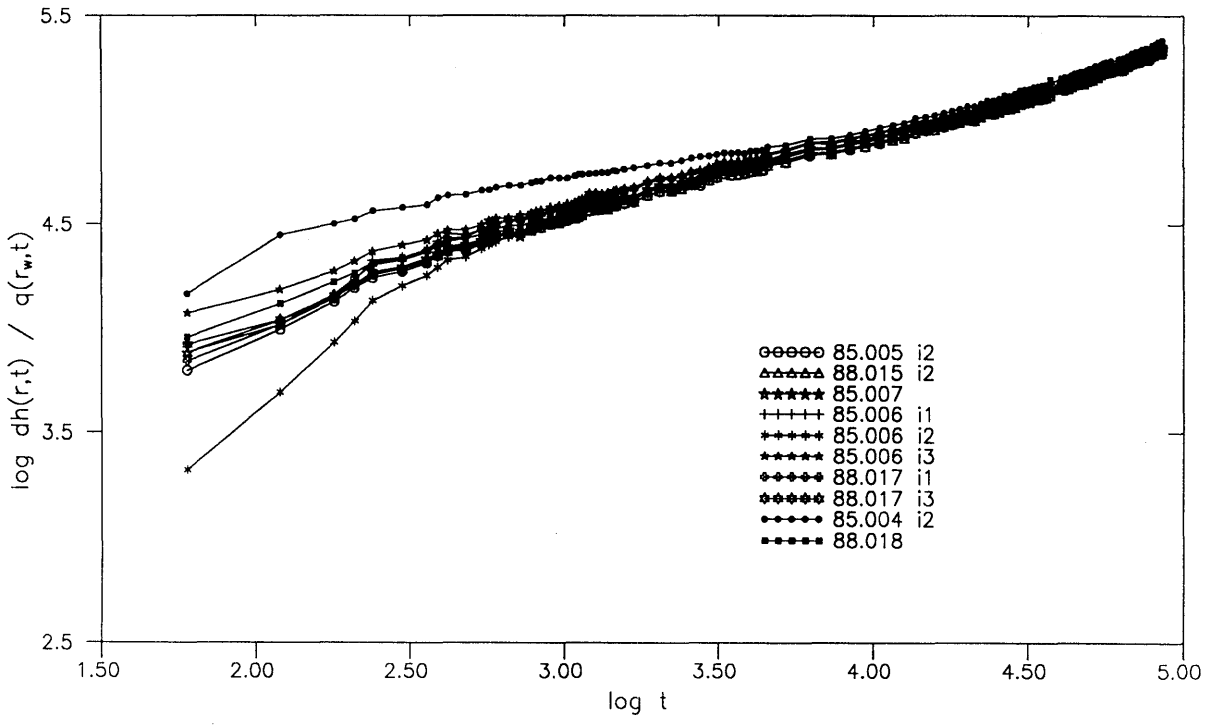

Figure III.18: Responses in selected intervals during test VE457.

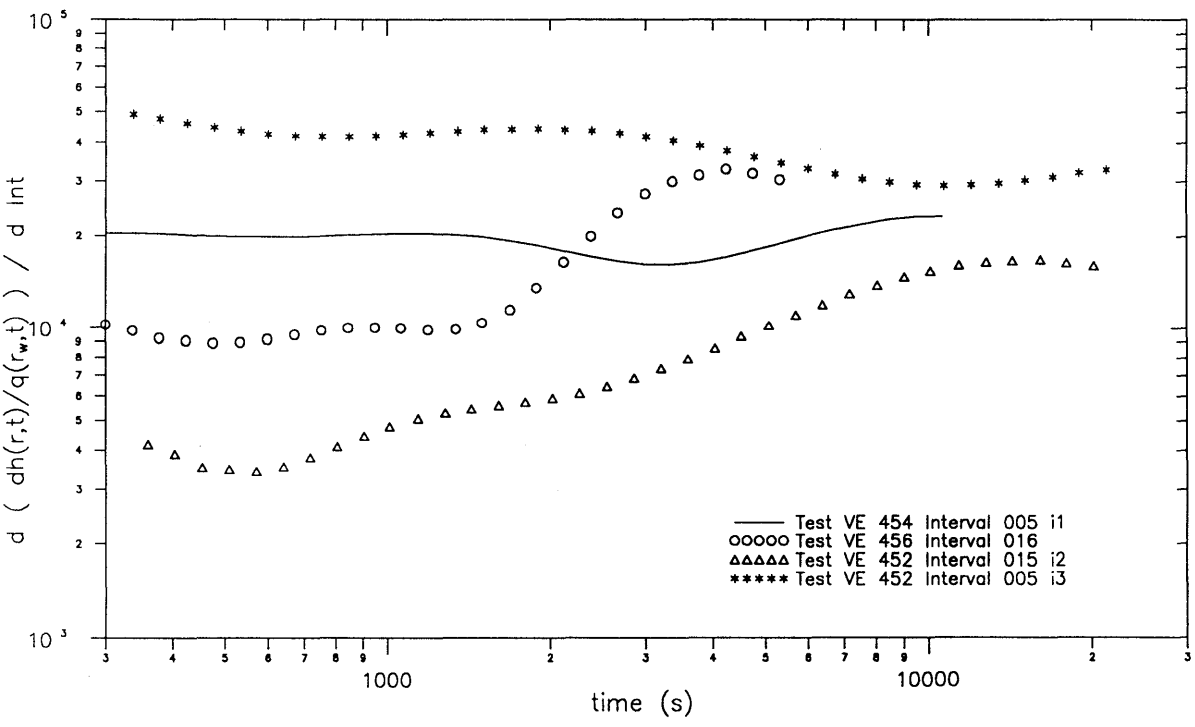

Figure III.19: Selected semi-log derivative plots for dimensional analysis.

The dimensional analysis showed that for many tests, the early-time pressure-response indicate flow characteristics which tend towards radial flow. Nearly all intervals show evidence of boundaries at late times which affect the pressure response and make flow dimension recognition difficult. Clear indications of borehole storage effects were not identified.

The results of the flow dimension analysis are in agreement with those of the single-hole test analysis (Section III.1). The response measured in the injection interval during test VE 457 for example, clearly showed evidence of radial flow at early times which was followed by linear or bounded-flow at late times due to the presence of a no-flow boundary.

In the analysis presented in Section III.2.3., a 2-D radial flow model is applied to the response measured in all the observation intervals during tests VE 451 through VE 457. Late-time data which showed the influence of boundaries were discarded for this analysis.

III.2.3 Determination of Hydraulic Parameters

III.2.3.1 Methodology

As was shown in MISHRA (1992, this volume), the pressure response at the observation intervals during a constant-head injection test in a 2-dimensional flow system can be analyzed and hydraulic parameters calculated using a modification of the Theis equation, where the drawdown in the observation interval is normalized with respect to the time-dependent flow rate at the injection interval according to:

$$\Delta h(r,t)/q(r_w,t) \approx 1/4\pi T \; Ei \; (-Sr^2/4Tt) \qquad \text{(III.7)}$$

where:
$\Delta h(r,t)$ is the drawdown at distance r and at time t
$q(r_w,t)$ is the flow rate at the injection interval and at time t
T is transmissivity
S is storativity
r is the radial distance to the observation interval
r_w is the radius of the injection interval
and Ei is the exponential integral

As for Equation III.4, Equation III.7 does not hold for observation intervals situated very close to the injection interval at early times. For practical purposes, the error due to the approximation can be assumed negligible at all times at a distance $r \approx 200\ r_w$.

If $\Delta h(r,t)/q(r_w,t)$ is plotted versus t/r^2 on a log-log plot for each interval, then the data can be matched with the Theis type curve to obtain estimates of T and S. The type curve matching was performed using an automatic fitting routine, EIFIT (Mishra pers. comm.), which makes use of the Levenberg-Marquardt algorithm to minimize the deviation between the measured and calculated points. The method was used to calculate T and S on a synthetic data set for which T and S were al-

ready known. Results show that while T is within 5 % of the true value, S is within 10 %. This error is due to the approximate nature of Equation III.7. As mentioned above, error increases as the distance to the observation well decreases.

Since the head at the injection interval during tests VE 451 through 457 was not always constant (see in particular test VE 457), a sensitivity analysis was performed to test the validity of Equation III.7 when the assumption of a constant head at the active well is not fully satisfied.

III.2.3.2 Sensitivity Analysis

Three sets of injection interval head data were generated (Figure III.20); one in which the head is constant throughout the test (case 1), one in which the head at the injection interval increases in a hyperbolic fashion (case 2) and one in which the hydraulic head was perturbed by a random noise component (case 3). The magnitude of the artificial head perturbations was comparable to that observed during the BK tests VE 451 through VE 457. The three sets of data were used as input to a borehole simulator (GTFM) to generate the flux at the injection interval and the head response at an observation well situated 20 m from the injection interval.

The hydraulic parameters used to simulate the response at the observation interval were:

$T = 5.0E\text{-}06\ m^2/s$
$S = 5.0E\text{-}05$

The head response calculated at the observation interval was then normalized with respect to the time-dependent flux at the injection interval and the resulting data set was matched with the Theis type curve using EIFIT, to obtain estimates of T and S. The results are presented in Table III.8.

Table III.8: Results of Sensitivity Analysis

	T (m2/s)	S ( )
Input Value:	5.0E-06	5.0E-05
Output Values		
Case 1:	4.97E-6	4.51E-5
Case 2:	4.97E-6	4.88E-5
Case 3:	4.89E-6	4.47E-5

The maximum error in the parameter determination is seen to occur as

expected for case 3 and is approximately 10 % of the true value. This error is on the same order as that introduced by the use of Equation III.7. The pressure responses at the observation interval calculated for all three cases are plotted in dimensionless form on Figure III.21 and compared to the Theis Solution. The results presented in Table III.8 and the good match between the dimensionless pressure curves and the Theis curve suggest that Equation III.7 is a valid approximation even when there are perturbations in the head at the injection interval such as those observed in tests VE 451 through 457.

III.2.3.2 Results of Hydraulic Parameter Calculations

The pressure responses measured in all the intervals during all the tests were normalized with respect to the flux at the injection interval and the resulting data sets were matched with the Theis type curve using Eifit. Late time data which showed evidence of boundary effects was discarded. The distance r was first assumed to be the straight line distance between the injection interval midpoint and the observation interval midpoint. Best-fits to the Theis curve for several intervals monitored during test VE 453 are shown as an example in Figure III.22. The data are seen to fit the Theis curve fairly well. It is interesting to note that the data do not show any significant evidence of borehole storage effects. Such effects would be indicated by a lag in the measured response with respect to the Theis curve. The calculated values of T and S are presented in Table III.9 and plotted on Figure III.23. It is seen that values of transmissivity show good agreement with the transmissivities calculated during the single hole test analysis (Section III.1). The range of transmissivities estimated from numerical simulations of the responses measured in the injection intervals (Section III.1) is represented in Figure III.23 by the dashed lines.

Calculated storativities are seen to spread over a much larger range which covers nearly 4 orders of magnitude. However it must be taken into account that there is a lot of uncertainty concerning these values of S due to the uncertainty with respect to the true diffusion path length of the pressure pulse (r). As was shown previously, for the intervals listed in Section III.2.2.1.2, the true distance travelled by the pressure pulse is not equal to the straight line distance. For these intervals, the pressure response was re-analyzed with Eifit while taking r as a unit value for all the intervals (r=1). The values of T and S when r is taken as the straight line distance or as a unit value are shown in Figures III.24 and III.25 respectively. The coordinate axis on the two plots are the same for comparison purposes. It is seen that when r is taken as the straight line distance, the plot shows a spread, whereas if r is taken as a unit value, all the points for a given test cluster together. This is a further illustration of the fact that certain intervals are reacting identically independently of the radial distance which separates them from the injection interval.

It is interesting to note that varying r has no effect on the fitted value of transmissivity. This is because on a log-log graph, changing r simply shifts the data in the horizontal direction without changing the shape of the curve, and T is obtained from the matched value along the Y-axis of the Theis type curve.

	VE451		VE452		VE453		VE454		VE455		VE456		VE457	
Interval	T	S	T	S	T	S	T	S	T	S	T	S	T	S
009	8.3E-06	2.0E-05	6.1E-06	2.5E-05	8.7E-06	3.2E-05	6.5E-06	4.7E-05	8.6E-06	2.0E-05	2.3E-06	2.9E-05	8.8E-06	2.6E-05
013	9.3E-06	7.4E-05	3.9E-06	7.1E-05	4.0E-06	8.2E-05	2.8E-06	6.6E-05	3.5E-06	7.6E-05	1.0E-06	7.8E-06	4.1E-06	5.8E-05
014	1.1E-05	3.0E-05	4.5E-06	4.5E-05	7.6E-06	2.6E-04	7.0E-06	2.6E-04	1.1E-05	2.5E-04	3.4E-06	2.4E-05	1.0E-05	2.2E-04
016	1.2E-05	2.9E-05	4.8E-06	5.7E-05	1.0E-05	4.3E-04	6.7E-06	6.4E-04	1.1E-05	3.3E-04	3.3E-06	3.7E-05	1.1E-05	3.6E-04
015 i1			1.2E-05	2.4E-06	5.1E-06	2.8E-04	2.6E-06	1.4E-04	4.5E-06	3.1E-04	2.9E-06	7.1E-06	4.7E-06	4.1E-05
015 i2	1.0E-05	5.8E-05	4.8E-06	7.5E-05	4.8E-06	2.6E-06	3.4E-06	4.8E-06	3.6E-06	1.7E-06	8.4E-07	9.0E-06	5.2E-06	3.2E-06
005 i1			5.4E-06	5.2E-05	5.9E-06	3.4E-05	3.9E-06	2.8E-05	3.3E-06	5.5E-05	8.6E-07	5.5E-06	4.5E-06	3.2E-05
005 i2	1.3E-05	6.9E-05	5.2E-06	1.1E-04	4.8E-06	1.2E-05	3.5E-06	2.3E-05	3.5E-06	8.7E-06	8.4E-07	3.5E-05	5.1E-06	1.2E-05
005 i3	1.6E-06	3.7E-06	2.0E-06	2.6E-06	7.6E-06	6.1E-05	5.3E-06	8.9E-05	9.3E-06	4.1E-05	3.4E-06	5.7E-06	7.1E-06	3.4E-05
005 i4	1.6E-06	2.3E-06	2.0E-06	1.6E-06	7.6E-06	3.4E-05	5.5E-05	4.3E-05	9.1E-06	2.5E-05	3.2E-06	2.2E-06	7.0E-06	1.8E-05
004 i1			1.2E-05	1.4E-05			3.3E-06	2.3E-05			1.2E-06	7.3E-06	5.7E-06	2.2E-05
004 i2					7.2E-06	5.1E-05			3.4E-06	2.0E-05				
007	8.8E-06	9.0E-05	4.7E-06	1.2E-04	4.5E-06	4.3E-06	3.3E-06	8.0E-06	3.4E-06	2.6E-06	8.4E-07	1.7E-05	4.7E-06	4.4E-06
011			1.2E-05	2.9E-04	1.6E-05	3.1E-04	7.6E-06	2.5E-04	1.9E-04	1.2E-04			2.7E-05	2.2E-04
006 i1	1.2E-05	2.1E-05	4.6E-06	2.8E-05	4.0E-06	9.1E-06	3.1E-06	6.6E-06	3.2E-06	1.2E-05	8.0E-07	3.6E-06	4.4E-06	6.3E-06
006 i2	1.2E-05	4.0E-05	5.0E-06	4.6E-05	3.8E-06	3.0E-05	2.9E-06	2.8E-05	2.7E-06	2.5E-05	7.6E-07	7.4E-06	4.0E-06	2.7E-05
006 i3	1.1E-05	8.1E-05	5.0E-06	8.3E-05	4.7E-06	8.0E-06	3.4E-06	1.8E-05	3.5E-06	5.0E-06	8.5E-07	2.1E-05	5.0E-06	8.3E-06
006 i4	2.3E-06	8.7E-05	2.6E-06	9.2E-05	3.3E-06	1.5E-05	1.9E-06	2.3E-05	2.9E-06	1.5E-05	5.2E-07	1.9E-05	3.0E-06	1.3E-05
017i1	9.7E-06	2.0E-05	4.5E-06	2.8E-05	4.5E-06	6.0E-06	3.2E-06	5.1E-06	3.3E-06	9.0E-06	8.0E-07	3.2E-06	4.4E-06	5.2E-06
017i2	2.4E-05	9.2E-05	4.6E-06	9.2E-05	4.2E-06	7.0E-06	1.8E-06	8.2E-05	2.4E-06	9.7E-05	8.2E-07	7.0E-06	2.9E-06	8.2E-05
017i3	8.8E-06	3.8E-05	4.3E-06	5.9E-05	2.7E-06	2.8E-05	3.3E-06	3.1E-06	3.5E-06	1.4E-06	8.4E-07	4.9E-06	4.8E-06	2.0E-06
018	1.3E-05	2.4E-05	4.7E-06	4.0E-05	4.6E-06	1.4E-05	3.7E-06	8.7E-06	3.8E-06	3.3E-05	9.0E-07	4.7E-06	5.4E-06	1.1E-05
008	1.5E-05	5.3E-05	2.9E-06	8.5E-05	4.8E-06	1.3E-05	3.4E-06	9.0E-06	3.7E-06	1.2E-05	8.7E-07	4.5E-06	4.7E-06	1.2E-05
010			1.6E-06	5.3E-05	3.1E-06	2.5E-05	3.2E-06	1.1E-05	2.6E-06	2.2E-05	1.0E-06	2.7E-06	2.7E-06	1.9E-05

Table III.9 Transmissivities and storativities obtained from the best-fit matching procedure

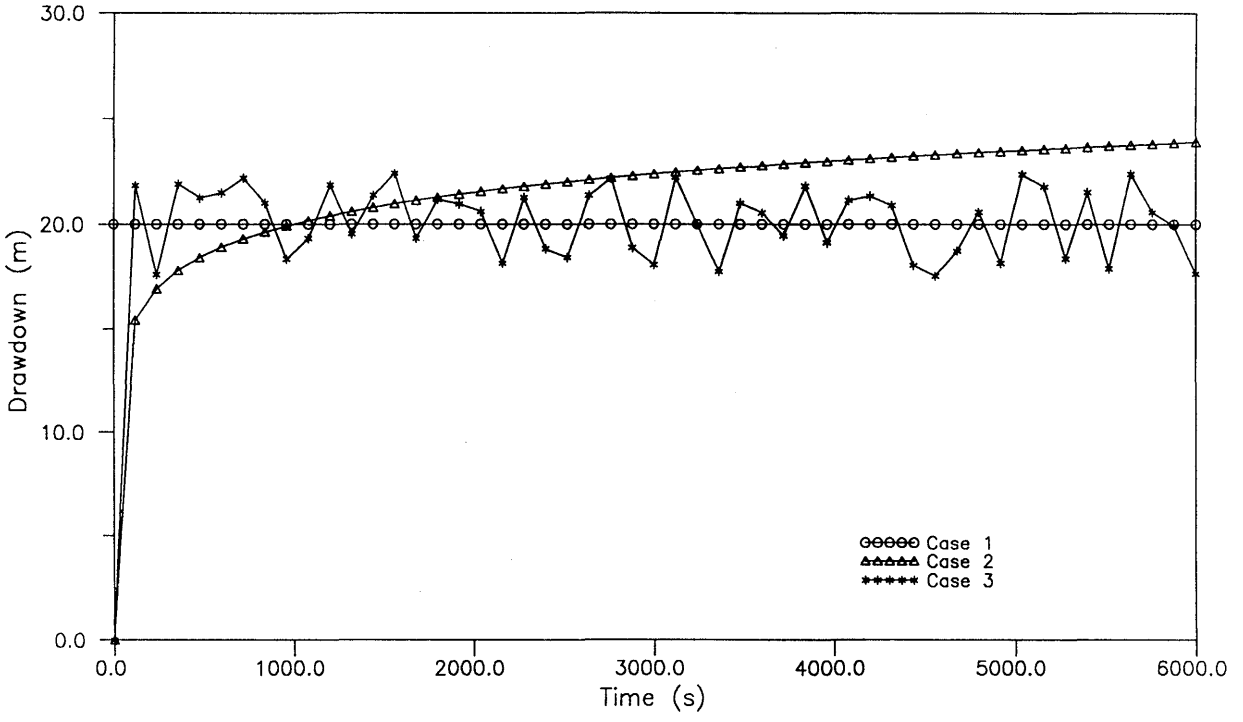

Figure III.20: Head variations used in the sensitivity analysis.

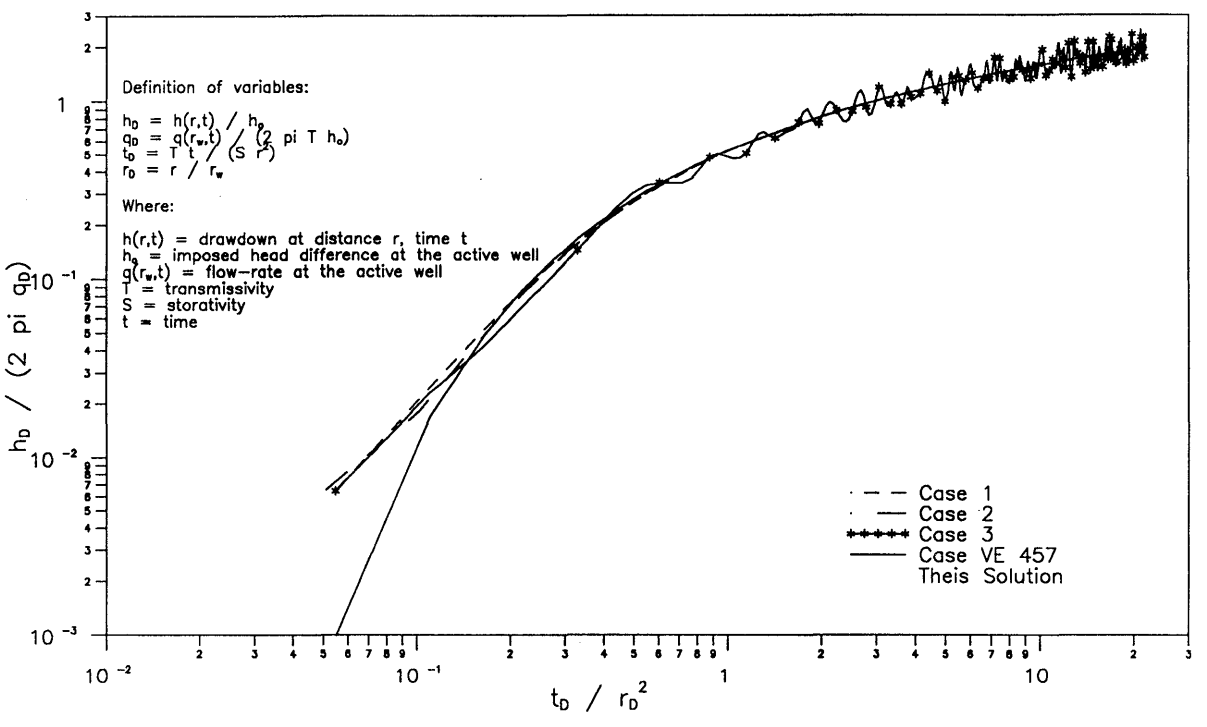

Figure III.21: Evaluation of the flux-normalized Theis approach.

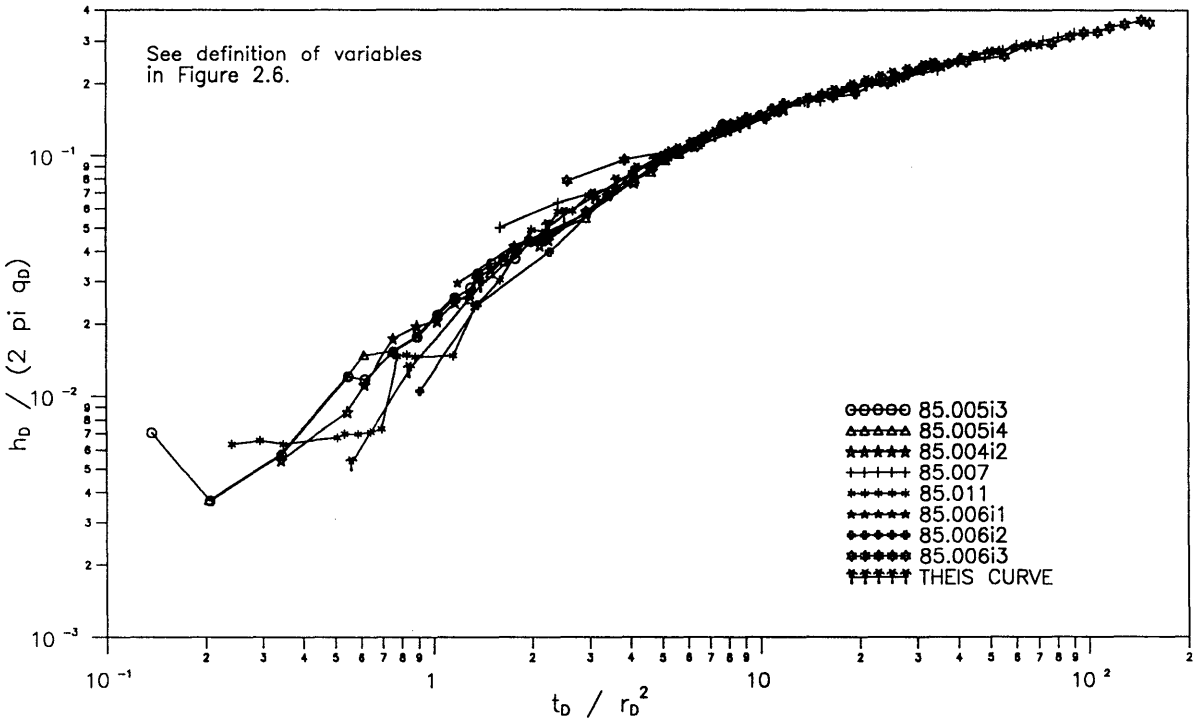

Figure III.22: Best-fit matches to the Theis curve. Test VE453.

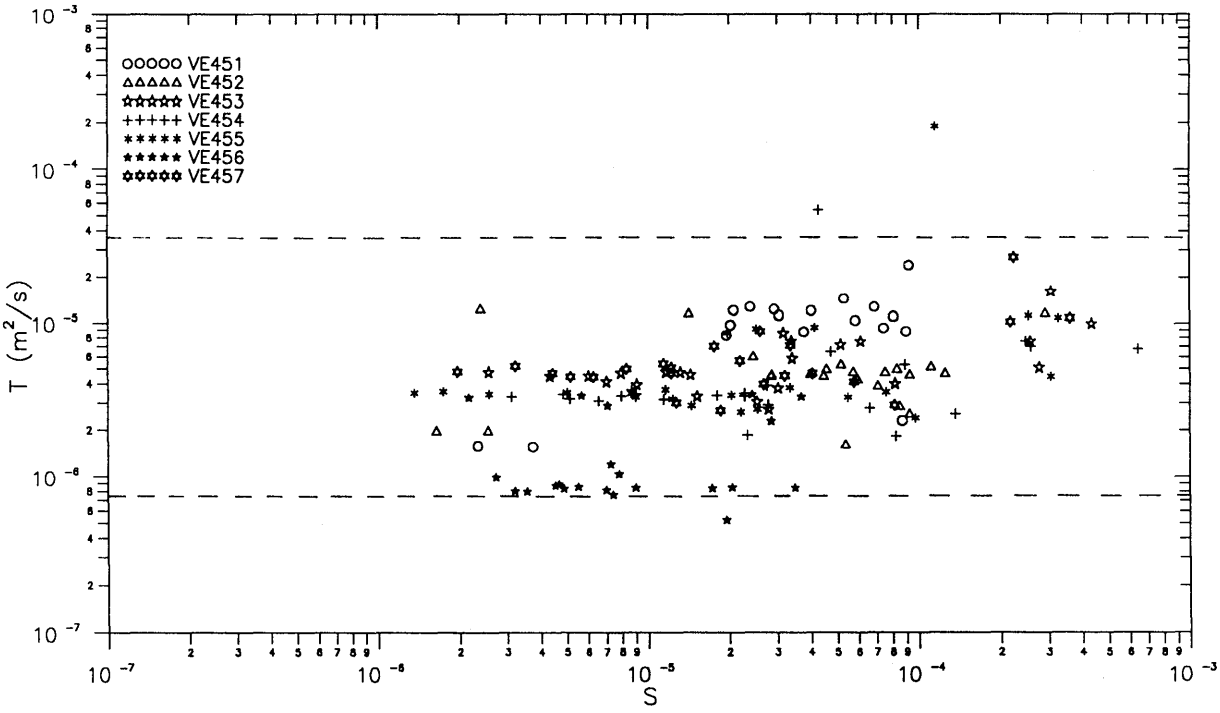

Figure III.23: Parameters obtained from the best fits to the Theis solution for all observation intervals.

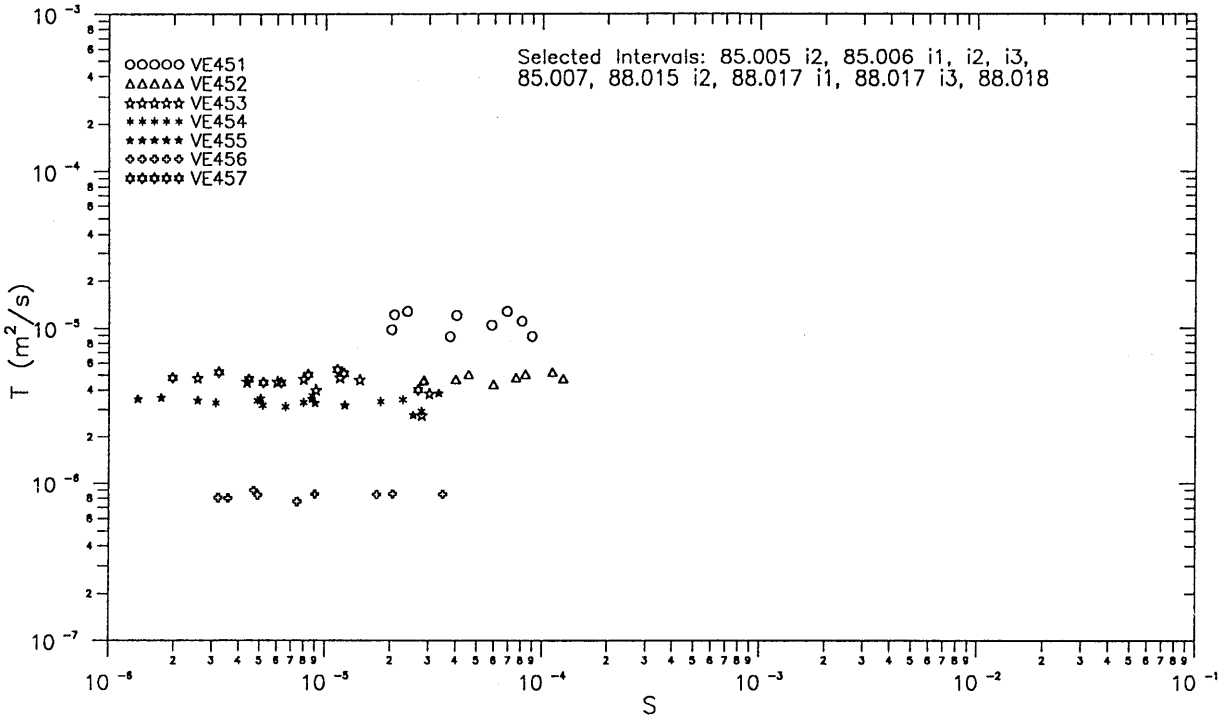

Figure III.24: Parameters obtained from best fits to the Theis solution. r is taken as straight line distance.

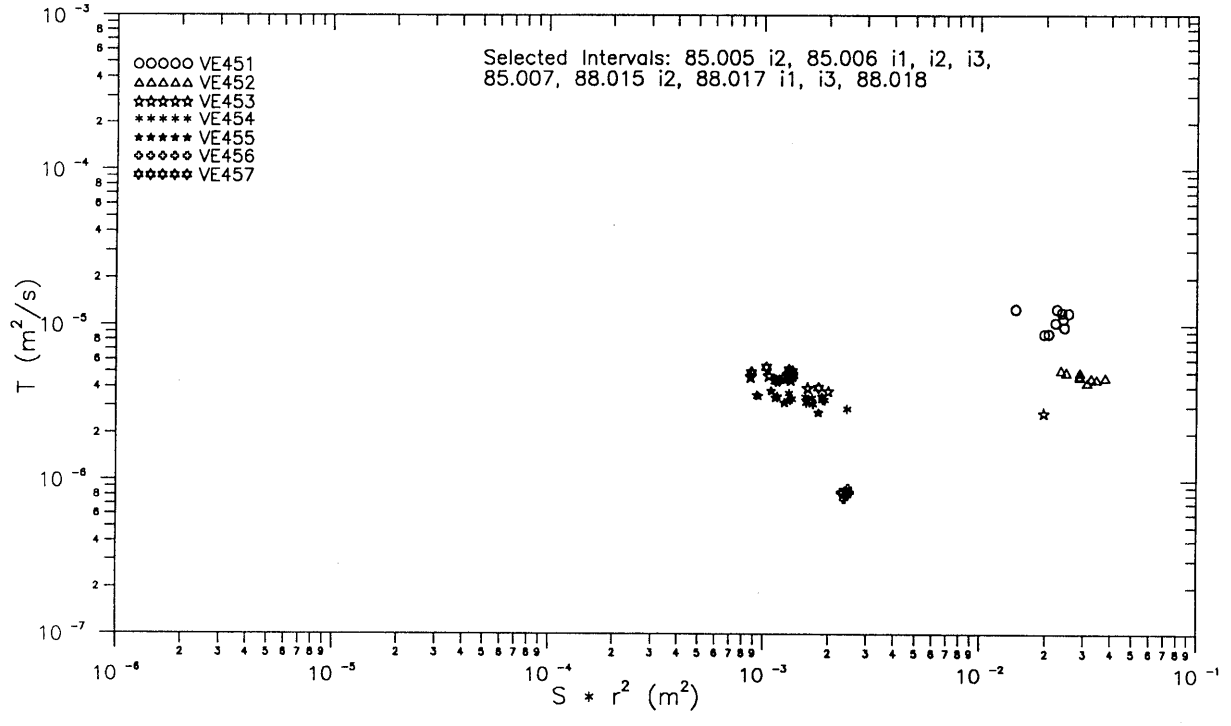

Figure III.25: Parameters obtained from best fits to the Theis solution. r is a unit value.

This is not true for S which is obtained from the matched value along the X-axis of the type curve, and this parameter will be strongly affected by errors in the value of r.

III.2.4 Summary and Conclusions

III.2.4.1 Implications for the Conceptual Model of the BK Zone

Certain intervals showed a similar response during each tests regardless of the relative distances between these intervals and the injection interval. This implies that the BK zone is not behaving as a homogeneous porous medium. Somehow these intervals must be connected by a highly transmissive feature such that when the pressure pulse reaches that feature, all the intervals intersecting it react in a similar fashion. The intervals which react in an identical fashion are:

borehole 85.005 i1
85.006 i1, i2, i3
85.007 i1
88.015 i2
88.017 i1, i2, i3
88.018 i1

The results presented in this section and in Section III.1 lead to a conceptual model of flow at the BK site which is schematically represented in Figure III.26. This flow model is compatible with the occurrence of radial or sub-radial flow at early times, followed by linear or bounded-system type flow at late times, due to the presence of boundaries. Also represented in this figure is the highly transmissive feature which affects the response in the intervals listed above.

The coordinates of the intervals which appear to intersect the feature were calculated and the intervals were plotted on a three dimensional representation of the BK site (Figure V.2). This image of the BK zone shows the selected intervals which are represented by their upper and lower packer positions. The surfaces represent the connection between the injection interval and points of maximum tracer inflow as observed during fluid logging (KELLEY & LÖW 1992, this volume). The correspondence between the results of the hydraulic tests and those of the fluid logging test is seen to be very good.

Correlation with existing geologic information is also convincing since it appears that the selected intervals intersect an important shear zone previously put in evidence by geologic fracture mapping (MARTEL and PETERSON, 1991, PAHL et al., 1992) and also by radar crosshole tomography (NIVA et al., 1988), (see Part V).

III.2.4.2 Significance of the Calculated T and S Values

Due to severe uncertainty in the true value of the diffusion path length (r), the calculated values of storativity presented in Table III.9 cannot be considered with any confidence. A meaningful value of storativity can only be determined if a good knowledge of the flow path

is known using detailed geological information and results from tracer tests. The storativity values determined during the single-hole test analysis (Section III.1) are not affected by the uncertainty on r, but these storativities cannot be considered representative of the bulk formation but rather of the immediate vicinity of the well.

As mentioned in Section III.2.3.2., the calculated transmissivities are not affected by the uncertainty on r. The main uncertainty with respect to the transmissivity values is related to the relevance of the flow model which was used for their determination. Transmissivities estimated from the analysis of the observation interval responses are in good agreement with those obtained from the single hole analysis (Section III.1).

An important question is how representative are these calculated transmissivity values with respect to the whole BK site? Since the total transmissivity in the direction of flow is the harmonic mean of the individual transmissivities, the values calculated for the intervals intersecting the high transmissivity feature are not representative of this feature, but relate to the bulk mass of rock investigated during the test. In order to have an estimate of the transmissivity of the feature, it is necessary to test that specific feature. Unfortunately, the plots of the measured response as a function of time (Section III.2.2.1.2) suggest that the injection interval did not intersect the highly transmissive feature during either of the tests. If it had, the response measured in the injection interval would collapse onto the ones measured in the intervals listed in the previous paragraph. This was not the case for either of the tests, the response in the injection interval was always higher than those observed in the observation intervals. The test which showed an injection interval response closest to the responses measured in the intervals intersecting the high transmissivity feature was test VE 457 (injection interval 6.7 - 10.7 m).

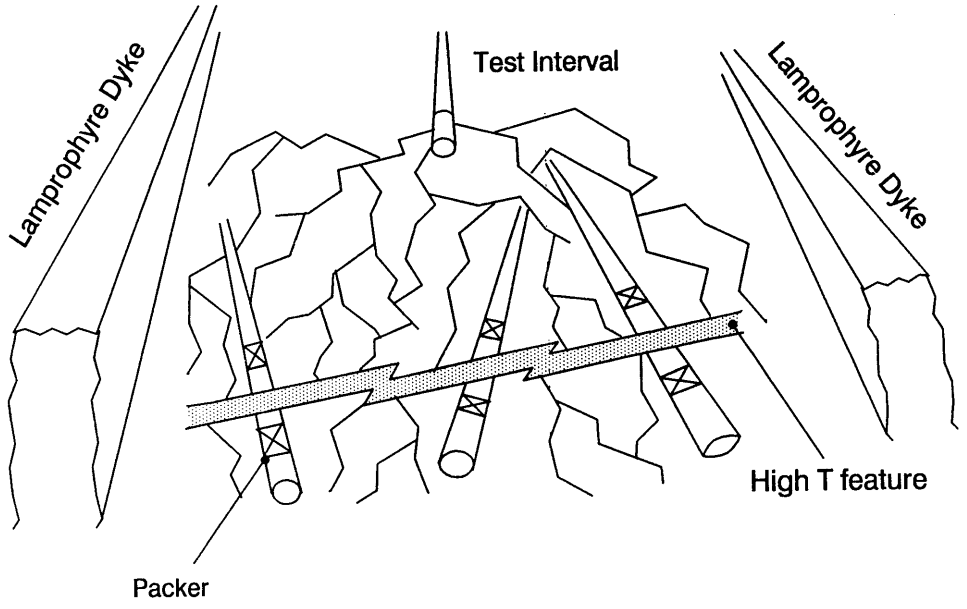

Figure III.26: Conceptual model of flow at the BK site.

PART IV

ANALYSIS OF A PILOT CROSSHOLE FLUID LOGGING TEST AT THE BK-SITE, GRIMSEL TEST SITE

Van Kelley and Simon Lõw

ABSTRACT

A pilot crosshole fluid logging test was performed in the BK-Area of the Grimsel Test Site (GTS). The fluid logging test ran from January 29, 1990 until February 8, 1990. The pilot crosshole fluid logging test consisted of logging various boreholes in the BK-Area with temperature-conductivity logs while a constant injection of tracer with constant concentration occurred somewhere in the well array. As each borehole was opened, flushed, and logged, connected fractures to the injection zone would produce traced fluid. From this experiment additional knowledge was hoped to be gained concerning the inter-borehole connections within the BK-Area. In addition, the test technique is experimental and for this reason interest also centered around implementation and performance of the crosshole fluid logging experiment.

The pilot crosshole fluid logging study was a success based upon the objectives of the experiment. The study (1) identified fractures with some form of connection between the injection borehole and the logged observation boreholes, (2) identified fractures at the observation wells which were apparently not connected to the injection well, and (3) because of the success in 1 and 2 validated the crosshole fluid logging technique for fracture system characterization. With the testing method described in this report it was possible to determine a great amount of information on fracture locations in a very short time span (in this case 9 days of testing). In total, 53 individual inflowing fractures were clearly defined and isolated to a specific borehole depth. Of these, 34 were connected to the injection borehole as indicated by tracer inflow and 19 were apparently not connected and did not receive tracer breakthrough.

The measured conductivity logs exhibited a very complex behavior indicative of the complex transport characteristics associated with a fracture system. There was evidence in the observed logs of transient inflowing concentration occurring at given inflows. This was surely expected, as each test emulates a complicated unequal strength dipole tracer test. In addition to having time varying inflowing concentration, each inflow is a unique tracer breakthrough and, for this reason, inflowing concentration also varies as a function of inflow location within the borehole.

Quantitative analysis focused using the Method of Partial Moments to calculate interval flow rates within each logged borehole. The measured logs were not optimal for this analysis method because of (1) quick peak development, (2) strong peak interference due to lots of inflows over short intervals, and (3) a large percent of the inflows are of low mass flux. However, the utility of this method proved substantial even under less than ideal conditions, as the method reproduced total borehole flow rate extremely well in the six boreholes in which it was applied. The finite difference conductivity log simulator BORE was used to calibrate inflow parameters for two suites of logs, Borehole 88.015 (Test VE463) and Borehole 85.009 (Test VE464). These calibration attempts were largely successful and resulted in first order estimates of inflow volumetric rates and concentrations. BORE calibration provides both flow rate and concentration which are both important to know in these types of experiments because flow rate is indicative of interval transmissivity

and inflowing interval concentration is indicative of the degree of connection between the injection and inflow intervals.

The success of this pilot study warrants additional investigations of this type. This report also makes recommendations for further crosshole fluid logging investigations.

IV.1 INTRODUCTION

A pilot crosshole fluid logging test was performed in the BK-Area of the Grimsel Test Site (GTS) from January 29 to February 8, 1990. The BK-Area is situated in a granitic to granodioritic rock that shows a slight foliation striking E-NE and dipping approximately 70 degrees to the south (KEUSEN et al., 1989). Based upon radar tomography and geologic mapping two steeply dipping major fracture zones occur to the south and northwest of the BK testing drift (NIVA et al., 1988) and are intersected in part by the testing boreholes drilled from the drift (BRÄUER et al., 1989). A detailed geologic description of the BK-Area is given in BRÄUER et al., (1989) and PAHL et al., (1992). The BK-Area of the GTS has been set aside for the study of flow and conservative tracer transport within a complex fracture zone on a scale of tens of meters.

The BK-Area has 17 boreholes drilled in it for characterization and testing purposes. Figure III.1 in GUYONNET and LAVANCHY (this volume) presents a plan view of the BK-Area with the boreholes designated by number. There are four curtains of boreholes which radiate out from the tunnel wall in vertical planes, A through D. Figure III.2 section III, shows these four planes as viewed normal to them. The relative coordinates (last three digits of Swiss Coordinate System), the dip and azimuth, and apparent depth of each well are listed in Table 1.1 of KELLEY and FRIEG, (1990).

The pilot crosshole fluid logging test consisted of logging various boreholes in the BK-Area with temperature-conductivity logs while a constant injection of tracer with constant concentration occurred somewhere in the well array. As each borehole was opened, flushed, and logged, connected fractures to the injection zone would produce traced fluid. From this experiment additional knowledge was hoped to be gained concerning the inter-borehole connections within the BK-Area. In addition, the test technique is experimental and for this reason interest also centered around implementation and performance of the crosshole fluid logging experiment.

The implementation of the fluid logging pilot test was a cooperative effort between NAGRA (Nationale Genossenschaft für die Lagerung radioaktiver Abfälle) and BGR (Bundesanstalt für Geowissenschaften und Rohstoffe). The design and fielding of this test was performed in part by the COLENCO/INTERA group for In-Situ Testing (UGIV) and is described in KELLEY and FRIEG (1990). The measurement of the electrical conductivity and temperature logs was performed by GEOTEST AG under the direction of Mr. P. Holub.

IV.2 TEST HISTORY

IV.2.1 Test Objectives and Test Design

The primary objective of the pilot crosshole fluid logging test was to acquire as much knowledge as possible concerning the connection of fractures between the various BK-Area wells. The BK-Area rock is a fractured granite with a low primary porosity. The granite matrix has little retardation capacity for transport because of the low primary porosity (i.e., storage capacity). For this reason, local-scale transport within the BK-Area would probably be controlled by the secondary porosity made up of fractures and some shear zones.

Two primary methods are available for the modeling of a fracture network. The easiest method is through the use of continuum-based models which assume that a REV can be defined and is much smaller than the scale of the modeled region. A second technique is the discrete modeling of a fracture network. In this case, the assumption of a REV within the scale of transport is not a requirement. However, to determine which approach is suitable, one must know something of the density of fractures, and more importantly, the fractures contributing to flow (HSIEH et al., 1983). Because of the large data requirements and the typical unavailability of this data, the models have been restricted to research application. Therefore, it is not enough to determine interval transmissivities; we must also know such things as fracture density and geometry.

Various methods are available to evaluate the location of fractures, such as geophysical logging and cores, but these methods do not give one clear insight into which fractures are active with respect to flow. PAILLET et al. (1987) found that highly transmissive fractures did not differ from significantly less transmissive fractures when evaluated by televiewer and resistivity logs. Standard hydraulic tests can provide a vertical distribution of transmissivity, but attributing discrete features to the transmissivity is indirect and resolution is limited to the packer separation. In addition, these methods are time and budget intensive. The need for techniques to gain insight into borehole connections in a fractured rock has been well documented (SILLIMAN and ROBINSON, 1989). These investigators have reported on using temperature logging of observation wells during pumping at a central well to infer crosshole fracture connections in the Oracle Granite (Arizona, USA). They concluded that their technique provided good insight into fracture connections through a nondestructive method which introduced no foreign substances to the ground-water system.

Previous investigations aimed at better understanding the fracture location, connections, orientations, and transmissivities within the BK-Area have been performed by BGR and NAGRA. Of the activities performed by BGR, two are of particular interest. The first, referred to in this report as the Bräuer fracture list, is a list of water-transmissive fractures compiled by Bräuer and published in PAHL et al., (1992). This list was compiled by drilling a given borehole with overpressure and then monitoring various other boreholes with multipacker systems. When a significant pressure response was monitored, the fracture system thought to be transmissive was located through core descriptions. The second data base regarding fractures in the BK-Area is the results of a series of Lugeon tests (injection) performed in a series of boreholes. During these tests, a constant head injection was

performed in 1 m intervals over the entire length of the borehole. From this, a transmissivity distribution could be defined for the borehole. These results are simply referred to as the Lugeon tests and are presented in LIEDTKE (1988). In addition, BGR performed a series of dipole tracer tests in various isolated fractures, the results of which were not directly usable for the investigation described herein.

NAGRA, in cooperation with the Swedish Geological Co., performed geophysical measurements in an attempt to learn something about fracture locations. In the BK-Area of the GTS, electromagnetic Geo-tomography was used to determine borehole connections and major area fracture zones (NIVA et al., 1988). Based on the radar tomography results and geologic mapping, the presence of two steeply dipping major fracture zones to the south and northwest of the BK testing drift were discovered (NIVA et al., 1988). These primary fracture zones intersect some of the BK-Area boreholes.

To gain additional information concerning fracture zone locations and well-to-well fracture connections, NAGRA designed a crosshole electrical conductivity fluid logging test. The test was designed so that a central well injects a tracer and then boreholes are sequentially logged to determine inflow points. A primary design criterion was that the test was limited to a two-week time period. In the design, there were four fundamental items in need of specification. They were (1) the injection interval, (2) the order by which boreholes were opened and logged, (3) the injection rate, (4) and the injection concentration. The injection interval chosen was based on the hydraulic tests performed immediately prior to the fluid logging test, which are described in GUYONNET and LAVANCHY (this volume). The hydraulic tests were injection tests performed over various intervals in Borehole 85.004. The interval chosen as the tracer injection interval (6.7 to 10.7 m) was the most transmissive interval and created the strongest pressure transience over the BK-Area during testing.

The order in which the boreholes would be logged was based upon their location and their reactions as observed in the hydraulic interference testing. An advantageous and natural borehole sampling order would be to first log the closest and best connected boreholes to the injection borehole and through time move away from the injection borehole to further, presumably less connected, boreholes. The order proposed for opening and logging was 85.007, followed by 85.006, 88.017, 85.018, and 85.010. From Figure III.1 (GUYONNET and LAVANCHY, this volume), it can be seen that these boreholes extend away from the injection borehole in a NE direction. An overall test objective was to maximize the amount of information (i.e., borehole coverage) in a two-week test period. Therefore, if all these boreholes could be logged in the first week of the test, then in the second week of testing the logging order would move away from borehole 85.004 in a SW direction. If tracer travel was slower than expected, or difficulties arose and by a week's time not all these boreholes were logged, then the investigation of the boreholes to the SW of 85.004 would still be adopted for the second week. The order of borehole logging in a SW direction was first 85.005, followed by 88.015, 85.009, 88.013, and 88.016. To maintain a gradient in the direction of logging, it was considered essential to keep at least one borehole in the direction of logging open at all times.

The design injection rate was proposed to be 1.0 l/min. In the field

prior to testing, the rate was decreased by a factor of two to 0.5 l/min and this was the rate maintained during testing. The design injection tracer concentration was 10,000 µS/cm. This value was based upon dilution factors (C_{inj}/C_{max}) observed by BGR in unequal dipole tracer tests. The factors they received varied from 36 to 79 for tests VE439 and VE449 respectively. With a maximum dilution factor of 79, we still could receive enough conductivity difference to detect inflows. However, the contrast would be at the limit for quantifiable results.

IV.2.2 Test Description

The pilot fluid logging test was performed after the hydraulic interference tests analyzed in GUYONNET & LAVANCHY (this volume). The fluid logging test ran from January 29, 1990 to February 8, 1990. Over the course of 9 days, 7 boreholes were examined with full temperature and electrical conductivity profiles. These boreholes are, in the order of logging, 85.007, 85.006, 88.017, 85.008, 85.005, 88.015 and 85.009. Therefore, 4 boreholes were logged in a NE direction and 3 boreholes were logged in a SW direction from the injection borehole. A total of 67 electrical conductivity and temperature logs were measured over the 11-day test period. These logs will be referred to as logs 1 through 67 in this report.

The tracer injection was started on January 30, 1990 at 10:10. At 10:17 the pump failed due to a system failure. The injection was re-started at 10:29 and was continuous until the end of the logging campaign at 14:58 on February 8, 1990. Figure IV.1 shows the time period of the test, with the injection period and the period each borehole was open. This figure allows for an easy method to see the relative time each borehole was open, as well as the periods when more than one borehole was open.

Because the logged boreholes are all inclined at varying angles from the vertical, the fluid logging apparatus had to be modified to perform at these angles. The apparatus is fully explained in the field report prepared by GEOTEST (KELLEY & FRIEG, 1990). As the logging conditions are thought to be important for understanding the conductivity log development, the method will be described briefly. The conductivity probe will at all times be in contact with the borehole wall in the inclined boreholes, therefore the probe will not pass smoothly down the borehole. As a result, a pulley assembly was installed in the bottom of each borehole prior to logging. As the probe was lowered into the borehole, a line attached to the bottom of the probe and leading through the pulley assembly and back to the surface was maintained at some pressure to allow easy movement of the probe.

The basic test procedure for a given borehole was as follows. First the packers were deflated in the borehole and the pulley assembly and logging tool were installed. An initial log was then run to determine if tracer breakthrough had occurred. When tracer was detected in the open borehole the borehole was flushed with fresh water with a conductivity of approximately 28 µS/cm. After flushing, a series of conductivity logs were measured in the borehole on a time scale appropriate for the maximum borehole velocity.

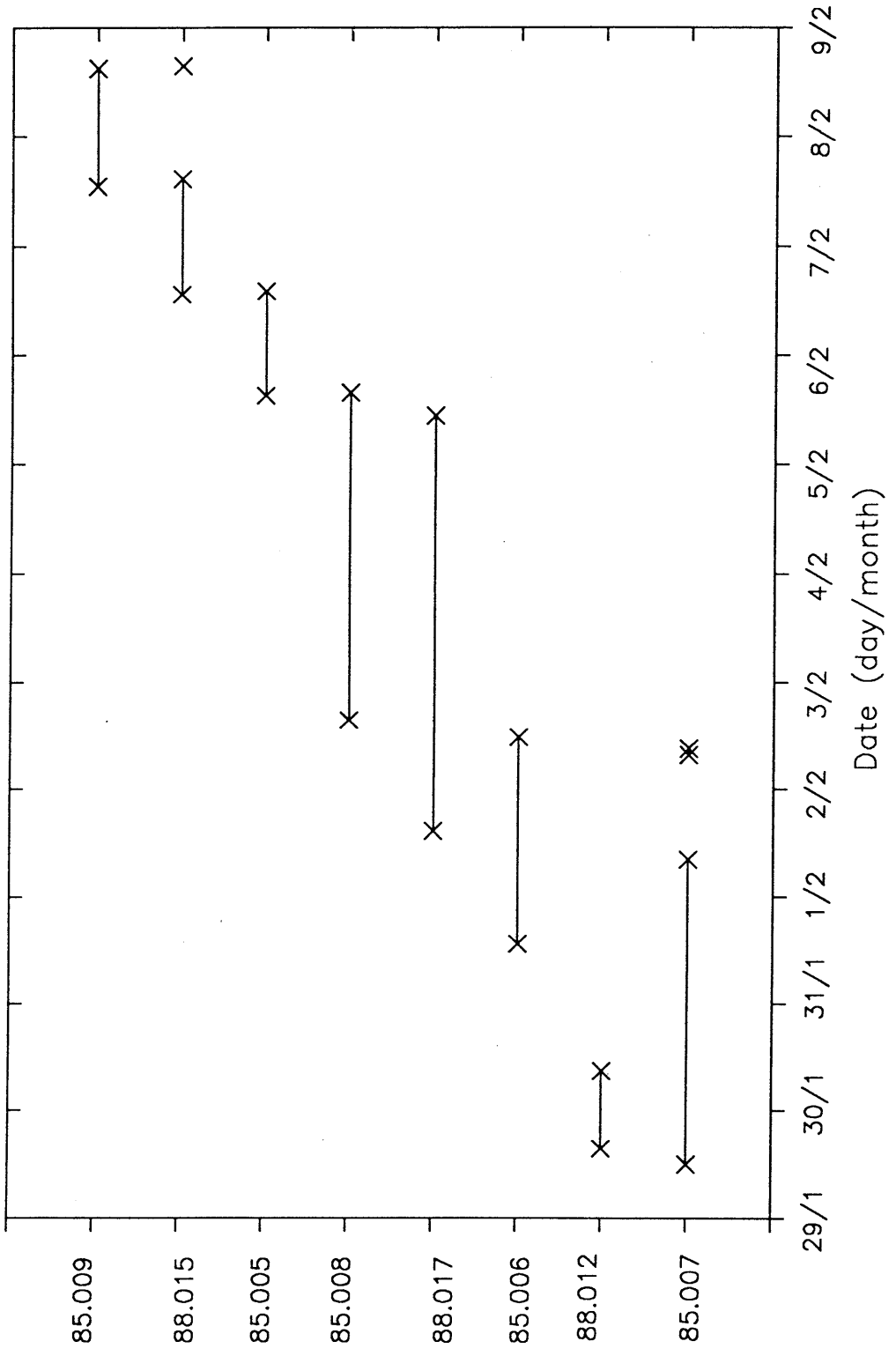

Fig. IV.1: Time Line Showing When BK Boreholes Were Open During the Pilot Fluid Logging Cross-Hole Test

IV.3.0 ANALYSIS OF FLUID LOGGING TESTS

IV.3.1 Conceptual Model for Analysis

Before the analysis of the fluid logs is performed, it is appropriate to briefly discuss the governing conceptual model used for analysis. By definition, the conceptual model is less complex than the physical system and processes actually existing. This is considered a simple borehole conceptual model which shares predominant traits with the physical borehole system but cannot fully share the inherent complexity. The conceptual model used to analyze conductivity logs requires assumptions. By establishing what these assumptions are, non-idealities in the data being analyzed can be better understood.

The conceptual model used herein is taken from a series of sources but most recently was presented by TSANG et al., (1990). Figure IV.2 shows a schematic of a borehole with a series of inflows. To detect an inflow with a conductivity log requires that the inflowing feature produce into the borehole with a fluid of different concentration than that already existing in the borehole. For the sake of discussion, we will consider the borehole fluid to have a concentration which is negligible compared to the produced formation fluid.

As the inflow produces water into the borehole a concentration peak develops emanating from the inflow point. The mass flux from a given inflow (i) is simply the product of volumetric flow rate (q_i) and inflowing concentration (C_i). As the mass flows into the borehole it is transported up the borehole through an advective-dispersive process. As can be seen in Figure IV.2, the borehole flow rate, and therefore mean borehole velocity, will increase as you move up the borehole and encounter more inflows. The governing equation which is accepted to apply to our borehole transport is the 1-dimensional advection dispersion equation written (TSANG et al., 1990)

$$K \frac{\partial^2 C}{\partial x^2} - v \frac{\partial C}{\partial x} + G = \frac{\partial C}{\partial t} \qquad \text{(IV.1)}$$

where C is concentration, K is the dispersion coefficient, and G is a source term which represents the mass flux occurring at the various inflows produced by their borehole intersection. Equation IV.1 is one dimensional and for this reason it assumes that the concentration measured and used in the above equation is a cross-sectional averaged concentration. For non-turbulent and turbulent conditions TAYLOR (1953 and 1954b) described the conditions when Equation IV.1 could be used to describe transport of a conservative tracer in a smooth tube. The conceptual model of the borehole is that of a simple tube which is fed by multiple inflows.

The determination of whether the flow regime is laminar or turbulent is easily calculated by calculation of the Reynolds Number. The Reynolds Number is equal to:

$$Re = 2 v r_w / p_k \qquad \text{(IV.2)}$$

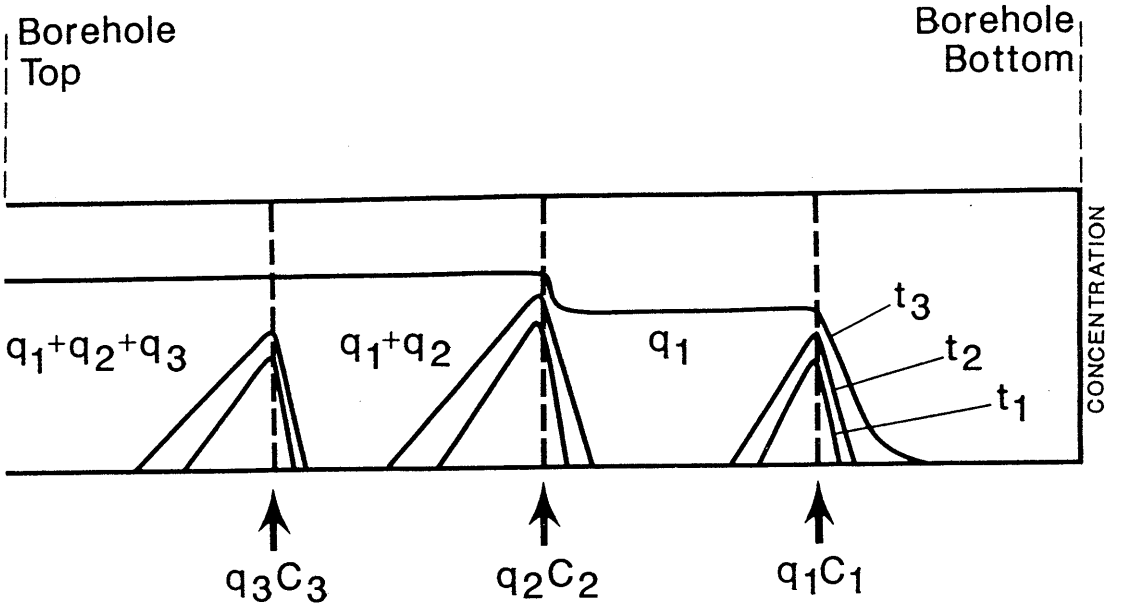

- $(C_3 = C_2) > C_1$
- t_1 and t_2 are early times
- t_3 is late time, "saturated" conditions
- At late time the theoretical maximum borehole concentration is calculated by

$$C_{max} = \frac{\sum_{n=1}^{i} q_n C_n}{\sum_{n=1}^{i} q_n}$$

Fig. IV.2: **Borehole Conceptual Model (after Tsang et al., 1990)**

where v is equal to the mean borehole velocity, r_w is equal to the borehole radius, and p_k is equal to the kinematic viscosity. The hydraulic regime is considered laminar for Reynolds Numbers less than 2000. For all boreholes logged in this pilot field test, the radius was equal to 0.043 m. If we assume a fluid density of 1000 kg/m^3 and a viscosity of 0.001 kg/m s, then the Reynolds Number criteria is never violated during any test.

For laminar flow conditions, Taylor defined an apparent dispersion coefficient which would theoretically be the applicable dispersion term for Equation IV.1. As to the validity and applicability of Taylor's apparent dispersion term under laminar flow conditions, he specified a detailed set of criteria to be met. Taylor understood that the velocity profile in a tube was parabolic rather than radially constant, and that the transport of a conservative constituent in a tube was a two-dimensional process at least for some time. However, TAYLOR (1953 and 1954a) found that, after a certain distance of travel, a traced pulse moved in the tube at a mean velocity and the mass was symmetrically distributed about the center of mass which migrated at the mean velocity. This was true even though the axial velocity profile in the tube was asymmetric. From this finding, he established that a 1-dimensional advection-dispersion equation was adequate to describe the concentration migration where the dispersion term was defined

$$K = r_w^2 \, v^2 \, / \, 48 \, D_o \qquad \text{(IV.3)}$$

where D_o is the free-water diffusion coefficient. The two criteria which Taylor defined where 3.3 is applicable can be written

$$v \geq 69 \, D_o \, / \, r_w \qquad \text{(IV.4)}$$

and

$$L \geq 690 \, r_w \, / \, 4 \qquad \text{(IV.5)}$$

The criterion identified by Equation IV.4 insures that the longitudinal molecular diffusion is significantly less than the dispersive effects caused by velocity variation. The second criterion represents a minimum distance over which the concentration front must advect before the Taylor dispersion term is applicable. By the time the pulse has traveled this far, a balance exists between the longitudinal advective transport and the axial diffusive transport.

Assuming a free water diffusion coefficient of 1E-9 m^2/s, the velocity in the borehole must exceed 1.6E-6 m/s, which corresponds to a borehole flow rate of approximately 0.1 l/min. The transport length calculated in Equation IV.5 is 7.4 m. This length is significant when one considers that most of the boreholes logged were in the order of 40 to 50 m deep. The applicability of these equations, or their meaning, for the case of moving a displacing tool through the concentration profiles as is done during logging is suspect. One would expect the fluid logging tool to effectively relax both criteria. In practice, the theoretical Taylor dispersion coefficient is not the dispersion coefficient (Equation IV.3)

which best describes observed field data (LÖW et al., in preparation). This is not surprising as the borehole is not a smooth tube and the tool should have the effect of increasing the observed dispersion. Also, given that fluid logging tool is used without borehole centralizers (i.e., it rests on the borehole wall), it is almost certain that the measured concentration will not be an axially averaged value. This is in violation of the use of Equation IV.1. This problem will be further discussed in light of the observed fluid logs in Section IV.4.

Before moving into the analysis one last equation will be introduced. A useful equation for the analysis of conductivity logs is that which calculates the theoretical maximum (i.e., steady state) concentration that a given inflow (i) should obtain. This equation is given by (TSANG et al., 1990)

$$C_{max,i} = \sum_{n=1}^{i} q_n C_n \Big/ \sum_{n=1}^{i} q_n \qquad \text{(IV.6)}$$

Where q_n and C_n are volumetric flux and concentration respectively coming from inflow n (see Figure IV.2). In this equation it is assumed that the initial borehole concentration is zero and that no volumetric or mass flux enters through the bottom of the borehole. In this case, if all inflows are of a similar concentration (C_i), then no matter what the variation of flow rates, the C_{max} for each peak will be equal to the inflowing concentration C_i. If however, the inflowing concentrations are different, and potentially transient as in these logs, then the theoretical C_{max} for each inflow will be different. When all inflows in a given borehole attain their relative C_{max} concentrations, the conductivity profile is referred to as being saturated (TSANG et al., 1990). An important assumption for the use of Equation IV.6 is that q_i and C_i are constant. In regards to the expected behavior of our fluid logs, it can be expected that the inflowing concentration will be transient as at each inflow point we are effectively sampling a breakthrough curve.

IV.3.2 Data Measured and Analysis Tools

The raw data measured during each logging run is electrical conductivity and temperature. Temperature is measured because the electrical conductivity is temperature dependent. Immediately after logging the conductivity data is temperature compensated to 20°C by GEOTEST. In addition to the two raw data types recorded, GEOTEST also computes a temperature gradient log. This gradient log is typically computed in real-time on-site by the logging contractor.

The analysis of the 7 fluid logging tests, designated VE458 through VE464, will be done in the chronological order they were tested. The analysis of each test will first be of a qualitative nature, identifying inflow points and tracer arrival times. For the qualitative identification of inflow points all three basic data types described above are used. Each data type offers a unique advantage in their use and each type has problems associated with it. In the next few paragraphs, some detail will be given as to how the three data types can be used to interpret the borehole inflow conditions.

The first type of data, and the primary type of data, used to identify inflows is the temperature compensated conductivity log. These logs identify where mass flux is occurring into the borehole. These data are good for determining borehole connections by identifying traced versus non-traced inflows. These are the only data which give a measure of the inflowing concentration occurring from an inflow. Saturated profiles yield good information concerning relative inflowing concentration and through quantitative analysis these logs can yield estimates of q_i and C_i (TSANG et al., 1990). The problem with these logs is that inflows which have little mass flux may be hard to detect and minor peaks which are downstream of a major inflow are strongly interfered with and therefore are hard to delineate.

An assumption used in this analysis is that the injected fluid is approximately the same temperature as the ambient groundwater in the local BK-Area. This assumption is felt to be a good one because the injection reservoir rests in the tunnel which is temperature controlled by the rock mass. BORE calculations also support this assumption as will be discussed later. The temperature log gives a measure of relative volumetric flux as it is distributed about the various inflows. This response is independent of C_i and fully dependent upon q_i and the accumulated inflowing volumetric rate which occurs downstream of inflow i (see Figure IV.2). The first log after flushing holds the most information as this log contains the least amount of inter-peak interference. The good thing about this data type is that it decouples volumetric flux from mass flux and it is very good at identifying low mass flux inflows which may be high volumetric flux features. The problem with this data type is similar to the conductivity logs in that interference downstream from a high volumetric flux is high.

The final data type is the temperature gradient which contains the high frequency information present in the temperature profile. Because this log exaggerates changes in temperature, this data can make more obvious minor inflows. The primary strength of using this data is that it does allow for the best resolution of inflows which are interfered with. The best example would be the identification of minor inflows on the downstream side of a large volumetric flux interval. The combined use of these three data types gives a relatively complete look at the inflowing regions in a given borehole.

Where possible, a quantitative analysis will follow a qualitative analysis of the measured conductivity logs. The primary codes used for this phase of analysis are MOMENT and BORE. The code MOMENT and its method are fully described in LÖW et al. (1991). Very little theory will be provided in this report. However, a complete nomenclature section in which the various MOMENT quantities are defined is included as Appendix A of this report. BORE is a 1-dimensional finite difference code which has been developed for the analysis of electrical conductivity logs through forward analysis. This code is fully documented in HALE & TSANG (1988) and the use of this code in the analysis of fluid logs is documented in TSANG et al. (1990). MOMENT was applied in the analysis of 6 out of the 7 boreholes in which logs were measured. BORE was applied in only 2 of 7 boreholes in which logs were measured. BORE was applicable for all suites of logs; however, due to a finite amount of time available for analysis, it was only applied on logs from boreholes 88.015 and 85.009.

IV.3.3 Test VE458, Borehole 85.007

IV.3.3.1 Qualitative Description and Analysis

Borehole 85.007 was opened on January 29, 1990 at 12:00. The logging runs designated 01 to 04 were experimental logs used to formalize techniques and to calibrate the system. Typically, the logging tool is run with centralizers which keep the tool in the center of the borehole. From experience gained from these first logs it became evident that the tool centralizers offered too much resistance to be used. During the course of testing each borehole, manual measurements of the borehole flow rate and the concentration of the effluent were taken. The summary of these data for Borehole 85.007 are listed in Table IV.1. The borehole was left open overnight with no injection of tracer occurring.
On the morning of January 30, 1990 the borehole was flushed from 7:30 until 8:46. The first suite of logs (05 - 13) were run after flushing (Figure IV.3). Continuous injection of the tracer at Borehole 85.004 did not start until 10:29. Logs 05 and 06 were measured before injection started whereas logs 07 through 13 were measured after the beginning of tracer injection. From Table IV.1 we see that outflow during the measurement of logs 01 through 13 was approximately 0.1 l/min. This corresponds to a very low Reynolds Number equal to 25 and a mean maximum borehole velocity of 1 m/hr.

The logs 05 through 13 were measured approximately 15, 53, 122, 158, 198, 262, 326, 380, and 425 minutes after the end of flushing. The flushing fluid has a mean concentration of approximately 27 to 28 μS/cm corrected to 20°C. The Grimsel formation water has a mean concentration of approximately 80 μS/cm corrected to 20°C. Because of this contrast, identification of inflows was possible even without getting tracer breakthrough. The tracer did not breakthrough at the well during the measurement of logs 05 through 13 and therefore all inflow points identified in these logs contained non-traced, ambient formation water. These logs are very noisy because of the low concentration values. From Figure IV.3 plots both the conductivity and temperature Logs 05 through 13. The lowermost well defined inflow occurs at a depth of 30.4 m. The next highest inflow appears at approximately 26.6 m. On the earliest logs 5 and 7 there is evidence for a inflow at a depth of 24 m. There is some evidence for minor inflows around 35 m which appear as a concentration plateau which is non-Fickian in nature in log 11.

From reviewing the temperature logs, more insight can be gained. The Grimsel formation water is slightly (2°C) warmer than the flushing fluid. This gives a secondary method of identifying inflows. In addition, the temperature logs are an indicator of non-traced inflows of formation fluid. From log 05, the three primary peaks are located at 30.4, 26.8, and 24.1 m, respectively. When reviewing the temperature gradient logs 05 through 13, the main inflows are easily seen. In addition, the temperature gradient logs (not shown) indicate that minor inflows are potentially occurring between the depths 7 and 20 m. After measurement of log 13, the borehole was again left open until the next morning.

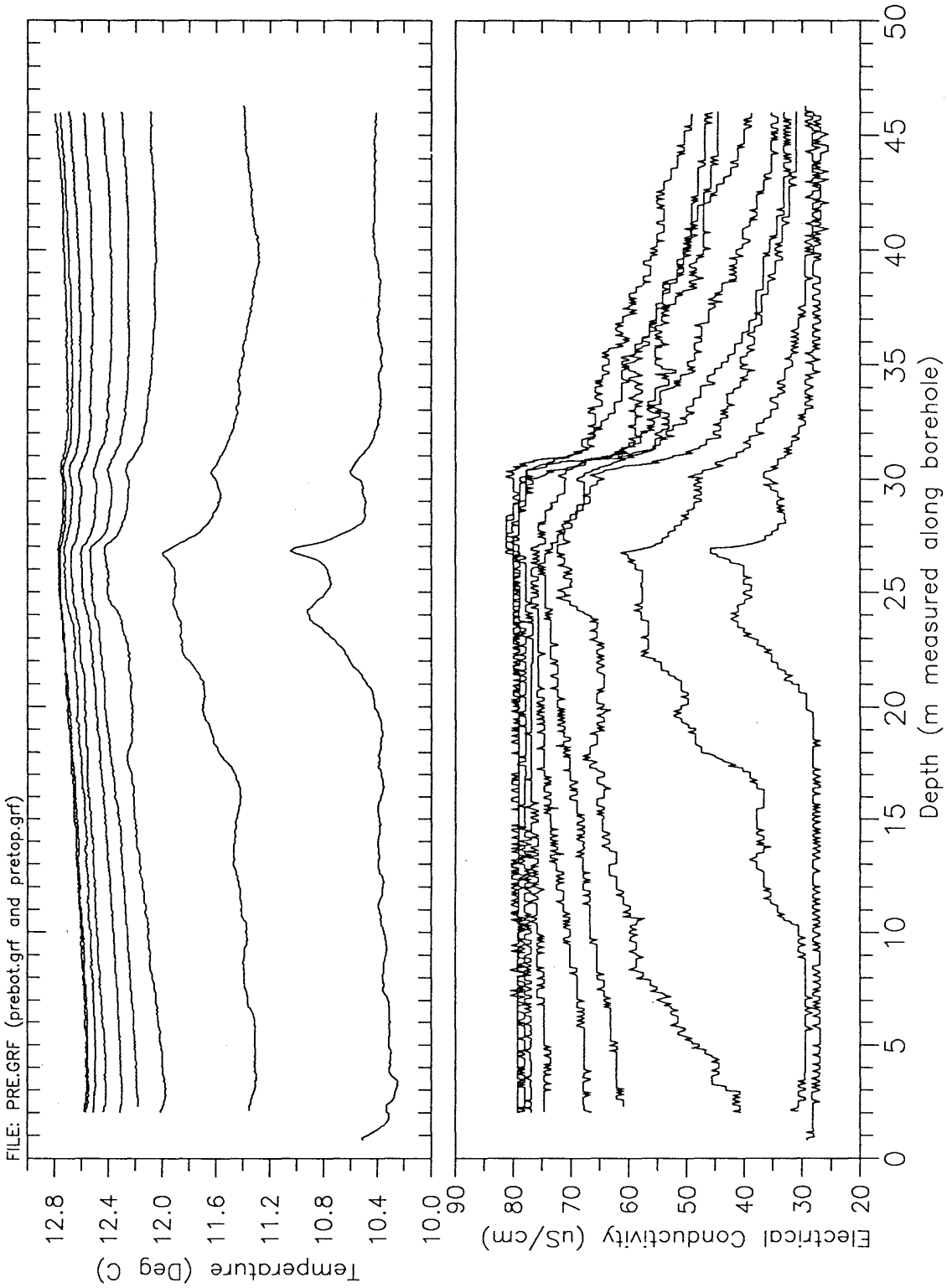

Fig. IV.3: Conductivity and Temperature Logs 5,6,7,8,9,10,11,12, and 13 Borehole 85.007, Logging Times 15,53,122,158,198,262,326,380, and 425 Minutes After First Borehole Flushing

Table IV.1 Measurements of Conductivity and Flow Rate Measured at the Borehole 85.007 Wellhead During Logging.

Date (Day/Month)	Time	Conductivity (μS/cm)	Flow Rate (l/min)	Comments
29/1	14:00		0.1	
30/1	08:46	30		Meas. at end of flushing
30/1	11:30		0.1	
30/1	15:15		0.1	
31/1	07:25	140 - 150	140 - 150	Uncorrected

On the morning of January 31, 1990 the first log (14) was measured before flushing the borehole. Figure IV.4 shows the last log taken on the afternoon of January 30 (log 13), with the first log taken on January 31. It is evident that the tracer has arrived at borehole 85.007 and other interesting things have occurred. In log 14, the inflow around 24 m dominates the other two in terms of mass flux. The peak at 30.3 m is still seen as a concentration plateau of approximately 137 to 138 μS/cm. If we consider that Log 14 is a late time log (at or near saturation conditions) then we can use Equation IV.6 to examine the saturation concentrations. From Equation IV.6 it can be said that the highest inflowing concentration emanates from the interval 24 to 25 m. The inflows around 27.1 and 30.4 have traced, but smaller inflowing concentrations.

After log 14, the borehole was again flushed from 8:32 to 8:55. Figure IV.5 plots the 5 conductivity and temperature Logs 15 through 19 which were measured after borehole the second flushing. Again we see that the three primary inflows are located around 24.6, 27.1, and 30.4 m. There is some evidence on logs 16 and 17 of a non-traced inflow occurring somewhere between 4 and 5 m. On the last log, the concentration increases from the bottom of the borehole in a stepwise fashion from a depth of approximately 39 to 40 m and 35 m. The step at 35 m appears as a very low volumetric inflow of non-traced fluid that has reached a saturation concentration of 80 μS/cm (ambient conductivity). The temperature logs again clearly delineate the three primary inflows. On log 16 there is some evidence for inflow at 5 m which also is seen on the conductivity logs. The temperature gradient of log 15 (not shown) shows a large number of gradient minimums indicative of inflow between the depths 7 to 21 m as was the case in the first set of logs. This would give support to a series of minor inflows occurring within this zone. However, gradient log 5 does not show the same minimums as gradient log 15. Because these two logs do not support each other, inflows in this interval (7 - 21 m) cannot be identified with certainty. The following Table IV.2 summarizes the inflows detected by fluid logging as well as the Bräuer fracture system. These inflows detected during fluid logging are graphically summarized in a wellbore schematic shown in Figure IV.6. It is important to note that the primary inflows at 24.6 and 27.1 m coincide well with the two primary transmissive fracture systems as identified by Bräuer.

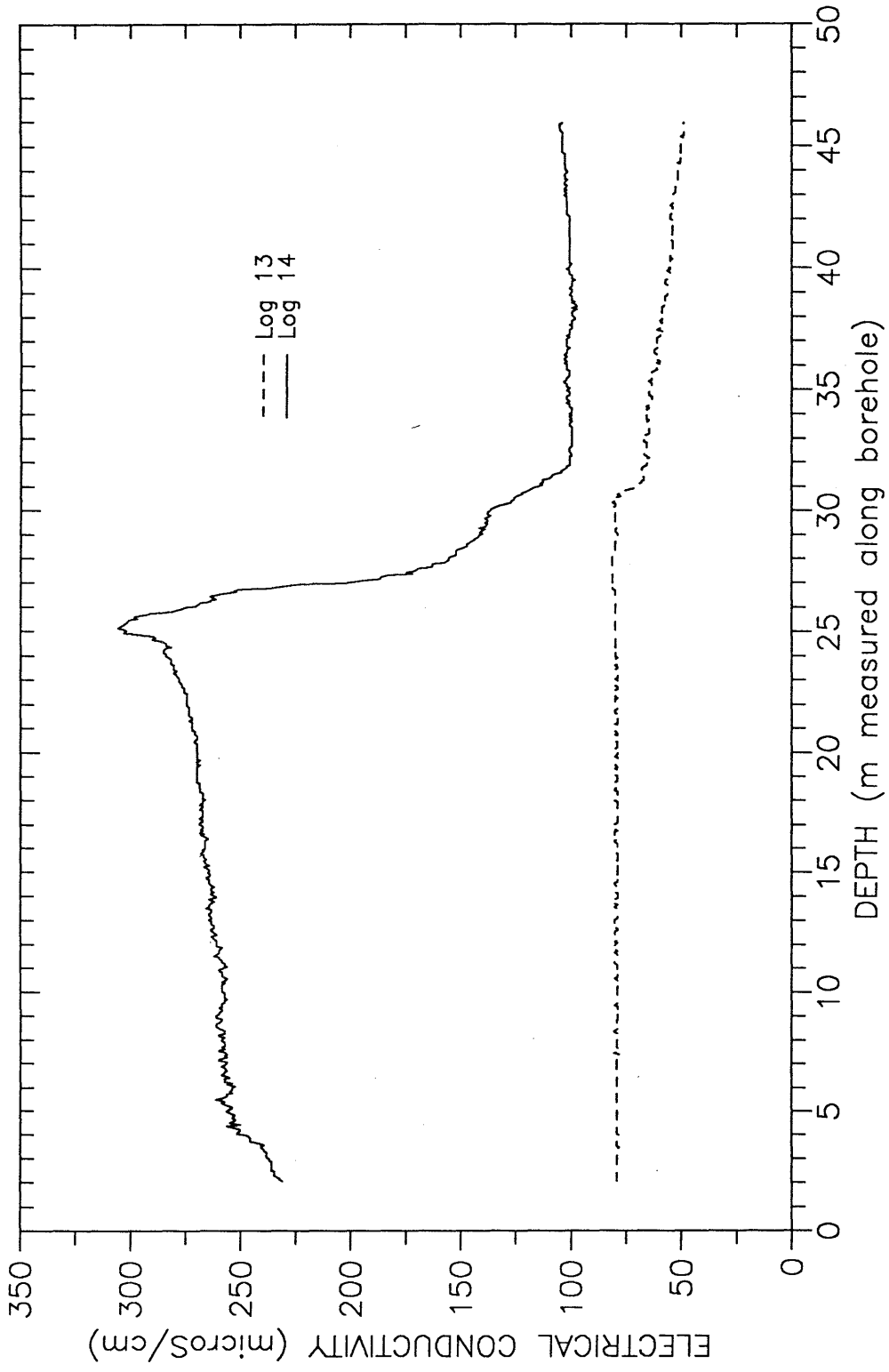

Fig. IV.4: Conductivity Logs 13 and 14, Borehole 85.007
Logging Times 425 and 1372 min After Flushing

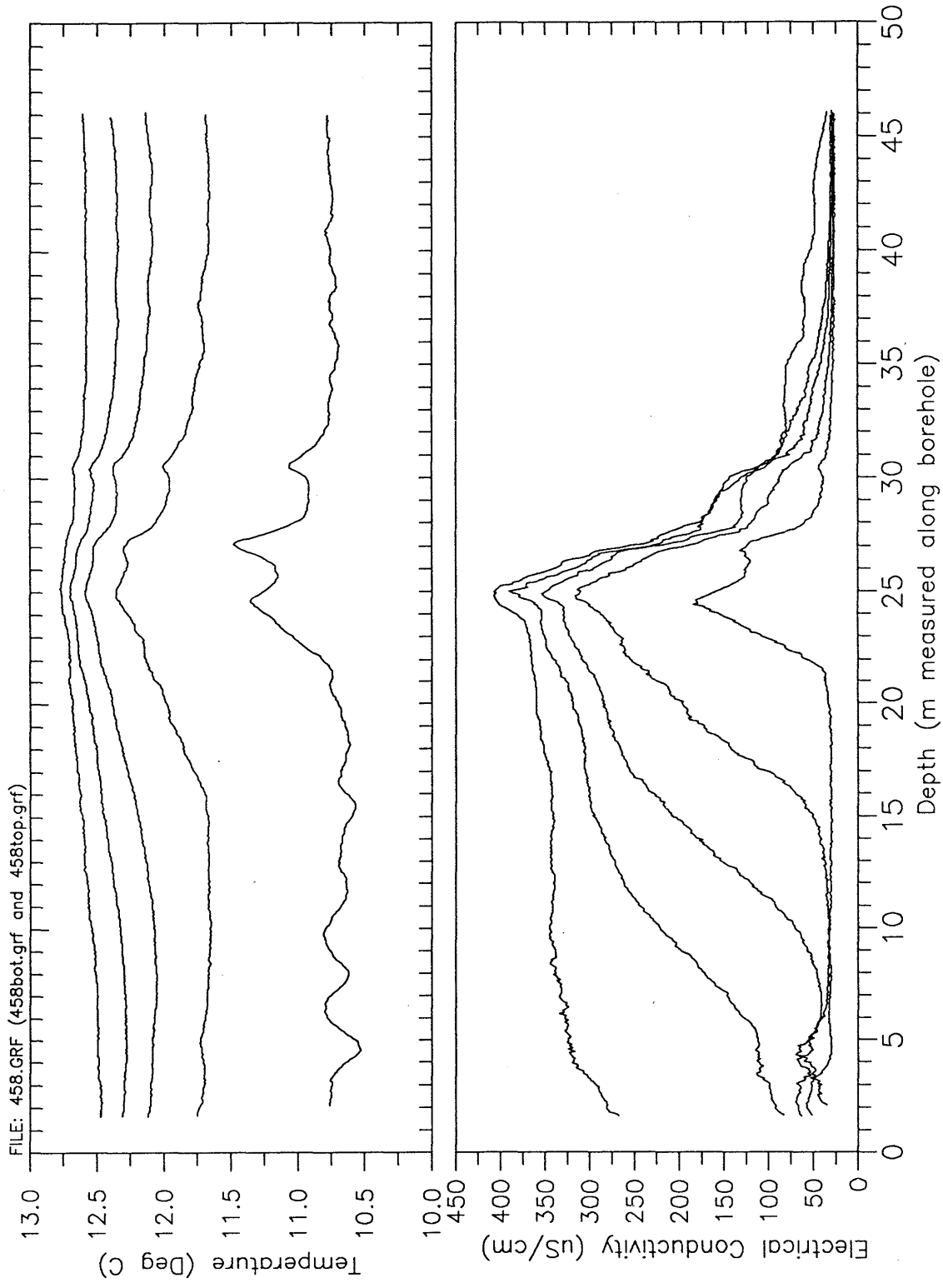

Fig. IV.5: Conductivity and Temperature Logs 15,16,17,18 and 19, Borehole 85.007, Logging Times 5,36,54,95, and 153 Minutes After Second Borehole Flushing

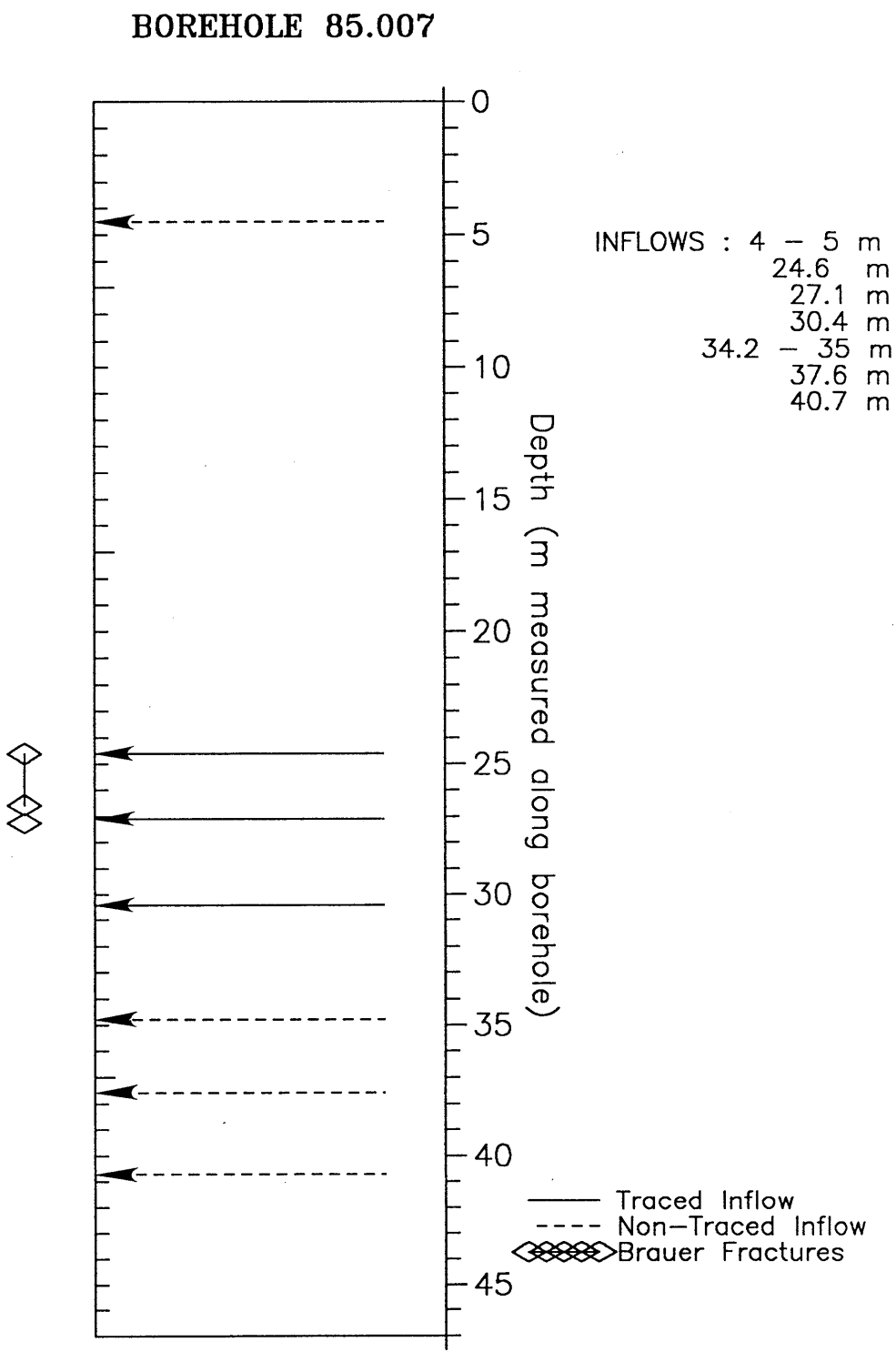

Fig. IV.6: Inflow Locations, Borehole 85.007

Table IV.2: Comparison of Significant Permeability Zones as Determined by Fluid Logging and Bräuer, Borehole 85.007

Fluid Logging Inflows	Bräuer Fracture System	Inflow (1) Concentration
4 - 5		NT
24.6	24.6 - 26.55	T
27.1	27.25	T
30.4		T
34.2 - 35		NT
37.6		NT
40.7		NT

(1) (T) equals a traced inflow, (NT) equals non-traced

Because the first arrival of the traced fluid occurred overnight, the estimation of first arrival time is bracketed. First arrival of the tracer occurred between 15:39 January 30 and 7:26 on January 31. Therefore, between 5.17 and 20.9 hours after continuous injection started. By comparison of Logs 14 and logs 18 and 19 it can be seen that the concentration inflowing to borehole 85.007 was transient and increasing during logging. The increase in concentration at 20 m was approximately 100 μS/cm over the time between measurement of Logs 14 and 19 (approximately 242 minutes).

IV.3.3.2 Quantitative Analysis

Manual estimates of flow rate during the measurement of logs 7-13 indicate that the flow rate was approximately 0.1 l/min. The Reynolds Number for this flow rate is very low at a value of 25. This flow rate corresponds to an approximate mean borehole velocity of 1 m/hr. The Logs 7 through 13 are not ideal for quantitative analysis because of the low concentrations measured. These low concentrations create problems when considering mass balance calculations. Because the borehole concentration profile at late time levels off at background concentration we can say that the inflowing concentration is formation fluid.

During the measurement of logs 15 through 19, a manual measurement of flow rate was not recorded for borehole 85.007. A rough estimate can be made by neglecting the effects of dispersion and recording the movement of the advection front. By noting the location of a given concentration (in this case 175 μS/cm) between two logs, one can calculate borehole velocity, and therefore borehole flow rate. This was done between logs 16 and 17 and 17 and 18. The corresponding flow rate estimates were 1.07 and 1.09 l/min, respectively. It is important to note that this flow rate is an order of magnitude larger than the measured flow rate prior to tracer injection. It is interesting that the observed flow increase at 85.007 is 0.5 l/min larger than the injection rate at 85.004. The

explanation for this is not intuitive.

A simple quantitative analysis can be performed using the classical zero moment of each log measured over the entire borehole interval. By calculating the zero moments of the logs a mass balance can be performed over the logged interval. The definition of the classical zero moment is given in Appendix A and simply represents the mass under the conductivity profile. We assume that the logged borehole is flowing at some constant rate (Q) and that the point A represents the top of the well and point B represents the bottom of the well. Therefore the segment AB defines the length of the logged interval. For this borehole a simple mass balance for time t can be written

Mass in AB at time t	=	Initial Mass in AB	-	Mass Leaving Across Boundary A, t_o to t	+	Mass Inflows via Fractures t_o to t

This expression assumes that no flow occurs across the lower boundary B. The expression can be explicitly written as

$$M_o(t)\pi r^2 = C_o(B-A)\pi r^2 - Q\int_{t_o}^{t} C_A(t)\,dt + Q\int_{t_o}^{t} C_i(t)\,dt \qquad (3.7)$$

where $M_o(t)$ is the classical zero moment as calculated by MOMENT for the interval A to B at time t, r is the wellbore radius, C_A is the concentration at boundary A, and C_i is the average inflowing concentration from A to B.

If we consider that a given conductivity log is measured at early time and no inflowing mass has exited the boundary A, then the second term on the right hand side goes to zero. Thus, if C_i were constant from t_o to t, then the function $M_o(t)$ would be linear with respect to time with the y-intercept equal to $C_o(B-A)$ and the slope equal to $(C_iQt/\pi r^2)$. Therefore, by multiplying the slope by borehole area one could calculate the average fracture mass flux and further by assuming that Q is known, a average inflowing concentration C_i. For the case when the mass lost out of the boundary A is not negligible, then this mass must be estimated and when the zero moment contains this correction it will be termed the corrected zero moment.

For logs 15 through 19, the classical zero moment was calculated by MOMENT and is plotted on Figure IV.7. As can be seen, the zero moment becomes very non-linear for Logs 18 and 19. This is a result of significant mass being transported across the upper boundary A and flowing out of the borehole. Also plotted is the corrected zero moment assuming that the borehole flow rate is 1.07 l/min. From the corrected moment an average inflowing concentration can be estimated as a function of time. Table IV.3 summarizes the variation in mass flux and the calculated inflowing concentration as a function of time. The calculation of the corrected zero moment assumes that Q was constant and equal to 1.07 l/min. The resulting mass flux and inflowing concentration are borehole averaged quantities.

Table IV.3: Borehole Average Mass Flux and Inflowing Concentration, Borehole 85.007

Time (min)	Mass flux (kg/s)	Ci (kg/m^3)	Ci $\mu S/cm$
36	3.17E-6	0.178	332
64	3.47E-6	0.195	363
95	3.64E-6	0.204	380
153	3.61E-6	0.203	377

This calculation supports what has been qualitatively observed above, that the inflowing concentration is transient and increasing for those inflows which are traced. Because all inflows are not traced, and there is significant variation in inflowing concentration between inflows, there is dilution occurring in the borehole. Thus, the measured borehole concentration is different from the concentration in a given fracture. In most cases it would be larger.

An estimate of the time rate of change of the average inflowing concentration can be calculated which requires no a priori estimate of total borehole flow rate, as in the preceding calculations. By reading the outflowing concentration from the log prior to flushing and the final log recorded after flushing one has a delta concentration. By dividing this concentration by the elapsed time between the logs one has a concentration time derivative which is a measure of the time rate of change of the average inflowing concentration. For this set of logs the concentration for logs 14 and 19 was recorded for a depth of 20 m. The top of the borehole was not used in this case because of the large decrease in concentration near the top of the borehole. The concentration derivative between these two logs is 0.381 $\mu S/cm$ min. The purpose of this calculation is to have a quantitative estimate of how much the average inflowing concentration is varying over the time window in which the analyzed logs were measured. The simple derivatives can be compared between boreholes in a simplistic nature. It is clearly understood that these derivatives are simplistic.
A method has been developed to estimate borehole velocities from estimation of partial moments quantities for a series of conductivity logs (LÖW et al., 1991). This method is called the Method of Partial Moments and can be used to estimate borehole velocities (flow rates) for the entire logged interval or for specific sub-intervals. Since a NAGRA document exists with a complete description (LÖW et al., 1991), MOMENT will be used as a black box in this report with little description offered. The partial moment quantities are defined in Appendix A. The calculation of interval flow rate by MOMENT is strongly dependent upon the behavior of the calculated partial moment quantities. To understand the calculated flow rates from MOMENT, it is helpful to plot the zero partial moment as a function of time. Through sensitivity studies and review of the governing equations it has been found that the partial moment method yields correct results when the zero partial moment is large and when it changes smoothly as a function of time (LÖW et al., 1991). In addition, it was suggested that the time derivative

of the zero partial moment equal or exceed a value of 0.05 kg/m^2 hr. For all intervals for which the method of partial moments was applied, a plot of the zero partial moment as a function of time will be included. Two general rules of thumb concerning the choice of appropriate integration intervals are (1) the integration interval must never contain an inflow as velocity must be constant within an interval, and (2) the larger the integration interval, the better.

Figure IV.7 plots the zero partial moment calculated for two different integration intervals (15-19 m and 12-19 m). Both of these intervals should estimate the total borehole flow rate with the exception of the inflow at 5 m which is considered to be relatively small. Because of the possibility of capturing minor inflows, it was decided to keep the integration intervals somewhat smaller than was strictly possible. This was justified as the zero partial moment time derivatives were still substantial. From a review of the behavior of the zero partial moment with respect to time for the two intervals, the best estimates for borehole flow rate were thought to come from logging times 1.07 and 1.58 hours. Figure IV.8 plots the flow rate as calculated by MOMENT for the two integration intervals. By averaging the calculated flow rates from the two runs at times 1.07 and 1.58 hours we receive an arithmetic average equal to 1.01 l/min (n=4). This is in good agreement with the flow rate estimated from advection front tracking of 1.07 l/min. No manual flow measurement at the wellhead was measured during this time period therefore there is no direct flow rate with which to compare.

Because the concentrations were relatively small (therefore the mass fluxes were small) for the portion of the borehole below 28 m, trying to determine interval flow rates for smaller intervals below this depth was not practical with the method of partial moments. BORE could be used to attempt to fit the observed conductivity logs through forward calibration but this analysis was not performed for these logs.

IV.3.4 Test VE459, Borehole 85.006

IV.3.4.1 Qualitative Description and Analysis

The packers were deflated in 85.006 on January 31 1990 at 13:28. Only one log was successfully measured on the day the borehole was opened and that was Log 21. Boreholes 85.006 and 85.007 were left open through the night and Borehole 85.007 was packed off on the next morning (February 1) at 8:20. Borehole 85.006 was flushed at 8:36 on February 1 and a series of logs were run (logs 022 through 025). A series of flow and conductivity measurements were made at the top of the borehole during logging and these are listed in the following Table IV.4 as they aid in the following discussion of the measured logs.

The flow rate coming from the well was manually measured to be approximately 5 l/min immediately after opening the well. Over the course of logging the flow rate stabilized at 4 l/min. This flow rate corresponds to a Reynolds Number of 987 and a maximum mean borehole velocity of 41 m/hr. The last manual flow rate measurement was performed with a packer and is considered the best estimate. From Table IV.4 it can be

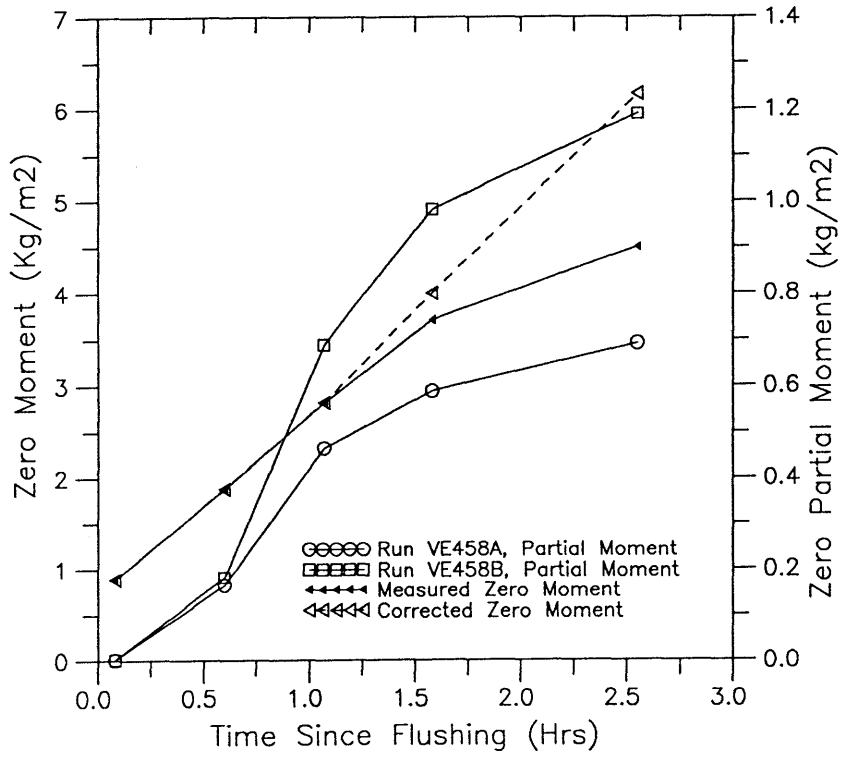

Fig. IV.7: Zero Moments for Fluid Logging Test VE458 Borehole 85.007, Logs 15,16,17,18, and 19

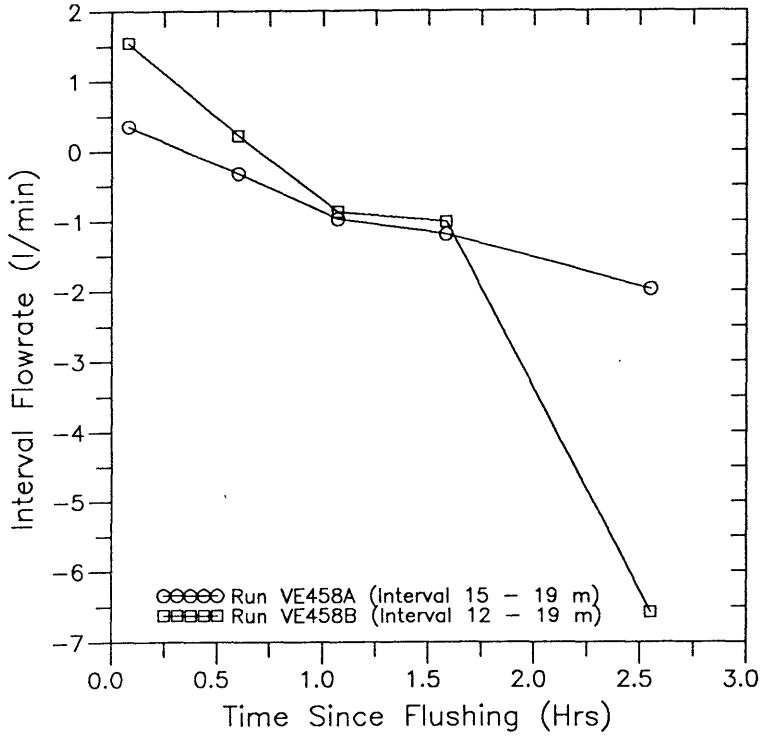

Fig. IV.8: Interval Flowrate as Calculated by MOMENT, Test VE458, Borehole 85.007, Logs 15,16,17,18 and 19

seen that two measurements of effluent conductivity were recorded on January 31. These were on the order of 1700 μS/cm, which indicates that the tracer had arrived at 85.006 sometime prior to the earliest measurement at 14:25 (53 minutes after borehole 85.006 was opened). Interestingly, the first measurement on the morning of February 1 was significantly less.

Figure IV.9 shows the measured conductivity and temperature logs 21 through 25. Log 21 was measured on February 1, the day the borehole was opened and prior to borehole flushing. On the morning of February 2, the borehole was flushed from 8:36 to 9:04. A log was not run before flushing because, after measuring Log 21 the day before, it was known that breakthrough had occurred. Logs 21 through 25 were measured -1036, 6, 27, 63, and 123 minutes after the end of borehole flushing. Log 21 was measured approximately 132 minutes after the borehole was opened. From Log 21 we can see that the outflowing concentration (approximately 1600 μS/cm) was 100 μS/cm less than the effluent concentrations measured immediately after opening 85.006. The apparent saturated profile exhibited by Log 21 had a maximum concentration peak occurring at approximately 23 to 24 m. Below this depth the concentration quickly falls off to background levels. Above this depth the concentration decreases in a series of steps which appear to coincide with inflow intervals. From Equation IV.6 we can say that these inflows downstream of a depth of 23 m produce a reduced concentration relative to the inflow(s) at 23 to 24 m.

Table IV.4: Measurements of Conductivity and Flow Rate Measured at the Borehole 85.006 Wellhead During Logging.

Date (Day/Month)	Time	Conductivity (μS/cm)	Flow Rate (l/min)	Comments
31/1	13:30		3.8 (5.0)	40% lost
31/1	14:03		3.0 (4.2)	40% lost
31/1	14:25	1710		
31/1	14:47	1745		
01/02	07:30	1396		
01/02	07:40		1.8 (2.9)	60% lost
01/02	09:55		3.0 (4.0)	30% lost
01/02	11:00		3.0	
	12:00		3.5	
	13:19		2.0 (4.0)	50% lost
	14:00		3.25	Meas. with Packer

(#) Represents an estimate compensating for fluid lost while making the manual flow measurement.

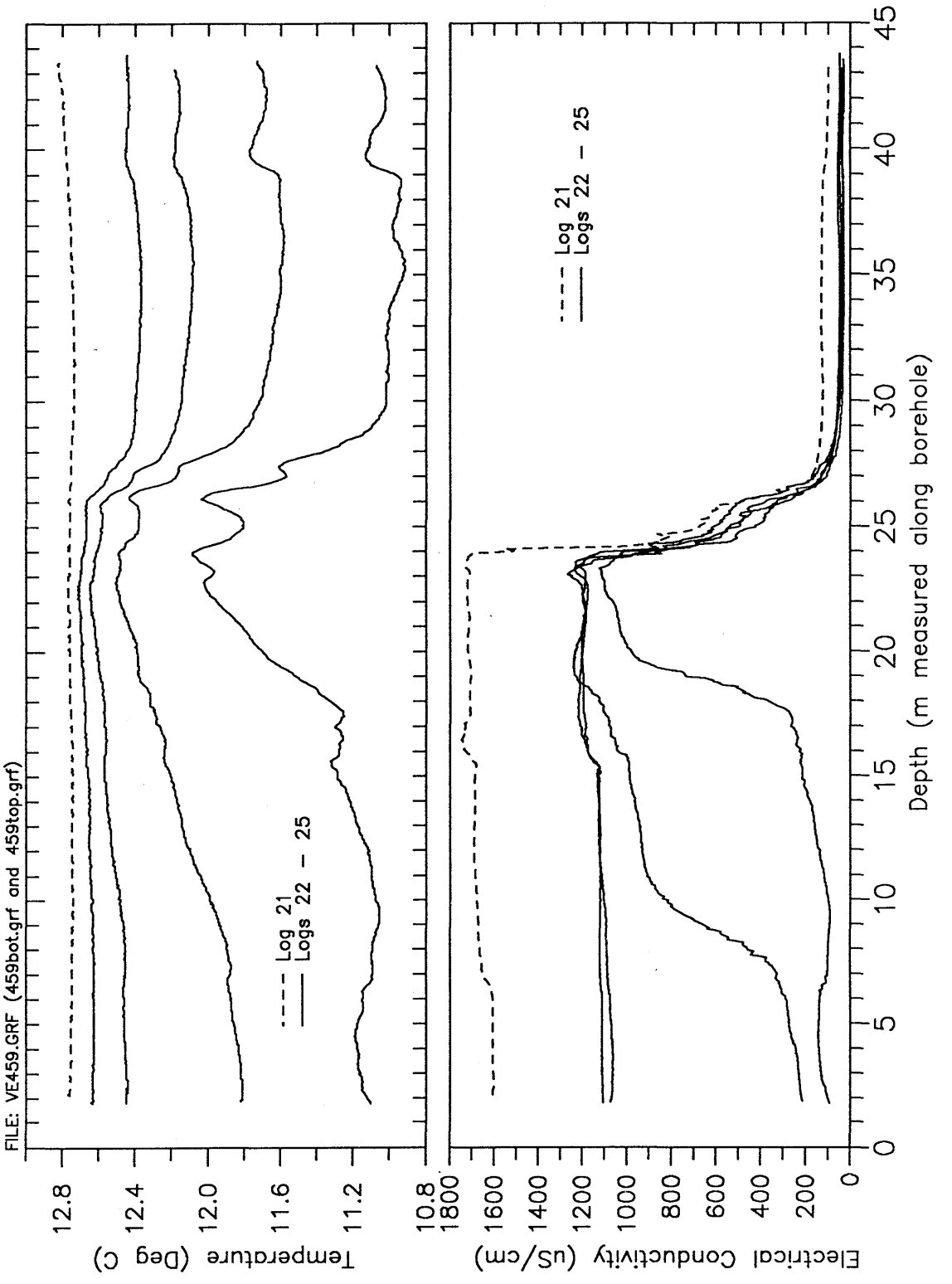

Fig. IV.9: Conductivity and Temperature Logs 21,22,23,24 and 25, Borehole 85.006, Logging Times −1036,6,27,63, and 123 Minutes After Borehole Flushing

Logs 22 through 25 quickly develop because of the significant flow rates in the borehole. It is interesting that the new semi-saturated concentration level exhibited by late time Logs 24 and 25 represents an approximate 40% decrease as compared to Log 21, which was measured 132 minutes after the borehole was opened. A possible conceptual model to explain this observation will be proposed in Section IV.4.1 of this report. Temperature logs 22 through 25 offer a good source of information for the delineation of inflows. The three largest volumetric inflows occur between the depths 22 and 28 m. By inspecting both temperature and conductivity logs, the major inflows are detected at 22.7, 23.9, 26.1, and 27.4 m. Other traced peaks are identified at 6.5 m, 15.6 m, and 17 m. One non-traced inflow was detected at a depth of 40.5 m. The temperature gradient logs, and to a lesser degree, the temperature logs, also suggest that minor inflows are occurring around the depths 33.8 and 37 m, but these are not considered important. The temperature gradient log 22 indicates a minor inflow occurring at a depth of 20.2 m which is also vaguely evident in conductivity log 22. The evidence for inflows at 33.8 and 37 m is not clearly defendable.

Table IV.5 summarizes the identified inflow zones as determined through the pilot cross-hole fluid logging test. Also included in Table IV.5 is the Bräuer Fracture System for the BK Site and the Lugeon Test results which were performed by BGR.

The inflow points show good correlation with the Bräuer Fracture System for the BK Site and the Lugeon Tests performed by BGR. Figure IV.10 shows a borehole schematic with the data in Table IV.5 shown. The three primary inflow points, 22.7, 23.9, and 26.1 m correlate well with the main water transmissive fracture systems identified by Bräuer. Many more inflows have been delineated through the fluid logging method. The Lugeon Tests found that the entire interval between 15-18 m and 22 to 30 m had transmissivity equal to or greater than 1E-8 m^2/s.

The results from the Lugeon Tests give good insight into the difficulties in resolving inflows from 17 to 27 m. There may be several inflows present within this interval but if they are small relative to the primary inflows they would be hard to detect due to interference.

IV.3.4.2 Quantitative Analysis

The first step in quantitative evaluation is to estimate a borehole flow rate from tracking of the advection front using Logs 22 and 23. The concentration used is 600 μS/cm. For Log 22 the 600 μS/cm concentration is at a depth of 18.73 m and for Log 23 is at 8.73 m for a net displacement of 10 m. The elapsed time between log measurement was 21 minutes which results in a borehole velocity of 7.94E-3 m/s and a borehole flow rate of 2.8 l/min. This value is less than the final measured manual flow rate of 3.25 l/min which was measured accurately with a packer assembly. One would expect the advection front estimate to overestimate flow because the calculation ignores dispersive flux. Some portion of the discrepancy may reside with measurement error and also because the inflow(s) occurring at a depth of 6.5 m was not accounted for by the advection front calculation.

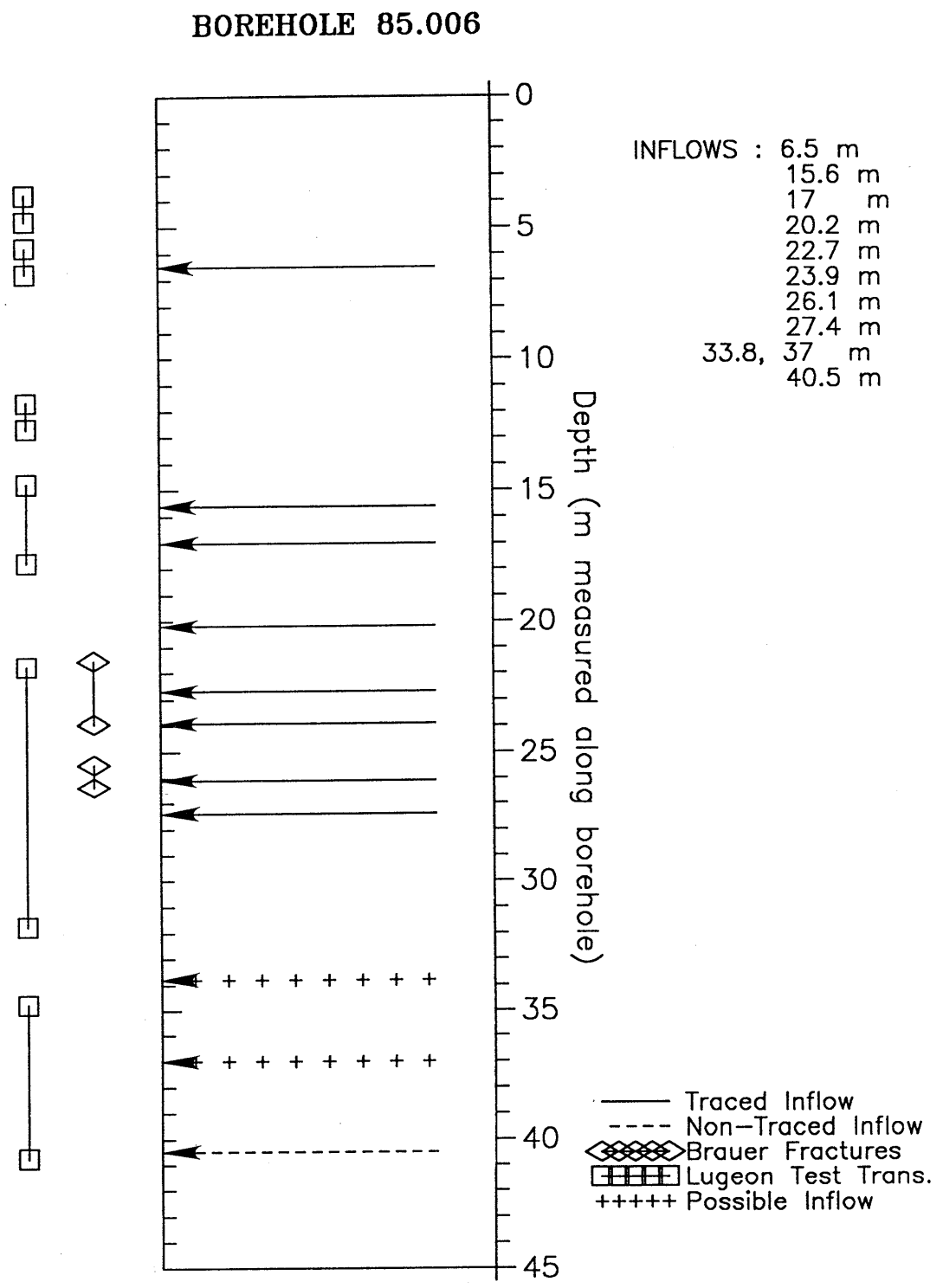

Fig. IV.10: Inflow Locations, Borehole 85.006

Table IV.5: Comparison of Significant Permeability Zones as Determined by Fluid Logging, Lugeon Tests, and Bräuer, Borehole 85.006

Fluid Logging Inflows	Bräuer Fracture Systems	Lugeon Testing (1)	Inflow Conc. (2)
		3.7 - 4.7	
6.5		5.7 - 6.7	T
		11.6 - 12.6	
15.6		14.7 - 17.7	T
17		14.7 - 17.7	T
20.2			T
22.7	21.49 - 23.88	21.7 - 31.7	T
23.9	21.49 - 23.88	21.7 - 31.7	T
26.1	25.45 - 26.33	21.7 - 31.7	T
27.4		21.7 - 31.7	T
(33.8)			NT

(#) Means that inflow point is poorly defined.
(1) Intervals where K greater than or equal to 1E-11 m/s
(2) (T) equals a traced inflow, (NT) equals non-traced

As with the last test, the average inflowing borehole concentration can be estimated by mass balance relationships. For this calculation it is assumed that the borehole flow rate is constant at a value of 3.25 l/min. Because borehole velocity is high, a good deal of mass is transported out of the borehole through the upper boundary during logging. Therefore, the calculation of an average C_i relies heavily on the zero moments corrected for the mass lost through the upper boundary. Figure IV.11 plots both the measured zero moment and the corrected zero moment for the interval from 3 to 40 m. The concentration calculated is relatively constant around 1000 μS/cm. This is smaller than the concentration flowing from the borehole in the last log 25 which was approximately 1100 μS/cm. Possible sources for error in this mass balance calculation arrive from evaluating the mass lost through the borehole effluent. The integration assumes a linear change of concentration between time measured logs. Because of dispersion affects and borehole velocity variations the concentration does not vary linearly and thus errors are accrued. Secondly, this calculation only accounts for advective losses and does not account for dispersive flux across the boundary. The net effect of these errors is to underestimate the borehole flux and subsequently the average inflowing concentration. Table IV.6 summarizes the calculated borehole inflowing mass flux and the average borehole inflowing concentration.

Table IV.6: Borehole Average Mass Flux and Inflowing Concentration, Borehole 85.006

Time (min)	Mass Flux (kg/s)	Ci (kg/m^3)	Ci ($\mu S/cm$)
27	2.87E-5	0.529	978
63	2.92E-5	0.539	996
123	3.04E-5	0.561	1036

Estimation of the concentration time rate of change for this borehole is complicated by the fact that the average inflowing concentration decreased. Log 21 was measured after borehole opening and 1036 min prior to the end of flushing. The outflowing concentration for this log was 1607.9 $\mu S/cm$. For Log 25, taken 123 min after flushing, the outflowing concentration had decreased to 1108 $\mu S/cm$. This results in a concentration derivative of -0.431 $\mu S/cm$ min. Because the change in concentration as a function of time is not expected to be linear, this derivative is not representative of the relatively short time period over which the suite of logs were measured.

Again, Partial Moment methods can be used to try to independently estimate a borehole flow rate. The interval chosen for MOMENT integration intervals was 7 to 15 m. The inflow at 6.5 m was excluded from the estimate. Two MOMENT runs were performed which shared this same integration interval and differed only in order of the line used to extrapolate concentration to the integration boundaries. Figure IV.11 plots the zero partial moments for these two runs. The difference between the two runs causes no observable difference in the partial moment which would be expected. The behavior of the moments suggest that the evaluation of flow rate at 0.45 and 1.05 hours should be the most robust. Figure IV.12 plots the flow rate as a function of time as calculated by MOMENT. As we can see, the estimated flow rates for the two runs are nearly identical. The flow rate estimate at 0.45 hours for both runs was approximately 1.1 l/min which is significantly less than the known borehole flow rate. MOMENT calculated flow rates at 1.05 hours which were close in magnitude to that manually measured. The average flow rate at 1.05 hours between the two runs is 3.15 l/min. This compares well with the best manual estimate of 3.25 l/min especially when it is considered that the inflow which was identified at 6.5 m is not contributing to the MOMENT estimate.

Again it is not advisable to apply the partial moment method on the lower intervals because of the low mass flux rates and short potential integration intervals. BORE could be used to attempt to fit the observed conductivity logs through forward calibration but this analysis was not performed for these logs.

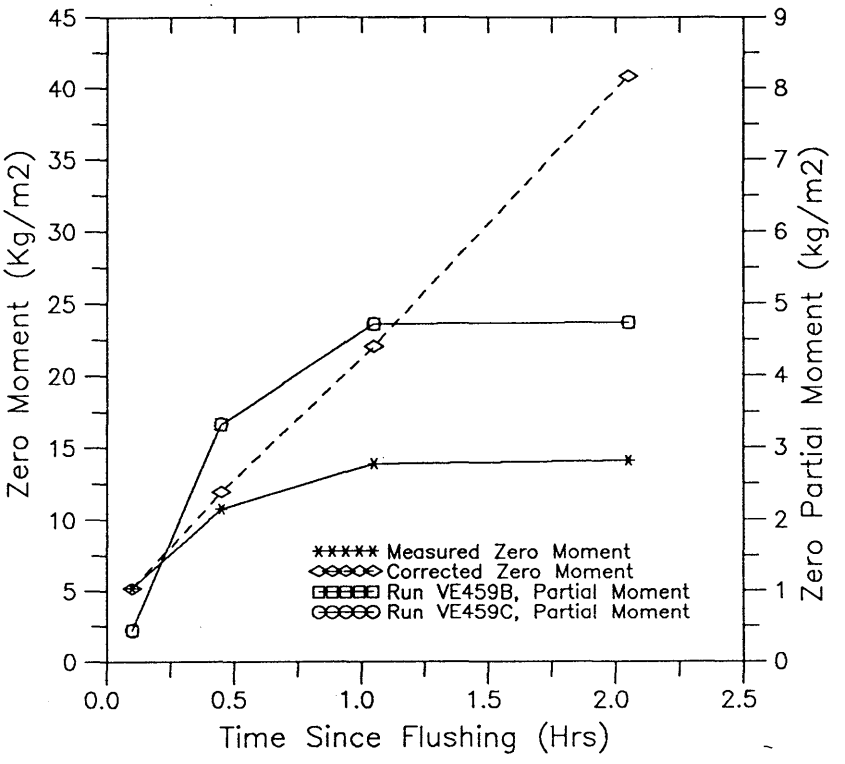

Fig. IV.11: Zero Moments for Fluid Logging Test VE459 Logs 22,23,24, and 25, Borehole 85.006

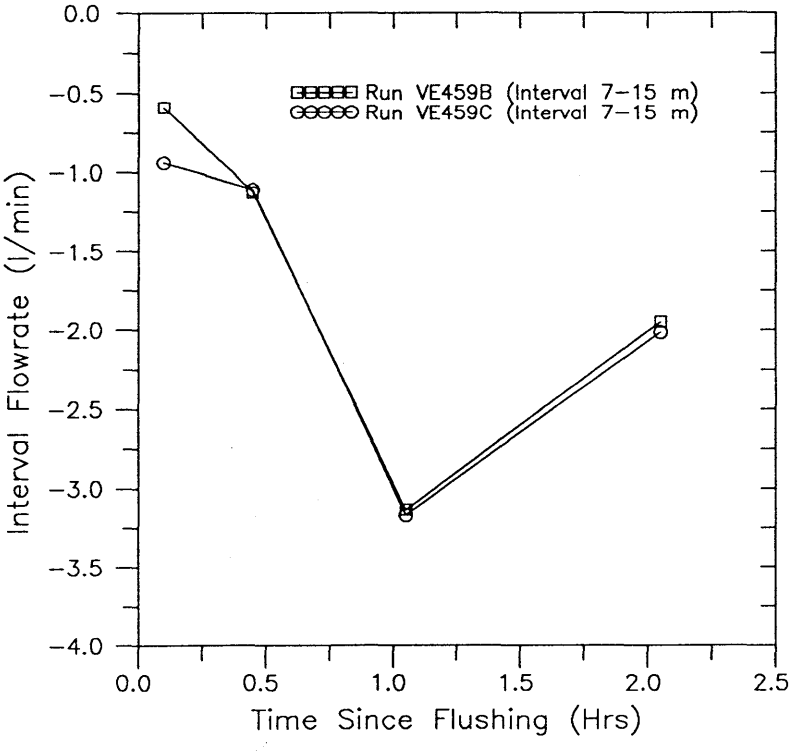

Fig. IV.12: Interval Flowrate as Calculated by MOMENT, Test VE459,Logs 22,23,24, and 25, Borehole 85.006

IV.3.5 Test VE460, Borehole 88.017

IV.3.5.1 Qualitative Description and Analysis

Borehole 88.017 was opened for logging on February 1 at 14:35. By this time Borehole 85.006 had not been closed. To complicate further, Borehole 85.007 started leaking water into the tubing at approximately 22:00 on February 1 and was re-opened February 2 at 7:35. The first log run in Borehole 88.017 was Log 26 and was started on February 2 at 7:30. Therefore, when logging started in Borehole 88.017, three boreholes were open. This is shown schematically in Figure IV.1 and the following will summarize which boreholes were open during logging of Borehole 88.017.

[Feb 2] 07:35 - 08:56	Boreholes 85.006,85.007, and 88.017 were open.
[Feb 2] 08:56 - 11:30	Boreholes 85.006 and 88.017 open.
[Feb 2] 11:30 - 15:25	Borehole 88.017 open.
[Feb 2] 15:25 - [Feb 5]	Boreholes 88.017 and 85.008 open. Through weekend.

Prior to logging Borehole 88.017 on February 2, manual measurement of effluent conductivity and flow rate were made at the wellhead. Unfortunately these measurements were only made once and therefore they will not be summarized in a table. At 7:15 on February 2 the effluent concentration was measured to be 1067 μS/cm and the total volumetric flow rate was estimated to be between 3 and 4 l/min. If we conservatively assume that 4 l/min flow rate is representative, then the corresponding Reynolds Number is 987 and the mean maximum borehole velocity would be equal to 41 m/hr.

Before flushing the borehole with fresh water, the borehole was logged once (Log 26). This log confirmed that tracer breakthrough had occurred therefore the borehole was flushed for the first time from 8:06 until 9:00. After the first flushing period a suite of 4 logs were recorded at times 7, 28, 47, and 108 minutes after the end of flushing. Figure IV.13 plots the conductivity and temperature Logs 26, 27, 28, 29 and 30. Log 26 shows what appears to be a saturated conductivity profile with the major mass flux inflow point occurring around 26 m. An inflow 5 m is delineated by a step increase in the concentration profile. From Equation IV.6 this tells us that the inflowing concentration at this inflow is the largest. There is also a traced inflow evident at 34.6 m and a non-traced inflow occurring around 42 m.

After flushing, the development of logs 27 through 30 was very quick. This results in strong peak interference which results in poor resolution of small inflows. For these reasons, the temperature and temperature gradient logs become useful tools in locating inflow points. The use of the temperature logs as an indicator of inflows is very useful. From review of the conductivity logs there is evidence that traced inflows occur at depths 5, 26.2 m. For some inflows it is very hard to determine if they are traced due to interference. Inflows at 42 m and at a depth of 44 m or greater are not traced. Inflows at 29 to 30 m and 34.9 m might be traced. There is evidence for a traced inflow(s) from 27 to 29 m but this inflow(s) is hard to detect because of interference. It is clear that the inflow at 5 m is of a higher concentration than 850 μS/cm. The temperature logs also delineate the inflows

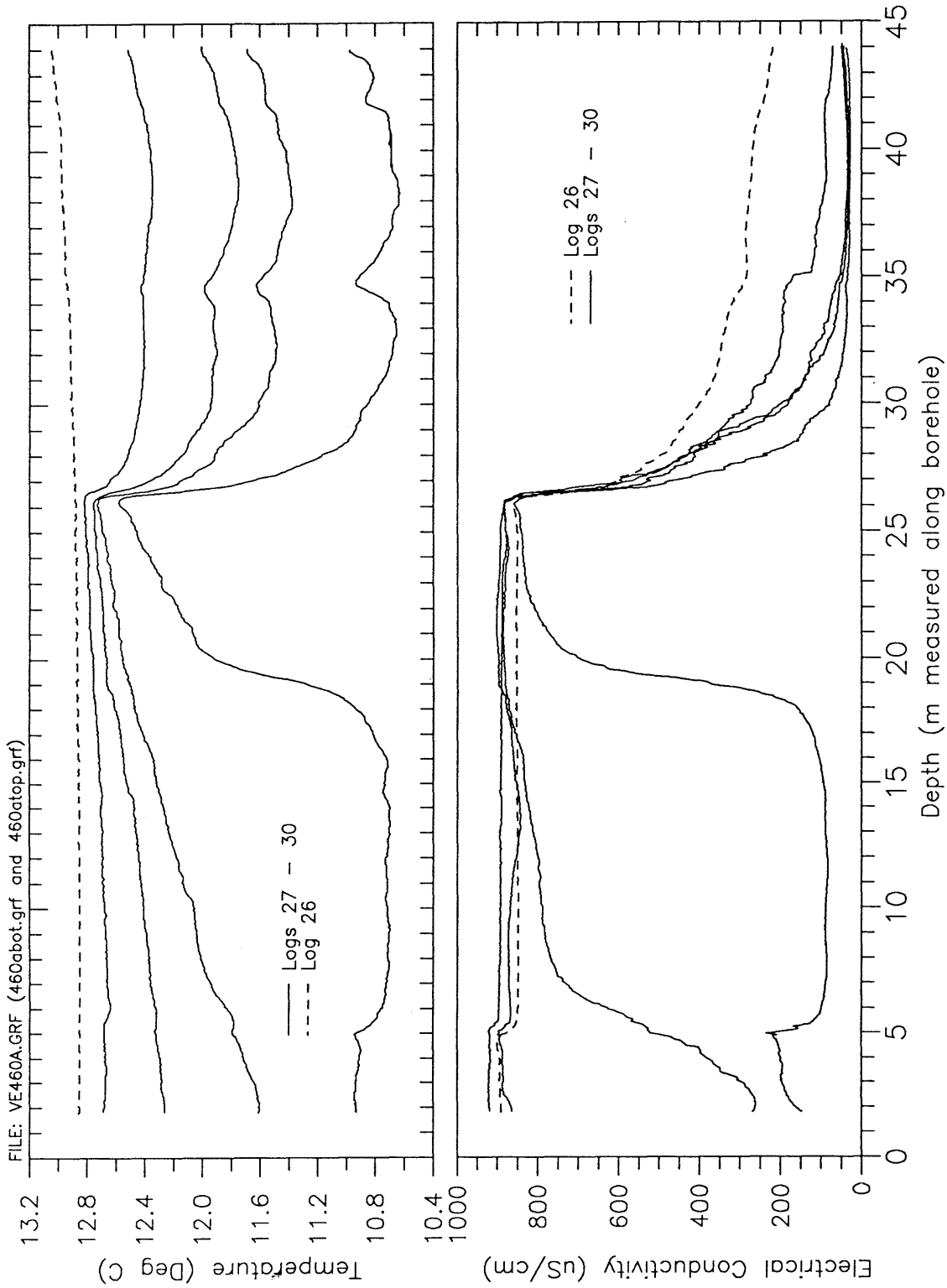

Fig. IV.13: Conductivity and Temperature Logs 26,27,28,29 and 30, Borehole 88.017, Logging Times −84,7,28,47, and 108 Minutes After First Borehole Flushing

listed above and additionally delineate a minor inflow around 15.2 m which also shows as a small local minimum on the temperature gradient Log 27. The existence of this inflow is considered not certain.

A second flushing event was started after measuring Logs 27 through 30. The reason for two flushing periods was that the first set of logs was not performed while Borehole 88.017 was the only borehole open. This was the case for the logs taken after the second flushing period. Also, because the peak development was so quick, it was advantageous to measure more conductivity logs in Borehole 88.017. Therefore, from 11:22 to 12:49 on February 2, the borehole was flushed with fresh water for a second time. After the second flushing period, a series of four additional logs were measured at times 6, 26, 43, and 100 minutes. Figure IV.14 shows logs 31, 32, 33, and 34.

The conductivity logs look very similar in detail to Logs 27 through 30. Again we see traced inflows at 5 m, 26.2 m, and 34.6 m. The inflow detected in the earlier logs around 29 to 30 m does not show up as clearly. Because the inflow around 29 to 30 m is not well reproduced with a second set of logs, the existence of this inflow is considered only a possibility. Non-traced inflows exist at 42 m and at 43.9 m or greater. At 14.3 m there appears to be an inflow which may also not be traced. The evidence for this inflow is not conclusive and this inflow is lumped with the inflow detected in the previous set of logs at 15.2 m and both are taken as intervals where flow may exist. Finally, there still appears to be inflow(s) in the interval 27 to 29 m but interference is strong and clear resolution is not possible.

Boreholes 88.017 and 85.008 were left open over the weekend (February 2 to 5). A final log was measured in Borehole 88.017 at approximately 8:00 on the 5th, 3940 minutes after the second flushing. Figure IV.15 plots this log with the last log measured on February 2 (log 34). As can be seen, the inflowing concentration increased by over a factor of 2 with the inflow at 5 m becoming even more prevalent. Obviously, the inflowing concentration at 5 m is greater than 1900 μS/cm. What is strange about this saturated profile is the distinct concentration peak at approximately 5.2 m. There could be diluting inflow occurring immediately after the main inflow around 5 m which creates the observed profile . Other reasons for the peak may be related to inclined borehole effects discussed in Section IV.4 of this report. Table IV.7 summarizes the inflows detected by fluid logging and lists the Bräuer Fracture System as detailed for this borehole. Figure IV.16 is a schematic of the borehole with the same information depicted as is in Table IV.7.

IV.3.5.2 Quantitative Analysis

The first step in quantitative evaluation is to estimate a borehole flow rate from tracking of the advection front using Logs 27 and 28. The concentration used is 600 μS/cm. For Log 27 the 600 μS/cm concentration is at a depth of 19.52 m and for Log 28 is at 5.83 m for a net displacement of 13.7 m. The elapsed time between log measurement was 21 minutes which results in a borehole velocity of 1.09E-2 m/s and a borehole flow rate of 3.8 l/min. This value falls within the manually measured value which was from 3 to 4 l/min.

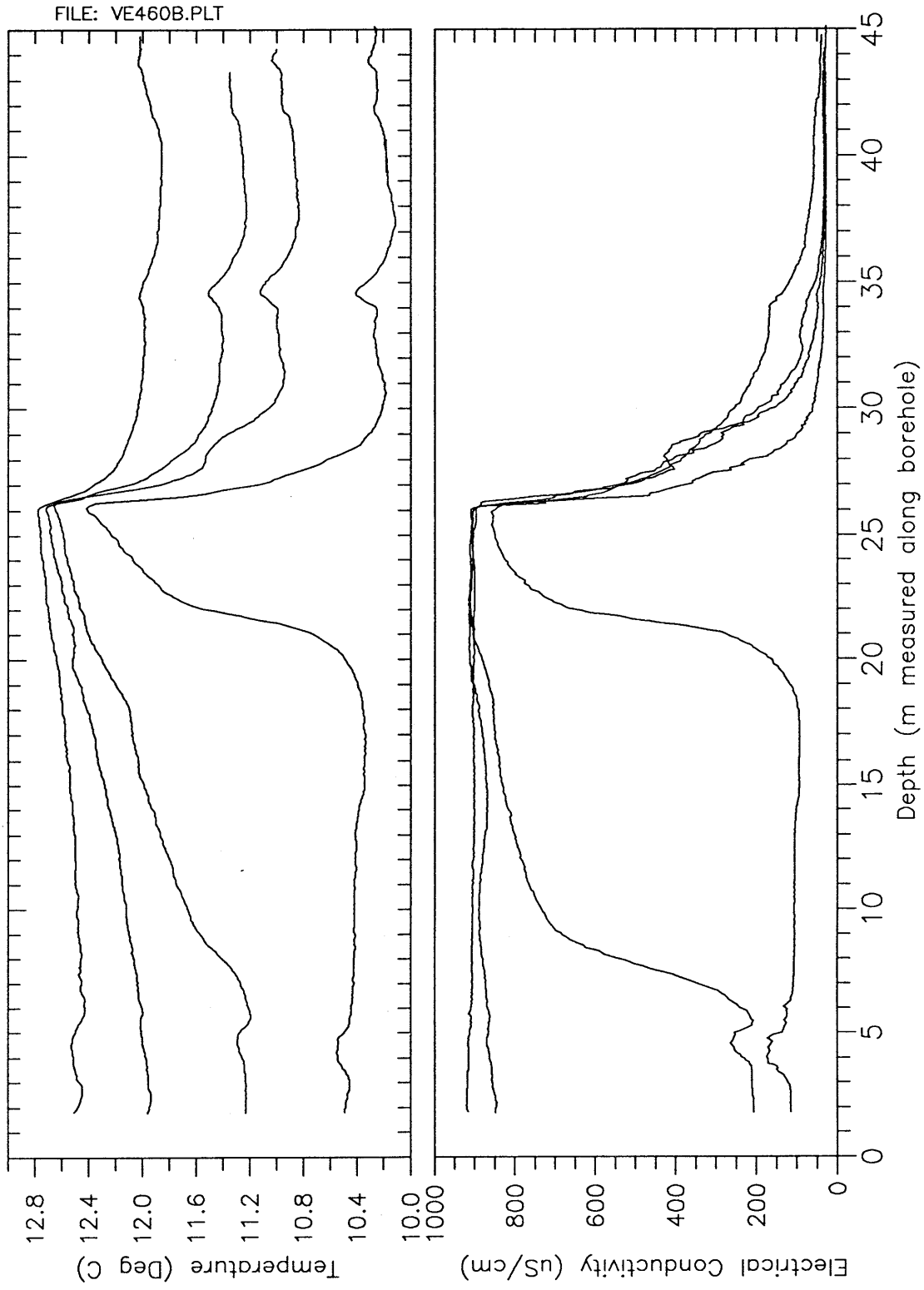

Fig. IV.14: Conductivity and Temperature Logs 31,32,33, and 34, Borehole 88.017, Logging Times 6,26,43, and 100 Minutes After Second Borehole Flushing

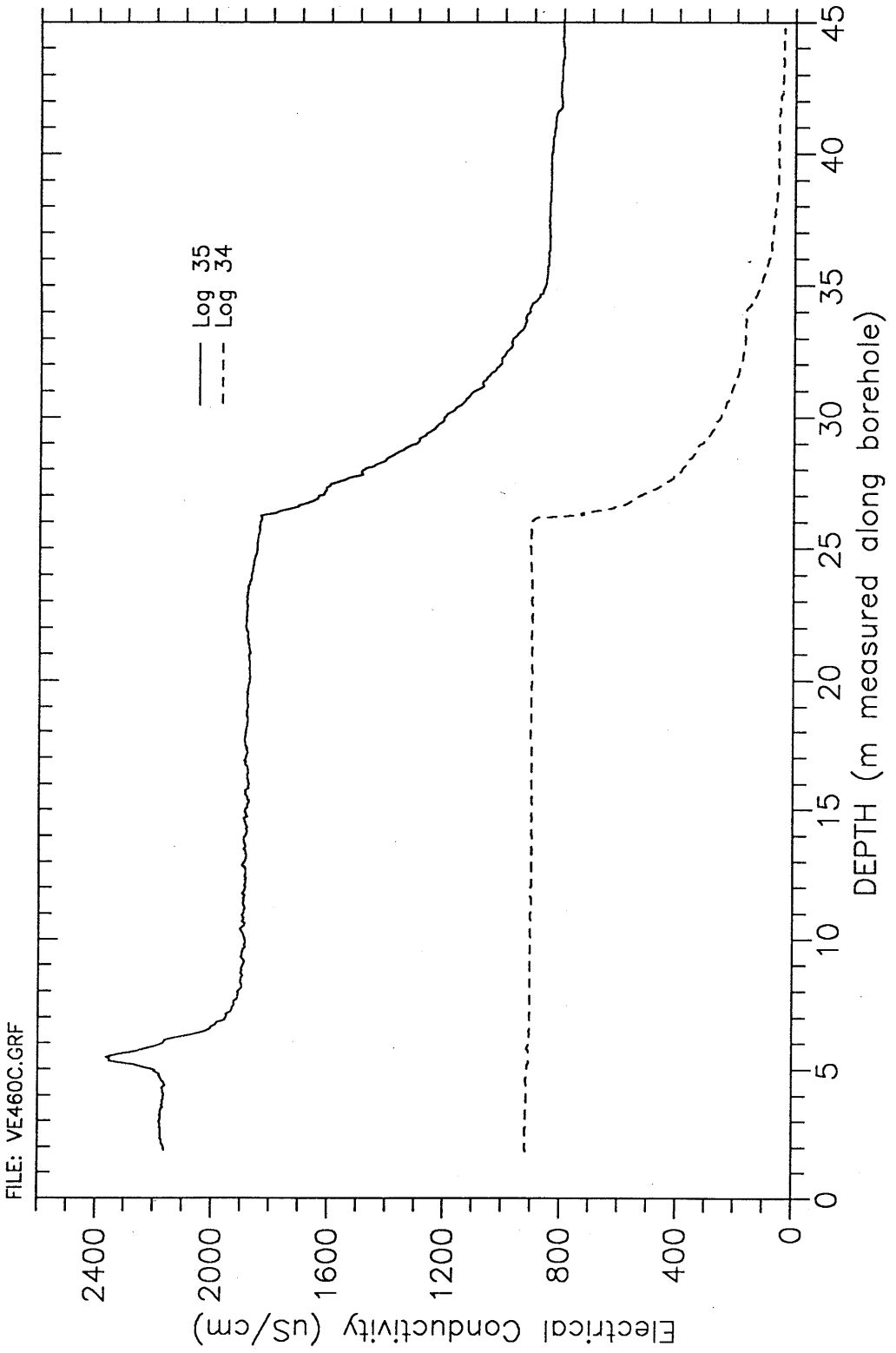

Fig. IV.15: Conductivity Logs 34 and 35, Borehole 88.017
Logging Times 100 and 3940 Minutes After
Second Borehole Flushing

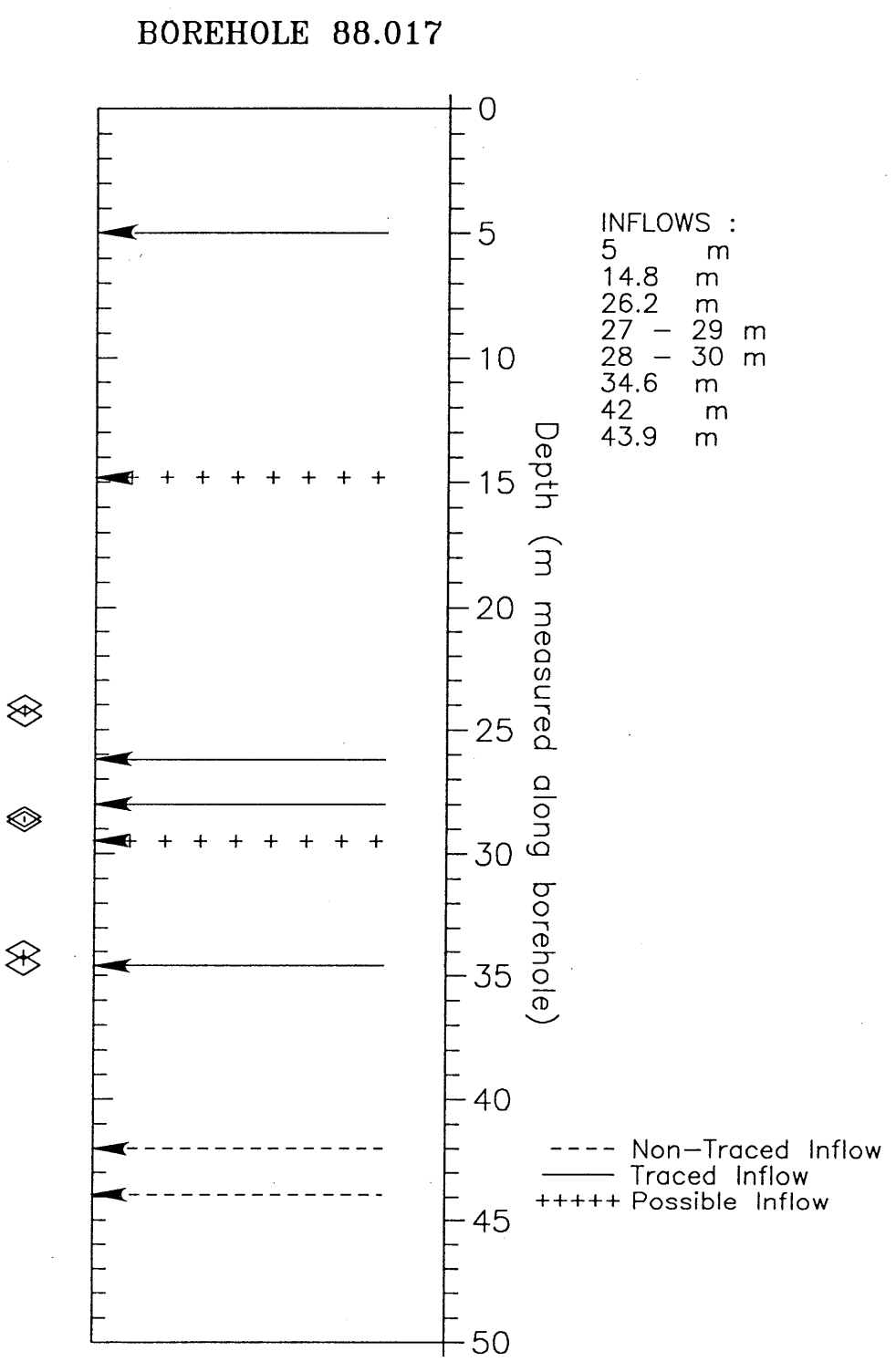

Fig. IV.16: Inflow Locations, Borehole 88.017

Again, the average inflowing borehole concentration can be estimated by mass balance relationships. For this calculation it is assumed that the borehole flow rate is constant at a value of 3.8 l/min as was calculated above. The average borehole mass flux is dependent upon the correct correction of the zero moment. As was stated for Test VE459, when the borehole velocity is high the correction of the zero moment is harder to estimate without error because of significant mass being lost through the upper borehole boundary. Figure IV.17 plots both the measured zero moment and the corrected zero moment for the interval from 2 to 43 m. Again the slope of the measured zero moment decreases at late times because of the large amount of mass exiting the borehole during logging. The measured zero moment quickly levels off which indicates near saturation conditions. The corrected moment shows a slight decrease in slope at late times. From review of the observed conductivity logs it is evident that the mass flux is relatively constant. For this case the corrected zero moment should have a constant slope. Table IV.8 summarizes the calculated borehole inflowing mass flux and the average borehole inflowing concentration. The average inflowing concentration calculated for 28 minutes is close to the observed outflowing concentration for Log 30.

Table IV.7: Comparison of Significant Permeability Zones as Determined by Fluid Logging and Bräuer, Borehole 88.017

Fluid Logging Inflows	Bräuer Fracture System	Inflow (1) Concentration
5		T
(14.3 - 15.2)		T
	24.01 - 24.46	
26.2		T
(27 - 29)	28.52 - 28.71	T
29 - 30		T
34.6	33.94 - 34.58	T
42		NT
43.9		NT

(1) (T) equals a traced inflow, (NT) equals non-traced
(#) Means that the inflow point is poorly defined.

Table IV.8: Borehole Average Mass Flux and Inflowing Concentration, Borehole 88.017

Time (min)	Mass Flux (kg/s)	Ci (kg/m^3)	Ci ($\mu S/cm$)
28	3.12E-5	0.492	910
47	2.86E-5	0.451	836
108	2.94E-5	0.463	858

The difference between the outflowing concentration at Log 26 and Log 30 is 28.9 $\mu S/cm$. The time difference between the two logs is 202 minutes. This results in an average inflowing concentration time rate of change equal to 0.143 $\mu S/cm$ min. This derivative does not appear to be applicable for the logs 31 through 34. Log 34 was measured 211 minutes after Log 30 and has approximately the same outflowing concentration. If we take the difference between the outflowing concentration taken for Log 34 and Log 35, we receive a high change in concentration equal to 1248.1 $\mu S/cm$. However the time difference between logs is 3840 min. The time rate of change of the average inflowing concentration between Logs 34 and 35 is 0.325 $\mu S/cm$ min which is a factor of 2.3 greater than the derivative between Logs 26 and 30. Log 35 was taken after borehole 88.017 flowed all weekend and just before packer re-inflation. The difference in the two concentration derivatives calculated over two different time periods illustrates the transient nature of the inflowing concentration. Apparently the concentration change had almost gone to zero by the measurement of Log 34. However, over the weekend breakthrough strengthened and the change in average inflowing concentration increased by greater than a factor of two.

The measured conductivity logs are not well suited for analysis by the partial moment method because velocities are high causing fast profile saturation. It was decided to attempt a limited analysis with Logs 27, 28, 29, and 30 in an attempt to estimate the total borehole flow rate. Because a potential inflow is thought to occur at a depth of 14.8 m, three integration intervals were defined. These are 5.5 to 25.5 m, 6 to 13.5 m, and 16.5, to 25.5 which correspond to the MOMENT runs VE460B, VE460C, and VE460D respectively. The first integration interval assumes that an inflow does not occur at 14.8 m whereas the last two intervals assume an inflow does exist at that depth and therefore straddle this depth. Figure IV.17 plots the zero partial moments for the intervals described above. For all three intervals analyzed the time derivative of the partial zero moment exceeds in magnitude the threshold value reported by LÖW et al. (1991) of 0.5 kg/m^2 hr. However, the partial zero moment behavior is very poor because of the quick saturation of the logs. MOMENT uses central difference time derivatives for calculational purposes so the better this derivative approximates a tangent to the time function at a given measurement time the better the MOMENT calculation for that time. From review of Figure IV.17, it appears that the best chance for a good MOMENT flow rate evaluation should be at time 0.47 hours.

Figure IV.18 plots the flow rates calculated for the three intervals by MOMENT. For the three integration intervals the flow rate at 0.47 hours was -4.4, -3.6, and -7.2 l/min for simulations B, C, and D, respectively. The estimate by manual means was between 3 and 4 l/min and the advection front tracking yielded a flow rate of 3.8 l/min. Two of these runs reproduce a flow rate in the order of 3.8 l/min. If we average the estimated flow rate at 0.47 hours for runs B and C we receive an average of 4 l/min which shows good agreement with prior flow rate estimates. The interval 31.5 to 34 m was also evaluated for flow rate by the partial moments and MOMENT but the results were poor. This was expected as the logs show a complicated behavior in this interval because they show irregular growth as a function of time. Further analysis of these logs could be performed with BORE but this was not done on these logs.

IV.3.6 Test VE461, Borehole 85.008

IV.3.6.1 Qualitative Description and Analysis

Borehole 85.008 was opened on February 2, 1990 at 15:25 and flowed all weekend. Borehole 88.017 was also open all weekend. Again a limited number of flow and conductivity measurements were made at the wellhead during testing. For this reason they will not be summarized in tabular form but rather recounted in the next few sentences. When Borehole 85.008 was opened, a flow rate of approximately 6 l/min was measured. On the morning of February 5 at 7:36, the flow rate was again measured and was from 2 to 3 l/min. At 8:41 on February 5, the conductivity of the effluent borehole fluid was measured to be 213 μS/cm corrected to 20°C. At a flow rate of 3 l/min, the Reynolds Number corresponds to 740. A maximum mean borehole velocity would be 31 m/hr.

The first log measured in Borehole 85.008 was measured prior to borehole flushing. This log (Log 36) was measured at 9:18 on February 5. After measurement of this log it was confirmed that breakthrough had occurred and the borehole was flushed with fresh water from 9:35 to 10:31. After flushing a series of 5 conductivity logs were measured. Logs 37 through 41 were measured at times 9, 30, 50, 83, and 166 minutes after the end of borehole flushing. Borehole 88.017 was not closed until 10:40 which corresponds to a time between logs 37 and 38. Figure IV.19 plots the temperature and conductivity logs measured after wellbore flushing and Log 36 which was measured prior to flushing. From review of Log 36 it can be seen that there exists an apparent saturated concentration profile. Inflows are clearly evident at 25 m and at 13.8 m, with the inflowing concentration at 13.8 m being greater than the inflowing concentration at 25 m (see Equation IV.6). The outflowing concentration as measured by Log 36 is 185 μS/cm. Interestingly, This is less than the measured conductivity recorded at the well head at 8:41 (213 μS/cm). The reason for this discrepancy is not known.

From the first logs measured after flushing, we can more clearly see the various inflow points encountered in Borehole 85.008. From review of logs 37 through 41 it can be seen that inflows of traced fluid occur at 13.8, 16.2, 21.8, and 24.9 m. There is some inflow at approximately 40 m, which is non-traced. From the first temperature log after

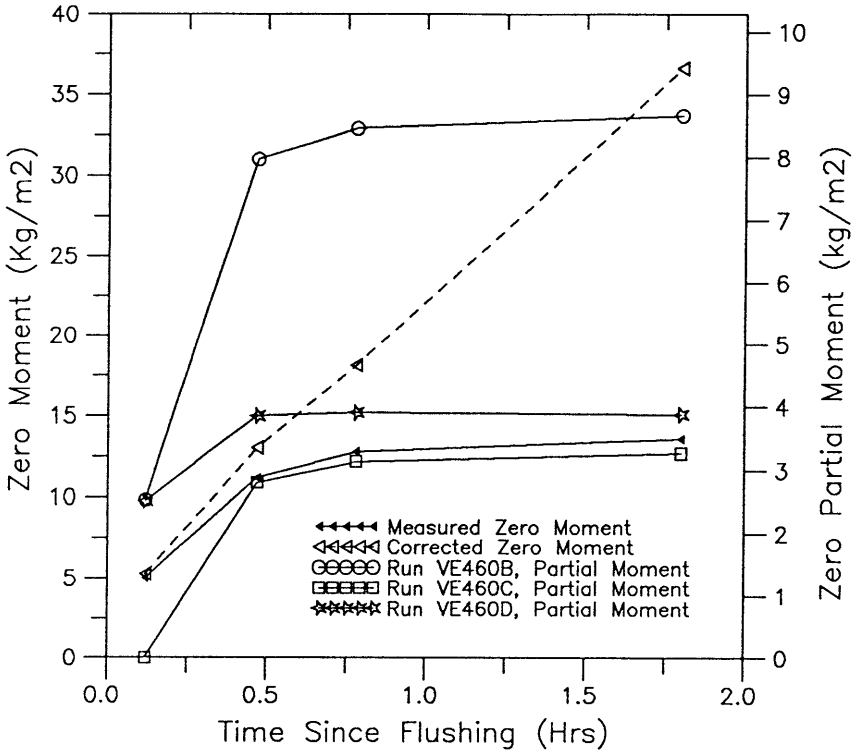

Fig. IV.17: Zero Moments for Fluid Logging Test VE460 Borehole 88.017, Logs 27,28,29, and 30

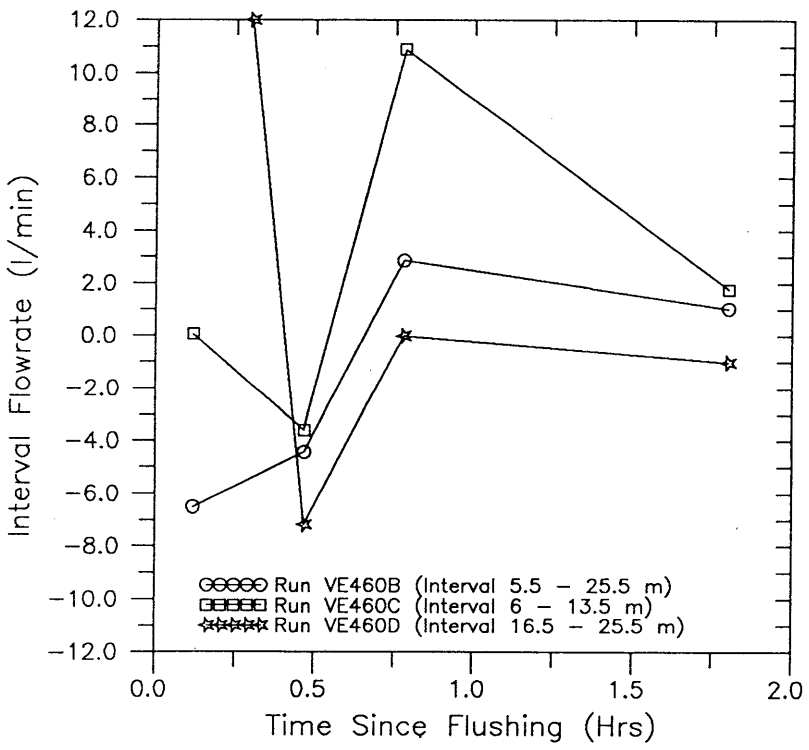

Fig. IV.18: Interval Flowrate as Calculated by MOMENT, Test VE460,Logs 27,28,29, and 30, Borehole 88.017

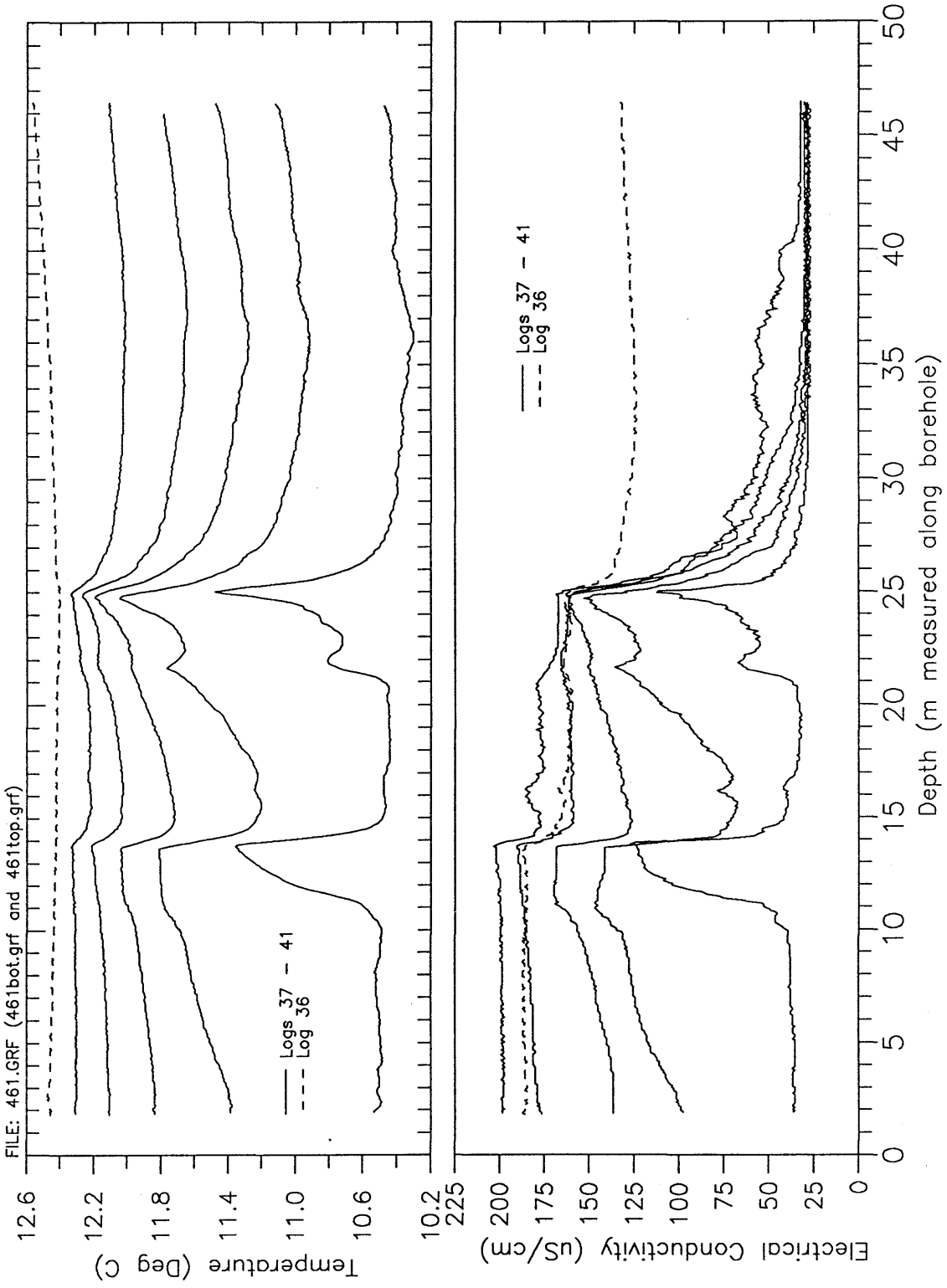

Fig. IV.19: Conductivity and Temperature Logs 36,37,38,39,40 and 41, Borehole 85.008, Logging Times −73,9,30,50,83, and 166 Minutes After Borehole Flushing

flushing, it can be said that the inflow at 13.8 m is the greatest with respect to volumetric flux. From the late time conductivity logs it can also be seen that this inflow contributes the greatest inflowing concentration. The inflow at 16.2 m shows up as a very low volumetric flux in the temperature logs but the late time conductivity logs show this inflow has a relatively high inflowing concentration relative to those inflows below it. The second highest volumetric flux occurs at 24.9 m followed by the inflow at 21.8 m. From the late time conductivity log 41 it appears that the inflowing concentration at 21.8 m is somewhat greater than that inflowing at 24.9 m. In general it appears that the inflowing concentration increases as depth decreases. The first temperature log measured after flushing shows some evidence for a minor inflow occurring at approximately 40 m. Further evidence to support this possibility will be presented later in this section. There is also some hint of inflow between the depths 26 to 29 m. Through study of the temperature gradient log 37 and there could be a very minor inflow at approximately 28 m. It would appear that it would be non-traced. There is also minor evidence on this log of very minor inflows at 33.5 and 35.6.

It is important to note that the last log after flushing (Log 41) is higher in concentration than the log measured prior to flushing (Log 36). This implies that the concentration inflowing was transient during logging. This could imply that the mean inflowing concentration was changing since first arrival (not known), or this transience could result from Borehole 88.017 being closed while logging Borehole 85.008. With the closing of 88.017 between the measurement of Logs 37 and 38, it is certain that flow field transience was created. It can only be speculated as to the signature of these effects upon the measured logs.

Table IV.9 summarizes the best defined inflows as determined through fluid logging and compares these results with the results of BGR Lugeon Tests performed in this borehole and the fracture mapping presented by Bräuer. Figure IV.20 also summarizes the information in Table IV.9 but in a schematic format. By comparing the results below we can see that the fluid logging reproduces the results from Lugeon Testing for all inflows with the exception of the permeable region identified by Lugeon Testing between 43.7 and 45.7 m. An important point can be made by reviewing the Lugeon Tests more closely. Of the permeable region identified by Lugeon Tests between 12 and 17 m, the most permeable region is between 12.7 to 13.7 m. This peak in permeability corresponds well with our observed peak at 13.8 m. Likewise, the permeable region identified by Lugeon Tests between 23.7 and 27.8 has its maximum between 23.7 and 24.7 m which again corresponds well with the fluid logging maximum peak for the interval at 24.9 m. The Lugeon Test typically shows very transmissive areas as being a distribution of transmissivity over a few meters which typically has a interval of maximum transmissivity isolated to 1 to 2 m. This supports the suspicion that the fluid logging clearly identifies these maximums but that the entire area of inflow is poorly defined because of interference encountered by being close to a large volumetric and mass flux interval.

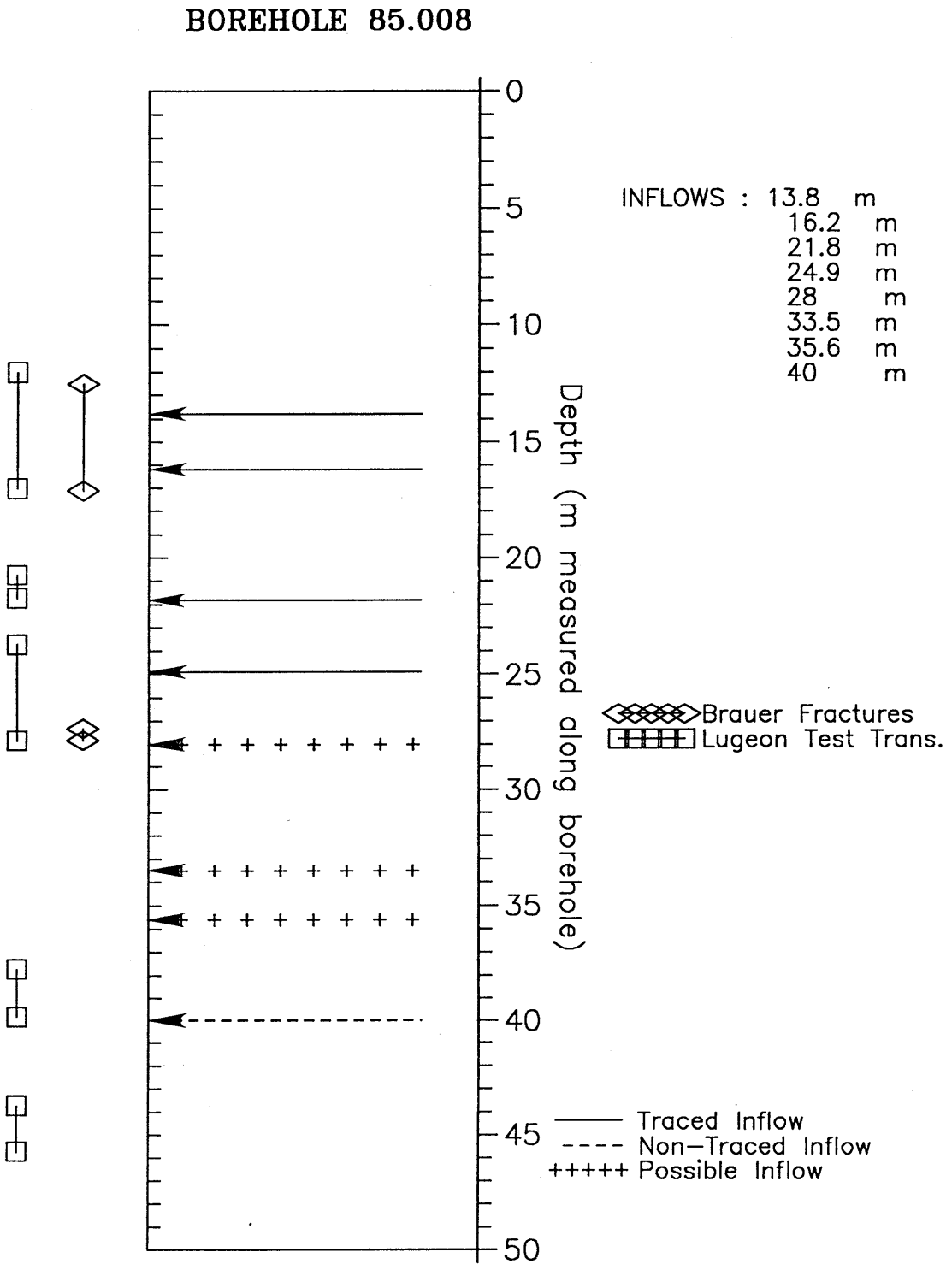

Fig. IV.20: Inflow Locations, Borehole 85.008

Table IV.9: Comparison of Significant Permeability Zones as Determined by Fluid Logging, Lugeon Tests, and Bräuer

Fluid Logging Inflows	Bräuer Fracture System	Lugeon Testing (1)	Inflow Conc. (2)
13.8, 16.2	12.5 - 17.1	12 - 17	T
21.8		20.7 - 21.7	T
24.9		23.7 - 27.8	T
(28)	27.3 - 27.8	23.7 - 27.8	NT
(33, 35)			NT
40		37.7 - 39.8	NT
		43.7 - 45.7	

(1) Intervals where K greater than or equal to 1E-11 m/s.
(2) (T) equals a traced inflow, (NT) equals non-traced.
(#) Means that the inflow point is poorly defined.

IV.3.6.2 Quantitative Analysis

Because of the evolution of the measured logs it was not possible to estimate borehole flow rate from advection front tracking. The flow rate measured at the wellhead was from 2 to 3 l/min during the period of logging. The first step will again be to estimate the average inflowing concentration through a mass balance calculation. The total borehole flow rate is relatively uncertain in this test and this will add some uncertainty to our calculation. The measured zero moment and the corrected zero moment for the interval from 4 to 45 m are plotted on Figure IV.21. Again the measured zero moment levels off in the late time logs which is indicative of saturated conditions. The slope of the corrected zero moment decreases with time which is not supported by the log evolution and is the result of a erroneous estimation of the corrected zero moment. Again it is expected that the corrected moments are in error and this is believed to occur for the same reasons as in previous examples. The resulting average inflowing concentration and mass flux are summarized in Table IV.10. Again the best estimate is evaluated at 30 minutes. Estimates at greater times are thought to be in error.

The difference between the outflowing concentration at Log 36 and Log 41 is 12.5 μS/cm. The time difference between the two logs is 239 minutes. This results in an average inflowing concentration time rate of change equal to 0.052 μS/cm min. This derivative is considered appropriate for the time period of 73 minutes before end of borehole flushing and 166 minutes after.

Table IV.10: Borehole Average Mass Flux and Inflowing Concentration, Borehole 85.008

Time (min)	Mass Flux (kg/s)	Ci (kg/m^3)	Ci ($\mu S/cm$)
30	5.36E-6	0.107	200
50	4.48E-6	0.090	167
83	4.42E-6	0.088	165
166	4.58E-6	0.092	171

These logs were potentially well suited for partial moment analysis because (1) the logs reached saturated conditions relatively slower than previous tests with the exception of VE458, and (2) the primary inflows were relatively uncrowded in terms of close neighboring inflows. The logs are potentially ill-suited for the partial moment method because of low mass flux and the transient average inflowing concentration. Three integration intervals were chosen for partial moment analysis. They were, 4 to 8.5 m, 17.5 to 20.3 m, and 29 to 32.5 m. The first interval was to measure the total borehole flow rate and the other two were to measure sub-interval flow rates. Figure IV.21 plots the zero partial moments for the three integration intervals. As has been previously mentioned, MOMENT makes good estimates of flow rate at times where the central difference time derivative (slope) is representative of the tangent at that point and when this derivative is of a significant magnitude. LÖW et al., (1991) suggest that the time derivative of the zero partial moment should exceed 0.05 kg/m^2 hr.

For interval 29 to 32.5 m none of the time derivatives of the zero partial moments exceed the suggested threshold of 0.05 kg/m^2 hr and for this reason the results from MOMENT will not be used. For interval 4 to 8.5 m the time derivatives are only large enough for times 0.5 and 0.83 hours. From review of the plot of the partial zero moments for this interval we can see that the evaluation of the derivative should be meaningful for both of these times as well. Figure IV.22 plots the MOMENT estimates of interval flow rate for the intervals 4 to 8.5 m and 17.5 to 20.3 m. For interval 4 to 8.5 m the estimates at 0.5 and 0.83 hours were averaged to give best guess estimate for that interval. The average is 3.4 l/min which is slightly greater than the manual borehole flow rate estimates of 2 to 3 l/min. The MOMENT estimate is considered a reasonable estimate in light of the difficulties in manual flow rate measurement encountered and the relative lack of measurements for this borehole. For the interval 17.5 to 20.3 m again the time derivative exceeded 0.05 kg/m^2 hr only at times 0.5 and 0.83 hours. From review of the zero partial moment as a function of time in Figure IV.21 it appears that the best flow rate estimate should occur at 0.5 hrs. MOMENT calculated a flow rate of -1.43 l/min for the interval 17.5 to 20.3 m at a time of 0.5 hours. Through review of the temperature logs this interval flow rate estimate is considered to be in order and within expectation. Additional simulation with BORE was not performed with these logs.

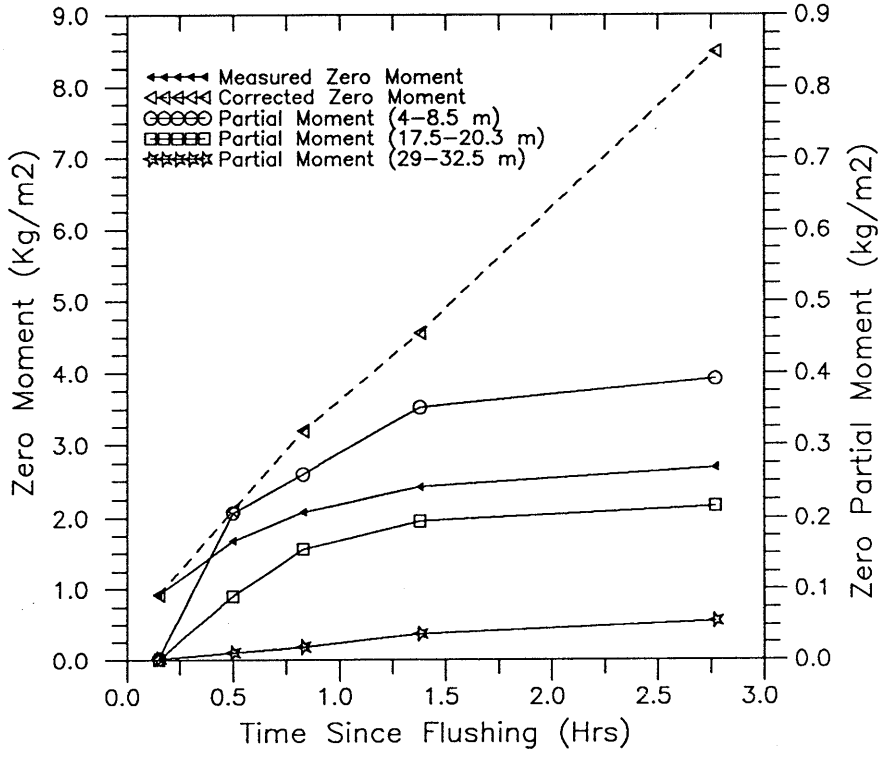

Fig. IV.21: Zero Moments for Fluid Logging Test VE461 Logs 37,38,39,40, and 41, Borehole 85.008

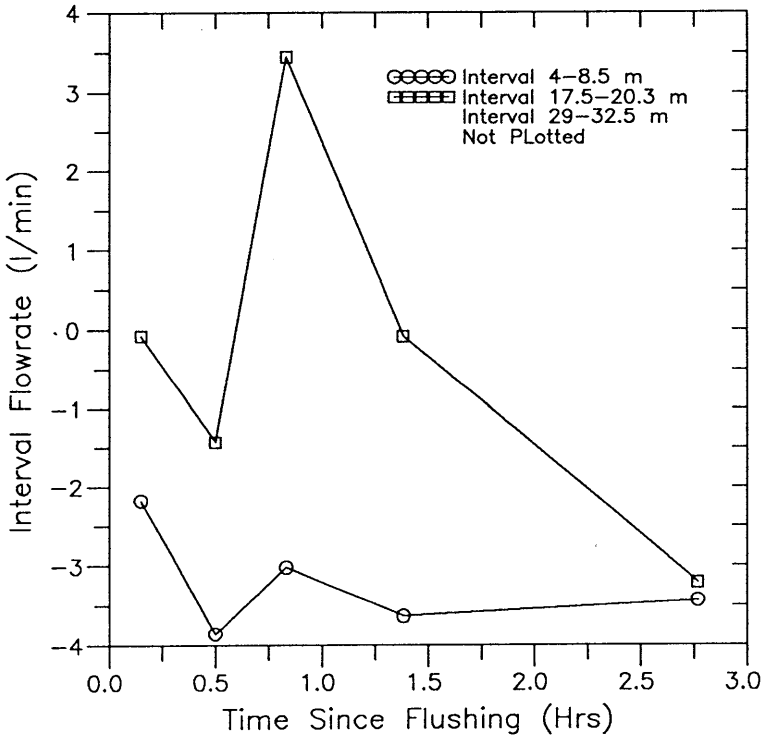

Fig. IV.22: Interval Flowrate as Calculated by MOMENT, Test VE461,Logs 37,38,39,40 and 41, Borehole 85.008

IV.3.7 Test VE462, Borehole 85.005

IV.3.7.1 Qualitative Description and Analysis

Borehole 85.005 was opened on February 5, 1990 at 14:58. The packers in Borehole 85.008 were inflated at 15:40 on the same afternoon. Because of time constraints, the packer assembly was left in borehole 85.005 over the night. Upon arrival on February 6, 1990, the packers were pulled from 85.005 and the logging assembly was installed. A series of flow and concentration measurements were manually collected of the effluent coming from the wellhead during testing. These measurements are summarized in Table IV.11.

Table IV.11: Measurements of Conductivity and Flow Rate Measured at the Borehole 85.005 Wellhead During Logging.

Date (Day/Month)	Time	Conductivity (μS/cm)	Flow Rate (l/min)	Comments
5/2	14:58		6.0	
5/2	15:07	208		
6/2	07:17	1142		
6/2	08:04		5.0	
6/2	09:10	$\simeq$ 200		
6/2	10:17		3.5	Meas. at end of flushing

The flow rate from the borehole was high (4 to 5 l/min) during logging and therefore peak development was quick. These flow rates correspond to maximum Reynolds Numbers of 987 and 1234 respectively. These two flow rates also correspond to maximum borehole velocities of 41.2 m/hr and 51.5 m/hr respectively. The concentration in the borehole was higher than background when first measured 9 minutes after packer deflation (208 μS/cm). By the next morning the concentration measured at the wellbore head was significantly increased at a magnitude of 1142 μS/cm.

The first conductivity log was run at 8:06 on the morning of February 6 and was measured prior to borehole flushing. The conductivity and temperature profile from Log 42 are shown as a dashed line in Figure IV.23. The conductivity profile showed a saturated concentration profile at background concentration from the bottom of the borehole up to a depth of 21 m where the concentration started rising sharply to a maximum at 17.6 m. There are several inflows evident between 21 and 17.6 m. The maximum concentration at 17.6 m is approximately 1100 μS/cm which abruptly falls off to a concentration of 950 μS/cm between 17.6 m and 15 m. Of interest with this suite of logs is the presence of a definite and sharp concentration peak occurring at 17.6 m even on late time (apparently saturated) logs.

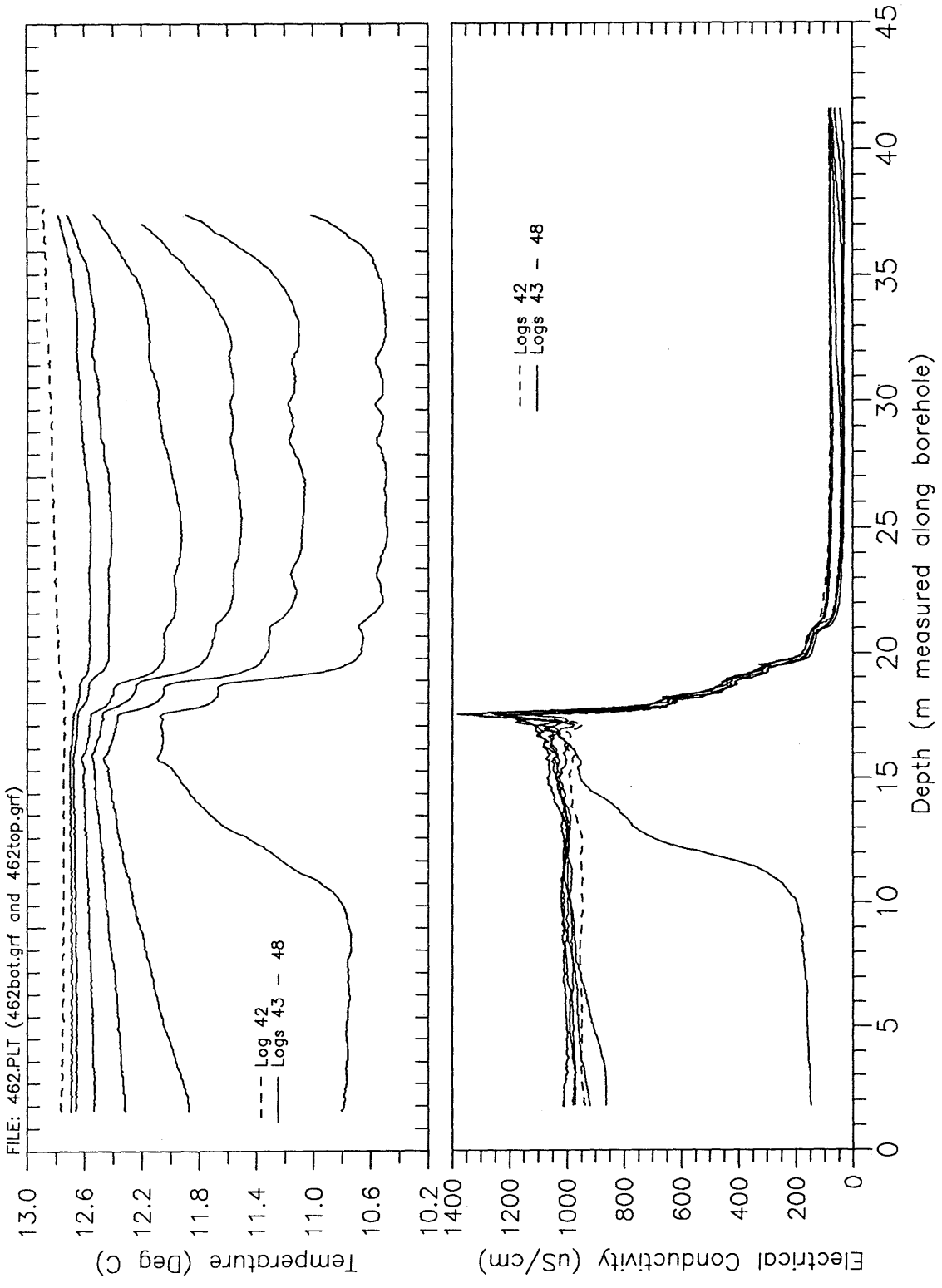

Fig. IV.23: Conductivity and Temperature Logs 42,43,44,45,46,47 and 48, Borehole 85.005, Logging Times −64,8,22,38,68,149 and 226 Minutes After Borehole Flushing

The borehole was flushed with fresh water from 8:27 until 9:15. During flushing the outflowing borehole water stabilized at a concentration around 200 µS/cm which is at least 140 µS/cm greater than the flushing fluid. This is indicative of the high volumetric flux entering borehole 85.005. After flushing, conductivity logs 43 through 48 were recorded at times 8, 22, 38, 68, 149, and 226 minutes after borehole flushing ended. Figure IV.23 plots the conductivity and temperature logs for Logs 43 through 48. Certain things are immediately evident upon viewing these logs. The major concentration influx is occurring at 17.6 m. However, the temperature log shows that the bulk of the volumetric flux occurs in the interval 20.7 to 17.6 m which corresponds in part to the largest borehole intersection with the S1/S2 fracture system. From review of the conductivity logs 5 traced inflows are clearly evident at depths 17.6, 18.2, 18.8, 19.5, and 20.7 m. Additionally, a non-traced inflow occurs in the bottom of the borehole in the vicinity of 40 m.

Several non-traced inflows deeper than 20.7 m did not clearly show up on the conductivity logs but did on the temperature logs. These additional minor non-traced inflows occur at depths 23.4, 25.7, 31.6, 33.2, and 35.2 m. All of these inflows are very low in volumetric flux and are not producing injected fluid. Because the mass flux and volumetric flux are so high that minor inflows cannot be easily delineated for depths 0 to 17.6 m. For this region, the temperature gradient log, which is the most sensitive to minor inflow points, was used to delineate inflows. The temperature gradient log offers the best resolution for peaks which are quickly interfered with. The temperature gradient log gave evidence for minor inflows at the approximate depths 5.5, 8.5, 12.7, and 16 m. The late time conductivity logs (Logs 42 and 48) provide further evidence of these inflows as slope changes in the conductivity profiles. Because the concentration falls off greatly above 17.6 m, it is felt that these inflows are of a lesser concentration than that which inflows at 17.6 m.

Table IV.12 summarizes the inflows detected from the fluid logging test. Also included on the table is the fracture system locations as reported by Bräuer and the intervals of the borehole which have a hydraulic conductivity greater than 1E-8 m/s as determined from BGR Lugeon testing. The results from Lugeon testing in this borehole found that almost the entire borehole had a transmissivity greater than 1E-11 m^2/s as measured in 1 m intervals. Because of this, intervals listed in the table only represent intervals with a transmissivity greater than 1E-8 m2/s. This was an effort to increase better resolution for this borehole. There is good agreement between the primary volumetric and mass flux inflow interval and the primary fracture zones as defined by Bräuer. In addition, the intervals identified by BGR Lugeon Testing as having a hydraulic conductivity greater than 1E-8 m/s show very close correlation with the inflowing intervals as defined by fluid logging. Perhaps the most important observation is that all inflows identified below 20.7 m are thought to be non-traced. These are not in the primary fracture zone which is considered to be the S1/S2 and the K4 zones identified by Bräuer to intersect the 85.005 borehole from 14.2 m to 20.5 m. Figure IV.24 is a schematic of the Borehole 85.005 which shows the information contained in Table IV.12.

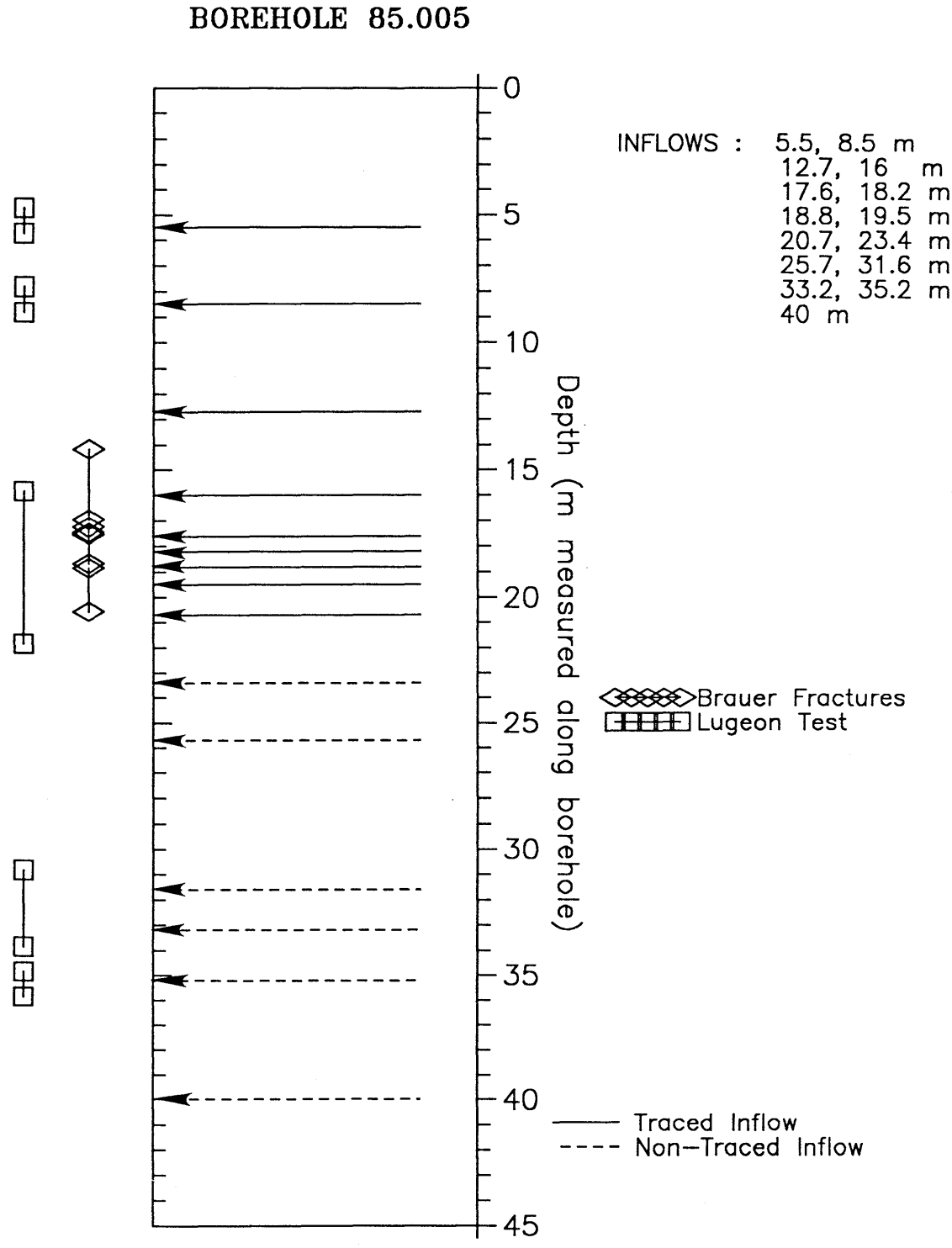

Fig. IV.24: Inflow Locations, Borehole 85.005

Table IV.12: Comparison of Significant Permeability Zones as Determined by Fluid Logging, Lugeon Tests, and Bräuer, Borehole 85.005

Fluid Logging Inflows	Bräuer Fracture Systems	Lugeon Testing (1)	Inflow Conc. (2)
5.5		4.7 - 5.7	T
8.5		7.8 - 8.8	T
12.7			T
16	14.16 - 16.93	15.8 - 21.8	T
NA	17.23 - 17.43	15.8 - 21.8	
17.6	17.51 - 18.66	15.8 - 21.8	T
18.2	17.51 - 18.66	15.8 - 21.8	T
18.8	18.83 - 20.54	15.8 - 21.8	T
19.5	18.83 - 20.54	15.8 - 21.8	T
20.7	18.83 - 20.54	15.8 - 21.8	T
23.4			NT
25.7			NT
31.6		30.8 - 33.8	NT
33.2		30.8 - 33.8	NT
35.2		34.8 - 35.8	NT
40			NT

(1) Intervals where T greater than or equal to 1E-8 m2/s
(2) (T) equals a traced inflow, (NT) equals non-traced

IV.3.7.2 Quantitative Analysis

Because of the very quick log development, it was not possible to estimate total borehole flow rate through advection front tracking. In addition, the method of partial moments is ill-suited for this suite of logs because of the extremely fast log saturation. The use of BORE would be a practical analysis tool for this log suite. However, BORE simulations were not performed on these logs. It was possible to estimate the time rate of change of the average inflowing concentration during measurement of these logs. The difference between the outflowing concentration for Log 42 measured 64 minutes prior to end of flushing and Log 48 measured 226 minutes after flushing is 76.2 μS/cm. The time difference between the two logs is 290 minutes. This results in an average inflowing concentration time rate of change equal to 0.263 μS/cm min. This derivative is considered appropriate for the

time period of 64 minutes before end of borehole flushing and 226 minutes after.

IV.3.8 Test VE463, Borehole 88.015

IV.3.8.1 Qualitative Description and Analysis

Borehole 88.015 was opened on February 6, 1990 at 13:31. Table IV.13 summarizes the manual measurements of conductivity and flow rate of the borehole effluent. The flow rate stabilized at approximately 3 l/min which corresponds to a Reynolds Number of 740 and a maximum mean borehole velocity of approximately 30 m/hr. Two conductivity logs were measured (Logs 49 and 50) on the afternoon the borehole was opened. Log 49 was measured approximately 78 minutes after the borehole was opened. The profile has a maximum concentration plateau from approximately 23 to 25 m of 112 μS/cm which is slightly higher than background concentrations. At depths deeper than 26 m the concentration remains at 92 μS/cm which is 12 μS/cm over the background concentration observed in the other logged boreholes. The reason for this change in apparent background concentration is not understood. A second log was run (Log 50) 124 minutes after the borehole was opened. This log shows a similar, apparently saturated log, with an increased concentration from 23 to 25 m at 152 μS/cm. Concentrations below 26 m remained at 92 μS/cm. The borehole flowed overnight.

Upon arrival the next morning (February 7), conductivity log 51 was measured prior to borehole flushing. Figure IV.25 plots the temperature and conductivity log 51. This log shows apparent saturated conditions just as Log 50 did however the concentration has increased to over 950 μS/cm at the major inflow at 25.1 m. In addition, a new inflow has occurred at 35.8 which also produces traced fluid. After measurement of Log 51 the borehole was flushed from 7:36 to 8:25. A suite of 6 logs (Logs 52 through 57) were measured at times 6, 22, 42, 78, 160, and 263 minutes after flushing ended. These logs are also plotted in Figure IV.25.

Table IV.13: Measurements of Conductivity and Flow Rate Measured at the Borehole 88.015 Wellhead During Logging.

Date (Day/Month)	Time	Conductivity (μS/cm)	Flow Rate (l/min)	Comments
6/2	14:27	102 (12.4°C)	1.2	Leakage around surface casing
6/2	14:59		3.0	
7/2	07:33		2.3	
7/2	08:21	88 (10.4°C)		Measured at end of flushing
7/2	09:51		3.0	

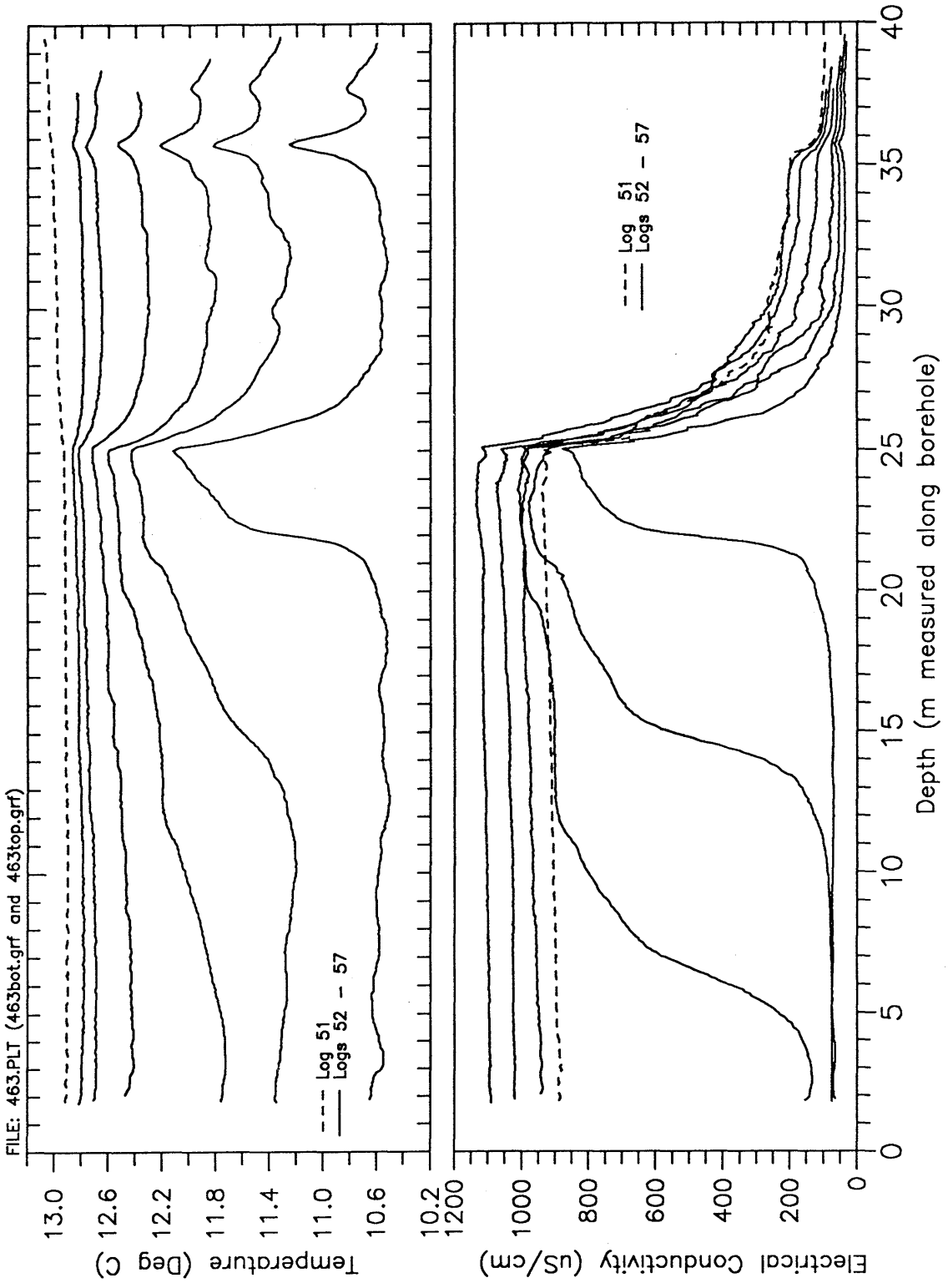

Fig. IV.25: Conductivity and Temperature Logs 51,52,53,54,55,56, and 57, Borehole 88.015, Logging Times −67,6,22,42,78,160 and 263 Minutes After Borehole Flushing

The major volumetric and mass flux appears to emanate from approximately 25 m. A secondary inflow again occurs at a depth of 35.8 m. A review of these logs reveals some interesting findings. First, there is a very complicated concentration distribution for all logs from approximately 21 m to 25.1 m. The peak concentration is not at 25.1 m, but somewhat further up the borehole at approximately 23.5 m. Also, the last three logs measured look like saturated curves but the concentration level rises with every log for all points above the major inflow at 25.1 m. These logs show strong evidence that the concentration inflowing from 23 to 25 m is transient and increasing. The fact that Logs 55, 56, and 57 decrease monotonically from 23 m to the surface supports this argument. Interestingly, the inflow occurring at 35.8 m does not seem to be significantly transient. By significantly transient, it is meant that the concentration changes significantly within the sampling frequency. Logs 51 and 57 show that the inflow approaches a similar saturation concentration of about 200 μS/cm.

No major inflows appear to be occurring over the first 23 meters of the borehole. The first temperature and temperature gradient log measured after flushing (Log 52) showed signs of minor inflows occurring in this interval however these trends are not supported by either late time conductivity or temperature logs. The major volumetric flux is occurring at a depth of approximately 25.1 m which is in agreement with the location of the S1/S2 fracture zone as mapped by BGR. This inflow also represents the highest inflowing concentration. It is felt that another inflow(s) is occurring within the interval 23 to 25 m but hard evidence is lacking. Minor inflows might occur on the steep upstream flank of the major inflow (25.1 m) but are hard to substantiate due to severe interference. The best evidence of such inflows is the pronounced step in concentration at 25.6 m in Log 51. A relatively strong traced inflow is occurring at a depth of 35.7 m. This inflow is not flowing at a concentration as high as the inflow at 25.1 m. A much more minor inflow (apparently non-traced) is occurring at depth of 37.7 m. This inflow shows up most clearly on temperature log 52. The following table summarizes the inflows detected by fluid logging and compares their location to the mapped fracture systems of BGR (Bräuer). Figure IV.26 is a schematic of this table showing the inflows.

Table IV.14: Comparison of Significant Permeability Zones as Determined by Fluid Logging and Bräuer, Borehole 88.015

Fluid Logging Inflows	Bräuer Fracture System	Inflow (1) Concentration
23 - 25		T
25.1	25.09	T
25.6		T
35.7		T
37.7		NT

(1) (T) equals a traced inflow, (NT) equals non-traced

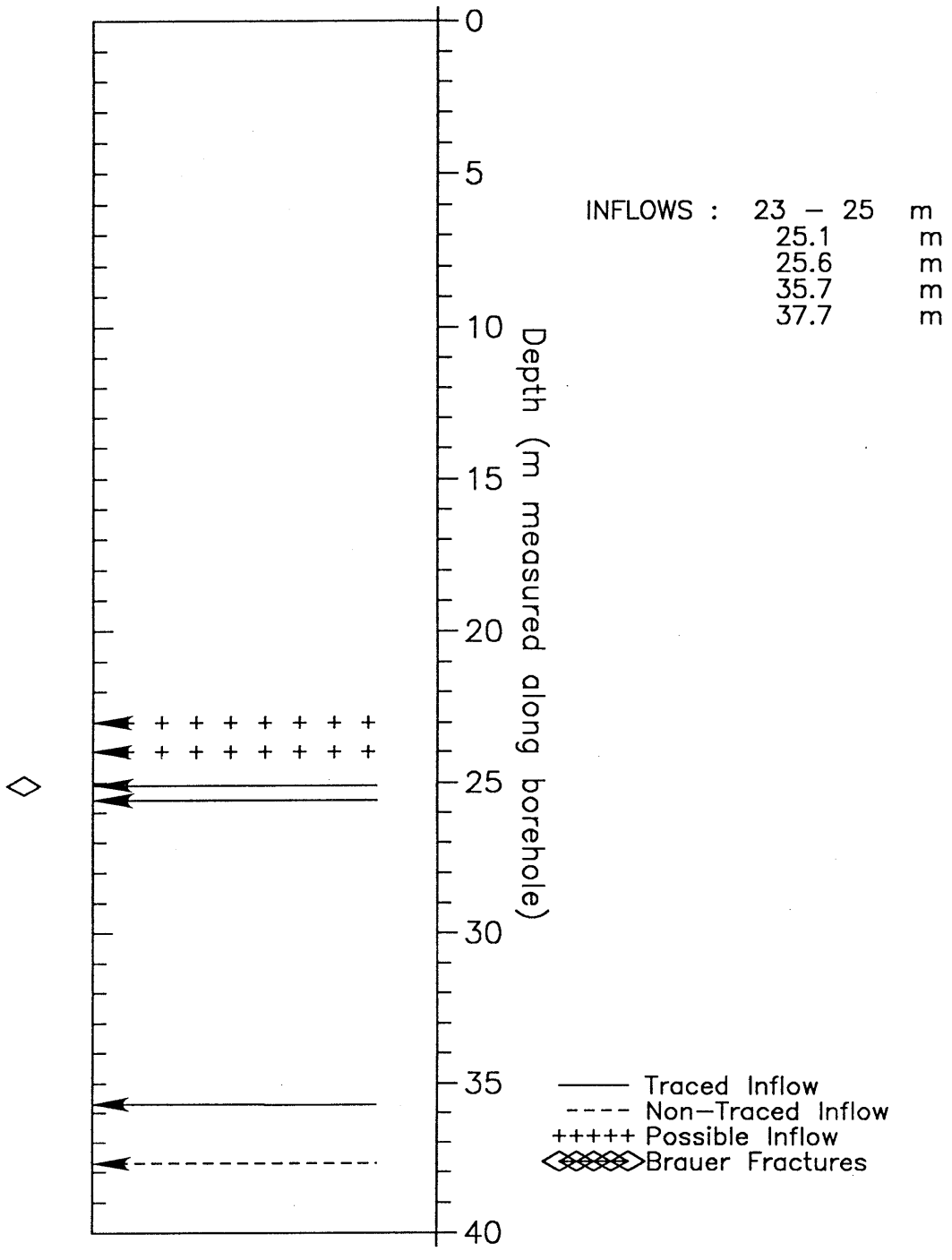

Fig. IV.26: Inflow Locations, Borehole 88.015

IV.3.8.2 Quantitative Analysis

First total borehole flow rate can be calculated based upon the advection (ignoring dispersion) of the 500 μS/cm concentration between Logs 52 and 53 and 53 and 54. The estimated flow rates are 2.5 and 2.3 l/min respectively. This corresponds to a Reynolds Number of 592 and a maximum mean borehole velocity of 24 m/hr. This suite of logs shows a strong concentration transience which shows up in the late time logs. If the average borehole inflowing concentration calculation is good, it should reflect this mass flux transience. The calculation assumes a total borehole flow rate of 2.5 l/min. Figure IV.27 plots both the observed and corrected zero moments for the entire borehole (Interval 3 to 37 m). The measured zero moment quickly levels off, indicating a saturated profile. However, the magnitude of the moment does increase slightly in the last three logs. This is the result of the increasing saturation level evident in the last observed logs. The corrected zero moment shows a slight decrease for Log 55 but the slope increases from that log. Below the calculated average borehole mass influx and inflowing concentration are summarized.

Both early time and late time estimates should be good because in the early time logs the moment does not require correction and in the late time logs the change in concentration between logs at the top of the borehole is relatively linear making the calculation of the accumulated mass exiting the borehole accurate. From review of Log 57 we can see that in fact the outflowing concentration was approximately 1100 μS/cm as is calculated for this time in Table IV.15.

Table IV.15: Borehole Average Mass Flux and Inflowing Concentration, Borehole 88.015

Time (min)	Mass flux (kg/s)	Ci (kg/m^3)	Ci (μS/cm)
22	2.27E-5	0.544	1005
42	2.02E-5	0.484	895
78	2.21E-5	0.530	980
160	2.42E-5	0.582	1074
263	2.49E-5	0.598	1103

Again it was possible to estimate the time rate of change of the average inflowing concentration during measurement of these logs. The difference between the outflowing concentration for Log 51 measured 67 minutes prior to end of flushing and Log 57 measured 263 minutes after flushing is 199.8 μS/cm. The time difference between the two logs is 320 minutes. This results in an average inflowing concentration time rate of change equal to 0.624 μS/cm min. This derivative is considered appropriate for the time period of 67 minutes before end of borehole flushing and 263 minutes after.

This set of logs seemed to be well suited for analysis through the

partial moment method because the mass flux rates were high and the primary peaks were few and not strongly interfered with at early times. Four integration intervals were selected for analysis by partial moments. A potential problem in analyzing this suite of logs is the strong transient nature of the inflowing concentration at the primary inflow. Three integration intervals were chosen for partial moment analysis and flow rate estimation. Intervals 5 to 22 m and 5 to 15 m were both chosen to estimate a total borehole flow rate. Ideally, one would prefer to choose integration intervals as large as is possible which would make the interval 5 to 15 m appear redundant. However, interval 5 to 15 m was chosen because of the odd behavior of logs 52 and 53 from approximately 18 to 25 m and the potential calculational problems this portion of the borehole might offer. Further, intervals 26.5 to 34 m and 27 to 34 m were chosen to determine the cumulative borehole flow rate coming from inflows located at 35.7 and 37.7 m. Again these two intervals are sampling the same flow rate. This is done as a consistency check to see how different the estimates might be for low velocity intervals.

Figure IV.28 plots the Zero Partial Moments for these four analysis intervals. For all three intervals, the time derivative of the zero partial moments exceed the threshold value of 0.05 kg/m^2 hr. The partial moment behavior for the interval 5 to 22 m is fairly ideal. MOMENT estimated negative (flowing out of the borehole) borehole flow rates for the last five logs (see Figure IV.29). The average between these five values is 2.8 l/min. For the interval 5 to 15 m, the moment behavior is a little less ideal with the moment possessing two regions of low slope, one at early time and one at late time. It is expected that the flow rate estimates at times 0.7, 1.3, and 2.67 hours should yield the most defendable results. The average flow rate from these three times is 2.9 l/min. Both of these values are in good agreement with the total borehole flow rate estimates from advection front tracking and from manual flow measurements. The moments for intervals 26.5 to 34 m and 27 to 34 m are small relative to the first two intervals. However, they should be large enough to give good estimates. Through review of the zero partial moments for these two intervals we can see that they are quite similar and it is not possible to discriminate between them in terms of which would yield the more robust calculation. Generally the best estimate comes from the interval with the highest magnitude moments (see LÖW et al., 1991), which in this case is the interval 26.5 to 34 m. Figure IV.30 plots the flow rates calculated by MOMENT for these two intervals. The interval 27 to 34 yields the most stable estimate of flow rate which, in most cases, is a smaller value relative to the interval 26.5 to 34 m. The average for all times other than 0.1 hrs for the interval 26.5 to 34 m is 0.14 l/min. The average for all time other than 0.1 hrs for the interval 27 to 34 m is 0.07 l/min. The difference between these two runs is a factor of two. From Figure IV.30 we can see that the estimate of flow rate at 0.7 hours for the interval 26.5 to 34 m is anomalously high. If we pull this value from the average for this interval, we receive an average interval flow rate of 0.1 l/min, which is very close to the interval 27 to 34 m results. The order of magnitude of the flow rate within this portion of the borehole is surely represented by the MOMENT calculations. The correct magnitude within that order of magnitude cannot be estimated with certainty. The next calculation is a forward calibration of the logs with the numerical borehole simulator BORE. BORE

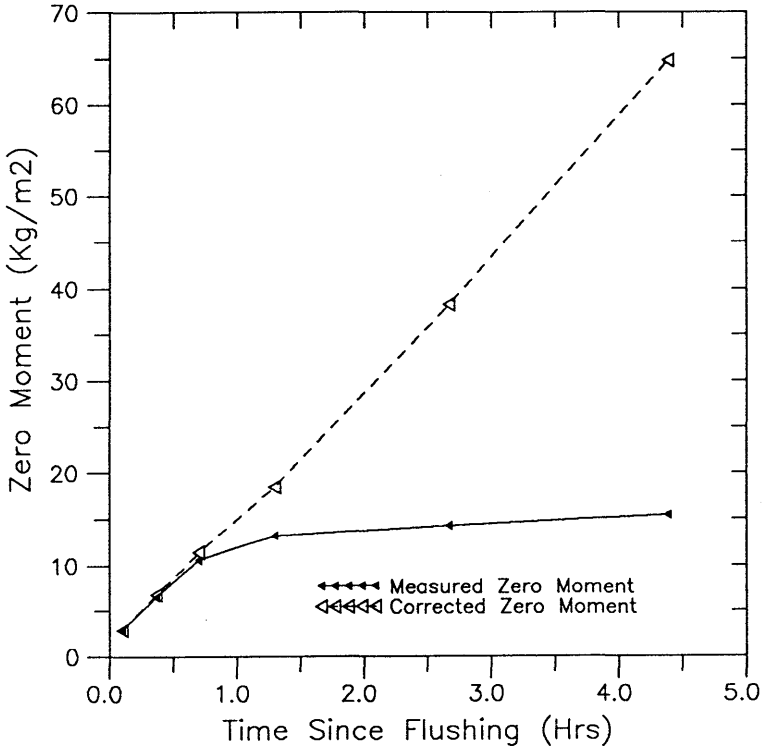

Fig. IV.27: Zero Moments for Fluid Logging Test VE463 Logs 52,53,54,55,56 and 57, Borehole 88.015

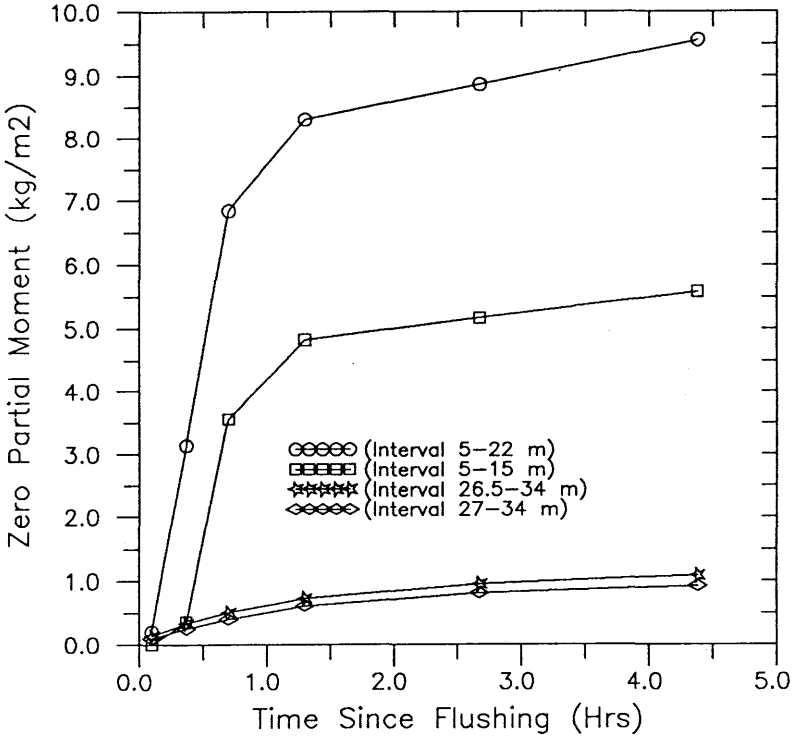

Fig. IV.28: Partial Zero Moments Calculated by MOMENT, Test VE463,Logs 52,53,54,55,56 and 57, Borehole 88.015

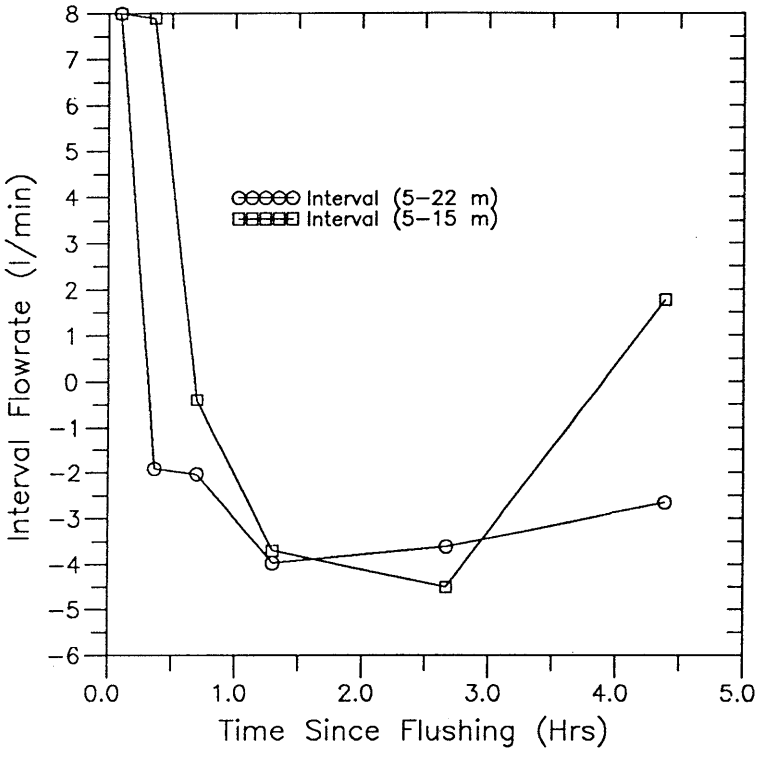

Fig. IV.29: Borehole Flowrates Calculated by MOMENT Logs 52,53,54,55,56 and 57, Borehole 88.015

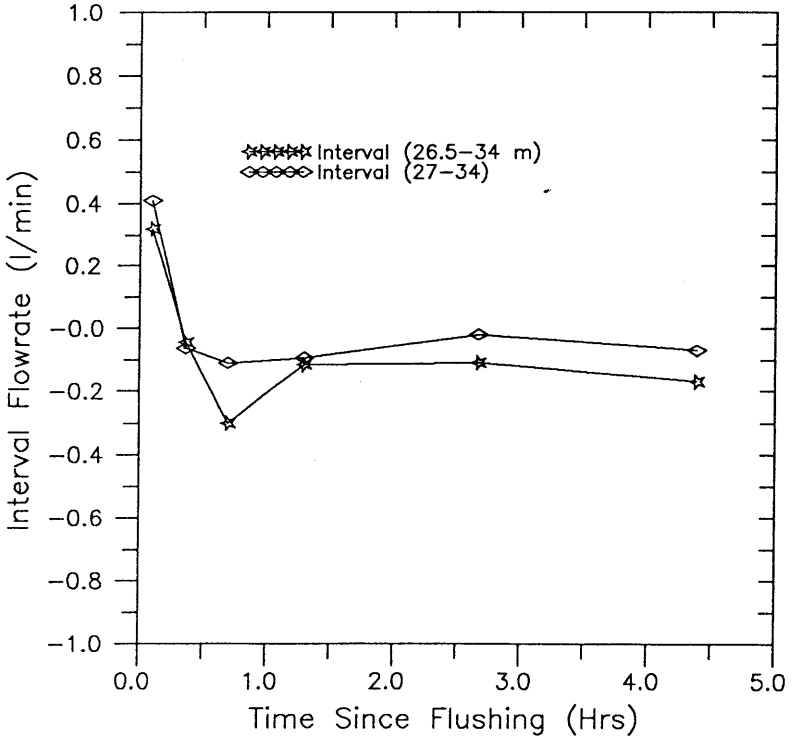

Fig. IV.30: Interval Flowrate as Calculated by MOMENT, Test VE463,Logs 52,53,54,55,56 and 57, Borehole 88.015

should be able to indicate how close MOMENT was in estimating the borehole flow rate in this low flow interval of the borehole.

The final analysis method used on this suite of logs is forward calibration with BORE. The analysis technique is trial and error calibration, starting from the bottom of the borehole and methodically progressing up the borehole with the specification of each inflow volumetric rate and inflowing concentration. The calibration is meant to be a first order analysis and significant time was not spent in optimization of parameters. Figure IV.31 plots the 6 conductivity logs measured after borehole flushing along with the BORE simulated logs. It is obvious upon review of the measured logs that the average inflowing concentration is increasing during logging and this is confirmed by the fact that the time rate of change of the average inflowing concentration was the largest for this suite of logs (0.624 μS/cm min). In fitting the logs, a constant set of flow rates were used for all times. A set of inflowing concentrations were held constant for the simulation of Logs 52 to 55 (6 to 78 minutes after flushing). A different set of inflowing concentrations were used for simulating between Log 55 to 56 (78 to 160 minutes after flushing). And a final set of inflowing concentrations were used to simulate between Log 56 and 57 (160 to 263 minutes after flushing). The fit is acceptable for this level of analysis and the input flow rates and concentrations are listed in Table IV.16.

The calibration started with the knowledge that the lowermost inflow had an inflowing concentration of 80 μS/cm and the relative flow rates could be initially estimated from the first temperature log after borehole flushing (Log 52). From this calibration continued on a trial and error educated guess method. It was very difficult to fit the conductivity peak emanating from 25.1 m for the first log. It was necessary to add inflows at 23 and 24 m which were felt to exist from qualitative review of the logs. The exact location of these inflows is still considered unknown. We see that the BORE calibration is possible even under relatively transient inflowing conditions. In addition, the use of BORE gives the analyzer another method by which to investigate the possibility of inflows. The inflows at 23 and 24 m are strongly interfered with and direct evidence is lacking. With BORE, it became obvious that some inflows between 23 and 25 m were necessary to fit both late time and early time logs. Finally, and perhaps most importantly, BORE yields estimates of inflowing concentration which cannot be had by other analysis methods. BORE can tell where the high concentration inflows are occurring. This is extremely important as the higher the inflowing concentration, the higher the degree of connection to the injection interval. The distribution of inflow volumetric rates gives a relative distribution of transmissivity within the borehole which is also of interest but is not related to the injection interval.

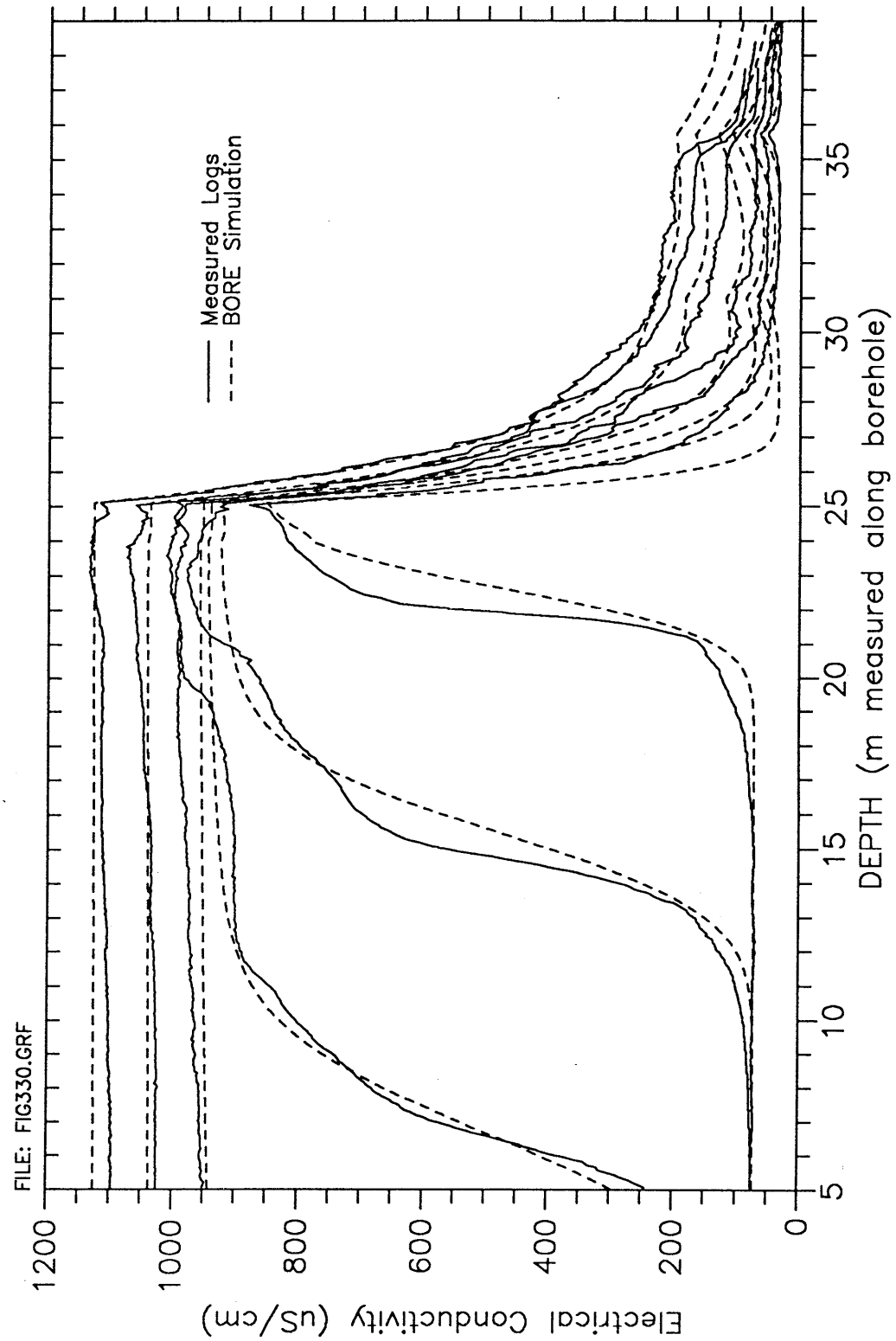

Fig. IV.31: Trial Bore Simulation, Test VE463, Borehole 88.015
Calibration to Logs 52, 53, 54, 55, 56 and 57 Measured 0.1, 0.37, 0.7, 1.3, 2.67 and 4.38 Hours After Borehole Flushing

Table IV.16: Calibrated Parameters Input to BORE for Test VE463 Calibration

Inflow Depth (m)	Inflow Rate (l/min)	Inflow Concentration (μS/cm)		
		Logs 52 to 55	Logs 55 to 56	Logs 56 to 57
23.0	0.05	1000	1080	1150
24.0	0.3	1000	1080	1150
25.1	2.1	1050	1130	1220
31.0	0.05	450	450	450
35.7	0.10	350	350	350
37.5	0.05	80	80	80

IV.3.9 Test VE464, Borehole 85.009

IV.3.9.1 Qualitative Description and Analysis

Borehole 85.009 was opened on February 7, 1990 at 13:03. Table IV.17 summarizes the manual measurements of conductivity and flow rate of the borehole effluent. The flow rate stabilized at approximately 6 l/min which corresponds to a Reynolds Number of 1481 and a maximum mean borehole velocity of approximately 62 m/hr. A second estimate of borehole velocity could not be calculated based upon the advection front movement between logs because of the high borehole velocities and the subsequent fast log development.

Two conductivity logs were measured (Logs 58 and 59) on the afternoon the borehole was opened. Log 58 was measured approximately 84 minutes after the borehole was opened, by which time the tracer had arrived. The concentration profile increases from the top of the borehole to a depth of 18.2 m with a maximum concentration of 102 μS/cm. The concentration from 19 to 28 m is slightly greater than the background concentration, indicating a slightly traced inflow at 28.3 m. From a depth of 28.3 m to the total depth, the concentration stays at background concentrations, indicating non-traced inflows. A second log was run (Log 59) 153 minutes after the borehole was opened. This log shows similar behavior to Log 58, except the concentrations have increased. For this log, the maximum at 18.2 m is now 148 μS/cm. The borehole flowed overnight.

The next morning (February 8), conductivity log 60 was measured prior to borehole flushing. Figure IV.32 plots the temperature and conductivity log 60. This log shows apparent saturated conditions, just as Logs 58 and 59 did. However, the concentration maximum at 18.2 m has increased to 497 μS/cm. The inflow at 28.3 has increased in concentration to a magnitude of 216 μS/cm. After measuring Log 60, the borehole was flushed from 7:35 to 8:35. A suite of 7 logs (Logs 61 through 67) were measured at times 6, 25, 44, 77, 118, 181, and 278 minutes after flushing ended. These logs are also plotted in Figure IV.32.

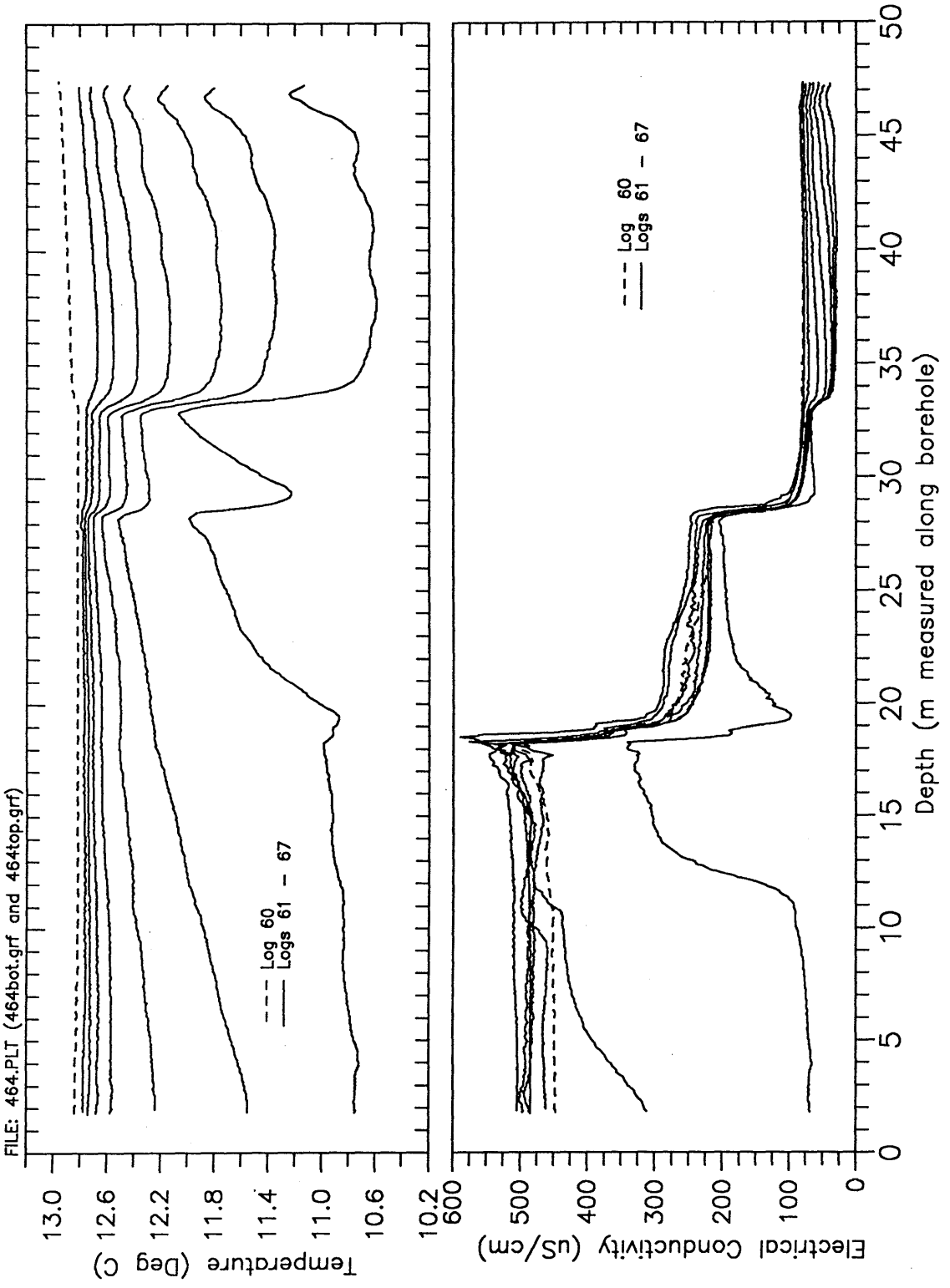

Fig. IV.32: Conductivity and Temperature Logs 60,61,62,63,64,65,66 and 67, Borehole 85.009, Logging Times −70,6,25,44,77,118,181 and 278 Minutes After Borehole Flushing

Table IV.17: Measurements of Conductivity and Flow Rate Measured at the Borehole 85.009 Wellhead During Logging.

Date (Day/Month)	Time	Conductivity (μS/sm)	Flow Rate (l/min)	Comments
7/2	13:03		6.9	Immediately after packer deflation
7/2	13:11		7.5	
7/2	13:14	80 (12°C)		
7/2	14:41		6.0	
8/2	07:12		6.0	

Log 60 was measured prior to flushing and is indicated by a dashed line. Three primary inflow zones are evident by looking at the conductivity logs. The maximum inflowing concentration occurs at a depth of approximately 18.2 m, with a lesser concentration inflowing at 28.3 m, and the background concentration inflowing at 32.8 m. From the first temperature log it can be seen that the inflow at 18.2 m is smaller in magnitude than those at 28.3 and 32.8 m in terms of volumetric flow rate. A traced inflow occurs at approximately 19 m which is indicated by a concentration step on the upstream side of the 18.2 m inflow peak. Three non-traced inflows are present in the bottom of the borehole at depths 39.5, 43.5, and 46.9 m. These are most clearly evident on the temperature logs. Conductivity logs 60, 66, and 67 show the presence of some diffuse inflow occurring at depths 23.5 and 25.6 m. These are strongly interfered with on early time logs but become more apparent on these late time logs. The location of these inflows is taken from the temperature gradient log 61. Gradient log 61 suggests that some minor inflows could occur at depths 9 to 11 m and 14.4 m. These are also hinted at by the conductivity logs but there is no strong evidence of their location. A final inflow is thought to occur between 3 and 4 m. This inflow shows up best on Log 61 and is quickly interfered with in later logs. The inflow is very minor and there is no strong evidence to suggest whether it is traced or non-traced.

The inflows are summarized in Table IV.18 along with the BGR Lugeon Test Intervals of Transmissivity greater than 1E-11 m^2/s and the Braüer Fracture System. They are all shown together in Figure IV.33 in a borehole schematic diagram. From Table IV.18, it can be seen that the observed inflows which are not poorly identified are in very good agreement with the BGR Lugeon test results and also the Bräuer Fracture System as it was defined for Borehole 85.009. As was rarely the case, the highest inflow concentration interval (18.2 m) does not correspond directly to a Bräuer Fracture System as mapped. For the inflows which are considered poorly defined, only the interval 14 to 15 m is supported by other data, namely the Lugeon testing.

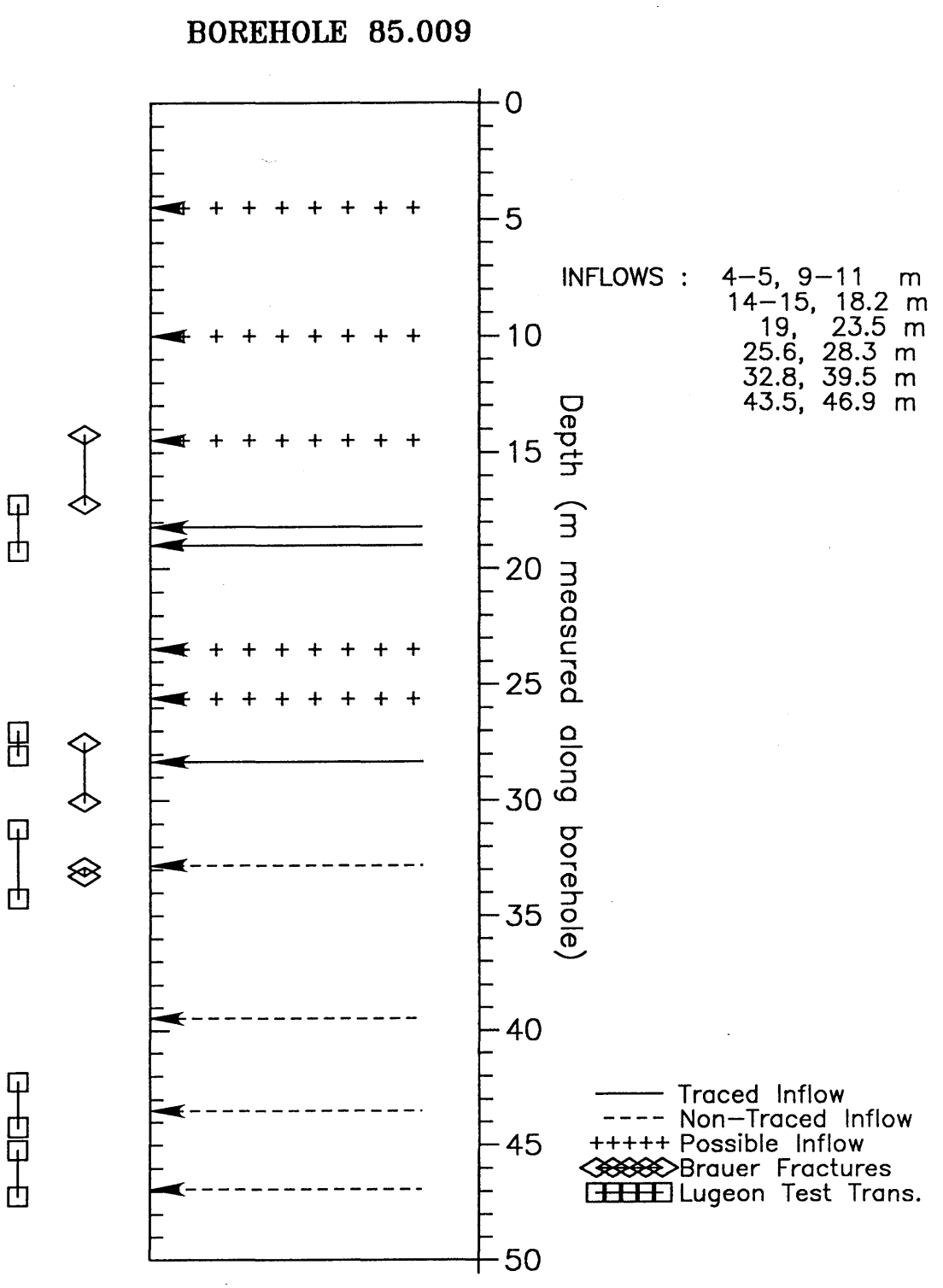

Fig. IV.33: Inflow Locations, Borehole 85.009

Table IV.18: Comparison of Significant Permeability Zones as Determined by Fluid Logging, Lugeon Tests, and Bräuer, Borehole 85.009

Fluid Logging Inflows	Bräuer Fracture System	Lugeon Testing (1)	Inflow Conc. (2)
(4 - 5)			?
(9 - 11)			T
(14 - 15)	14.26 - 17.2		T
18.2		17.2 - 19.2	T
19		17.2 - 19.2	T
(23.5)			T
(25.6)			T
28.3	27.48 - 30.04	27 - 28	T
32.8	32.86 - 33.26	31.2 - 34.2	NT
39.5		39.2 - 40.2	NT
43.5		42.2 - 44.2	NT
46.9		45.2 - 47.2	NT

(1) Intervals where K greater than or equal to 1E-11 m/s.
(2) (T) equals a traced inflow, (NT) equals non-traced.
(#) Means that the inflow point is poorly defined.

When comparing the two conductivity logs 60 and 67, it can be seen that for the two inflows which produced the greatest mass flux, inflows 18.2 m and 23 m, the concentration was increasing with time during logging. Logs 60 and 67 collapse on to each other at a depth greater than 30 m because all of these inflows are of a equal, non-transient background concentration. The transient inflowing concentration at 18.2 m does not explain the extreme concentration peak present at that depth. It is possible that this is caused by inclined borehole effects and there are also more possible explanations. This phenomena will be discussed in some detail in Section IV.4.2. It is interesting to note that this extreme peak is only half as evident on Log 60.

IV.3.9.2 Quantitative Analysis

Log development was too fast to track the primary advection front and get an estimate of total borehole flow. The manual measurements of total borehole flow rate were on the order of 6 l/min during the measurement of the conductivity logs. This flow rate was used in the calculation of the average inflowing concentration. Figure IV.34 plots the measured zero moment and the corrected zero moment for the entire borehole as a function of time. One can see that the measured zero moment quickly flattens which is indicative of quick attainment of

saturated conditions. This is to be expected with the high borehole flow rate. This makes estimation of the corrected zero moment very difficult and subsequently the average inflowing flux calculation prone to error. The following Table IV.19 summarizes the results of these calculations. As can be seen, the calculated concentration is at all times less than the late time outflowing concentration of approximately 505 μS/cm. This implies that these calculations are in error.

Table IV.19: Borehole Average Mass Flux and Inflowing Concentration, Borehole 85.009

Time (min)	Mass Flux (kg/s)	Ci (kg/m^3)	Ci (μS/cm)
25	2.39E-5	0.239	445
44	2.12E-5	0.212	395
77	1.83E-5	0.183	340
118	1.48E-5	0.148	275
181	1.48E-5	0.148	275
278	1.57E-5	0.157	292

Again it was possible to estimate the time rate of change of the average inflowing concentration during measurement of these logs. The difference between the outflowing concentration for Log 60 measured 70 minutes prior to end of flushing and Log 67 measured 278 minutes after flushing is 57.7 μS/cm. The time difference between the two logs is 348 minutes. This results in an average inflowing concentration time rate of change of 0.166 μS/cm min. This derivative is considered appropriate for the time period from 70 minutes before end of borehole flushing to 278 minutes after.

These logs are not well suited for partial moment analysis because the logs saturate very quickly for depths less than 35 m and below this depth mass fluxes are marginal. For this reason, the partial moment method is limited to the analysis of one integration interval which will estimate the total borehole flow rate. The interval chosen for analysis was 6 to 15 m. Figure IV.34 plots the partial zero moments for this interval and, as expected, the moments level off quickly, which is indicative of the very high borehole velocity. Figure IV.35 plots the estimated borehole flow rate for the interval 6 to 15 m for all logging times. We see significant scatter in the calculated flow rate, which is typical for intervals where the time derivative of the moments quickly goes to a very small number. A review of the partial moment plot on Figure IV.34 and the zero partial moment time derivatives calculated by MOMENT indicates that the only potential robust estimate of flow rate should occur at 0.42 hours. The flow rate estimated for this interval at this time is 6.4 l/min, which is in good agreement with the manual estimate of 6 l/min. Other analysis intervals were tried on these logs but the results were not considered defendable due to the very low time derivatives of the zero partial

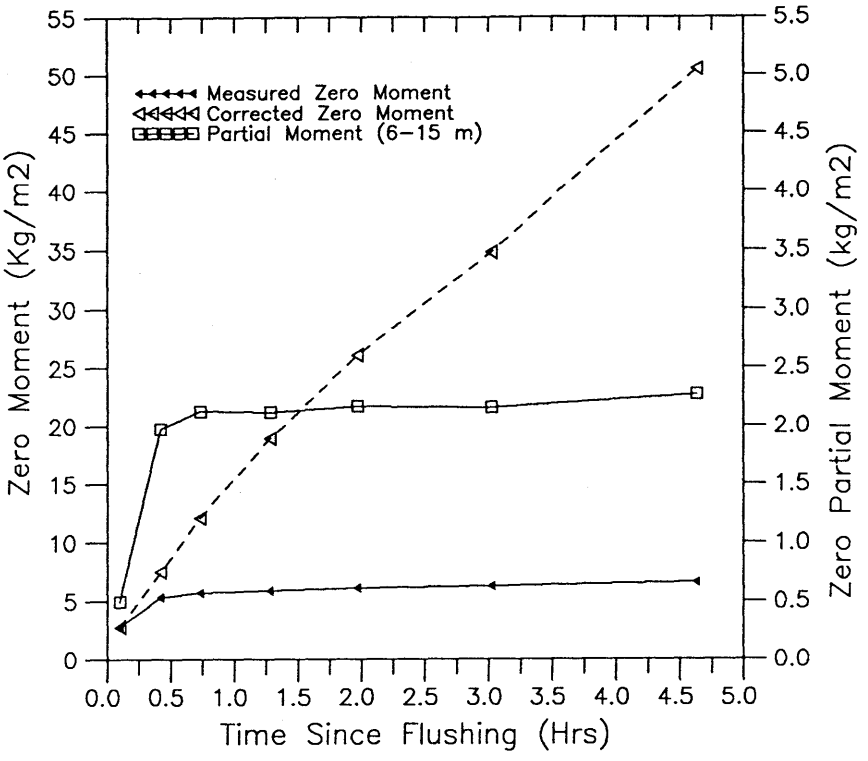

Fig. IV.34: Zero Moments for Fluid Logging Test VE464
Borehole 85.009, Logs 61,62,63,64,65,66 & 67

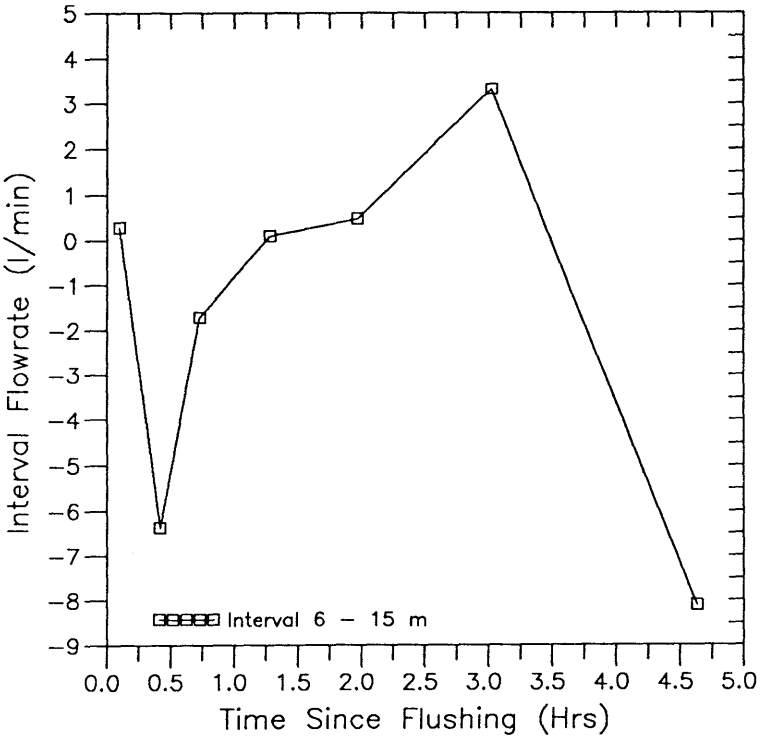

Fig. IV.35: Interval Flowrate as Calculated by MOMENT, Test VE464
Borehole 85.009, Logs 61,62,63,64,65,66, & 67

moment. These were generally low and very close to or less than the suggested threshold of 0.05 kg/m^2 hr.

BORE has been used in the analysis of the measured conductivity logs from the preceding Test VE463 and this Test VE464. The analysis technique is trial and error calibration starting from the bottom of the borehole and methodically progressing up the borehole with the specification of each inflow volumetric rate and inflowing concentration. These calibrations were meant to be trial calibrations and significant time was not spent in optimization of parameters. Figure IV.36 plots the first three measured logs after flushing along with the BORE simulated logs. The fit is acceptable for this level of analysis and the input flow rates and concentrations are listed in Table IV.20.

The results shown in Table IV.20 are quite remarkable. The largest inflowing concentration comes from two relatively insignificant volumetric inflows. This is supported by the temperature logs in Figure IV.32 which yield a measure of relative inflow volumetric fluxes. Again it was necessary to add inflows into the calibration which were considered as only potential inflows through qualitative analysis (inflows 23.5 and 35.6 m). We see a greater discrepancy in this calibration between individual inflow concentrations and the average inflowing concentration as compared to the previous BORE analysis of VE463. This is because the highest concentration inflows from a relatively low volumetric inflow point, which is contrary to VE463. Again, the BORE calibration yields important information concerning which intervals are more greatly connected to the injection interval. A final conclusion from this calibration exercise has to do with an earlier assumption, i.e., that the injected fluid was at the same temperature as the formation fluid. This assumption is consistent with the calibration parameters summarized in Table IV.20 and the nature of the first temperature log measured after flushing (Log 61). The size of the temperature anomaly is taken to be a function of volumetric flux and not related to the relative percentage of injected versus ambient fluid which might make up that volumetric influx.

Table IV.20: Calibrated Parameters Input to BORE for Test VE464 Calibration

Inflow Depth (m)	Inflow Rate (l/min)	Inflow Concentration (μS/cm)
18.2	0.2	6055
19.0	0.05	5735
23.5	0.05	410
25.6	0.05	410
28.3	2.8	410
32.8	3.0	80
43.5	0.15	80
46.9	0.40	80

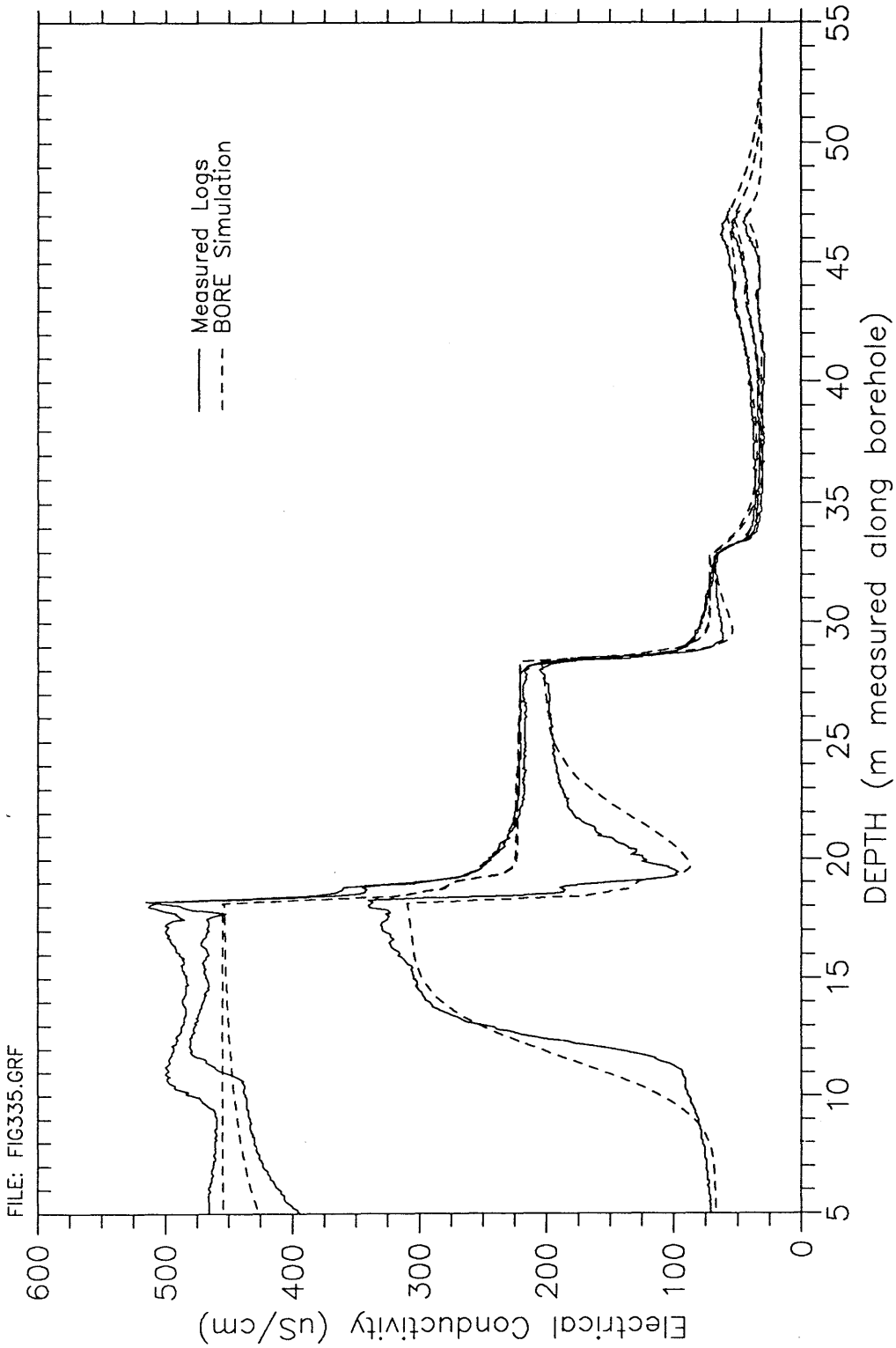

Fig. IV.36: Trial Bore Simulation, Test VE464, Borehole 85.009 Calibration to Logs 61, 62 and 63 Measured 0.1, 0.42, and 0.73 Hours After Borehole Flushing

IV.4.0 ASSESSMENT OF THE COMPLEX DEVELOPMENT OF THE MEASURED CONDUCTIVITY LOGS

From the qualitative and quantitative analysis of the measured conductivity logs presented, it becomes obvious that the detailed behavior or evolution is a complicated process. There are a number of observations which do not satisfy the simple borehole conceptual model which was explained in Section IV.3.1. Primary elements to the simple model are the assumptions that (1) the inflowing volumetric flux and concentration are not transient, and (2) that the measured concentration is a radially averaged quantity. We should expect a complicated model to apply to the crosshole test and therefore evidence should exist in the observed logs. The purpose of this section is to introduce the various processes that can create a more complicated "non-typical" conductivity profile development under conditions present during the BK crosshole fluid logging test. After these are introduced, examples will be cited from the measured conductivity logs.

IV.4.1 Transient Flow Rate

During logging of each borehole the borehole is flowing in response to being open to atmospheric pressure. Assuming that atmospheric pressure is approximately constant over the course of logging the borehole is kept at constant pressure conditions which results in a transient volumetric flux. All of the boreholes logged reached a relatively steady flow rate within 12 hours of opening. All boreholes were flushed, and subsequently logged, at least 18 hours after the borehole was opened. For this reason, it is felt that transient flow rate did not detectably influence the development of the measured logs.

IV.4.2 Transient Inflowing Concentration

Because the injection borehole is injecting a constant concentration source at rates which are in all cases less than the rate of withdrawal at the observation borehole, the test is essentially a complex unequal strength dipole tracer test. Therefore, each inflowing fracture which is in some way connected to the injection well undergoes tracer breakthrough. This process of transport is assumed to occur in accordance with the advection-dispersion equation which is inherently transient. Therefore, it is obvious that there are fundamental reasons why one might observe a transient inflowing concentration.

If the two well dipole were started at some time the concentration at the observation borehole would increase over time until at some late time the concentration would reach some maximum (C_{max}) which would represent a steady-state concentration. This C_{max} would occur under conditions of a steady-state flow field and would be described by the equation

$$C_{max} = Co\ (\theta\ /\ 2\pi) \qquad (IV.7)$$

where θ represents the subtended angle (expressed in radians) between the two streamlines which define the limits to the capture zone of the observation borehole for the injected traced fluid. The C_o is the

constant concentration injected at the injection well. The angle θ is a function of the ambient groundwater velocity and the magnitudes of the participating sink and source. If the dipole were of equal strength and there were no ambient flow field then the angle θ would effectively become 2π and from Equation IV.7 we see that the C_{max} would be equal to C_o. Because our dipole is unequal with the observation well being the strongest, and because some global gradient might exist, the angle θ will be some quantity less than 2π.

Therefore, as the concentration builds to a C_{max} value, it will have a significant effect upon the observed conductivity profiles. The factor which would determine if the transient inflowing concentration were observed or not is the relation between the time rate of change of concentration relative to the logging time period. Figure IV.37 shows a possible breakthrough curve for a single inflow in a borehole. As can be seen, the concentration builds to a maximum in some time scale. Superimposed upon this breakthrough curve are two potential logging start and end times. The first logging time window is from time A to A′ and is relatively short as compared to the logging time B to B′. In the bottom portion of this figure, two possible suites of logs are shown. In the first case, where logging time was small relative to the time rate of change of inflowing concentration, we see no irregular peak development and we see a normal saturated profile. However, for the logging time B to B′ there is significant change in inflowing concentration during logging and this is easily seen in the conductivity profiles in an increasing saturated level.

This effect is much more complicated in this field study as there are many inflows which are breaking through with relatively independent breakthrough curves much like a layered system. The measured conductivity log represents a complex superposition of all of these breakthroughs as well as borehole transport.

We can find evidence for both strongly transient and weakly transient inflowing concentrations in the measured logs in the BK-Area. For the case of a relatively stable inflowing concentration it is not possible to determine if this is because of attainment of a theoretical Cmax or if it is an apparent condition resulting from the time scale of observation. The inflowing concentration at 23.9 m of Borehole 85.006 remains relatively constant during logging. This is also true for the average inflowing concentration during logging in Borehole 85.008. In contrast, several boreholes showed evidence of strongly increasing inflowing concentration as a function of time. The most obvious example is Borehole 88.015 (see Figure IV.25). The conductivity curve continues to reach an apparent saturated profile only to be increased upon by the next measurement. Other boreholes which exhibited strongly transient inflowing concentrations include boreholes 85.007 and 85.005.

A second mechanism which will cause an increase in the inflowing concen-tration has to do with the observation borehole flow rate. As mentioned in the previous section, transient flow rate effects are considered minimal in comparison to the one listed above but will be brought out here for completeness. Because the observation well is open to atmospheric conditions, the well is kept under constant head conditions and therefore flow into the well is transient. From Equation IV.7, we have seen that the maximum concentration C_{max} which

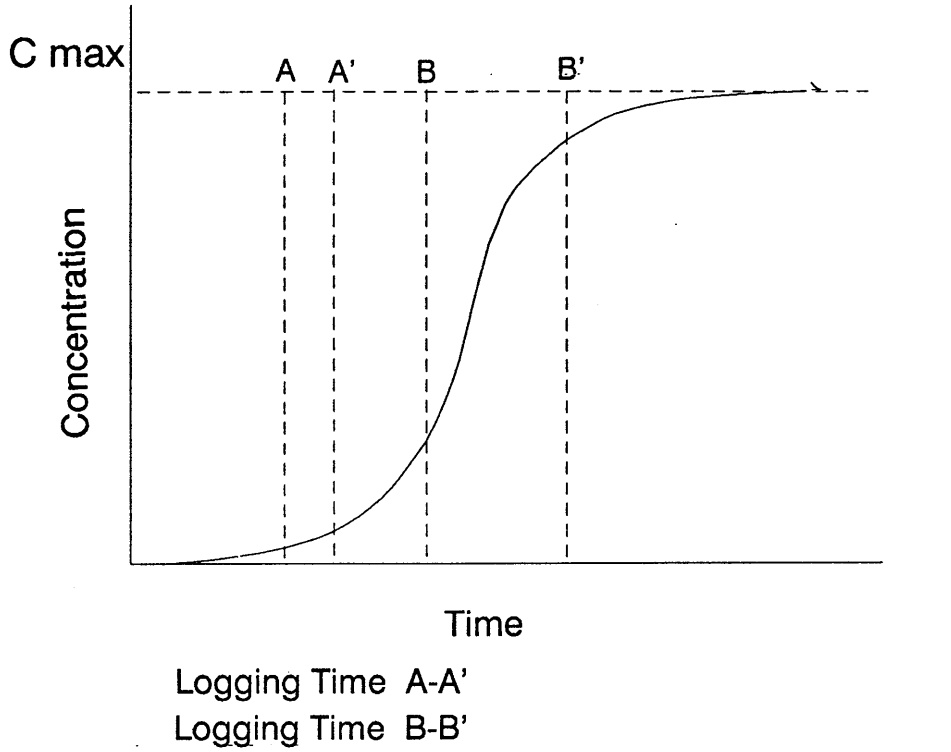

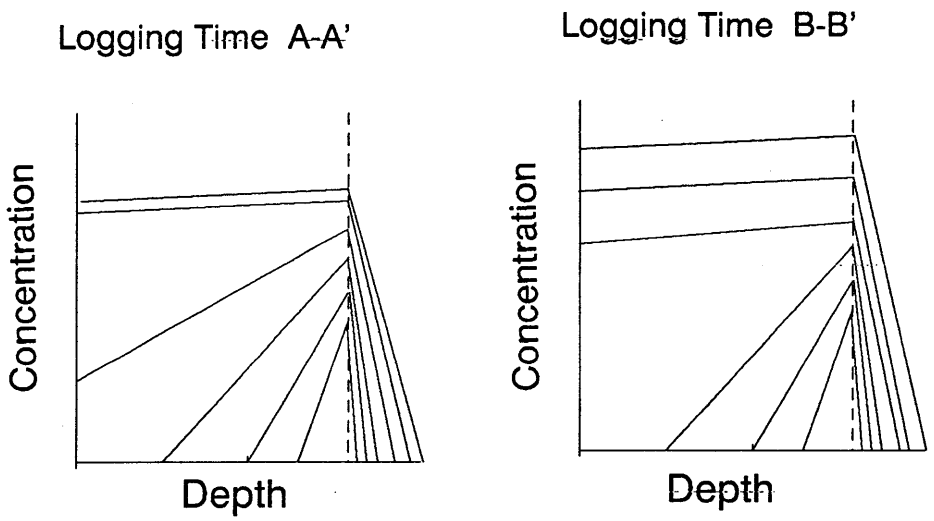

Fig. IV.37: Potential Effect of Transient Inflowing Concentration

enters the observation borehole is dependent the angle θ. The angle θ is in part a function of the strength of the observation borehole volumetric inflow (Q). As Q decreases, θ increases. This means that a larger fraction of the inflowing water will be coming from the injection borehole and that the diluting effects of the other water will be decreased. From Equation IV.7 we can see that the concentration inflowing would theoretically increase.

It is also possible to have a decreasing inflowing concentration as a function of time. If the borehole receives tracer breakthrough prior to opening, then the tracer plume has moved past the observation borehole. If the borehole is opened, again there is some angle θ which defines the capture zone of traced fluid being injected at the injection well. However, in the region outside of the region defined within θ also exists traced water. Therefore, the theoretical maximum concentration (if indeed it were possible to reach steady-state transport) would be greater than that defined by Equation IV.7. However, the amount of traced fluid which moved past the borehole is assumed to be finite and exhaustible therefore the concentration at the integrator well could decrease as a function of time.

Although it is admitted that this is somewhat of a special case, there is evidence to suggest that this type of process did occur while logging Borehole 85.006. Borehole 85.006 is located in the same plane as the injection borehole 85.004, and they are in proximity. The first conductivity log measured in 85.006 was Log 21 measured 132 minutes after the packers were deflated. The conductivity profile appears to be saturated with the concentration from a depth of 24 m to the drift surface equal to 1608 μS/cm (see Figure IV.9). The borehole flowed throughout the night and was flushed the next morning prior to logging. These logs saturated quite quickly, due to fast a fast flow rate. However, the concentration from a depth of 24 m to drift now was at a concentration approximately 40% less than Log 21. The decrease in inflowing concentration at borehole 85.006 is thought to be the result of the tracer moving past the observation borehole before packer deflation, as described above.

IV.4.3 Measurement of Non-Radially Averaged Concentrations

All of the boreholes tested during this crosshole test dip at angles less than 90° to the horizontal (BK drift floor). This fact necessitated the development of an apparatus which allowed for tension to be applied both from the top and bottom of the tool as it was lowered through the borehole. This was performed by installing a pulley on the bottom of the borehole. In vertical boreholes the conductivity probe is typically used with centralizers which insure that the probe travels in the center of the borehole. Because of the increase in friction associated with these sub-horizontal boreholes, centralizers could not be used. The net effect of not using centralizers was that the conductivity probe travelled along the bottom of the borehole wall. As a result, it is possible that concentrations which were measured are not representative of a radially mixed cross-sectional borehole average. Because this concentration is measured prior to mixing and dispersing with the borehole stream, it is anomalous in magnitude relative to a radially averaged value. Figure IV.38 shows a concentration profile

Scenario A

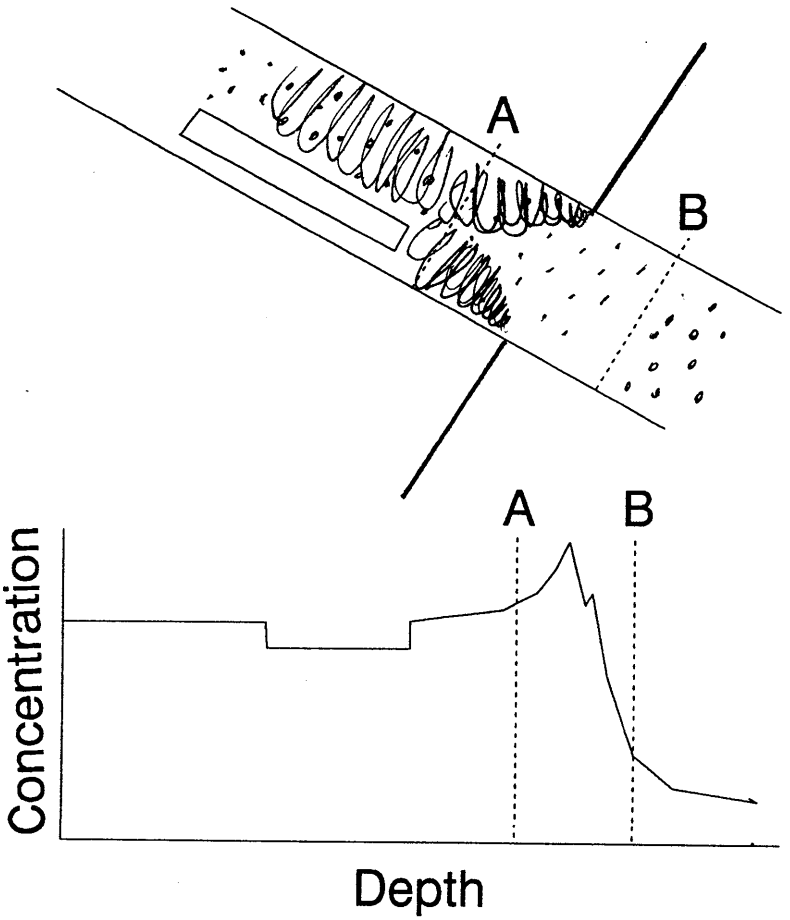

Scenario B

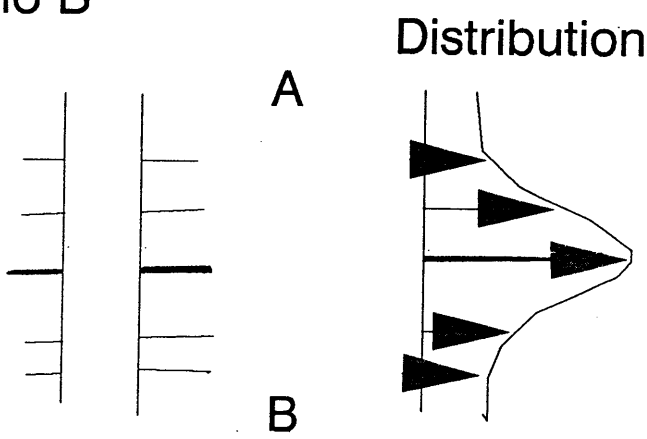

Fig. IV.38: Possible Scenario For Late Time Peaks

which might occur and in fact was encountered in the observed crosshole tests. For the interval A to B, we see that there exists a significant concentration maximum even under apparent saturated conditions. As shown in Figure IV.2, theoretically at saturated conditions the concentration should plateau to a maximum value. The saturated behavior in the segment AB is not clearly explained by the simple borehole model represented in Figure IV.2. The simplest explanation of this time of log behavior is when the inflowing concentration varies greatly on a time scale which is significantly less than the borehole residence time. However, the magnitude of the concentration derivatives calculated for each borehole during logging are not large enough to create significant concentration changes on a time scale much less than the borehole residence times.

The concentrations shown in Figure IV.2 are assumed to be radially averaged concentrations. One explanation is that the conductivity probe measures a concentration which is a maximum and is indicative of fracture concentrations, not of two-dimensional mixing which occurs axially in a borehole under inflow conditions. This concentration would be in direct violation with the assumptions which were defined by TAYLOR (1953, 1954a) and which make possible the assumption of 1-dimensional advective-dispersive transport. The explanation of late time maximums as being caused by measurement of non-radially mixed concentrations will be referred to as Scenario A because there is at least one other process which might produce a similar signature.

The observed concentration profile represented by segment AB in Figure IV.38 could be explained by an alternative method. The conductivity profile could be the result of variations in mass flux over a relatively small borehole interval. This will be termed Scenario B and is shown in Figure IV.38. In this case, we have a segment of borehole (AB) which is intersected by a swarm of fractures. Each fracture represents a unique flow path and is therefore associated with a unique mass flux (the product of $C_{i \text{ and }} q_i$). If we consider that one fracture is the dominant flow path, then we could conceivably get a mass flux distribution over a segment AB which is shown in Figure IV.38. Therefore, this could also create the observed conductivity profile as was measured for segment AB. In reality, the response we see in our observed logs of late time concentration maximums might better be thought of as the net result of both of the scenarios A and B. Both processes contribute to the production of a similar conductivity signature. In the following paragraphs we will look for evidence for Scenario B in the measured logs. Direct evidence for Scenario A cannot be provided so it must remain a theoretical possibility.

Borehole 85.008 has a very pronounced late time maximum in the measured conductivity logs which occurs at a depth of 17.6 m (see Figure IV.23). It is very hard to determine if this late time concentration maximum is the result of a poorly mixed concentration measurement or if additional diluting mass flux is occurring immediately above 17.6 m. The results from Lugeon Testing from this borehole indicated that almost 90 % of the borehole had a transmissivity greater than 1E-9 m^2/s. In fact, although a transmissivity maximum was discovered between 17 and 20 m, the transmissivity was evenly distributed about this maximum. We see evidence for minor inflows downhole from 20 m from review of the Lugeon Test results and these are well represented in the conductivity and

temperature logs. The potential for minor inflows at depths immediately above 17.6 m is again shown by the Lugeon Test results. However, we do not see a lot of evidence for these inflows in the conductivity and temperature logs. This is probably because of significant interference from below. The concentration fall off immediately up borehole from 17.6 m could be the result of additional inflows contributing small mass flux.

The logs measured for Borehole 85.009 showed a similar late time concentration maximum at the depth of maximum mass flux (18.2 m). Again, it is not possible to say which scenario best describes the reason for the anomaly. Lugeon Testing again identified a transmissive interval from 17 to 20 m which was approximately centered about 18 m. Just as there is a minor inflow clearly defined at 19 m, there may also be an inflow just above 18.2 m which is imputing a smaller mass flux than the main mass inflow at 18.2 m.

IV.5 SUMMARY OF RESULTS, CONCLUSIONS, AND RECOMMENDATIONS

The pilot crosshole fluid logging study can be considered a success based upon the objectives of the experiment. The study (1) identified fractures with some form of connection between the injection borehole and the logged observation boreholes, (2) identified fractures at the observation wells which were apparently not connected to the injection well, and (3) owing to the success in 1 and 2, validated the crosshole fluid logging technique for fracture system characterization. With the testing method described in this report, it was possible to determine a great amount of information on fracture locations in a very short time span (in this case 9 days of testing). In total, 53 individual inflowing fractures were clearly defined and isolated to a specific borehole depth. Of these, 34 were connected to the injection borehole as indicated by tracer inflow and 19 were apparently not connected and did not receive tracer breakthrough. It is understood that these apparently unconnected fractures could in fact be connected to the injection well through a much higher effective porosity or through larger flow path lengths unsampled in the current test time scale.

The conductivity logs exhibited a very complex behavior indicative of the complex transport characteristics which are associated with a fracture system. There was evidence in the observed logs of transient inflowing concentration occurring at given inflows. This was surely expected as each test emulates a complicated unequal strength dipole tracer test. In addition to having time varying inflowing concentration, each inflow is a unique tracer breakthrough and for this reason inflowing concentration also varies as a function of inflow location within the borehole. Although it is expected that the total borehole flow rate would change as a function of time under constant pressure conditions, it was felt that this effect was minimal because each log suite was measured in excess of 12 hours after borehole opening.

In all boreholes logged there was an inflow which produced a significantly higher mass flux than the other inflows in the borehole. It was also quite common to have minor inflows in the bottom of each borehole which produced ambient non-traced fluid. Table IV.21 summarizes the locations of the inflows in each borehole which produced

the highest concentration into the borehole. In addition, Table IV.21 lists the fracture system identified by Bräuer (PAHL et al., 1992) which corresponds to the zone of highest inflowing concentration.

As can be seen in Table IV.21, in all boreholes except borehole 88.017, Bräuer identified a fracture system occurring at the same interval where the highest inflowing concentration occurred. There was a second major mass influx occurring at 26.2 m in Borehole 88.017 which was also not coincident with any Bräuer fracture systems. Generally the highest mass flux inflows were associated with the fracture system S1/S2. The correlation between inflows determined by fluid logging and fracture systems identified by Bräuer and zones of elevated transmissivity identified by the Lugeon Testing showed a high degree of correlation. In most boreholes the highest mass flux intervals were associated with the highest volumetric flux intervals. A significant exception to this was Borehole 85.009 where the highest inflowing concentration (as determined by BORE calibration) was associated with a relatively low volumetric flux (which is indicative of a low relative transmissivity).

The total borehole flow rate from each logged borehole was high, with most boreholes producing in excess of 3 l/min. The injection rate maintained at 85.004 was 0.5 l/min. With such high borehole flow rates, the logs developed relatively quickly and exhibited saturated, or apparent saturated, conditions by the end of borehole logging (less than 4 hours in most cases). The final fluid concentration flowing from the borehole under saturated conditions is a function of the accumulated volumetric and mass fluxes inflowing into the borehole (see Equation IV.6). The final outflowing borehole concentration measured during logging varied from 198 μS/cm to a high of 1108 μS/cm. Two higher effluent concentrations were measured in Boreholes 85.006 and 88.017. A concentration of 1608 μs/cm was measured in 85.006 one day prior to logging, and a concentration of 2165 μS/cm was measured in 88.017 three days after logging. The injection concentration was 10,000 μS/cm. In most logged boreholes the average inflowing concentration entering the borehole during logging was transient. There was evidence for a strongly transient inflowing concentration in some cases, and in other cases it was very weakly transient. Table IV.22 summarizes the final average outflowing concentration, the best estimate total borehole flow rate during logging, and the estimated average borehole mass flux at the end of logging. In addition, Table IV.22 summarizes the time rate of change of the average inflowing borehole concentration during logging.

In addition to the seven boreholes logged, the injection well is included in Table IV.22. Please remember that the borehole average inflowing concentration is simply a mixture of all inflowing mass with all inflowing water and does not represent any individual inflow. As we saw through BORE simulations of the logs for Boreholes 88.015 and 85.009, the inflowing concentration can be much larger than any concentration measured in the borehole. In general, we can see that four boreholes close to the injection well inflowed at average concentrations at approximately 1,000 μS/cm during flushing and logging. Boreholes 85.006, 88.017, 85.005, and 88.015 are closest to the injection borehole, with the exception of 85.007, which is in the same vertical plane as the injection borehole.

Table IV.21: Inflow Within Each Borehole having the Highest Inflowing Concentration

Well	Inflow Depth (m)	Bräuer Fracture System
85.007	25	K4 u
85.006	23.9	S1/S2 u
88.017	4.5 - 5	--
85.008	13.8	S1/S2 u
85.005	17.6	K4 u
88.015	25.1	S1/S2 u
85.009	18.2	Probably S1/S2 u (14.3 to 17.2 m)

Table IV.22: Average Borehole Inflow Parameters

BK Borehole	Final Outflowing Concentration (μS/cm)	Flow Rate During Logging (l/min)	Final Borehole Mass Flux (kg/s)	Average dC/dt During Logging (μS/cm min)
85.004	[10,000]	[0.5]	[5.1E-5]	NA
85.007	270	1.1	2.6E-6	0.381
85.006	1,108	3.3	3.3E-5	--
88.017	917	3.8	3.1E-5	0.143
85.008	198	3.2	5.7E-6	0.052
85.005	1,012	4.5	4.1E-5	0.263
88.015	1,092	2.5	2.5E-5	0.624
85.009	505	6	2.7E-5	0.166

NA = Not Applicable
[] = Injection Borehole

A large inflowing concentration was not measured at borehole 85.007, possibly because the borehole was being logged at the early part of tracer breakthrough. This is supported by the relatively high time rate of change of the average inflowing concentration (dC/dt) of 0.381 μS/cm min. Borehole 85.007 also had the lowest borehole flow rate which suggests that it has the lowest total transmissivity. This could again result in the low measured concentrations. Both boreholes 85.008 and 85.009 had lower average borehole inflowing concentrations which could in part result from their longer euclidean distances from the injection well. The borehole mass flux for most boreholes is quite high and within a factor of two of the mass flux being injected.

Quantitative analysis focused using the Method of Partial Moments to calculate interval flow rates within each logged borehole. This analysis method was not optimal for use on these conductivity logs because of (1) large borehole velocities (resulting in quick peak development "saturation"), (2) strong peak interference due to lots of inflows over short intervals, and (3) a large percent of the inflows are of low mass flux. Even though these conductivity logs were not well suited for analysis through the method of partial moments it should be stated that the partial moment method reproduced the total borehole flow rate extremely well in the six boreholes it was applied. This is a vote of confidence for the methodology and shows that the method can be effective even under less than ideal conditions.

BORE was used to calibrate inflow parameters for two suites of logs, Borehole 88.015 (Test VE463) and Borehole 85.009 (Test VE464). These calibration attempts were largely successful and resulted in first order estimates of inflow volumetric rates and concentrations. BORE calibrates both flow rate and concentration which are both important to know in these types of experiments. The estimation of inflow volumetric rate for each inflow interval gives a relative borehole distribution of transmissivity. With BORE, inflowing concentrations can additionally be estimated. These are not borehole mixed (averaged) concentrations and are thought to have strong correlation with the degree of connection between injection and inflow intervals. From an analysis standpoint it would be recommended that BORE be further used to define full parameter sets of flow rate and concentration.

Some recommendations will be offered which pertain to implementing further similar tests. Correct estimation of the total borehole flow rate is very important from an analysis standpoint. This measurement was difficult to perform because of the irregular drift-borehole interface. It is suggested that a measuring device be designed to perform these measurements accurately, even when the probe lines are in the borehole. Also, it is recommended that the manual measurement of conductivity be performed very frequently during the measurement of a suite of logs in a borehole. This will result in improved mass balance calculations.

Finally, it is recommended that additional similar crosshole fluid logging tests be performed. The injection parameters used in this pilot study were successful and it is considered advantageous to implement further test(s) with similar injection parameters (i.e., flow rate of 0.5 l/min and an injection concentration of 10,000 μS/cm). This will allow for more ease in comparison of these pilot study results to future studies. It might be interesting to choose an injection interval which showed high volumetric flux but low mass flux. The idea being that this fracture is transmissive but was not strongly connected to the injection interval in Borehole 85.004. This test could possibly result in a new set of inflows and borehole connections which do not intersect with the set defined by this pilot study. Finally, it would be interesting to perform an additional test where the injection interval is the interval which showed the strongest mass flux in the pilot study. The interest here would be in seeing if this study re-created the same pattern of inflows as defined by this pilot study.

PART V

INTERPRETATION OF SELECTED 1990 HYDRAULIC AND FLUID LOGGING TESTS: SYNTHESIS AND CONCLUSIONS

Dominique Guyonnet and Van Kelley

V.1 INTRODUCTION

Research at the Grimsel Test Site (GTS) is focused towards testing and developing methodologies for the characterization and instrumentation of crystalline rocks. The GTS was also conceived to be a site for flow and transport model validation. The research is motivated by a need for understanding the transport processes which govern nuclide migration within a crystalline host rock. It is generally accepted that transport from a repository in crystalline rock would be primarily controlled by secondary porosity i.e. fractures. The BK area of the GTS is reserved for the evaluation of methodologies for the characterization of flow and conservative transport within a fracture system.

The development of a conceptual flow model which is consistent with physical observations is a prerequisite for flow and transport modeling. Although pressure and tracer tests such as those described in GUYONNET & LAVANCHY and KELLEY & LOEW (this volume) provide valuable information regarding the flow system, a conceptual model must be based upon other sources of medium information due to the inherent non-unique character of flow and tracer tests. Information derived from geological and structural mapping, reconnaissance and geophysical investigations should be the basis upon which a conceptual flow model can be built. At the GTS, structural and geological mapping of surface and subsurface exposures and boreholes, along with geophysics, provide a wealth of information which cannot be matched by system response tests. However, system response tests such as those described herein are essential for determining which individual or groups of structural features identified by visual inspection or by geophysics have an influence on the flow system. An overview of important results from geological, structural, and geophysical investigations performed at the BK Site is presented in Section V.2 of this chapter.

The nature of the fracture geometry at the BK site is so complex that an exhaustive description of the flow system is probably not practically feasible. Rather than to attempt such an endeavour it is preferable to focus the effort upon accurately characterizing those particular structural features which are controlling the flow system. This approach is based upon experience and has been described by LONG et al. (1989) as trying not to lose the forest for the trees. In a fractured rock environment it is possible that a number of preferential pathways and flow boundaries describe 99% of the flow system. The effort needed to describe the remaining 1% may be enormous and unjustified from the standpoint of repository safety-analysis requirements. Perhaps the most important result from the hydraulic and fluid logging tests described in this report is the evidence of dominant features which control the flow system, and consequently the transport in the BK-Site vicinity. This evidence is summarized in Sections V.3.1 and V.3.2 of this chapter and evaluated in the light of the information presented in Section V.2.

In Section V.4, uncertainties concerning the flow system at the BK site are discussed and directions for future investigations designed to reduce these uncertainties are suggested.

V.2 BRIEF SUMMARY OF INFORMATION FROM PREVIOUS GEOLOGICAL, STRUCTURAL AND GEOPHYSICAL INVESTIGATIONS AT THE BK-SITE

The geology and fracture distribution at the Grimsel and BK area has already been described in detail in several Nagra reports among which KEUSEN et al., (1989) and BOSSART & MARTEL (1990). Fractures and lamprophyre dykes observed in the walls of the BK cavern and of the adjoining tunnel before they were cemented were mapped and classified into different systems. Some of these features could be correlated with structures observed in surface outcrops above the site. Fractures in boreholes drilled at the BK-Site are described in BRÄUER et al., (1989) and PAHL et al., (1992). In the latter, a list of water-transmitting fractures is presented and is referred to in KELLEY & LOEW (this volume) as the Bräuer list. A synthesis of the BK-Site structural geology by MARTEL & PETERSON (1991) proposes a preliminary geologic model of the site. The results of the hydraulic and fluid logging tests presented in Section V.3 of this chapter, will be evaluated in the light of this model.

At the BK site there are 4 major types of structures (Figure V.1):

- S-zones
- K-zones
- E-W striking lamprophyres
- N-W striking lamprophyres

The S-zones and K-zones have a very different morphology and can be expected to behave differently from a hydraulic standpoint. S-zones are ductile deformations which present a braided structure while K-zones exhibit brittle deformation characteristics.

The S-zones consist essentially of two families of fractures noted S1 and S2. The distinction between S1 and S2 fractures is based upon their relative ages rather than upon their orientations which are very similar. For this reason they are often grouped together and noted S1/S2. The average strike and dip of the S1/S2 fractures at the BK site are approximately N50°E and 65°SE respectively. This orientation is similar to that of the foliation of the granite and granodiorite host rock at the site. S-zones tend to follow the foliation of the rock and S-zone fractures are typically abundant where biotite is relatively abundant.

Unlike S-zones, K-zones strike at a high angle with the foliation. K-zone fractures are subdivided into 4 different fracture families numbered K1 to K4. They appear to be much less common in the BK boreholes than S-zone fractures. It should be noted however, that the great majority of the boreholes in the BK area strike N49°W. Considering the fracture orientations, these boreholes are much more likely to encounter S-zones than K-zones. This phenomena which has been referred to as "borehole bias" underlines the importance of three-dimensional sampling and observation provided by outcrops. A well developed K-zone can be observed at the entrance of the BK cavern and in boreholes BOBK 86.002 and BOBK 86.003 which do not have the same orientation as most boreholes. The strike and dip of this K-zone are approximately N80°W 80°S. In general K-zones are found to be more discontinuous than S-zones and are offset by steps where fracturing is

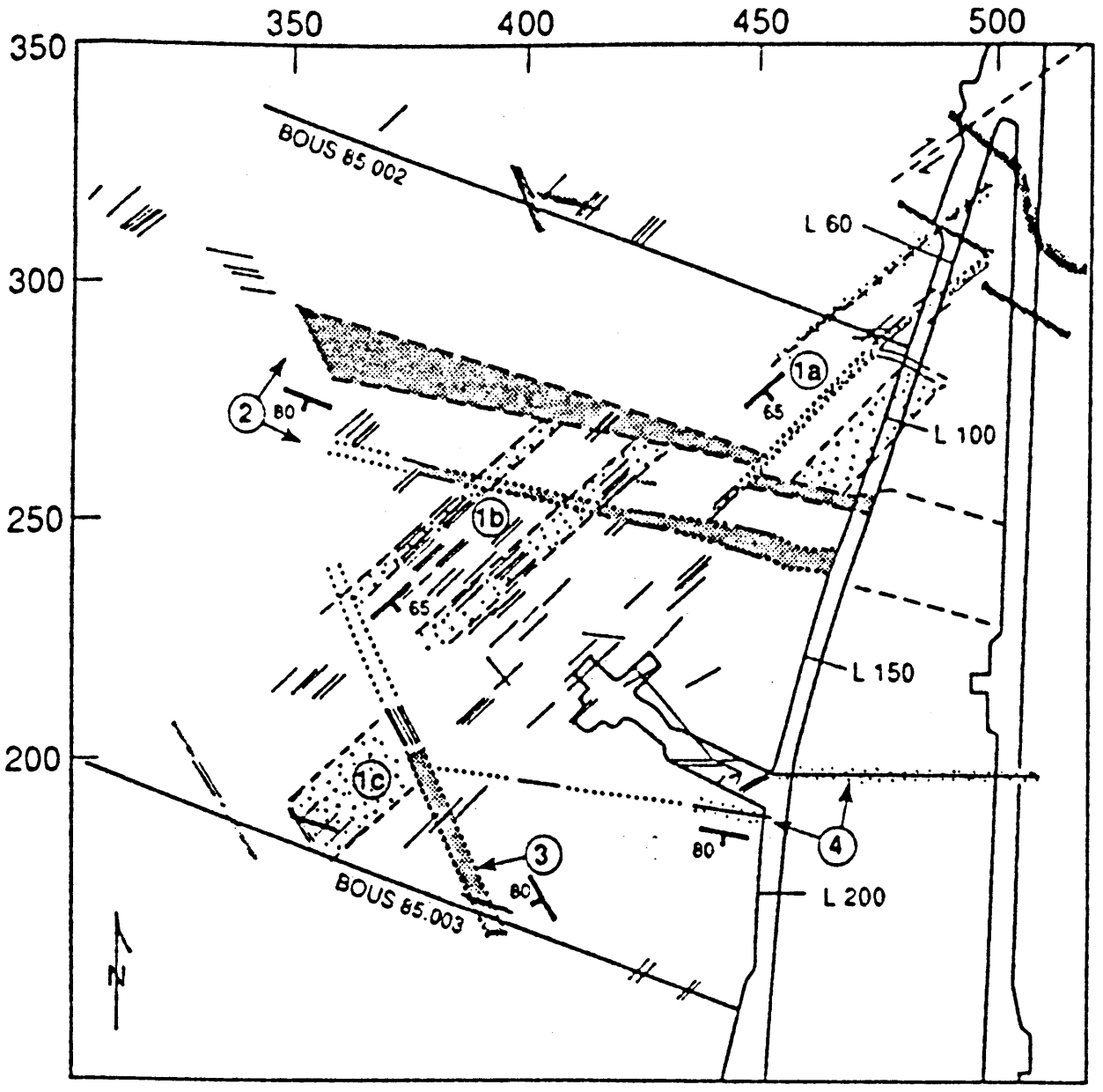

Fig. V.1: Preliminary geologic model of the BK site. (Martel and Peterson 1991).

Feature 1a, 1b, 1c: S-zones. Feature 2: EW-striking lamprophyres. Feature 3: NW striking lamprophyre. Feature 4: K-zone.

more intensive. Due to their structure, flow within K-zones is expected to be much more heterogeneous than within S-zones and to be concentrated in the vicinity of steps.

The BK site is limited to the N and to the S by two lamprophyre zones. The northern lamprophyre strikes approximately N80°W and dips 80°S (as the K-zone mentioned above), while the southern lamprophyre strikes N25°W and dips 80°W. Lamprophyres are often found to be discontinuous and are strongly sheared at their edges. Flow along lamprophyres can therefore be expected to occur preferentially along these edges. In the case of un-deformed lamprophyre, the permeability across the structures can be expected to be quite low and they may constitute hydraulic barriers to flow.

The information summarized above is incorporated into the preliminary geologic model of the BK site presented in Figure V.1. For this representation, the major structures are projected into the plane of the BK cavern (elevation: 1730 m asl). Of interest in Figure V.1 is that S-zones are interpreted as being discontinuous and are either limited or offset by the lamprophyres. This interpretation is of considerable consequence for the expected hydraulic behaviour of these fracture zones.

To assist in the extrapolation of borehole information to the rock mass located between the boreholes, radar crosshole tomography was performed at the BK site (NIVA et al., 1988). A signal was transmitted between the laboratory tunnel, borehole BOUS 85.003 and borehole BOUS 85.002. The basic principal behind the methodology is that a signal travels faster in un-deformed material than in deformed material. In addition to detecting geological structures, the technique was used to map groundwater transport paths. Tomograms measured after injection of a saline brine were subtracted from tomograms of the undisturbed system with the objective of obtaining an image of the tracer migration path.

In summary the results of the crosshole tomography supported the presence and general geometry of some major structures previously defined by borehole and outcrop mapping. However it was difficult to infer new structures from the tomograms which were not known beforehand by geological mapping. The main reason for this was that a considerable amount of filtering was required to rid the tomograms of anomalies which were interpreted as being artifacts of the inversion process, although their magnitudes were comparable to those of anomalies believed to reflect major structures. The relatively large pixel dimension used in the tomographic inversions (2.5 m) added to the uncertainty in resolving the internal structure of major features.

V.3 SUMMARY OF HYDRAULIC AND FLUID LOGGING RESULTS WITH RESPECT TO BK FRACTURE-SYSTEM CHARACTERIZATION

V.3.1 Results from hydraulic testing

Nearly all hydraulic tests performed by the Bundesanstalt für Geowissenschaft und Rohstoffe (BGR) showed evidence of hydraulic boundaries or outer zones of lower permeability which inhibited flow and caused deviations from the ideal radial infinite-acting pressure

response. The distance from the test interval to this hydraulic barrier was estimated to be approximately 70 m. Although the analysis does not allow the distance to the boundary to be determined with a precision greater than 50%, the estimated value is nevertheless on the same order as the distance separating the tested borehole from the lamprophyres in Figure V.1. The fact that the test borehole (BOBK 85.004) intersects a major S1/S2 zone (feature 1b in Figure V.1) brings credibility to the hypothesis derived from geological observations that the S-zones are discontinuous and limited laterally by the lamprophyres.

The single-hole analysis indicates that the hydraulic barrier is heterogeneous with respect to permeability. Table III.7 in GUYONNET & LAVANCHY (this volume) suggests permeability variations of several orders of magnitude along the barrier. These results are consistent with geological knowledge of the lamprophyres which shows that they are heterogeneous and deformed.

Despite their heterogeneity, the lamprophyres must constitute relatively effective pressure boundaries. Pressure recoveries performed at a later date and for a longer period of time than those described in this report, yield steady-state pressures which differ substantially on either side of the lamprophyres. Preliminary inspection of the data suggests steady-state hydraulic heads on the northern side of feature 2 (Figure V.1) of approximately 1760 m asl while on the southern side of feature 3, hydraulic head stabilized at around 2100 m asl. The steady-state heads within the zone delimited by these two lamprophyre structures were found to be relatively homogeneous and around 1815 m asl.

A particularly important aspect of the hydraulic pressure response analysis is the flow-dimension analysis. Dimensional analysis of the single-hole response suggests an initial flow period presenting radial flow characteristics followed by a later flow period which presents either linear or bounded flow characteristics. It is very difficult to clearly distinguish between linear and bounded flow as both geometries have the effect of inhibiting pressure relief at the test well compared to the radial flow case. This again underlines the non-unique behaviour of response tests and the relative importance of geologic information for derivation of a conceptual flow model. Dimensional analysis of single-hole response from tests performed at a later date than those described here, also exhibit this mixed response (early radial flow + late linear/bounded flow). Dimensional analysis of the crosshole response confirmed the results from the single-hole response. No evidence of an early flow period dominated by borehole storage in the observation interval was found in the data.

Analysis of the crosshole response reveals that several observation intervals have the same pressure response regardless of their location relative to the injection interval. These different observation intervals, located in different boreholes, acted as though they were one interval. This implies that they must be well connected by a fracture zone which is particularly transmissive. The list of these intervals is presented in Section III.2.4.1 of GUYONNET & LAVANCHY (this volume). The coordinates of the intervals which appear to intersect a high conductivity connecting feature were calculated and plotted on a 3-D representation of the BK site which is presented in

the following section.

Analysis of the pressure response from both the injection and observation intervals yielded estimates of hydraulic diffusivity and static heads. Extrapolation of the pressure response observed during the pressure recoveries (Horner analysis) suggest undisturbed heads between 1920 and 1940 m asl. However, extrapolation over a period of time neglects any boundary effects which may occur during this time. As stated previously, more recent pressure recovery tests showed steady-state heads in the central BK area around 1815 m asl. This lower value probably reflects the influence of the drift.

Transmissivity estimates from the single-hole response yielded values which range between 7.7E-07 and 3.6E-05 m^2/s for the area located between the lamprophyres. The range of transmissivities calculated from the crosshole response is very similar to the range presented above (see Figure III.23, GUYONNET & LAVANCHY this volume). Calculated storativities range between 1E-06 and 1E-04. However, very little confidence can be given to these values due to severe uncertainty concerning true flowpath lengths which are required in the type-curve matching procedure. Analysis shows that these lengths are not simply the straight line distances separating the injection and observation intervals.

V.3.2 Results from the pilot crosshole fluid logging test

The primary objectives, listed in order of priority, of the crosshole fluid logging test (KELLEY and LOEW, this volume) were (1) to determine if the proposed testing methodology was feasible, (2) to identify fractures in the BK observation boreholes which are in some way connected to the injection interval, and (3) to evaluate current electrical conductivity log analysis methodologies for logs measured under these tests conditions. The test was a success based upon these objectives and provided a considerable amount of information in a short amount of testing time. A total of 53 inflowing fractures were identified in 7 observation boreholes over 9 days of testing. Test design parameters such as injection flow rate and concentration were well designed and controlled, resulting in large tracer breakthroughs occurring at the observation boreholes on the time scale of the test.

Prior to logging each borehole, the boreholes fluid was displaced (flushed) with a low salinity water which was of a lower temperature than the injected or in-situ groundwater. It was observed that temperature log development was dependent upon inflowing volumetric flux and that electrical log development was dependent upon the product of volumetric flux and tracer concentration (i.e. mass flux). Because of this, all volumetric inflow would show up on the temperature logs and only traced inflows would be identified through the electrical conductivity logs. By examination of the electrical conductivity and temperature logs, some qualitative information could be gained relative to which fractures dominate volumetric flow and which dominate mass (tracer) flux. If a fracture produced a relatively significant volumetric flux but produced insignificant mass, it suggests that a fracture is relatively transmissive (at least in the vicinity of the borehole) but poorly connected to the injection interval.

Through qualitative analysis of the electrical conductivity and temperature logs, all inflowing fractures, traced or not traced, were identified for each borehole. These fracture locations showed good correlation with a list of "water transmissive" fractures compiled by BRÄUER et al., (1989) and the results of focused packer Lugeon testing. For each borehole the most highly connected fracture(s) to the injection interval was identified (see Table IV.21 of KELLEY & LOEW, this volume) and showed strong correlation with the BRÄUER et al., (1989) list. In the majority of boreholes it appears that the S1/S2 fracture family dominates transport which is consistent with the model proposed by MARTEL & PETERSON (1991) and illustrated in Figure V.1. Also, for the majority of boreholes, the fracture which produced the highest mass flux also produced the highest volumetric flux with the exception of borehole 85.009. This suggests that the most connected interval to the injection interval in borehole 85.009 is not the most transmissive and is not as transmissive as the most connected fractures in the other observation boreholes. This is consistent with the results from GUYONNET & LAVANCHY (this volume) where the pressure response for borehole 85.009 always showed a greater drawdown than highly connected intervals in other boreholes to which it was apparently connected.

As for the highly connected hydraulic intervals determined during pressure testing, the coordinates of the fractures most highly connected to the injection interval as determined from fluid logging were also calculated and plotted on a 3-D image of the BK-Site (Figures V.2.a and V.2.b). Figure V.2.a shows the BK-Site from the South-West while Figure V.2.b is a view from above. The yellow cylinders in these figures represent the locations of the highly connected interval packers, while the red spheres are the points of highest concentration inflow as determined from fluid logging. The blue surfaces link the tracer injection interval to the locations of highest concentration inflow. From these figures it is seen that the packer locations encompass and contain the inflows. The locations of highest concentration inflows more-or-less define a feature which has a similar location and orientation as the S1 zone in Figure V.1.

The correct quantitative analysis methodologies were evaluated for use in interpreting the measured electrical conductivity logs from the crosshole test. The methods applied were zero and partial moment relationships and the conductivity log simulator BORE (TSANG et al., 1990). Because of large borehole flow rates (velocities), conductivity log suites evolved quickly relative to the log measurement cycle. There was also a large amount of peak interference even in early logs as a result of high flow rates and closely spaced inflows. Because of these characteristics, moment methods, while found to be powerful analysis tools in classical fluid logging applications, were only of limited use in this case. BORE however, proved to be a useful interpretive tool allowing estimation of fracture inflowing concentration and flow rate. BORE simulations for borehole 85.009 showed that inflowing concentration (prior to borehole dilution) reached values as high as 60% of the injection concentration.

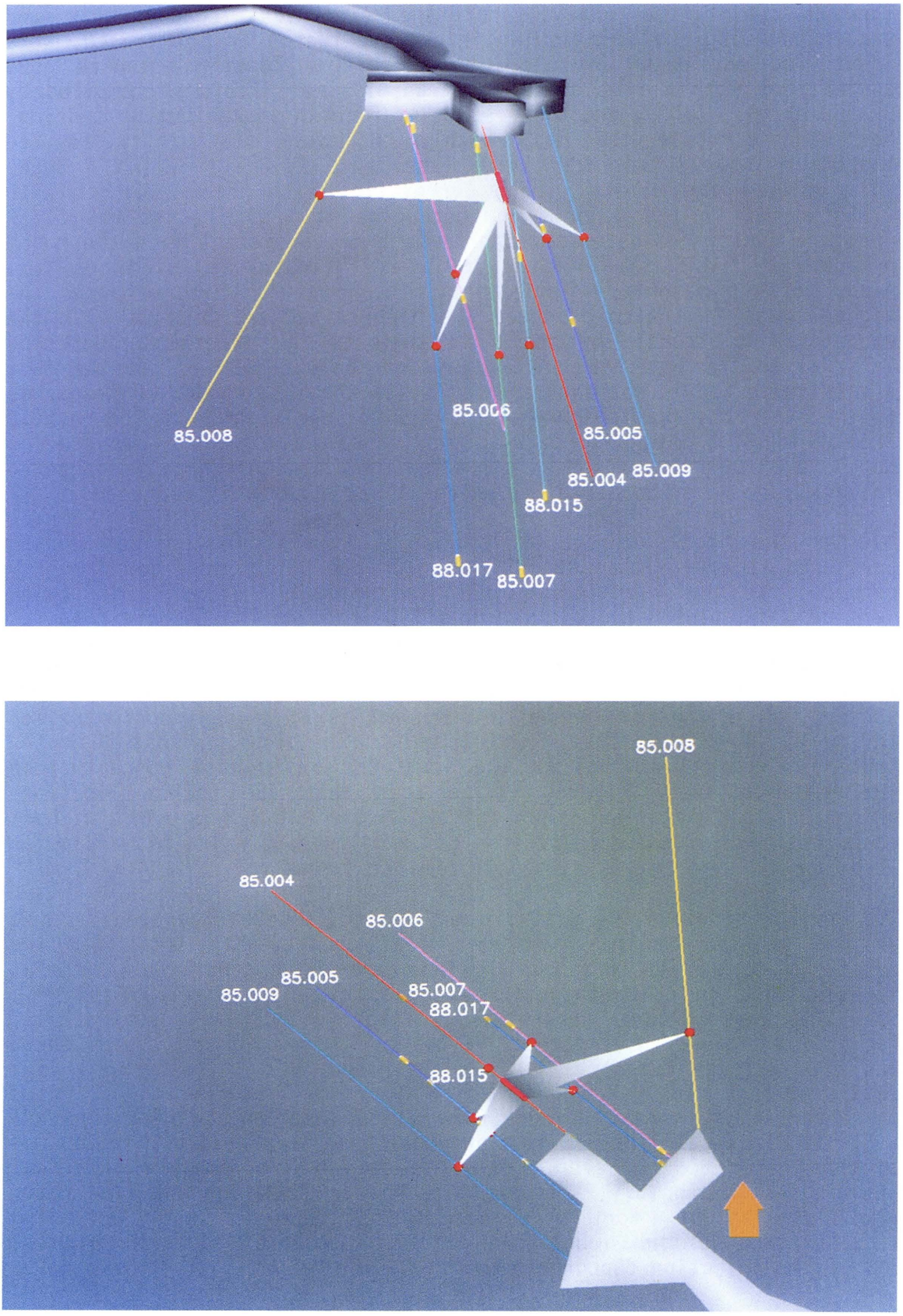

Fig. V.2: Three-dimensional views of the BK-Site.

V.4 OPEN QUESTIONS AND RECOMMENDATIONS FOR FUTURE INVESTIGATIONS

Flow and transport modeling in a fractured system requires knowledge of boundary conditions, the location and geometry of the controlling fractures, and the hydraulic properties of these fractures.

Hydraulic testing performed to-date at the BK site has already provided considerable insight into the boundary conditions which control flow at this site. The hydraulic data presented in this report as well as more recent tests performed by BGR underline the importance of the lamprophyre dykes as hydraulic boundaries which constrain flow. The hydraulic response of these structures is found to be heterogeneous. More pressure testing is needed to further characterize these structures and assess their influence on the flow system.

An important aspect which is not yet fully understood is the effect of the tunnel on the pressures at the BK-Site. Of particular interest is whether this effect has stabilized or whether it is still transient and if so, when will a steady-state be reached. The simplest way to address this problem is to install several long-term pressure monitoring systems in selected boreholes. The longest recovery periods performed to-date reached a pseudo-stabilization where the pressure increased to a plateau and then showed a very weak decrease. It would be of interest to follow the evolution of this decrease over the long-term.

Maybe the most significant result from both the pressure tests and the pilot fluid logging test was the evidence for the existence of a highly conductive preferential pathway for flow and transport. Two important questions remain relative to this feature. The first is what is the transmissivity of the feature and the second is are there other transmissive preferential pathways in the BK near-field which have not been identified. The pressure tests presented in this report do not really provide an answer to the first question. As mentioned in section III.2.4.2 of GUYONNET & LAVANCHY (this volume), the response from the test interval was always substantially higher than those of the intervals which show a high degree of connection. The responses were closest during test VE 457 in interval 6.7-10.7 m which was also the injection interval during fluid logging. Although the feature must necessarily be connected to this interval, this connection's transmissivity must be somewhat lower in the interval's vicinity. The best way to determine the transmissivity of the highly conductive feature would be to perform a pressure test in an interval covering one of the inflows which during fluid logging showed high mass as well as volumetric fluxes.

As for the presence of other highly conductive features, fluid logging identified some inflows with high volumetric fluxes and low mass fluxes which is indicative of a poorly connected but highly transmissive feature. An important aspect to investigate is whether such features are linked to others through a network which was not well connected to the injection interval. The pilot crosshole fluid logging test has demonstrated that this methodology is particularly well suited to this purpose. This is especially true at the BK site where the scale of investigation is relatively small and there are many boreholes. It should be reminded however that because most boreholes strike in a similar direction as the K-zones, it may prove difficult to evaluate

the potential existence of preferential K-zone pathways. For future conductivity log testing it is recommended that for comparison purposes, the injection tracer flux (QC) should be equal to that used in this pilot study.

Further investigations should rely more on the information from geologic and structural investigations. The combination of systematic feature classification based on geologic information, hydraulic tests and crosshole fluid logging provides a powerful methodology for the characterization of fractured rock flow systems.

REFERENCES

ALMEN, K.E., ANDERSSON, J.E., CARLSSON, L., HANSSON, K. & LARSSON, N.A. (1986): Hydraulic testing in crystalline rock: A comparative study of single-hole test methods. -Report SKB 86-27, Stockholm.

BARKER, J.A. (1988): A generalized radial flow model for hydraulic tests in fractured rock. -Water Resour. Res., Vol. 24, p. 1796-1804.

BOSSART, P., & MARTEL, S. (1990): Hydrogeological implications of ductile and brittle deformations in the Grimsel crystalline, upper Aare valley, Switzerland. -Nagra Internal Report, Baden (Switzerland).

BOURDET, D., WHITTLE, T.M., DOUGLAS, A.A. & PIRARD, Y.M. (1983): A new set of type-curves simplifies well test analysis. -World Oil (May), p. 95-106.

BRÄUER, V., KILGER, B. & PAHL, A. (1989): Felslabor Grimsel, Ingenieur geologische Untersuchungen zur Interpretation von Gebirgspannungsmessungen und Durchströmungsversuchen. -Nagra Technical Report, NTB 88-37, Baden (Switzerland).

COOPER, H.H. & JACOB, C.E. (1946): A generalized method for evaluating formation constants and summarizing well field history. -EOS, Trans. AGU, Vol. 27, p. 526-534, 1946.

EARLOUGHER, R.C., Jr. (1977): Advances in well test analysis. -Mono graph Series, Vol. 5, Society of Petroleum Engineers, Dallas.

GRINGARTEN, A.C. (1982): Flow test evaluation of fractured reservoirs. -in: Recent trends in hydrogeology (ed. T.N. Narasimhan).-Geol. Soc. Am., Special paper 182, Denver.

GRISAK, G.E., PICKENS, J.F., BELANGER, D.W. & AVIS, J.D. (1985): Hydrogeologic Testing of Crystalline Rocks during the Nagra Deep Drilling Program. -Nagra Technical Report, NTB 85-08, Baden (Switzerland).

GUYONNET, D., & LAVANCHY, J.-M. (1992): Analysis of single and cross-hole tests at the BK-Site, GRIMSEL Test Site. -Nagra Technical Report, NTB 91-09 (this volume).

HALE, F.V. & TSANG, C.F. (1988): A Code to Compute Borehole Fluid Conductivity Profiles with Multiple Feed Points. -Nagra Technical Report, NTB 88-21, Baden (Switzerland).

HORNER, D.R. (1951): Pressure buildup in wells. -Proc. Third World Pet. Cong., The Hague, Sec. II, p. 503-523.

HSIEH, P.A., NEUMAN, S.P. & SIMPSON, E.S. (1983): Pressure Testing of Fractured Rocks - A Methodology Employing Three-Dimensional Hole Test. -U.S. Nuclear Regulatory Committee, Washington, D.C., NUREG-/CR-3213, 176 p.

JACOB, C.E. & LOHMAN, S.W. (1952): Non-steady flow to a well of constant drawdown in an extensive aquifer. -EOS, Trans. AGU, Vol. 33, p. 559-569.

JARGON, J.R. (1976): Effect of wellbore storage and wellbore damage at the active well on interference test analysis. -J. Pet. Tech., Vol. 28, p. 851-858.

KELLEY, V.A. & FRIEG, B. (ed.) (1990): FLG: Field Investigations in the BK-AREA, Grimsel Test Site, December 1989 Until March 21, 1990. -Nagra Internal Report, Baden (Switzerland).

KELLEY, V. & LÖW, S. (1992): Analysis of a Pilot Fluid Logging Test at the BK-Site, Grimsel Test Site. -Nagra Technical Report, NTB 91-09, Baden (Switzerland) (this volume).

KEUSEN, H.R., BULETTI, M., GANGIN, J. & SCHULER, P. (1989): Felslabor Grimsel - Geologie. -Nagra Technical Report, NTB 88-37, Baden (Switzerland).

LAVANCHY, J.-M. (1990): Hydraulic Interference Tests. -In: Kelley, V.A., and Frieg, B. (ed.) (1990): FLG: Field Investigations in the BK-Area, Grimsel Test Site, December 1989 until March 21 1990. -Nagra Internal Report, Baden (Switzerland).

LIEB, R.W. (1988): The Grimsel Test Site from 1983 to 1990 - An overview. -Nagra Bulletin, Special Edition 1988.

LIEDKE, L. (1988): Felslabor GRIMSEL: Bohrlochkranzversuche (fracture system flow test). Abschlussbericht bis 1987. -Bundesanstalt für Geowissenschaften und Rohstoffe.

LONG, J.C.S, MAJER, E.L. MARTEL, S.A., KARASAKI, K., PETERSON, J., DAVEY, A., HESTIR, K., LANDSFELD, M. & MENSCH, A. (1989): Hydrologic Characterization of Fractured Rocks. An Interdisciplinary Methodology. -NDC-12. LBL, Berkeley California.

LÖW, S. & LAVANCHY, J.-M. (1990): Felduntersuchungen BK-Bereich Dezember 1989-Dezember 1990 Vorschlag NAGRA. -In: Kelley, V.A., and Frieg, B. (ed.), (1990): FLG: Field Investigations in the BK-Area, Grimsel Test Site, December 1989 until March 21 1990. -Nagra Internal Report, Baden (Switzerland).

LÖW, S., McNEISH, J.A. & ANDREWS, R.W. (1991): Determination of Transmissivities from Detailed Analysis of Leuggern 1987 Fluid Logging Data. -Nagra Internal Report, Baden (Switzerland).

LÖW, S., TSANG, C.F., HALE, F., & HUFSCHMIED, P. (1990): The Application of Moment Methods to the Analysis of Fluid Electrical Conductivity Logs in Boreholes. -Nagra Technical Report NTB 90-42, Baden (Switzerland).

MARTEL, S.J. & PETERSON, J.E. (1991): Interdisciplinary Characterization of Fracture Systems at the US/BK Site, Grimsel Laboratory, Switzerland. -Int. J. Rock Mech. Min. Sci. & Geomech. Abstr. Vol. 28, No. 4, pp. 295-323.

MISHRA, S., (1992): Methods for Analyzing Single- and Multi-Well Hydraulic Test Data. -Nagra Technical Report, NTB 91-09, Baden (Switzerland) (this volume).

MISHRA, S. &. GUYONNET, D. (1992): Analysis of observation-well response during constant-head tests. -Ground Water (in press).

NIVA, B., OLSSON, O., & BLÜMLING, P. (1988): Radar Crosshole Tomography with Application to Migration of Saline Tracer Through Fracture Zones. -Nagra Technical Report, NTB 88-31, Baden (Switzerland).

OGBE, D. & BRIGHAM, W.E. (1989): A correlation for interference testing with wellbore storage and skin effects. -SPE Formation Eval., Vol. 4., p. 391-396.

PAHL, A., LIEDTKE, L., NAUJOKS, A. & BRÄUER V. (1992): Abschlussbericht, Bohrlochkranzversuch BK im Felslabor Grimsel. -Nagra Technical Report, NTB 91-01, Baden (Switzerland).

PAILLET, F.L., HESS, A.E., CHENG, C.H., & HARDIN, E.L. (1987): Characterization of fracture permeability with high-resolution vertical flow measurements during borehole pumping. -Ground Water, Vol. 25, No. 1, pp 28-40.

RAGHAVAN, R. (1980): The effect of producing time on type-curve analysis. -J. Pet. Tech., Vol. 32, p. 1053-1064.

SILLIMAN, S. & ROBINSON, R. (1989): Identifying fracture interconnections between boreholes using natural temperature profiling: I. conceptual basis. -Ground Water, Vol. 27, No. 3, pp. 393-402.

STRELTSOVA, T.D., (1988): Well Testing in Heterogeneous Formations. -John Wiley, 413 pp., (New York).

TAYLOR, G.I. (1953): Dispersion of soluble matter in solvent flowing slowly through a tube. -Proceedings of the Royal Society of London, Series A 219, pp. 186-203.

TAYLOR, G.I. (1954a): Conditions under which dispersion of a solute in a stream of solvent can be used to measure molecular diffusion. -Proceedings of the Royal Society of London, Series A 225, pp. 473-477.

TAYLOR, G.I. (1954b): The dispersion of matter in turbulent flow through a pipe. -Proceedings of the Royal Society of London, Series A 223.

THEIS, C.V. (1935): The relation between lowering of the piezometric surface and the rate and duration of discharge of a well using groundwater storage. -EOS, Trans. AGU, Vol. 16, p. 519-524.

TSANG, C.-F., HUFSCHMIED, P., & HALE, F. (1990): Determination of fracture parameters with a borehole fluid conductivity logging method. -Water Resour. Res., Vol.26, No.4, pp. 561-578.

URAIET, A.A. & RAGHAVAN, R. (1980): Unsteady flow to a well producing at constant pressure.-J. Pet. Tech., Vol. 32, p. 1803-1812.

The zero'th moment of a single outflow peak located between L_0 and L as used in this QLR is defined by:

$$M_0(t) = \int_{L}^{L_0} C dx,$$

where C is the depth-varying electrolyte concentration and x the depth measured along the borehole with x=0 at the ground surface.

The zero'th moment as defined above can be related to the fracture outflow parameters q_i and C_i as follows (LÖW et al. 1991):

$$M_0(t)\pi r^2 = tq_i(C_i-C_0) + (L_0-L)C_0\pi r^2$$

where r = wellbore radius, and C_0 the background electrolyte concentration in the well prior to pumping.

The zero'th moment of an entire logging section located between X_0 (Bottom of Hole) and X as used in this QLR is defined by:

$$M_0(t) = \int_{X}^{X_0} C dx$$

The "corrected zero'th moment" (corrected for mass leaving through the x=X boundary) of an entire logging section located between X_0 and X is defined by:

$$M_{C0}(t) = \int_{X}^{X_0} C dx + Q/\pi r^2 \int_{0}^{T} C(X,t)dt,$$

where Q = the volumetric flux at x=X (pumping rate).

The corrected zero'th moment as defined above can be related to the mean fracture fluid concentration (averaged over all fracture outflows at a given time t, LÖW et al. 1991):

$$C_{mean}(t) = \frac{\pi r^2 \frac{d}{dt} M_{C0}(t)}{Q(t)}.$$

The n'th Partial Moment of a logging section between two inflows is defined as:

$$I_n(t) = \int_A^B (x-A)^n C(x,t)\,dx$$

The wellbore velocity v in this logging section can be related to the zero'th and first partial moment as follows (LÖW et al., 1991):

$$v = \frac{I_{0t}(lC_{xB}+C_A-C_B)-I_{1t}(C_{xB}-C_{xA})}{(C_A-C_B)(lC_{xB}+C_A-C_B)+lC_B(C_{xB}-C_{xA})-I_0(C_{xB}-C_{xA})}$$

with I_{nt} denoting the time derivative of the n-th Partial Moment, C_A the measured (or interpolated) concentration at point A, and C_{xA} the space derivative (slope) at point A.